Extending the possibilities of biopartitioning chromatography for improved prediction of in vivo drug absorption

Mike De Vrieze

Promotor: Prof. Dr. F. Lynen

Co-promotor: Prof. Dr. P. Sandra

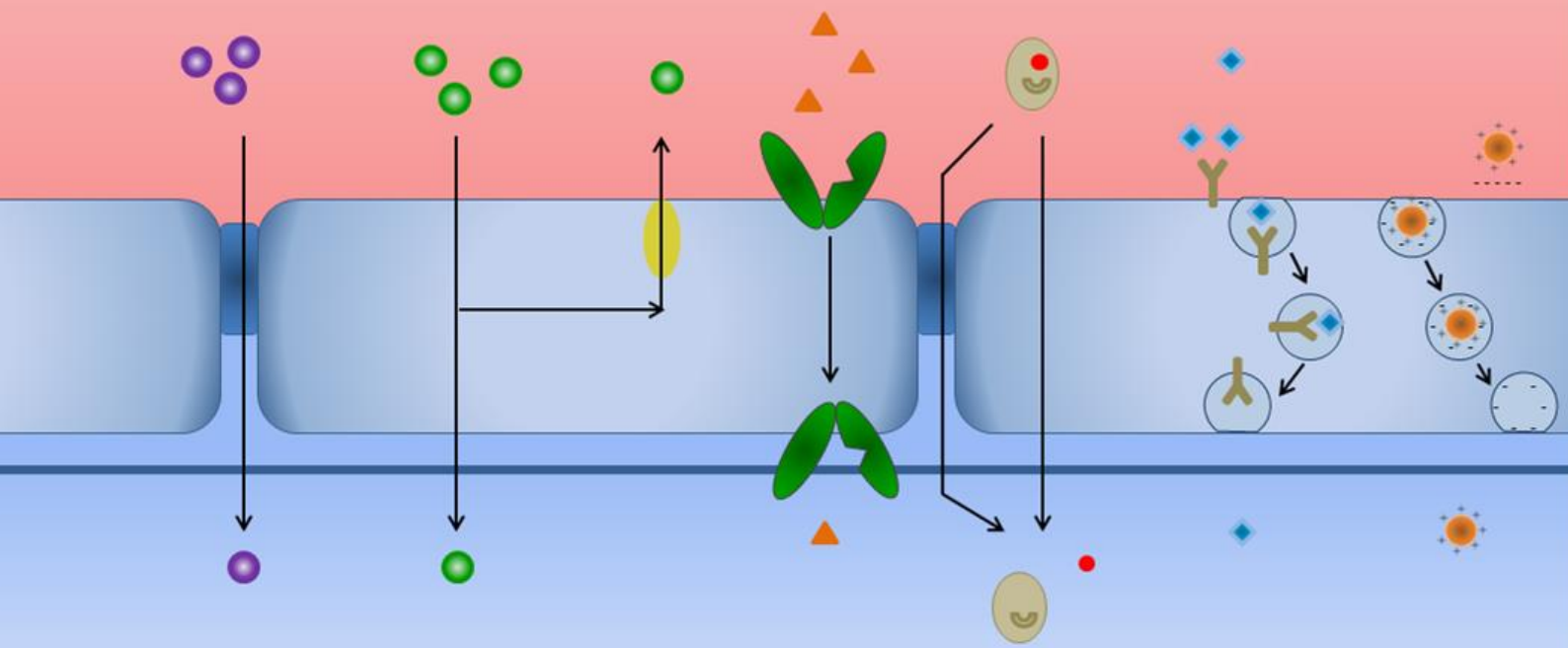

2015

Thesis submitted to obtain the degree of
Doctor in Sciences, Chemistry

Extending the possibilities of biopartitioning chromatography for improved prediction of in vivo drug absorption

Mike De Vrieze

Promotor: Prof. Dr. F. Lynen

Co-promotor: Prof. Dr. P. Sandra

2015

Thesis submitted to obtain the degree of
Doctor in Sciences, Chemistry

Table of contents

Table of contents

List of abbreviations

A

α	Total molar charge
ABC	ATP-binding cassette
ADME	Absorption, distribution, metabolism and excretion
ADMET	Absorption, distribution, metabolism, excretion and toxicity
AGP	α-acid glycoprotein
AIC	Akaike information criterion
AIDS	Acquired immune deficiency syndrome
ALS	Amyotrophic lateral sclerosis
ANN	Artificial neural network
ANS	8-Anilino-1-naphthalenesulfonic acid
ATP	Adenosine triphosphate

B

BAMPA	Bio-mimetic artificial membrane permeation
BBB	Blood-brain barrier
BCRP	Breast cancer resistance protein
BCSFB	Blood-cerebrospinal fluid barrier
BEC	Brain endothelial cell
BEKC	Bicelle electrokinetic chromatography
BIC	Bayesian information criterion
BMC	Biopartitioning micellar chromatography
BMEC	Brain microvessel endothelial cell
BPC	Biopartitioning chromatography
Brij 35	Polyoxyethylene (23) lauryl ether

C

C	Cholesterol
CAD	Charged aerosol detection
CE	Capillary electrophoresis
CEC	Capillary electrochromatography

List of abbreviations

CMC	Critical micellar concentration
CNS	Central nervous system
CO	Cholesteryloleate
CSF	Cerebrospinal fluid
CTAB	Cetyl trimethylammonium bromide
CV	Cross-validation
CZE	Capillary zone electrophoresis

D

DD	Drug discovery
DG	Diacylglycerol
DHPC	Dihexanoylphosphatidylcholine
DIC	N,N′-Diisopropylcarbodiimide
DIPEA	N,N-Diisopropylethylamine
DMF	Dimethylformamide
DMPC	Dimyristoylphosphatidylcholine
DPBS	Dulbecco’s phosphate-buffered saline
DRIFT	Diffuse reflectance infrared fourier transform

E

ECF	Extracellular fluid
EKC	Electrokinetic chromatography
EOF	Electroosmotic flow

F

FA	Fatty acid
FAME	Fatty acid methyl ester
FUS	Focused ultrasound

H

h	Height
HATR	Horizontal attenuated total reflectance
HBA	Hydrogen bond acceptor
HBD	Hydrogen bond donor

HIA	Human intestinal absorption
HILIC	Hydrophilic interaction liquid chromatography
HIV	Human immunodeficiency virus
HPLC	High-performance liquid chromatography
HR-MAS	High resolution magic angle spinning
HSA	Human serum albumin

I

IAM	Immobilized artificial membrane
IAMLC	Immobilized artificial membrane liquid chromatography
ILC	Immobilized liposome chromatography
ISF	Interstitial fluid

K

k	Retention factor
K	Partition coefficient
K_{in}	Unidirectional uptake coefficient

L

LEKC	Liposome electrokinetic chromatography
LGOCV	Leave-group-out cross-validation
Log BB	The logarithm of the brain:blood (or plasma) concentration ratio
Log D7.4	The logarithm of the distribution coefficient at pH 7.4
Log k	The logarithm of the retention factor
Log P	The logarithm of the partition coefficient
Log WSo	The logarithm of the intrinsic aqueous solubility
LOOCV	Leave-one-out cross-validation
LPC	Lysophosphatidylcholine
LPE	Lysophosphatidylethanolamine

M

MARS	Multivariate adaptive regression splines
MDCK	Madin-Darby canine kidney

MEEKC	Microemulsion electrokinetic chromatography
MEKC	Micellar electrokinetic chromatography
MELC	Microemulsion liquid chromatography
MG	Monoacylglycerol
MI(A)	Ames test mutagenic index
MLC	Micellar liquid chromatography
MLR	Multiple linear regression
MLV	Multilamellar vesicle
MR	Molar refractivity
MS	Mass spectrometry
MSA	Molecular surface area
MTBE	Methyl-tert-butyl ether
MV	Molar volume
MW	Molecular weight

N

NMP	N-Methyl-2-pyrrolidone
NMR	Nuclear magnetic resonance

O

ODS	Octadecyl silica

P

PA	Phosphatidic acid
PAMPA	Parallel artificial membrane permeation assay
PB	Plasma protein binding
PC	Phosphatidylcholine
PCA	Principal component analysis
PCR	Principal component regression
PD	Pharmacodynamic
PE	Phosphatidylethanolamine
PG	Phosphatidylglycerol
P-gp	P-glycoprotein
PI	Phosphatidylinositol

PK	Pharmacokinetic
PLS	Partial least squares
Pr	Parachor
PS	Phosphatidylserine
PSA	Polar surface area
PSP	Permeability-surface area product
PyBOP	(Benzotriazol-1-yloxy)tripyrrolidinophosphonium hexafluorophosphate

Q

QRAR	Quantitative retention-activity relationship
QSAR	Quantitative structure-activity relationship
QSRR	Quantitative structure-retention relationship

R

R	Correlation coefficient
RP	Reversed-phase
RPLC	Reversed-phase liquid chromatography
RR	Ridge regression
RT	Room temperature

S

SDC	Sodium deoxycholate
SDS	Sodium dodecyl sulfate
SFC	Supercritical fluid chromatography
SMILES	Simplified molecular-input line-entry system
Sphingo	Sphingomyelin
SPM	Sphingomyelin

T

t_0	Column dead time/ Void volume
TG	Triacylglycerol
THF	Tetrahydrofuran
TNBS	2,4,6-Trinitrobenzene sulfonic acid
TOF-MS	Time-of-flight mass spectrometry

t_r	Retention time

U

UV	Ultraviolet

V

V	Volume
VEKC	Vesicle electrokinetic chromatography
V_m	Volume of solvent within a column
V_s	Volume of the stationary phase within a column

W

WS7.4	Aqueous solubility at pH 7.4
wt	Weight

Chapter I. General introduction and aims of the work

Drug discovery and development is recognized as a long, costly, and financially hazardous process. Pharmaceutical companies are facing serious challenges because of rising R&D costs and declining success in new drug approvals. It now takes about 10 – 15 years to introduce a new therapeutic agent on the market, with costs ranging from hundreds of millions to several billion euro. Much of this expense is the result of costly late-stage failures [1]. Several stages can be distinguished in the development process, which are illustrated in Figure I-1.

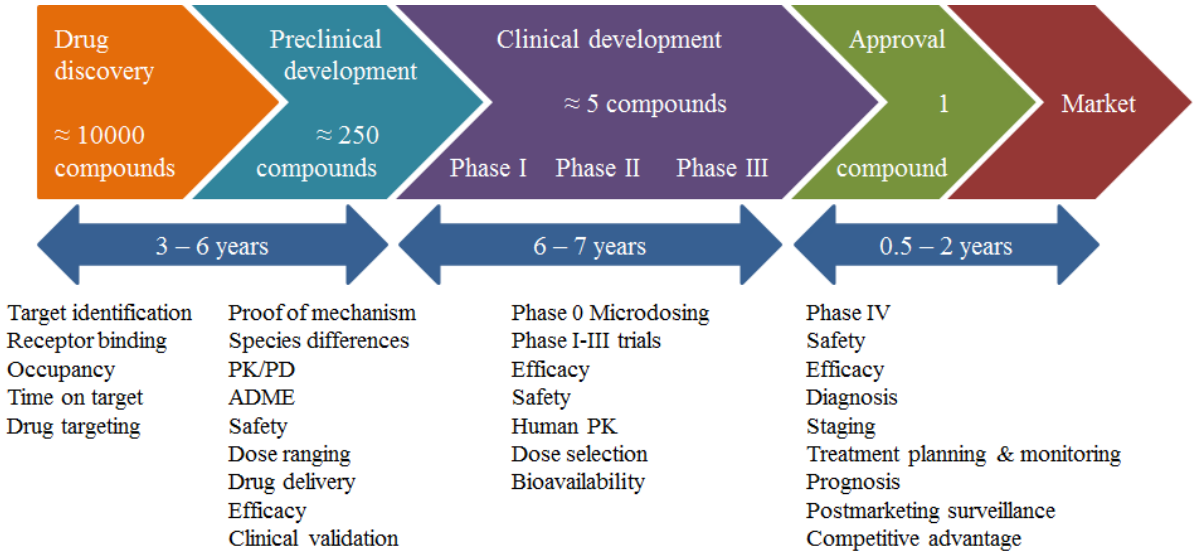

Figure I-1: From discovery to market launch of a new drug. Based on [1,2].

As can be seen in Figure I-1, a broad range of tests is needed during each stage of the development process, causing the elimination of most compounds after each consecutive step and a very high (> 99 %) overall attrition rate. In modern drug design, a lot of effort is put in the prediction of drug delivery. The reason for doing this is obvious: the sooner a lead

compound is found (or an uninteresting compound can be eliminated), the sooner the final drug can get marketed and the lower the total cost of the drug development.

In vivo, in vitro and in silico methods have been developed for the prediction of drug delivery. Prediction in these methods is mainly focused on absorption, distribution, metabolism and excretion (ADME) and drug delivery (see preclinical development, Figure I-1). Intestinal permeability and blood-brain barrier transport are predicted most often, although the prediction of drug delivery in specific organs (e.g. lungs, skin; [3]) has also been studied. Most methods are only capable to predict passive absorption, although some methods also try to account for carrier-mediated transport in the prediction [4]. Since total drug absorption is a combination of several mechanisms (see II.1.1), the latter type of methods is somewhat more realistic.

The fastest (and cheapest) way to predict drug delivery is based on in silico (= via computer simulation) predictions. This can even be performed before actual drug synthesis; therefore, it is a very good method to find lead compounds in initial studies.

As mentioned, predictions can also be made based on in vivo (in a living organism, e.g. rat) or in vitro (outside the body of an organism) measurements. Although in vivo measurements provide the best predictions, they are increasingly avoided (especially during the early drug discovery phases) because of high cost, low throughput and ethical considerations. In vitro methods are very useful after initial synthesis of the product, since they are much faster and cheaper than in vivo methods. Both for lead identification and optimization, there is a need for in vitro systems with high reproducibility and reliability. Several in vitro systems have been developed, each with certain advantages and disadvantages. These systems are experimentally simple and can model passive transport, which is mostly either completely or partially responsible for drug uptake. However, there is as yet no industrial standard for in vitro measurements to predict drug delivery. The search for such a method is still ongoing, since the creation of this method could lead to a significant reduction in the total cost of drug development.

This thesis will focus on in vitro systems based on high-performance liquid chromatography (HPLC), which has been proposed as an alternative to other in vitro methods. The basic processes of chromatographic separations are considered to be similar to the dynamic processes of drug action. Under adequate experimental conditions, the same basic properties (hydrophobic, electronic and steric) determine the behavior of chemical compounds in both the biological and chromatographic environments. Therefore, chromatography can be used as a powerful technique for estimating biological activity [5]. The two major HPLC-based

techniques in the prediction of drug delivery – micellar liquid chromatography (MLC) and immobilized artificial membrane liquid chromatography (IAMLC) – will be experimentally compared in this thesis. The general objective of this thesis is to develop improved in vitro methods which are able to provide useful data for the prediction of in vivo behavior of pharmaceutical compounds. More specifically, the aims are:

- The development of new in vitro methods, which could allow faster analyses, better predictions and/or a wider application range.
- A fundamental comparison of existing and new in vitro methods and evaluation of the performance of these methods. In order to get a realistic comparison, a range of in vitro methods should be tested. This should allow to conclude which method is suited best.

In chapter II, the prediction of blood-brain barrier (BBB) transport is explained. First, some general information about the BBB is provided. Then, the most common delivery systems are presented. Finally, most of the methods for the prediction of BBB transport are provided and the processing through mathematical modeling is discussed.
In chapter III, several common MLC and IAMLC methods are compared and evaluated towards the prediction of transport across the BBB.
In chapter IV, the synthesis of a sphingomyelin stationary phase for IAMLC is presented based on a solid-phase inspired methodology. The potential of this new stationary phase as an in vitro prediction tool was evaluated by a proof-of-concept model.
Chapter V compares the most common IAM phase and two other IAM phases (including the new sphingomyelin phase) towards in vitro prediction of transport across the BBB.
In chapter VI, the lipid composition of brain membranes is studied, with a focus on the main lipid classes. Both extraction and quantification procedures are presented. Afterwards, the main lipid classes in white and grey matter of newborn piglets are determined.
The results of chapter VI indicated that phosphatidylcholine is indeed the most prominent phospholipid in membranes and that C_{16} and C_{18} carbon chains are the most common in membrane phospholipids. Therefore, we decided to use the lipid analog miltefosine as MLC surfactant in chapter VII, since this phosphocholine-based lipid has a C_{16} carbon tail and thus has a similar (but less complicated) structure compared to phosphatidylcholine. In this chapter, not only transport across the BBB is predicted, but also the prediction of human intestinal absorption (HIA) was evaluated.

In chapter VIII, several topics are treated. The first section in this chapter involves a test, where MLC conditions are used on an IAM column; creating a different setup for the prediction of log BB and HIA values. In the second section, MLC and IAMLC methods from chapters III, V, VII and VIII are compared, in which both HIA and BBB transport are investigated. The third section shows how well the different descriptors are correlated. Finally, multiple linear regression was performed and compared to the partial least squares regression that was used throughout this thesis.

In chapter IX, the general conclusions resulting from this thesis are summarized and discussed. Proposals on how future research could contribute to better predictions are also made.

I.1 References

1. Buchanan L, Jurek P, Redshaw R (2007) Nuclear imaging drug development tools - PET and SPECT help enhance the quality of a product and prevent late-stage failure. Genet Eng Biotechn 27 (8):23-25.

2. Somerville S, Kloda JH (2015) FDA's Expedited Review Process: The Need for Speed. http://www.appliedclinicaltrialsonline.com/fda-s-expedited-review-process-need-speed.

3. Martin-Biosca Y, Torres-Cartas S, Villanueva-Camanas RM, Sagrado S, Medina-Hernandez MJ (2009) Biopartitioning micellar chromatography to predict blood to lung, blood to liver, blood to fat and blood to skin partition coefficients of drugs. Anal Chim Acta 632 (2):296-303.

4. Usansky HH, Sinko PJ (2003) Computation of log BB values for compounds transported through carrier-mediated mechanisms using in vitro permeability data from brain microvessel endothelial cell (BMEC) monolayers. Pharmaceut Res 20 (3):390-396.

5. Escuder-Gilabert L, Martinez-Pla JJ, Sagrado S, Villanueva-Camanas RM, Medina-Hernandez MJ (2003) Biopartitioning micellar separation methods: modelling drug absorption. Journal of Chromatography B-Analytical Technologies in the Biomedical and Life Sciences 797 (1-2):21-35.

Chapter II. Description of the structure, function and delivery across the Blood-Brain Barrier

In the first part of this chapter, the structure and function of the blood-brain barrier (BBB) is explained. Then, the focus is put on drug delivery across the BBB and prediction thereof. Finally, some prediction models are presented.

II.1 Structure and function of the blood-brain barrier

The blood-brain barrier (BBB) is a selective barrier formed by the endothelial cells that line cerebral microvessels (Figure II-1). The principal components of the BBB are the endothelial cells, astrocytes, and pericytes. Some other cellular elements like neurons or microglia may also play a significant role in the function of BBB. From the point of view of the permeability, the most important cell types of the BBB are the cerebral endothelial cells, which form a continuous sheet covering the inner surface of the capillaries. Endothelial cells are interconnected by tight junctions which form a belt-like structure at the apical region of the cells. Endothelial cells are sitting on the basal lamina. The basal lamina is the extracellular matrix layer produced by the basal cell membrane, used as an anchoring and signaling site for cell-cell interactions. Engulfed in the basal lamina are the pericytes, which cover approximately 22-32 % of the endothelium. Pericytes play an important role in the regulation of endothelial proliferation, angiogenesis and inflammatory processes. Astrocytes are capable to induce BBB properties in endothelial cells. Endfeet of astrocytes cover a significant part of the endothelial surface and provide the cellular link to the neurons. Neurons can regulate important aspects of BBB function and can induce the expression of BBB-related enzymes in cultured cerebral endothelial cells. Microglial cells are also found in the perivascular space. Their contribution to the BBB properties is not well characterized, although it is known that they play a very important immunological role [1-5].

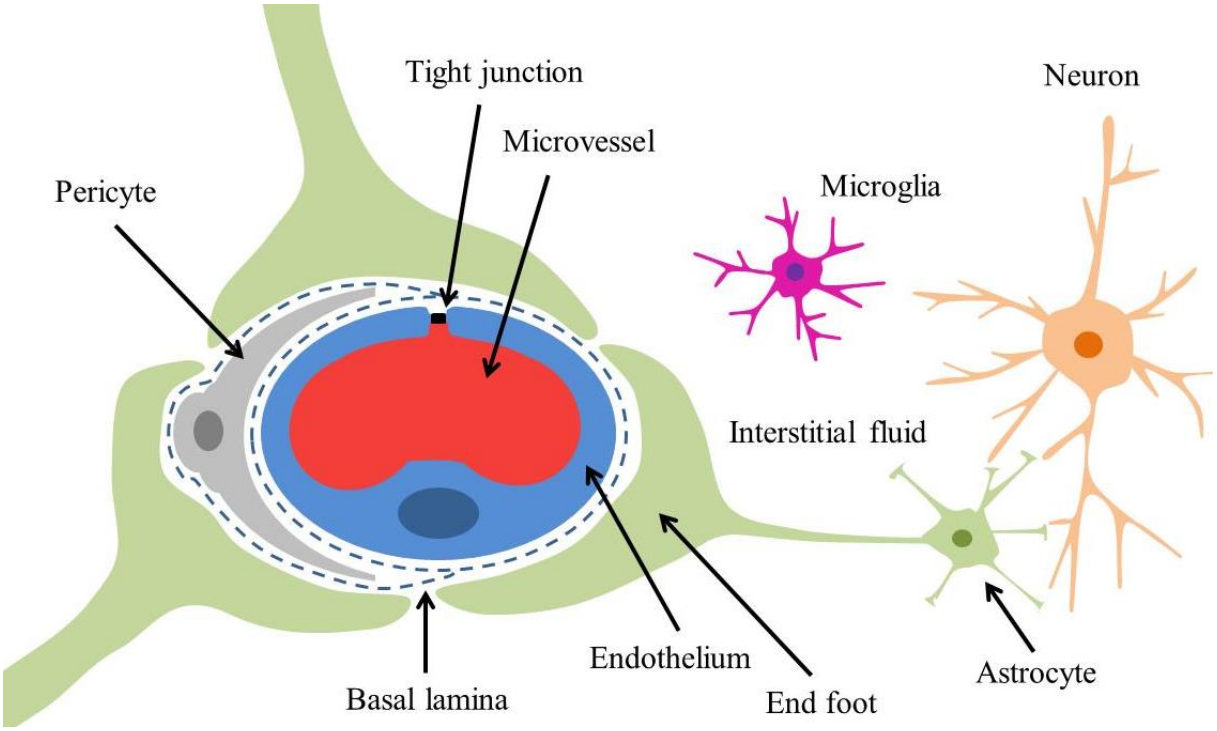

Figure II-1: Cellular constituents of the blood-brain barrier (BBB). Cerebral endothelial cells form tight junctions which restrict the paracellular pathway. Pericytes are distributed discontinuously along the length of the cerebral capillaries and partially surround the endothelium. Both the cerebral endothelial cells and the pericytes are surrounded by a basal lamina. Astroglial endfeet form a complex network surrounding the capillaries and provide the cellular link to the neurons. Microglia are CNS-resident immune cells. Modified from [6].

Barriers at three interfaces separate the blood from the brain interstitial fluid: the blood-brain barrier (BBB), formed by the endothelial cells that form the walls of the capillaries; the blood-cerebrospinal fluid barrier (BCSFB), formed by the choroid plexus epithelium, which also secretes cerebrospinal fluid (CSF); and the avascular arachnoid epithelium, which forms part of the meningeal covering. At each of these layers, cell:cell tight junctions form the 'physical' barrier, specific transport proteins mediate uptake and efflux ('transport' barrier), and enzymes add a 'metabolic' barrier. Together, these mechanisms regulate molecular traffic of drugs, nutrients, hormones, metabolites and other constituents between blood and brain, both inward and outward. The BBB, with the largest surface area (12-18 m^2 for the average human adult) and shortest diffusion distances (typically < 10-15 µm) to neurons, is the most important in regulating drug permeability to the brain. The BBB also supplies key nutrients and protects the brain from neuroactive and potentially toxic compounds circulating in the plasma. However, for some drugs and pathological conditions, the other two barriers may also be relevant [7,8]. The CSF is secreted across the choroid plexus epithelial cells into the brain ventricular system, while the remainder of the brain extracellular fluid, the interstitial fluid

(ISF), is derived by secretion across the capillary endothelium of the BBB. The avascular arachnoid epithelium, underlying the dura, completely encloses the CNS. This completes the seal between the extracellular fluids of the central nervous system and that of the rest of the body. The avascular nature and relatively small surface area of the arachnoid epithelium indicate that it does not represent a significant surface for exchange between the blood and the CNS. A schematic overview of the barriers at the three interfaces is given in Figure II-2.

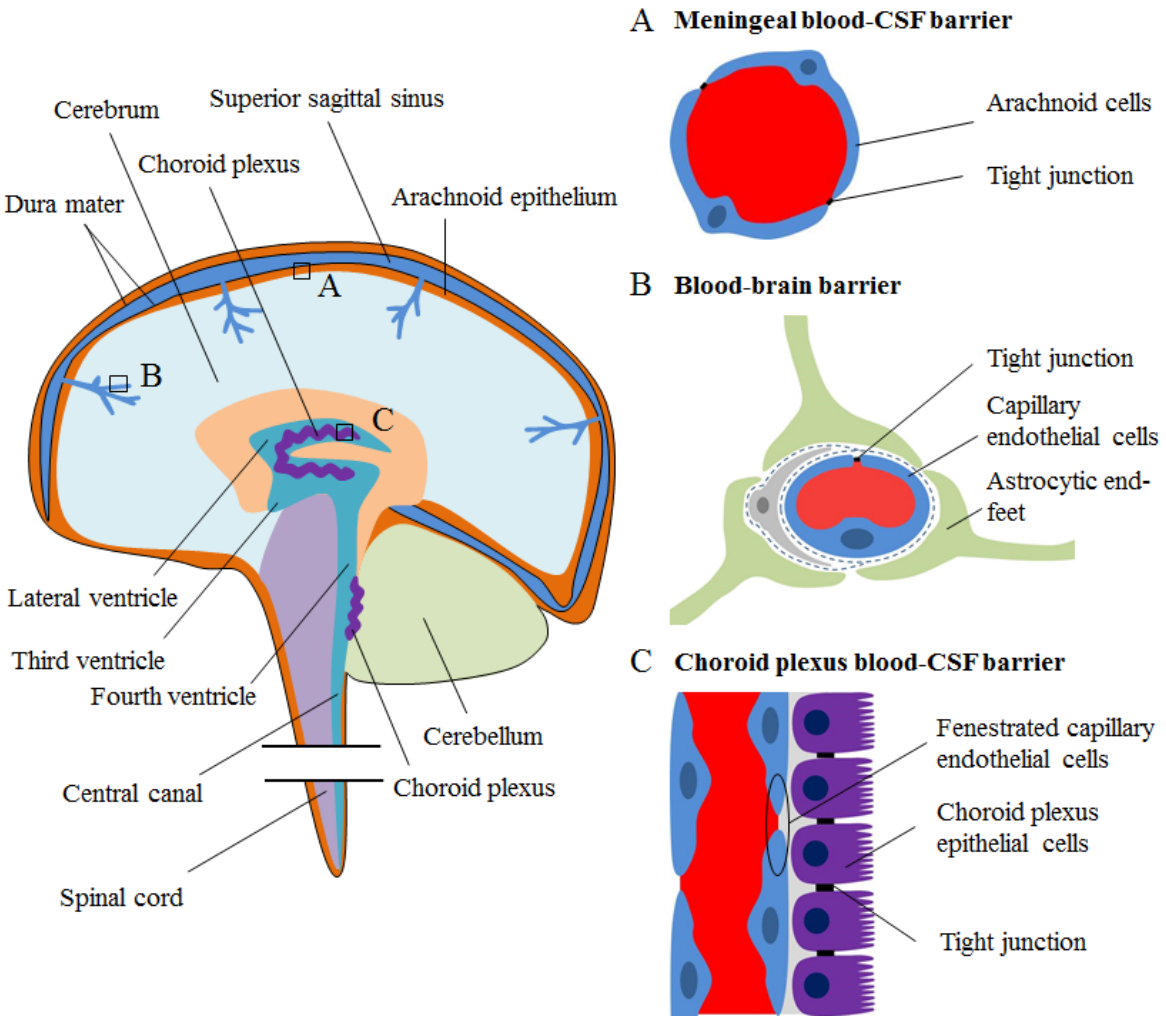

Figure II-2: Blood-brain and blood-CSF barriers. Three principal barrier sites exist between blood and brain: (A) The arachnoid barrier in the meningeal compartment. The brain is enveloped by the arachnoid membrane lying under the dura. Endothelial cells from the subarachnoid space are joined by tight junctions and form an effective seal. Transport across the arachnoid is not an important route for the entry of solutes into brain. (B) The BBB itself, created at the level of the cerebral capillary endothelial cells by tight junction formation. Once the BBB is crossed, diffusion distances to neurons and glial cells for solutes and drugs are short. Therefore, targeting a drug across the BBB is the favoured route for global delivery of drugs to all brain cells. (C) The blood-CSF barrier (BCSFB) lies at the choroid plexuses in the ventricles of the brain where tight junctions are formed between the choroid plexus epithelial cells. These epithelial cells produce the CSF. Barriers (A) and (B) continue into the spinal cord. Modified from references [3,6,9].

At all three interfaces mentioned in this figure, the barrier function results from a combination of physical barrier (tight junctions between cells reducing flux via the intercellular cleft or paracellular pathway), transport barrier (specific transport mechanisms mediating solute flux), and metabolic barrier (enzymes metabolizing molecules in transit). The barrier function is not fixed, but can be modulated and regulated, both in physiology and in pathology [10].

The blood-brain barrier has peculiar characteristics among the various physiological barriers. Diffusion of drugs across this endothelium separating the blood from the central nervous system (CNS) is more restrictive than elsewhere. Each of the cellular elements of the brain microvasculature that compose the BBB (endothelial cells, astrocyte end-feet, and pericytes) have specific functions [11].

Endothelial cells provide a crucial interface between blood and tissue environments. The free diffusion of chemicals across endothelia is prevented by endothelial tight junctions, of which the permeability varies considerably depending on tissue and conditions. In peripheral tissues (e.g. intestine, kidney, salivary gland) these cell barriers have fenestrations enabling almost free exchange of water and solutes. The endothelial barrier separating the blood from the CNS is however characterized by tight junctions of severely limited permeability (excluding molecules with a diameter larger than 10-15 Å), no fenestrae, and an attenuated pinocytosis. The tight junctions significantly reduce permeation of polar (hydrophilic) solutes through paracellular diffusional pathways between the endothelial cells from the blood plasma to the brain extracellular fluid [12]. This forces molecular traffic to take a largely transcellular route across the brain endothelium [13-15]. Adjacent endothelial cells are connected by tight junctions. The difference in tightness in different regions is explained by the number of fusion point between tight junctions [16].

Two main types of astrocyte cells can be distinguished in the brain. Protoplasmic cells exist in the grey matter, and fibrillary cells are present in the white matter. Protoplasmic astrocytes have large nuclei and thick cytoplasmic appendices. The endings of these appendices form cap-like structures known as end-feet that tightly attach to neurons on one side and blood vessels on the other [16].

Pericytes are small vessel wall-associated cells that are developed in the mesoderm. They are separated from endothelial cells by the basal lamina (basement membrane), but gap junctions provide contact spots. In the brain, pericytes are responsible for the regulation of endothelial cell activity, mediation of inflammation, and control capillary-like structure formation and capillary diameter. They therefore play an important and composite role in the maintenance of the BBB and brain homeostasis [16].

Although the blood-brain barrier has some typical characteristics, at a molecular level, the main building blocks of its biological membranes are similar compared to other physiological barriers. Biological membranes have as structural framework a bilayer resulting from the orientation of amphiprotic lipids (phospholipids, glycolipids) and cholesterol in the aqueous medium. In many biological animal membranes, these lipids are distributed asymmetrically. The outer half of the bilayer comprises mainly zwitterionic lipids, for example phosphatidylcholine (PC) and phosphatidylethanolamine (PE), whereas the inner part contains negatively charged lipids, particularly phosphatidylserine (PS) [17]. Figure II-3 gives a schematic representation of a typical biological membrane according to the fluid mosaic model. Proteins and other substances (e.g. steroids and glycolipids) are either associated with its surface or embedded in it to different degrees. The polar heads of phospholipid molecules are orientated to form an almost continuous polar layer on both the inner and outer side of membranes. In contrast, the long hydrophobic chains of phospholipids molecules extend into the central core of the membrane. The peripheral and integral proteins located in the membranes are responsible for carrying out many of the active functions of membranes, such as acting as receptors and transportation routes for various substances in and out of cells. The formation of pores, including ion channels, is also associated with integral proteins [18].

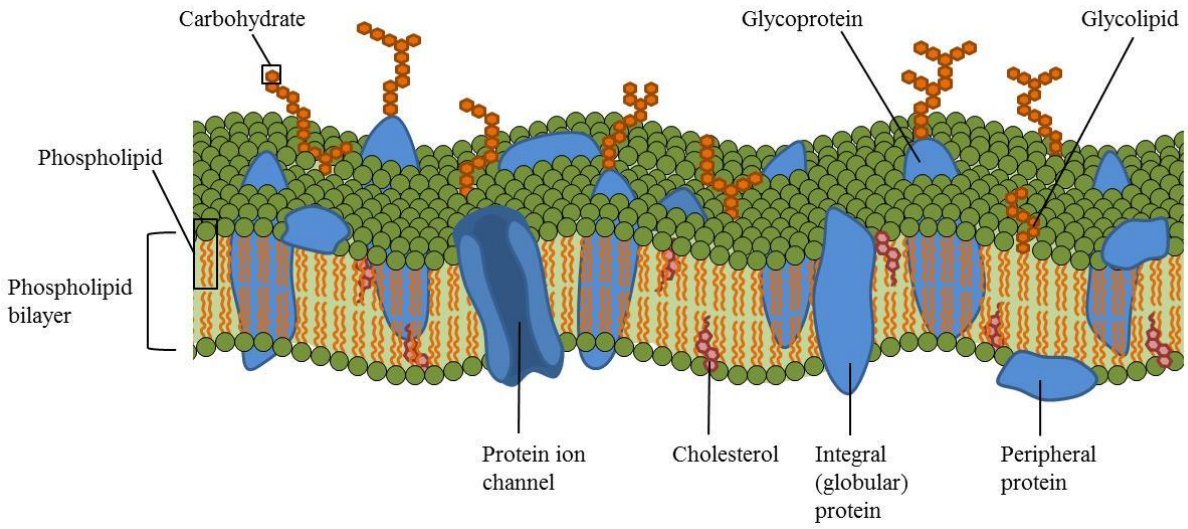

Figure II-3: The fluid mosaic model of biological membranes. Modified from references [18,19].

Most cell membranes are composed of both around 50 weight% lipid and protein. This means that about 50 % of the cell surface area (the semipermeable surface created by membrane lipids) is available for drug penetration. However, BBB cells are composed of only around 15

weight% of lipids (see Figure II-4), which means that only 15 % of the cell's plasma membrane area represents the surface area available for diffusion [20].

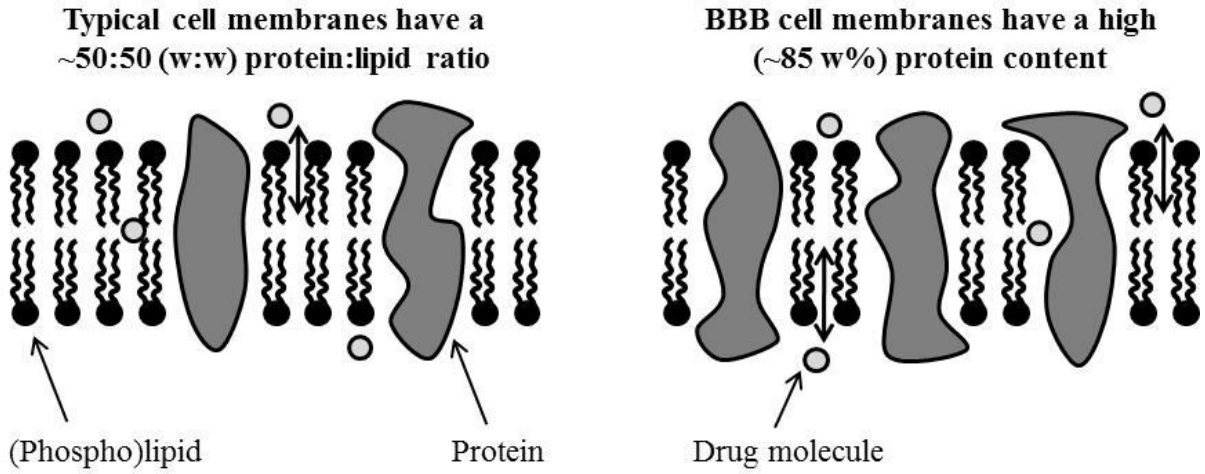

Figure II-4: Composition of typical and BBB cell membranes. Based on [20].

II.1.1 Transport across the blood-brain barrier

Cells forming the BBB depict a high negative charge density on the surface from PS. Negatively charged membranes are difficult for compounds to cross. This is one of the reasons why many CNS active compounds are hydrophobic amines since they have affinity for negatively charged surfaces and they can partition into the membrane as a result for their hydrophobicity [20]. CNS drugs can be classified according to their action mechanism as general or non-specific CNS drugs and selective modifiers of CNS functions [21]. Drugs whose mechanisms currently appear to be general or non-specific act by diverse molecular mechanisms affecting different target cells. They can have the ability to depress excitable tissue at all levels of the CNS or may stimulate the CNS (e.g. anesthetics, hypnotics and sedatives). Drugs classified as selective modifiers of CNS functions produce the effects through an identifiable molecular mechanism specific for the target cells that bear receptors for them. These drugs can be classified more definitively according to their site of action or specific therapeutic usefulness (e.g. anticonvulsants, psychopharmacological agents such as antipsychotics, antidepressants, etc.). Certain drugs that are unable to cross the blood-brain and blood-CSF barriers may sometimes produce a profound effect on the CNS as part of their pharmacological actions. Some of these drugs also produce side effects or toxic reactions that can affect the CNS (e.g. antihistamines) [22].

Since the BBB is the most important in regulating drug permeability to the brain, we will limit ourselves to this pathway. Permeation across the cell membranes takes place by three main mechanisms: transcellular diffusion, paracellular diffusion and active transport (either transport into the cells or efflux out of the cells). Paracellular permeation is mainly governed by the size and the number of the pores between the cells, as well as the size and charge of the drug. Active transport processes require specific binding of the drug to the transporter protein. Diffusion across the cell membranes and transcellular permeation through the cells constitute the most important mechanisms, by which drugs cross biological membranes [23]. The main physical barrier of the transcellular pathway is the lipid matrix of the membranes, whereas that of the paracellular pathway are the intercellular tight junctions [17]. Most common drugs traverse cellular barriers by transcellular pathways. These pathways require movement of solutes across and through cells and include passive diffusion, carrier-mediated and vesicular transport mechanisms.

It has long been assumed that synthetic drugs pass cellular barriers by passive diffusion only, which would favour lipophilic[1] drugs. However, carrier-mediated membrane transport is not only a pathway for endogenous molecules (i.e. amino acids, oligopeptides, monosaccharides, water-soluble vitamins, etc.), but also a transport route that can be used by xenobiotics (molecules found within an organism that are normally not present there) [24]. Large molecules can be transported through a vesicle-based migration mechanism across the cell, i.e. transcytosis [17].

Paracellular transport, the tendency of a solute to follow the aqueous extracellular route, might be the primary pathway by which hydrophilic compounds of relatively low molecular weight cross epithelial and some endothelial barriers. Transport of larger hydrophilic molecules might be enhanced by modulation of junctional pores or addition of so-called drug absorption promoters. Translocation of solutes via the paracellular route takes place primarily by passive diffusion. Because of ionisable side-chains in tight junction proteins, the junctional space has an electrostatic field with a negative net charge that might affect the paracellular flux of solutes via ionic interactions [25]. Even if paracellular penetration occurs, the compound must still cross the cell membrane at the target cell to have its effect. A schematic representation of the various pathways involved in the BBB permeability is shown in Figure II-5.

[1] Lipophilicity is a measure for the lipid solubility of an agent, typically estimated as log P, the octanol:water partition coefficient.

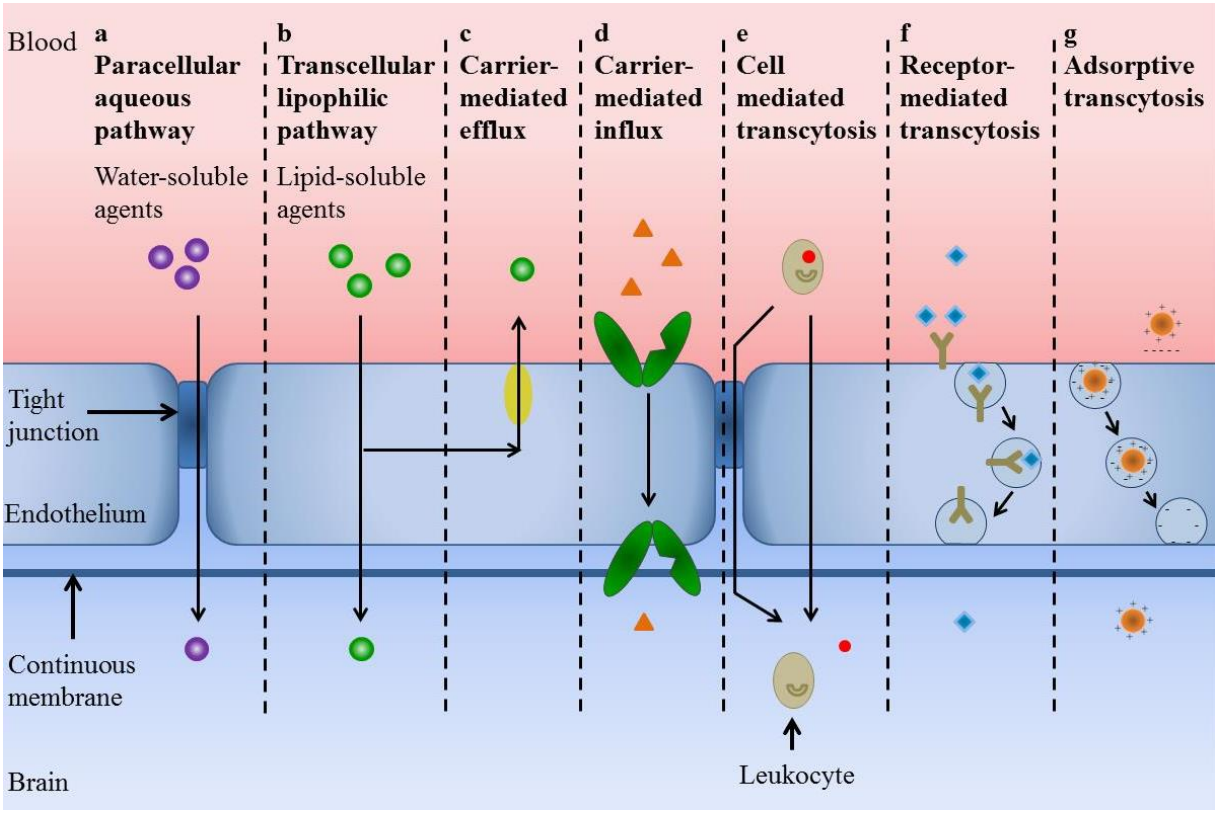

Figure II-5: Potential routes for transport across the brain endothelium forming the blood-brain barrier. **a** Tight junction modulation may occur, which gives way for the paracellular aqueous diffusional pathway. **b** Solutes may passively diffuse through the cell membrane and cross the endothelium. This process is favoured for solutes with greater lipid solubility. **c** Active efflux pumps intercept some of these passively penetrating solutes and pump them out of the endothelial cell. **d** Many essential polar molecules, such as glucose, amino acids and nucleosides are transported into the CNS by carrier-mediated influx. **e** Leukocytes may cross the BBB adjacent to the tight junctions or by modification of the tight junctions. **f** Some macromolecules, proteins and peptides are transported by receptor-mediated transcytosis. **g** Adsorptive transcytosis appears to be induced by positively charged macromolecules and may result in transport across the BBB. Modified from references [6,26].

Passage of compounds that are important in metabolism is facilitated by the presence of specific transporters in the plasma membranes of the endothelium. Separate transporters for glucose, large neutral amino acids and monocarboxylic acids, plus several others have been found. Common inorganic ions and essential trace metals also have specific transport systems at the barrier. Iron is present in extracellular fluids in combination with the protein transferrin. It is generally transported into cells by receptor-mediated endocytosis of this iron-transferrin [27].

Some of the uptake transporters of the brain endothelium may work bidirectional, also regulating efflux. However, several families of transporters have been identified that are capable of transporting solutes out of the brain endothelial cells. They are able to restrict the CNS entry of a number of potentially harmful, toxic or lipophilic agents circulating in the blood [8].

For many CNS drug-like molecules, plasma concentrations can quickly equilibrate with brain concentrations, even though their BBB permeability can vary substantially. Therefore, a lead compound should not be eliminated as a candidate compound only because it shows low BBB permeability [28].

II.1.2 Functions of the blood-brain barrier

The BBB has several roles. It controls molecular traffic, keeps out toxins, supplies the brain with essential nutrients and mediates efflux of many waste products. It restricts ionic and fluid movements between the blood and the brain, allowing specific ion transporters and channels to regulate ionic traffic, to produce a brain ISF that provides an optimal medium for neuronal function. ISF is similar in composition to blood plasma, but thanks to the BBB, it has a much lower protein content, and lower K^+ and Ca^{2+} concentrations but higher levels of Mg^{2+}. More importantly, the BBB protects the brain from fluctuations in ionic composition that can occur after a meal or exercise, which would disturb synaptic and axonal signaling. The barrier helps to keep separate the pools of neurotransmitters and neuroactive agents that act centrally (in the CNS) and peripherally (in the peripheral tissues and blood), so that similar agents can be used in the two systems without 'crosstalk' [3,6]. The restricted and highly controlled access to the brain is due to several factors: (i) tight junctions which are sealing the intercellular gap, (ii) reduced rate of pinocytosis from the luminal side which prevents uncontrolled cell entrance, (iii) no fenestration which blocks the intercellular passage of the endothelium, (iv) an enzymatic barrier which presents the second line protection against unintentionally entered molecules, proteins and viruses, and (v) efflux transporter systems such as P-glycoproteins and others which remove small molecules from the endothelial cells before they reach the abluminal or basal side [29].

II.1.3 Controlling the permeability of the blood-brain barrier

The apparent permeability of the BBB to a solute may be modified in at least three primary ways. Firstly, the effectiveness of transport depends on the magnitude and distribution of blood flow in the brain. Secondly, tight junctions may be partially or fully opened, introducing or enlarging a water-filled route for entry of solutes into cerebral interstitial fluid. Lastly, specific transport mechanisms may be regulated, e.g. the transport of glucose [27].

The BBB can be broken down by different physiological and pathological conditions, including hypertension, hyperosmolality of the blood, exposure to microwave or radiation, infection, trauma, ischemia and inflammation [30]. There is a growing list of pathologies involving alterations of BBB function and abnormal astrocyte-endothelial cooperation; some pathologies even cause multiple BBB deficits. A short overview of pathologies causing BBB breakdown or disorder is given in Table II-1.

Table II-1: Overview of several CNS pathologies together with (some of) their effects on the BBB. Based on [3,10,26].

CNS pathology	**Main expressions of BBB dysfunction**
Alzheimer ‘s disease	* Decreased levels of P-glycoprotein transporter expression * Decreased glucose transport * Altered cellular relations at the BBB
Brain tumors	* Breakdown of the BBB * Loss of the tight junctions in the tumor vascular system
Epilepsy	* Transient BBB opening in epileptogenic foci * Upregulated expression of P-glycoprotein and other drug efflux transporters in astrocytes and endothelium
Glaucoma	* Opening of the BBB
HIV	* Disruption of tight junctions in the BBB * Apoptosis of endothelial cells
Infectious or inflammatory processes	* Examples include bacterial infections, meningitis, encephalitis and sepsis * Permeability of BBB tight junctions is affected * Interferon-β prevents BBB disruption * Alterations in P-glycoprotein expression and activity in the BBB
Multiple sclerosis	* Breakdown of the BBB * Downregulation of laminin in the basement membrane * Tight junction disruption
(Inflammatory) pain	* Alters BBB tight junction protein expression and BBB permeability due to activated astrocytes
Parkinson's disease	* Dysfunction of the BBB by reduced efficacy of P-glycoprotein
Stroke	* Proteolysis of the vascular basement membrane/matrix * BBB disruption * Downregulation of the brain capillary endothelial
Trauma	* Opening of the BBB

Considering the BBB dysfunctions caused by CNS pathologies, a concern within the CNS drug discovery environment is that the vast majority of studies are conducted using healthy preclinical tissue, while this might not give a representative image [26,31,32]. Given the evidence for involvement of BBB damage in many neurological conditions, there is growing interest in the BBB as a therapeutic target. For many pathologies, directing therapies to

protect or repair the BBB endothelium may prove an effective way to reduce the severity of neurological symptoms or delay onset of neurodegeneration [8,3].

II.2 Principles of drug delivery across the blood-brain barrier

The BBB significantly hinders drug delivery to the brain. Because of this barrier, many therapeutics which could potentially treat neurological conditions cannot be delivered in an intravenous way. Overcoming this hindrance could mean potential therapies for a wide range of disorders, including Alzheimer's and Huntington's diseases, amyotrophic lateral sclerosis (ALS), neuro-AIDS, stroke, brain or spinal cord trauma, autism, lysosomal storage disorders, fragile X syndrome, inherited ataxias, and blindness [33].

For drugs that do not readily cross the BBB, there are several options. The existing molecule can be modified to cross the BBB directly, the barrier can be bypassed physically or specialized delivery vehicles can be used to evade the BBB mechanism [34]. An overview of possible methods for drug delivery across the BBB is given in this section. All developed brain-targeted delivery systems must be assessed for their safety, risk and benefit for patients. So far, the safety issue has been largely overlooked during the research stage, yet this issue will become critical when the drug to be delivered is intended for a long term therapy. It is extremely important that any developed delivery system should have no significant impact, short or long term, on the functions of the brain [26].

It has been suggested by Lennernäs [35] that purely passive diffusion is universal for membranes with different physiological functions and physicochemical properties. Therefore, the factors that determine a compound's intestinal absorption should also, to some extent, determine the BBB permeability. Some techniques mentioned in II.2 and II.3 are mainly focused on intestinal absorption, but are also illustrated based on their potential regarding BBB delivery or prediction.

II.2.1 Non-mediated delivery

Some compounds are able to cross the BBB directly making use of the paracellular aqueous pathway or the transcellular lipophilic pathway (passive diffusion). The extent and speed of penetration can however be totally different. Therefore, methods to improve penetration of these compounds are desirable. The improvement of passive penetration of the brain can be

achieved by developing lipophilic pro-drugs that are taken up into the brain and metabolized to release active parent compounds [36]. This lipidization strategy is limited since drug lipidization also increases its penetration in other tissues. In practice, lipidization modifications are difficult, and the only example of a (street) drug where the effectiveness of this approach can be demonstrated is heroine. This molecule, synthesized by di-acetylation of morphine, increases brain uptake more than 30-fold. This approach has limited applicability to drugs greater than 400-450 Da [37,38].

A lot of molecules showing lipophilic properties potentially enabling them of passive permeation of the BBB nevertheless exhibit unexpected low penetration rates. This observation may be explained by the presence of ATP-binding cassette (ABC) transporters, which effectively efflux a broad spectrum of molecules. Therefore, there are limits to the strategy to design CNS drugs exhibiting high lipid solubility as it increases the probability that the drug will not sufficiently reach the intended targets [39].

The major efflux transporters in the BBB are P-glycoprotein (P-gp), breast cancer resistance protein (BCRP) and multidrug resistance proteins. P-gp can be used for increase or decrease of brain delivery of drugs. P-gp is an ATP-dependent pump, the protein acts as an efflux pump with broad substrate specificity, resulting in the restricted accumulation of some cytotoxic and lipophilic drugs. Several drugs are potential ligands for P-gp and have restricted transfer through the brain endothelial cell and in brain tumors, since they are pumped out by the transporter. A pharmacological strategy consists of co-administration of P-gp reversing agents (inhibitors) such as verapamil as a means of increasing drug delivery to the brain by competition on the P-gp specific sites. Conversely, the use of inducers of P-gp such as phenobarbital could decrease adverse central side-effects of drugs acting in the periphery [40,41]. The BCRP efflux transporter plays an important role in the efflux of CNS acting drugs and anticancer therapeutics. Various attempts have been made for the development of predictive models for this protein [42]. A recent study [42] developed a model to calculate a BCRP value, after which is was incorporated in the model development for log BB (the logarithm of the brain:blood (or plasma) ratio, see section II.3.1). Compounds which fulfilled the criteria for BBB permeability, but showed low log BB values, were proven to be substrates for the BCRP transporter, thus indicating the important role of BCRP in BBB permeability.

Another possibility for the improvement of delivery across the BBB lies within the development of drugs which are transported into the brain via endogenous BBB transporters [37].

While these methods are promising and offer the ability to easily administer drugs to the CNS as in other organs, they do require the expense and time of developing new agents, and they result in drugs being delivered to the entire brain, which may not always be desirable [33].

II.2.2 Drug delivery across the blood-brain barrier by liposome systems

A possible alternative route would be the use of liposome systems. Liposomes have become more and more important as strategy for brain-targeted drug delivery. The most interesting features of liposomes are their ability to incorporate and deliver large amounts of drug and the possibility to place different ligands on their surface [43]. Liposomes can provide an increased cellular uptake and a reduced efflux through ABC transporters. New therapeutic strategies for using liposome-carried drugs in different conditions have been developed, affecting CNS tumors and neurodegenerative diseases to viral infections and epilepsy [44].
Liposomes (Figure II-6) can be prepared by weighing the desired lipids (e.g. dimyristoylphosphatidylcholine (DMPC, represented in Figure II-7)) and dissolving these lipids in an organic solvent. A lipid film is formed on the wall of a round-bottom flask following rotary evaporation. The resulting dried film can be hydrated in a swelling (e.g. a phosphate buffer) solution by vortex or mixing, which results in the formation of multilamellar vesicles (MLVs, multilamellar liposomes) [45,46]. Compared to classical micelles, these liposomes are much bigger. However, they offer more possibilities towards the incorporation of drugs, since both hydrophilic and hydrophobic spaces are available. Also, the bilayer of the liposomes is a much more realistic mimic of the membrane bilayers compared to micelles.

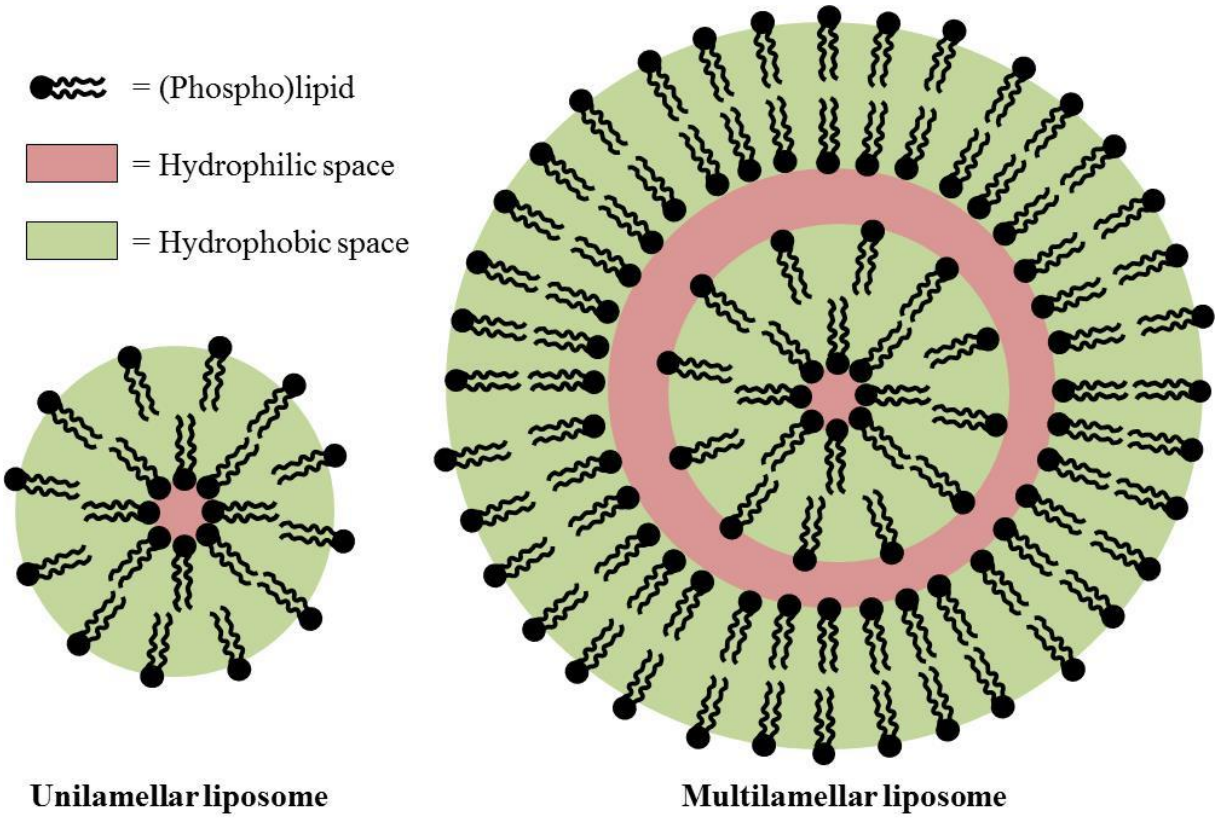

Figure II-6: Schematic representation of a unilamellar and a multilamellar liposome. Water-soluble compounds can be encapsulated in the aqueous core, while lipid-soluble compounds can be incorporated into the lipid bilayer of the liposome. Modified from references [20,47].

Liposome suspensions prepared from phospholipids exhibit structural similarities to the phospholipid bilayer found in cell membranes. Several quantitative structure-activity relationship (QSAR) studies have successfully correlated drug activities with drug liposome partition coefficients [48,49]. Liposomes can model both polar and nonpolar drug-membrane interactions, but they are difficult to model experimentally. Limitations of this delivery mechanism include the large size of liposomes and controlled release of the encapsulated drugs from the vesicles [41].

II.2.3 Bicelles as an alternative delivery system

Bilayered micelles, or bicelles, are a popular model membrane system. Depending on composition, concentration, and temperature, bicelle mixtures may adopt an isotropic phase or form an aligned phase in magnetic fields. Therefore, bicelles have interesting characteristics in Nuclear Magnetic Resonance studies.

To a certain extent, the morphology of bicelles is similar to liposomes. Bicelles consist of a mixture of long-chain phospholipids, such as DMPC, and short-chain phospholipids, such as dihexanoylphosphatidylcholine (DHPC). Bicelles were proposed to consist of disk-shaped bilayer domains, whose edges were coated by a curved DHPC rim. The radius of the disk-shaped bilayer depends on the chosen molar ratio (of long- to short-chain phospholipid). Figure II-7 depicts a bicelle, consisting of short- and long-chain phospholipids (i.e. DHPC and DMPC). As can be seen, DMPC lipids dominate the disk-shaped bilayer domain of radius R, which is coated with a DHPC rim with radius h/2 [50]. To the best of our knowledge, bicelles have not been used for brain-targeted drug delivery.

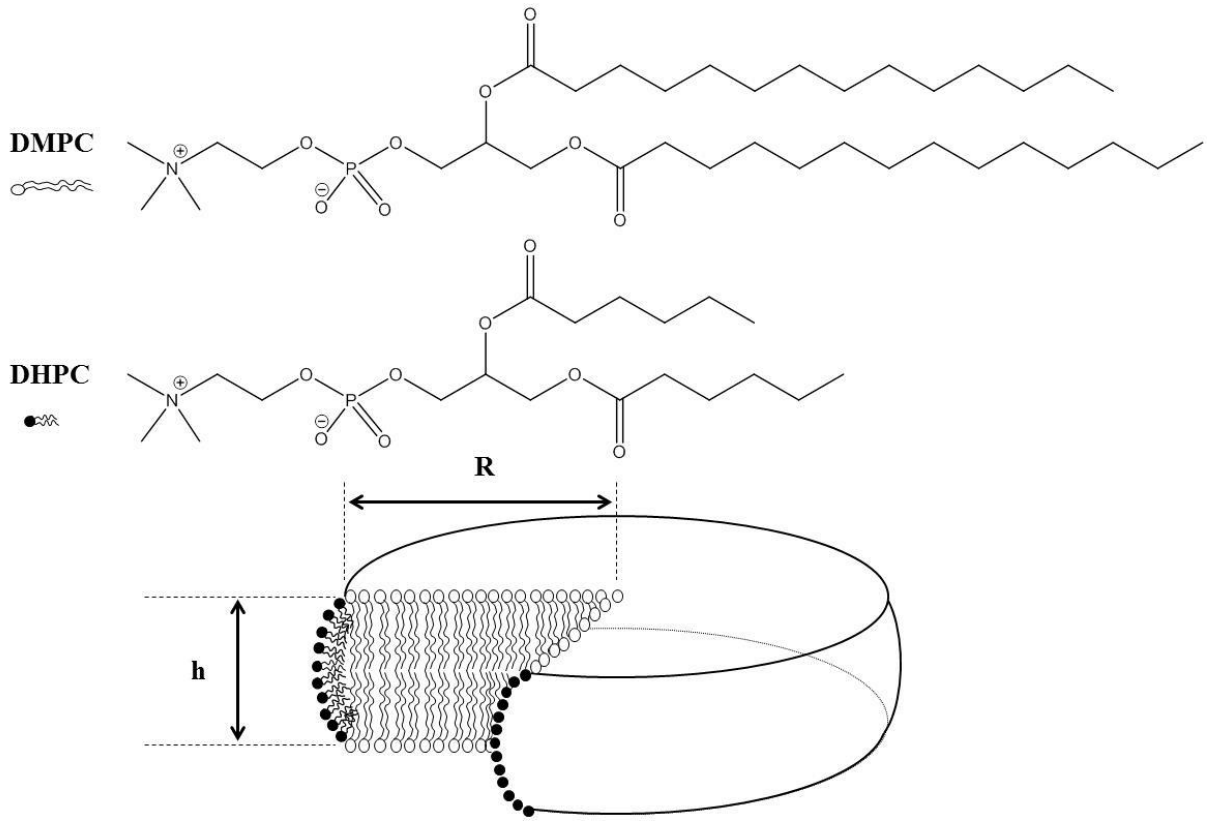

Figure II-7: The disk-shaped bicelle model, in which the planar bilayer domain consists of long-chain phospholipids (DMPC), and the rim consist of short-chain phospholipids (DHPC). R is the bicelle disk radius, h is the total bilayer thickness. Based on [50].

Like micelles, bicelles are noncompartmentalized, optically transparent, and effectively monodisperse. On the other hand, bicelles have a much lower detergent content than classical mixed micelles and maintain some key bilayer properties that are absent in micellar systems. Bilayers can – to a limited extent – mimic membrane bilayers. A more realistic model could

be achieved with other classes of lipids, such as those with longer acyl chains and higher degrees of chain unsaturation than DMPC [51] (see chapter VI).

II.2.4 Cell-penetrating peptides and molecular Trojan horses

Cell-penetrating peptides and molecular Trojan horses can be used for targeting the entire brain. They perform well as delivery molecules. Cell-penetrating peptides are not brain specific but can provide efficient traversal of the BBB, and tandem systems with targeting molecules may produce extremely effective brain drug delivery tools. The molecular Trojan horse technique involves using a targeting ligand such as a serum protein, monoclonal antibody, or another high affinity targeting molecule that binds to its receptor and activates endocytosis of the complex into a vesicle that is transported to, and released from the opposite pole (i.e. transcytosis; Figure II-5) [33]. Molecular Trojan horses are thus limited by the quantity of relevant receptors. They can however be very selective for the BBB endothelium and have shown promise in gene therapy [34].

II.2.5 Drug delivery through nanocarriers

Nanocarriers are an emerging class of drug delivery systems that can be easily tailored to deliver drugs to various parts of the body, including the brain. It has been attracting increasing attention for its use in transport of drugs across the BBB due to the rapid increase in our understanding of receptors and the fast development in polymer chemistry and nanotechnology. Nanocarriers are unique because of their size and easily tailored structures due to the material (biodegradable polymers) used. They can behave like macromolecules, but they can carry much more drug payload and are capable of controlling drug release. They can carry a range of drugs and their surface properties can be modified. These properties make nanocarriers an attractive alternative for transporting drugs across the BBB [26,52]. One of the limiting factors upon the systemic use of nanoparticles is their rapid clearance from the blood circulation. Nanoparticles with a longer circulation time are in contact with the BBB for an increased time, and thus have a longer time to deliver their cargo to the brain. Drug delivery through the BBB can be enhanced by cationic nanoparticles, since these can interact with the negative charges present on the cell membrane of endothelial cells [53].

Nanoscale drug carriers consist of particles in the size range from 10 to 1000 nm. Some ideal properties for drug delivery are: (i) nontoxic, biodegradable and biocompatible, (ii) particle size less than 100 nm (except for transport via monocytes or macrophages), (iii) stable in blood and prolonged blood circulation time, (iv) BBB-targeted moiety, (v) tunable drug release profiles, and (vi) applicable to carry small molecules, proteins, peptides or nucleic acids [54,55].

Despite a large variety of nanocarriers developed so far, only amphiphilic molecule-formed liposomes and polymeric nanoparticles have been extensively exploited for brain drug delivery (e.g. poly(butylcyanoacrylate) nanoparticles further coated with polysorbate-80 allow brain delivery of dalargin and loperamide) [56].

Solid lipid nanoparticles show several advantages as drug delivery systems, which explains why they can be used as vehicles to cross the BBB. Advantages include good biocompatibility, an interesting production process that can be performed easily on a large scale, a relevant drug loading capacity and a controlled drug release that can be made to last several weeks. However, the real potential of solid lipid nanoparticles for delivering drugs to the CNS is not clear, especially since data regarding the extent of permeation is often contradictory. It is however clear that the drug concentration in the brain is effectively increased using these nanoparticles, making them interesting to use for delivery across the BBB [53].

II.2.6 Tight junction opening using focused ultrasound

In the past two decades, some modulators have been discovered which can be used for opening the BBB (in several cases: opening of tight junctions). These modulators range from chemical (e.g. cyclodextrin and poloxamers) and biological (e.g. virus and macrophage) substances to physical stimuli such as high frequency focused ultrasound (FUS) and electromagnetic fields. FUS is a very promising technique since it provides a non-invasive alternative that may prove more desirable for acute treatment of brain tumors and other conditions requiring local tissue necrosis. An excellent overview of these modulators, their course of action and their impact on the BBB is provided by Chen et al. [26]. FUS has several advantages over other approaches because it is readily repeatable, noninvasive, and able to disrupt the BBB in a targeted way [41]. The rationale for modulating tight junction opening to enhance the paracellular approach is fourfold: (i) the tight junction opening (BBB leakage) is a phenomenon associated with many brain diseases (Table II-1) and stimuli, and many

modulators have already been characterized; (ii) enhanced paracellular transport will increase the delivery of small water soluble molecules into the brain; (iii) modulated tight junction opening may also improve the BBB passage of macromolecules and drug delivery systems including liposomes, nanocarriers, micelles, polymer conjugates, and their distribution in the brain; (iv) using physical stimuli such as ultrasound and electromagnetic fields will temporarily provide local BBB disruption, therefore, concentrated drug doses can be delivered locally [26].

FUS can be used in combination with circulating microbubbles. The microbubbles concentrate the ultrasound effects to the microvasculature, greatly reducing the FUS exposure levels needed to produce bioeffects. This offers a potential way to disrupt the BBB in a targeted, noninvasive, and repeatable manner to deliver a wide range of drugs to the brain and to brain tumors. The technique also offers the potential to control the magnitude of BBB disruption at each focal target through modification of the ultrasound parameters, enabling a level of control over drug delivery that is not available with other technologies. The gas-filled microbubbles interact with the vessel wall through oscillation. At higher acoustic pressures, they implode. After collapsing, their gaseous content or drugs packed within their shells are released. The sonifications do not appear to have any deleterious effects on the brain and studies on animals have demonstrated that treatments can be performed safely without causing tissue damage even after repeated weekly sessions. This flexibility, along with the noninvasiveness, and lack of need for general anesthesia make FUS a potentially transformative technology. Given the availability of clinical FUS devices capable of focusing ultrasound through the intact human skull, along with recent safety studies demonstrating the method can be performed safely in nonhuman primates, it appears that the method is ready for initial clinical tests [33,57,58].

II.2.7 Intranasal delivery as a drug delivery system

Two routes have been proposed for the direct passage of drugs from the nose to the brain: an intraneuronal and an extraneuronal pathway [59]. Even large molecules like peptides could be transported from the nasal cavity to the CNS. Most pharmaceuticals are water soluble or have MW > 400 Dalton, and do not freely traverse biological barriers [37]. The main advantage of intranasal administration is the minimal invasiveness, although the usefulness of this technique will be limited to compounds with large therapeutic indices. The major disadvantages of intranasal drug delivery are the challenge of reproducibility, the limited

absorption across the nasal epithelium, which restricts the application to particularly potent substances, and the fact that drugs are delivered to the whole brain through this route [60]. Nevertheless, the technique is a promising route to bypass the BBB and is currently being investigated by numerous researchers [33,61]. A wide range of therapeutics, such as peptides, proteins, gene vectors and stem cells, have been successfully delivered through intranasal administration to small animal brains and have shown efficacy in treating CNS diseases, such as Alzheimer's disease, Parkinson's disease, Huntington's disease, depression, anxiety, autism spectrum disorders, seizures, drug addiction, eating disorders and stroke [62].

Since neurological diseases do not generally affect the brain in a global manner, and drugs are delivered to the whole brain through intranasal delivery, a new strategy was proposed for enhancing drug delivery efficiency at the sites requiring treatment while minimizing the exposure to other brain sites. This method uses transcranial FUS in combination with microbubbles [62]. The authors concluded that FUS can enhance intranasal drug delivery efficiency at the targeted brain location and that this technique achieves similar drug delivery efficiency within the targeted region compared with the conventional FUS approach.

The field of drug delivery to the brain via the nasal route is rather immature. The mechanistic understanding of the pathways of drug transport from the nose to the brain is limited, and their efficiency is not clear [61].

II.2.8 Other delivery systems

Controlled-release intracranial polymer implants and particle injections are the clinical state of the art with regard to localized delivery, although these approaches can impose significant surgical risks [34]. This type of delivery yields the highest degree of targeting, although it is limited by invasiveness and diffusion restrictions [63].

High local drug concentrations can be achieved by inserting a needle or catheter into the brain and directly injecting or infusing drugs or by implanting drug-releasing devices. However, because of their invasiveness, there are some risks of infection or brain trauma, and they may not be amenable for repeated treatments or for drug delivery to large areas of the brain [33].

Intracerebroventricular and intrathecal administrations deliver the drug directly into the CSF compartment, either in the lateral ventricle or in the subarachnoid space. These routes are less invasive than direct intracerebral injection and allow access to a much wider area of the CNS through CSF circulation pathways. Limiting factors are diffusional and cellular barriers for penetration into surrounding tissue [64].

Opening of the BBB using intracarotid infusion of hyperosmolar solutions (such as mannitol) has had some success in increasing drug delivery to tumors. This procedure causes shrinkage of endothelial cells and consequent stretching of tight junctions through which drugs may pass [41,65,66]. While this procedure can be effective to deliver drugs to large brain regions, it is invasive, requires general anesthesia and can have side effects (e.g. oedema). Therefore, therapeutic BBB opening needs to be kept as brief as is practical or it would be desirable to have a less-invasive way to achieve this disruption [33].

Chemical-mediated BBB disruption involves exposing the BBB to an agent that increases BBB permeability. These agents induce a transient inflammatory reaction within the endothelium, resulting in enhanced paracellular permeability [67].

II.3 Measurement and prediction of drug transport across the blood-brain barrier

In the CNS related drugs, the probability of success in obtaining a marketing authorization is less than 7 % and the time needed, considering clinical and regulatory phases, is around 10.5 years, the longest compared to other therapeutic areas. Therefore, reliable methods for selecting the best candidates in the early preclinical phases are urgently needed in order to reduce the risk of costly later failures in clinical phases [68]. In vivo rodent models for studying BBB permeation are not time and cost effective enough to be applied as screening models during the early drug discovery phases. Owing to low costs and high throughput, in silico models are useful for the preliminary assessment of BBB permeability and classification of test compounds in the hit to lead phase. During the lead identification and optimization stages, there is a need for in vitro models with higher reproducibility and reliability [69]. During the lead optimization stage, the data resulting from in vitro and in vivo assessments of CNS penetration may be used for the development of more locally (regarding chemistry space) relevant and quantitatively predictive models [70]. In the last stages of drug discovery, in vivo tests become increasingly important. An overview of the commonly used methods during the drug discovery stages is given in Figure II-8.

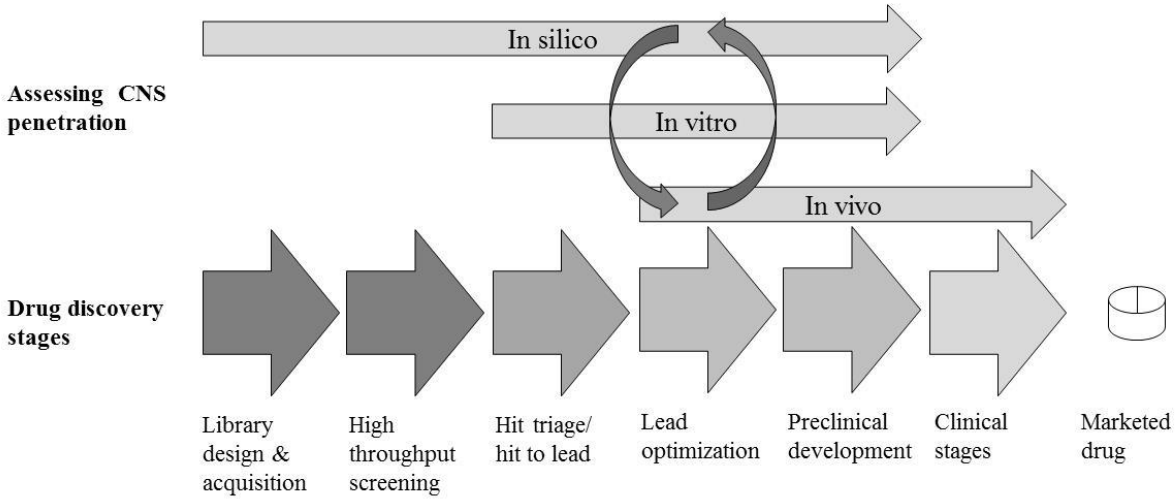

Figure II-8: Application of in silico, in vitro, and in vivo CNS penetration assessment methods during the various stages of drug discovery. Modified from [70].

II.3.1 In vivo methods for assessing blood-brain barrier permeability

The most important in vivo methods are discussed in this section. Two of the methods for assessing BBB permeability in vivo are widely used: determination of the logarithm of the ratio of the concentration in the brain versus blood (or plasma), leading to the log BB value (section II.3.1.1); and measurement of the permeability-surface area product (PSP) [7] (section II.3.1.2). In general, extrapolation of animal permeability or absorption data to humans should be performed with caution because of potential species differences [71]. Species similarity and differences in absorption, distribution, metabolism, excretion and toxicity (ADMET), with the limitations in extrapolating data from animals to humans, have been described previously [72,73].

When animals are required for experiments, a difference can be made between tissue assays and whole animal assays. The former indicates a long(er)-lasting method without constant need for the sacrifice of animals, while the latter indicates a single test per animal for oral bioavailability information. The main disadvantages of performing in vivo experiments are the cost and the time required for the surgical procedures, especially for brain microdialysis and in situ brain perfusion. This has continued to drive the development of in vitro and in silico based approaches [74].

II.3.1.1 Determination of the logarithm of the brain versus blood ratio (log BB)

A common measure of the extent of BBB permeation is the ratio of the steady-state concentration of a drug molecule in the brain to its concentration in the blood, usually expressed as log (C_{brain}/C_{blood}) or log BB [75]. Measurement of BBB permeation is typically based on intravenous administration of a radiolabeled compound to anesthetized rodents (mostly rats, sometimes mice or rabbits) followed by exsanguination when radioactivity in the blood reaches a plateau. The brain is removed and the concentration of the corresponding drug is measured by use of a scintillation counter. Measurement is time-consuming, expensive, and difficult, but it is still very important because in vivo animal experiments enable the best prediction of log BB values [76]. Single time-point log BB determinations are of limited value as they depend on the chosen time and the relation between the concentration in blood and brain at this time point. The ratio of the areas under the curve is more useful. However, these measurements are generally made over several hours, with several animals required per data point, increasing the cost and workload. Quite often, data at only one or two data points are obtained, and the assumption is made that equilibrium has been reached [77]. Some factors, like metabolism, also affect the brain distribution, so that log BB is not a pure measure of BBB permeability but rather a partitioning value [7,74].

Over the last few decades, the log BB values of some compounds were determined in vivo. An overview of these compounds is given in Appendix A. When several log BB values were found, the average value was calculated. The use of this data is however not without risk, since these values were obtained in several research groups and conditions of the experiments were not always identical (e.g. the use of mice, rats or rabbits).

II.3.1.2 Measurement of the permeability-surface area product (PSP)

Drug action in the brain is a function of drug receptor occupancy. This is a function of the free drug in brain cells and not the total drug concentration (as determined by log BB). Unfortunately, it is not easy to measure free drug in brain experimentally. A good index of BBB permeability is the BBB PSP, which has units of $\frac{\mu L}{\min g}$ and is a measure of unidirectional clearance from blood to brain across the BBB. The measurement of the BBB PSP can be performed either in vitro using a tissue culture model of the BBB, or in vivo using quantitative animal models [78]. The PSP is commonly regarded as the most relevant measure of a compound's ability to cross the BBB, because it is not compromised by metabolism,

plasma protein binding and nonspecific brain binding owing to the short exposure time [79]. The PSP values can be obtained after determination of the unidirectional uptake coefficient (K_{in}) using the in situ saline-based perfusion method. The saline composition of the perfusate can be controlled, and plasma protein included if needed to test the effect of protein binding. If perfusate flow is also measured, K_{in} can be converted to the PSP. These values can be compared across preparations and tissues, and used to follow changes under altered conditions (e.g. pathological) [7]. This method is resource-intensive, requires microsurgical expertise and has therefore a low throughput. However, considering the greater mechanistic clarity of log PSP compared with log BB, the former is likely to be more informative as a measure of CNS penetration for use in lead optimization. Unfortunately, only limited log PSP values are available in literature and few studies have thus far been published using this data [70].

II.3.1.3 Microdialysis for the measurement of brain penetration

Another technique for measuring brain penetration in vivo is intracerebral microdialysis. Using this method, a quantitation of the BBB permeability can be done in an intact animal. It allows determination of the brain extracellular concentrations of a drug over time. The basic principle is the stereotaxic[2] implantation of a microdialysis probe. The probe consists of a semipermeable membrane; molecules lighter than the molecular weight cut off can be transported into or out of the perfusate from a higher to a lower concentration. The concentration of the molecules of interest is then monitored using a sensitive separation method [30]. This method is relatively cheap and simple, measures free drug concentrations and is suited to characterize slowly changing brain drug concentrations [80]. The disadvantage is that brain microdialysis requires the most surgical skill of all the available in vivo methods [74].

Based on microdialysis, the unbound brain-to-unbound plasma concentration ratio can be determined. This ratio thus measures the unbound concentration gradient across the BBB, which equals 1 for drugs undergoing passive transfer. A value less than 1 suggests passage across the BBB is restricted by either inherently low permeability (e.g. atenolol) or by active efflux through a transporter, such as P-gp. A value greater than 1 would indicate that uptake into the brain is facilitated in some way, perhaps via active influx [74].

[2] A method to locate the site to be operated on within the brain using an external, three-dimensional frame of reference usually based on the Cartesian coordinate system.

II.3.1.4 The measurement of cerebrospinal fluid (CSF) concentrations

A lot of models concerning the prediction of BBB penetration have been published. In several of these models, the total (i.e. bound + free) drug concentration in the brain is predicted, expressed as the log BB. This total drug concentration is however not entirely relevant to pharmacological action, since effects in the CNS are mainly caused by the free drug concentration. The CSF has been suggested as a better indication for pharmacological activity, since the amounts of a drug in the CSF and in the free plasma are similar for most drugs [81].

This does however not necessarily mean that the drug concentration in the CSF is a good surrogate for the drug concentration in extracellular fluid (ECF). For compounds where BBB diffusion is both rapid and passive, CSF concentrations agree well with brain ECF concentrations. There are however instances where CSF and ECF brain concentrations do not correlate well, such as when the drug is subject to a slow rate of uptake across the BBB, active transport or local metabolism [74]. Despite these issues, the measurement of CSF provides a relatively simple means to estimate unbound drug concentration within the CNS system [82]. So far, the available CSF data is limited, which inhibits its use in prediction models [83].

Systematically administered drugs can reach CSF either directly via passage across the choroid plexus, or indirectly by passage across the BBB followed by diffusion/convection transport from the ISF to CSF. The major site of blood-CSF exchange is the choroid plexus, although microvessels in the pia- and dura-arachnoid membranes are also sites of exchange. It is generally assumed that diffusional exchange of solutes across the BCSFB is minimal because of the very limited (< 0.1 %) surface area compared to that of the BBB. However, in early drug discovery and development, CSF sampling is more practical than ISF sampling by microdialysis in terms of effort, cost and throughput. For antibiotics and antivirals, CSF sampling provides crucial information as to whether adequate drug concentration is achieved to eradicate the infectious organism or virus in the CSF. In these cases, CSF concentration serves as a direct therapeutic check. Overall, CSF concentration is a reasonably good discriminating indicator of drug availability to the CNS for hydrophilic or large molecular weight compounds with poor to moderate permeability. The presence of a drug in the CSF only reflects extracellular drug availability and does not reveal access of drugs to the intracellular sites within the brain parenchyma. The brain ISF concentration can differ remarkably from the CSF concentration, even if the receptor resides on the cell membrane

surface where it is readily accessible from the extracellular aspect. This has dispelled the simplistic notion that there is a free exchange of drug between the ISF and CSF, and that at steady-state CSF drug concentration represents the effective free drug concentration that pervades the CNS. A downward CSF-to-ISF concentration gradient is a concern when efflux transport at the BBB is likely [84].

II.3.1.5 In situ perfusion to study drug absorption

The development of the in situ brain perfusion technique by Takasato et al. [85] provided a simple method for performing short-term studies of brain uptake following feasible surgery. The in situ brain perfusion method involves cannulation of the carotid artery and infusing whole blood, physiological buffer, or saline containing the compound of interest. Because of the possibility of extending perfusion time, this model allows transport studies of slowly penetrating an metabolically unstable drugs [86]. Transport in the brain can be measured for an undisturbed BBB when a radiolabeled tracer is added to a suitable perfusate solution. The perfusate can be adjusted to study mechanistic aspects of permeation and identify the responsible transport systems [6].

After decapitation, the radiolabeled test and reference compounds are measured and the BBB permeability-surface area product (PSP) is quantitated. The radiolabeled tracer is quantitated in the brain tissue by scintillation counting or autoradiography [30]. The biggest advantage of the in situ system compared to the in vitro techniques (section II.3.2) is the presence of an intact blood and nerve supply in the experimental animals [71]. Compared to the determination of log BB, the in situ perfusion method offers the advantages of the ability to tailor the perfusion fluid, the constant infusion concentration, and the absence of compound metabolism in other organs [87]. This methodology is found to be highly accurate for predicting the permeability of passively transported compounds, although the use of a scaling factor has been recommended for predicting permeability of carrier-mediated compounds [88]. Disadvantages are that a large number of animals is required to get statistically significant absorption data and relatively high amounts (> 10 mg) of test compounds are required to perform studies [71].

In situ brain perfusion is a widely accepted method for measuring BBB permeability; the technique has been simplified over the years by using shorter perfusion time and less complex surgery. However, this method is not commonly performed, because it is labor intensive and it does not directly provide unbound brain concentration [79].

In situ experiments for studying intestinal drug absorption involve the perfusion of a drug solution prepared in a physiological buffer through isolated cannulated intestinal segments. Absorption is assessed based on the disappearance of the drug from the intestinal lumen. In this technique, the difference in the concentration of the inlet and outlet flow is used to calculate the permeability. The presence of an intact blood supply, nerve, and clearance capabilities at the site of absorption lead to an excellent experimental system that mimics in vivo conditions. Also, the input of compounds can be closely controlled with respect to concentration, pH, flow rate, and intestinal region [71].

II.3.1.6 Other in vivo methods

Other in vivo methods include intravenous injection [89], positron emission tomography imaging [80], bolus carotid intravenous method [90], indicator dilution technique [40], brain uptake index [91], capillary depletion technique [40], and brain efflux index [92]. Most of these methods need radiolabeled compounds, expensive infrastructure and are labor intensive, which prevents their use for high throughput screening [76].

II.3.2 In vitro systems for the prediction of drug transport

Transcellular routes of drug penetration include not only passive but also active and facilitated mechanisms. Although physicochemical methods are only able to model passive transport, they remain one of the most common screens used in drug discovery for two reasons:

- They are experimentally the simplest methods
- Passive transport is mostly either completely or partially responsible for drug uptake

Nevertheless, multiple drug transport pathways through cells should not be ruled out when evaluating data. This is why there is still no consensus on which model best predicts biologically relevant drug membrane interactions [20].

II.3.2.1 High-performance liquid chromatography

In High-performance liquid chromatography (HPLC), several techniques have been used to model drug action, although most attention has been paid to micellar liquid chromatography (MLC) and immobilized artificial membrane (IAM) LC. Possibilities offered by these techniques will be outlined below. General disadvantages of these techniques are that they do

not consider the potential role of paracellular transport, carrier-mediated transport, drug metabolism, and efflux transporters on permeability. Overlooking the possible influence of all these factors can be dangerous and may provide a very limited view of the true absorption potential of a compound [93].

Biopartitioning chromatography (BPC) has been proposed as a non-cell-based and high-throughput screening platform for drug membrane permeability and biological activity. BPC introduces biomembrane-mimetic structures (such as liposome, phospholipid monolayer, micelle, microemulsion, vesicle, bicelle, etc.) into chromatographic systems, i.e. liquid chromatography or capillary electrophoresis (CE), and thereby emulates drug-membrane interactions. BPC is therefore a generic name for micellar and microemulsion liquid chromatography (MLC and MELC), immobilized artificial membrane (IAM) chromatography, micellar and microemulsion electrokinetic chromatography (MEKC and MEEKC), liposome electrokinetic chromatography (LEKC), etc. [94-96]. An overview of HPLC-based BPC methods can be found in this section, some CE-based BPC methods are illustrated in section II.3.2.2.

II.3.2.1.1 Micellar liquid chromatography for the prediction of drug transport

In quantitative structure-activity relationship (QSAR) methods, the biological activities of solutes or their ability to penetrate the different hydrophobic barriers (membranes) are related to their physico-chemical properties. The hydrophobicity of a compound, expressed as log P, is of great importance in QSAR studies [97]. One of the main drawbacks is that many biologically active compounds of interest in QSAR studies are ionic at physiological pH and ionic organic compounds are not or only weakly retained in reversed-phase liquid chromatography (RPLC).

To circumvent this problem, micellar liquid chromatography (MLC), a mode of RPLC which uses a surfactant solution above the critical micellar concentration (CMC) as mobile phase [98], proved to be a very useful method. The use of micellar solutions produces the adsorption of surfactant monomers to the stationary phase and increases the thickness of the stationary phase. Above the CMC, a change in surfactant concentration is translated in an increase in the concentration of micelles in the solution, whereas the number of monomers of surfactant in the mobile phase remains constant. Adsorption of an approximately fixed amount of surfactant monomers on the stationary phase is also produced, giving rise to a stable modified column and regular retention behavior [99,100]. Micellar mobile phases have been used for

all kinds of purposes in RPLC. In this thesis, only the possibilities of this technique towards the prediction of drug absorption will be presented, an application based on previous publications, such as [22,101-103].

Surfactants in MLC can be charged positively, negatively or can be neutral. The retention of a compound in MLC depends on the type of interaction (electrostatic and/or hydrophobic) with the micelles and with the surfactant-modified stationary phase. Non-ionic solutes are supposed to be only affected by hydrophobic interactions, charged solutes can be subject to hydrophobic and/or electrostatic interactions [97]. When the net charge is the same for structurally related compounds, differences in retention arise from differences in hydrophobicity.

The main advantages of MLC are: (i) simultaneous separation of charged and uncharged compounds, (ii) direct on-column injection of physiological fluids, (iii) unique separation selectivity, (iv) low cost and toxicity, (v) enhanced luminescence detection, and (vi) the biodegradability of the solvents used [104,105]. However, MLC is not a very popular technique due to poor separation efficiency and the relatively weak solvent strength of micellar eluents. The two main approaches that have been used to enhance efficiency in MLC are to add low amounts of organic modifier to the mobile phase and to increase the temperature.

The use of an organic modifier is certainly not recommended for compounds with low hydrophobicity. For highly hydrophobic compounds, the addition of an organic modifier is advised to reduce compound retention times and to improve peak efficiency and resolution. The amount of organic solvent is however crucial, since a high percentage can disrupt the micelle structure; the maximal allowable concentration depends on the organic solvent and the nature of the surfactant [97,100].

The retention of a solute in a MLC system can be modified by changing the eluent composition in terms of the nature of the surfactant and its concentration, pH (in the case of ionizable compounds), ionic strength and/or by the addition of organic modifiers at different concentrations [106].

McCormick et al. [107,108], provided another possible solution to circumvent the weak eluting power of micellar mobile phases compared to conventional hydro-organic mobile phases in RPLC. According to them, a possible explanation for the weak eluting power is that micelles are excluded from the pores, within which most of the stationary phase is located and where analytes spend most of their time. In order to determine whether wide-pore stationary phases would overcome this limitation, a study was performed in which several C_8 and C_{18}

stationary phases with pores ranging from 100 to 4000 Å were investigated using a diverse set of test solutes and micellar solutions of anionic, neutral, and cationic surfactants as mobile phases. As the pore size of a porous material is increased, the specific surface area is reduced. As a consequence, the volume of bonded stationary phase is also decreased. Therefore, under equal mobile phase conditions, the retention of a solute in a large-pore column is smaller than on an otherwise identical small-pore column. Stationary phases with larger pore sizes augmented the eluting power of the MLC mobile phases, also taking into account the drop in retention factor with increasing pore size. This could be explained by a better penetration of the micelles into the larger pores, such that they are able to reach the solutes at the internal surface of the stationary phase better, and elute them in less time [100]. Although all surfactant types showed improvement, the greatest effect was achieved with a neutral surfactant. Large-pore stationary phases were also found to be effective for the analysis of mixtures with varying properties, including highly hydrophobic solutes, which are strongly retained on the conventional small-pore stationary phases.

In order to speed up MLC-analyses, Detroyer et al. [109] tested the performance of a monolithic column. In theory, due to the larger porosity, higher flow rates can be applied while maintaining the retention characteristics, providing better efficiency and performance. The authors concluded that the MLC methods on both monolithic and particle-based columns provided highly correlated information. MLC methods could thus be speeded up using monolithic columns without major changes in retention characteristics.

When organic solvents are used in MLC, they partition to the micellar aggregates, and the degree of association increases with their hydrophobicity. Like other compounds, organic solvent molecules can be located outside the micelles, entry into the palisade, or into the micelle core. The first two effects might favour the formation of micelles, whereas the latter can substantially increase the amount of organic solvent inside the micelle and produce a microemulsion [110].

Short-chain alcohols added to an ionic micellar mobile phase show an interesting range of behaviors [111]. Methanol, with the shortest carbon chain, is more polar and soluble than the other alcohols. It can solvate surfactant monomers more easily, which hinders micelle formation, and consequently, a greater amount of surfactant is required to form the micellar assemblies (i.e. the CMC increases with added methanol). The effect of ethanol and propanol is opposed to methanol. These alcohols remain mainly outside the micelles, dissolved in the bulk liquid, but they interact with the micelle surface, reducing repulsion among the ionic heads of the surfactant monomers. This favours the formation of micelles and reduces the

CMC. Finally, butanol and pentanol are inserted into the micellar assembly, owing to their particular structure that combines a polar group with a non-polar chain, similarly to surfactant molecules. These alcohols align with the surfactant molecules in the micelle palisade, the polar hydroxyl group of the alcohol oriented towards the outer layer and the alkyl chain located in the non-polar micelle core. This gives rise to swollen mixed micelles. The use of acetonitrile is another possibility, but it should be noted that the effect of acetonitrile on the CMC is similar to methanol, in spite of the differences in polarities and structure [100,111].

II.3.2.1.2 The use of microemulsion liquid chromatography to assess membrane permeation

Microemulsions are dispersions of nanometer-sized droplets of an immiscible liquid within another liquid. They can be classified as either oil-in-water or water-in-oil (see Figure II-9), of which the latter has only limited applications so far. Oil-in-water microemulsions contain droplets of oil (e.g. heptane, octane) dispersed throughout an aqueous buffer. Droplet formation is facilitated through the addition of a surfactant and usually also a cosurfactant. The surfactant lowers the oil-water surface tension and the cosurfactant usually has the effect of reducing the intermolecular repulsion experienced by the surfactant molecule head groups by positioning itself in-between them around the oil droplet. Droplets in the microemulsion are less than 10 nm in diameter, and therefore do not scatter white light, resulting in the solution being optically transparent [112]. As in MLC, the stationary phase is also modified by the adsorption of surfactant in microemulsion liquid chromatography (MELC) and a secondary partitioning mechanism also exists in MELC where solutes partition from both the mobile and stationary phase into the microemulsion droplets. Solutes can easily penetrate the microemulsion surface, since this is not rigid as in MLC. In MELC, more complex solute-solvent interactions exist since the cosurfactant (e.g. butanol) and oil molecules can also be adsorbed to the stationary phase. An increase in surfactant, cosurfactant or microemulsion oil content gives rise to a decrease in solute retention [113,112].

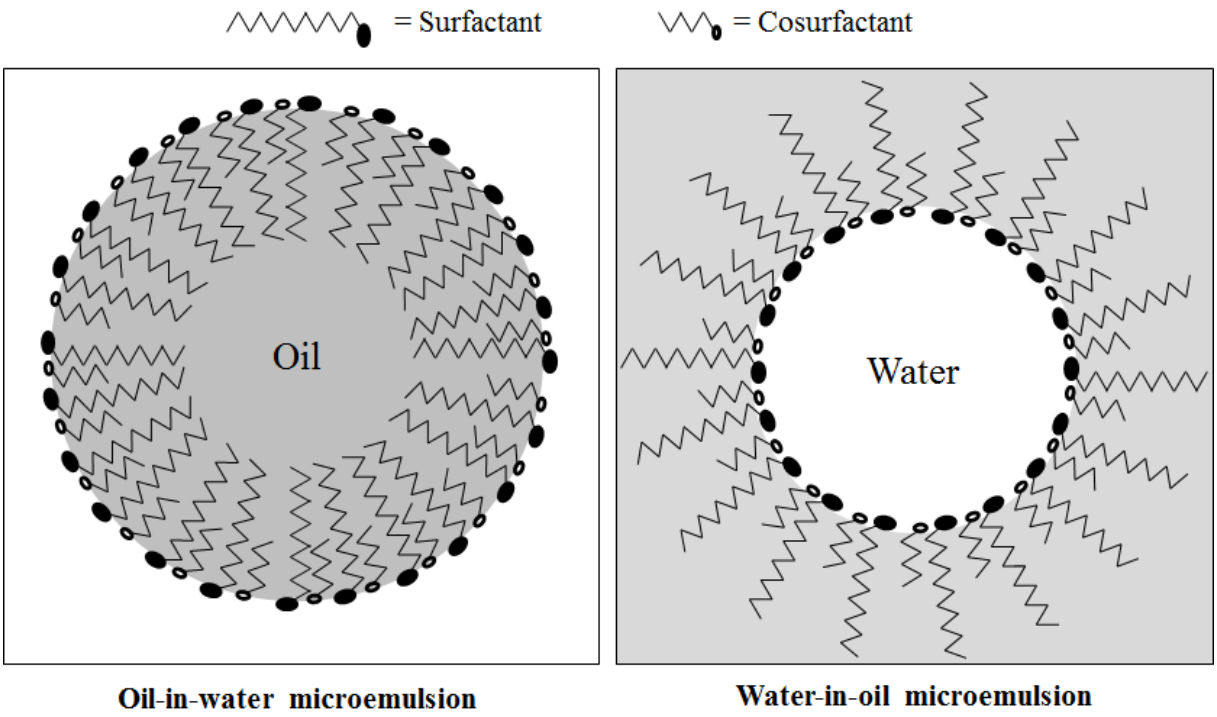

Figure II-9: Schematic representation of oil-in-water and water-in-oil microemulsions. Cosurfactant molecules position themselves between the surfactant molecules and reduce the intermolecular repulsion. Modified from [114].

According to Liu et al. [113], a MELC-SDS system containing 1.6 % heptane was superior to a MLC-SDS system (with butanol as organic modifier) concerning the capability of predicting drug penetration across the BBB for a set of 37 compounds. However, subsequent studies illustrated that retention times in some MELC systems were not stable for most drugs, with an increasing tendency over time. Therefore, Liu et al. [94] made some adaptions to the MELC-system, including optimized mobile phase compositions and a rinsing step with water (to remove the buffer salt) and with methanol (to remove the adsorbed components) at the end of a work session. Also, the retention times of compounds for long-term operations were corrected by an internal standard method. Methyl paraben and propranolol could be used as internal standards for correcting the retention times.

II.3.2.1.3 Immobilized Artificial Membrane Liquid Chromatography for the prediction of drug transport

Cell membranes provide an environment for several types of molecular processes. In IAMLC, an attempt is made to mimic the environment of cell membranes on a chromatographic solid support. This type of chromatography, pioneered by Pidgeon et al. [115], started with lecithin

as the bonded phase to a silica solid support. Since phosphatidylcholine (PC) is the most abundant fraction in lecithin, this is considered as the first phospholipid-based stationary phase.

Based upon this research, a series of innovative IAM chromatography packing materials was created. Rhee et al. immobilized lysophosphatidylcholine ligands on aminopropyl silica [116]. Hereby, the effect of differences caused by different endcapping groups was also studied, indicating that the chromatographic surface endcapped with dodecanoic cyclic anhydride provided the most stable column. Ong et al. created a whole new set of IAM chromatography packing material [117]. This time, single chain ether phospholipids were immobilized on aminopropyl silica. The ether phospholipid ligands were analogs of phosphatidylglycerol (PG), phosphatidylserine (PS), phosphatidylethanolamine (PE) and phosphatidic acid (PA). These ether phospholipid ligands were also prepared by Qiu et al. [118] using a general synthetic route. The biggest difference for these ligands compared to PC ligands, is the presence of amines, carboxyls, hydroxyls or phosphate groups that require protection prior to immobilization.

In 1994, the first mixed ligand immobilized artificial membranes were created [49]. These IAMs contained two immobilized membrane phospholipids: one PC analog and PE, PS, PG or PA as other analog. The second analog was however bonded at only 6-10 mol% relative to the molar amount of immobilized PC. The higher amount of PC is – to a certain extent – logical, since PC is usually the major phospholipid with a typical cell concentration of around 40 % of the total lipid. In BBB cells, PS can have a concentration of up to 15 %, creating a negatively charged cell membrane. This is why Yang et al. [20] were convinced that an IAM-surface prepared from PC and a negatively-charged phospholipid could provide a better IAM model. As assumed, they obtained better predictions using the IAM surface with both PC and PS than with the a purely IAM.PC column. The authors also suggested that the development of IAM columns with a phospholipid composition resembling various barriers, such as the intestinal barrier and the BBB, might provide intriguing results. However, technical limitations with concerns about column consistency and quality control impeded the development of this type of columns.

In 1995, Ong et al. compared a set of three different phosphatidylcholine ligands to study the effect of lipid structure on drug binding to IAMs [119]. The three ligands were: (i) a diacylated PC ligand, (ii) a single chain ether PC ligand, and (iii) a single chain PC ligand that lacks a glycerol backbone (Figure II-10). In this study, solute retention data were almost identical for those IAMs, indicating that the structure of the immobilized PC ligand was not

critical for the binding of solutes. The most interesting conclusion was that the removal of the glycerol backbone was not critical for drug binding of the solutes. Additional study showed that a normal IAM.PC column required end-capping with C_{10} and then C_3 alkyl groups. Only after end-capping the IAM surfaces, the exact structure of the immobilized phospholipid was not critical for predicting the binding of solutes to membranes. End-capping of the residual amines is also crucial for an increased column stability. On end-capped IAM surfaces, lipid leaching is reduced but not totally suppressed, and retention factors may decrease during a column's lifetime (aging) [116,120].

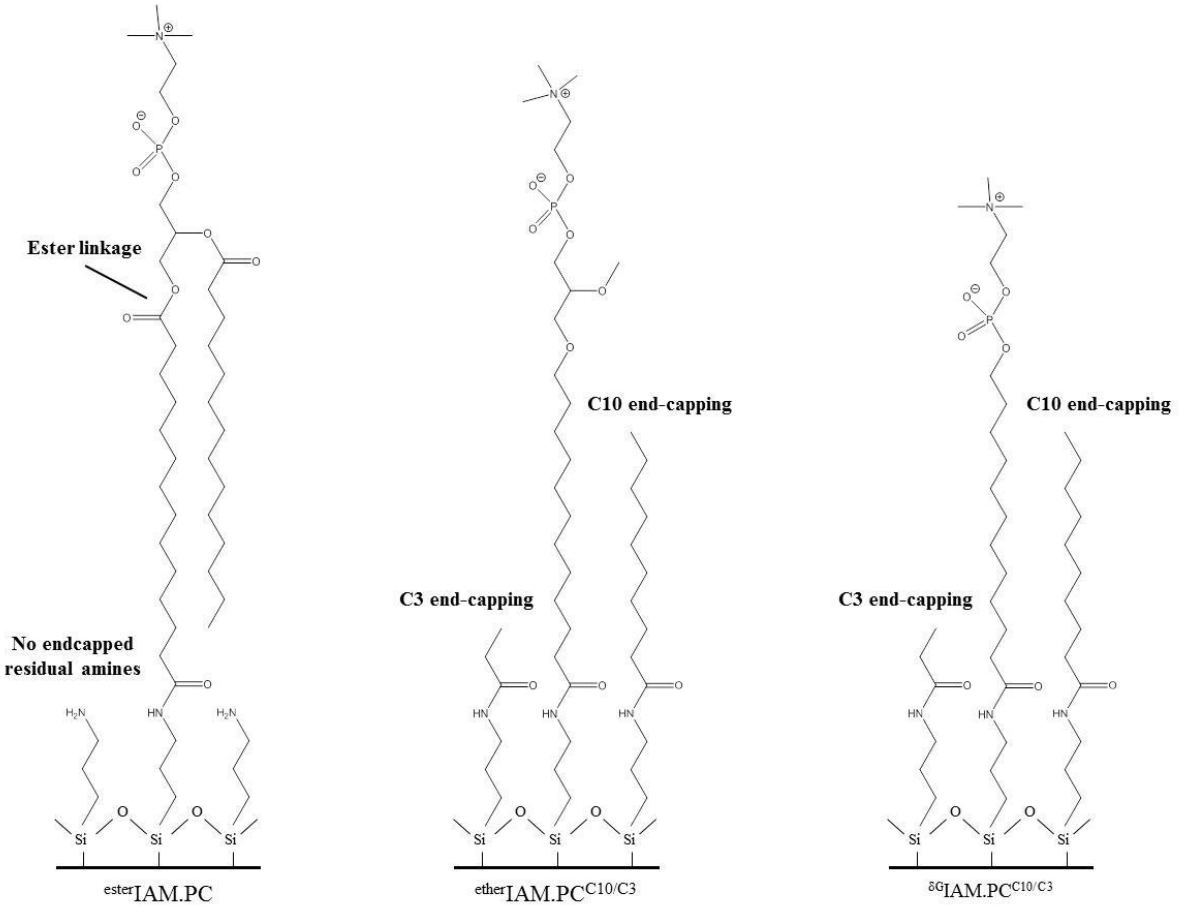

Figure II-10: Structures of three different IAM.PC surfaces used to study the effect of the lipid structure on drug binding to IAMs. From left to right: a diacylated PC ligand; a single chain ether PC ligand; a single chain PC ligand that lacks a glycerol backbone. The superscript C10/C3 indicates the end-capping with C_{10} and then C_3 alkyl groups. Modified from [119].

After additional tests, Pidgeon et al. [121] concluded that the glycerol backbone, the type of linkage (ester or ether) between the glycerol backbone and the acyl chain, and the number of acyl chains are not important in evaluating the rank order of drug partitioning into membranes containing phosphocholine analogues. Based on these findings, the $^{\delta G}$IAM.PC$^{C10/C3}$ column (=

silica solid support with a single chain PC ligand that lacks a glycerol backbone, end-capped with C_{10} and then C_3 alkyl groups) was chosen as column for predicting drug transport since it was the easiest to synthesize. Equally important, this column also had significantly shorter retention times compared with the other columns. The $^{\delta G}$IAM.PC$^{C10/C3}$ column has been commercialized by Regis Technologies under the name IAM.PC.DD (see Figure II-11), where DD denotes Drug Discovery. As illustrated by Caldwell et al. [120], IAM.PC.DD columns are somewhat subject to premature column failure. Data in this study suggested that either silica support dissolution occurred or that some of the stationary phase was removed by a buffered mobile phase after 7000 column volumes, leading to significant peak broadening and decreased k values.

Another IAM.PC surface has been developed and is known as IAM.PC.DD2 (see Figure II-11). This column type is less amenable to premature aging. This HPLC column is a combination of two other commercialized products: diacylated phosphatidylcholine is immobilized on aminopropyl silica and the residual amino groups are end-capped using C_{10} and C_3 alkyl chains. End-capping can also be established with glycidol and methyl glycolate (MG). This converts the residual amino groups into chemically neutral amides, but introduces hydroxyl groups, which causes a change in selectivity compared to the IAM.PC.DD and IAM.PC.DD2 surfaces. This type of surface is available as IAM.PC.MG (Figure II-11) [122].

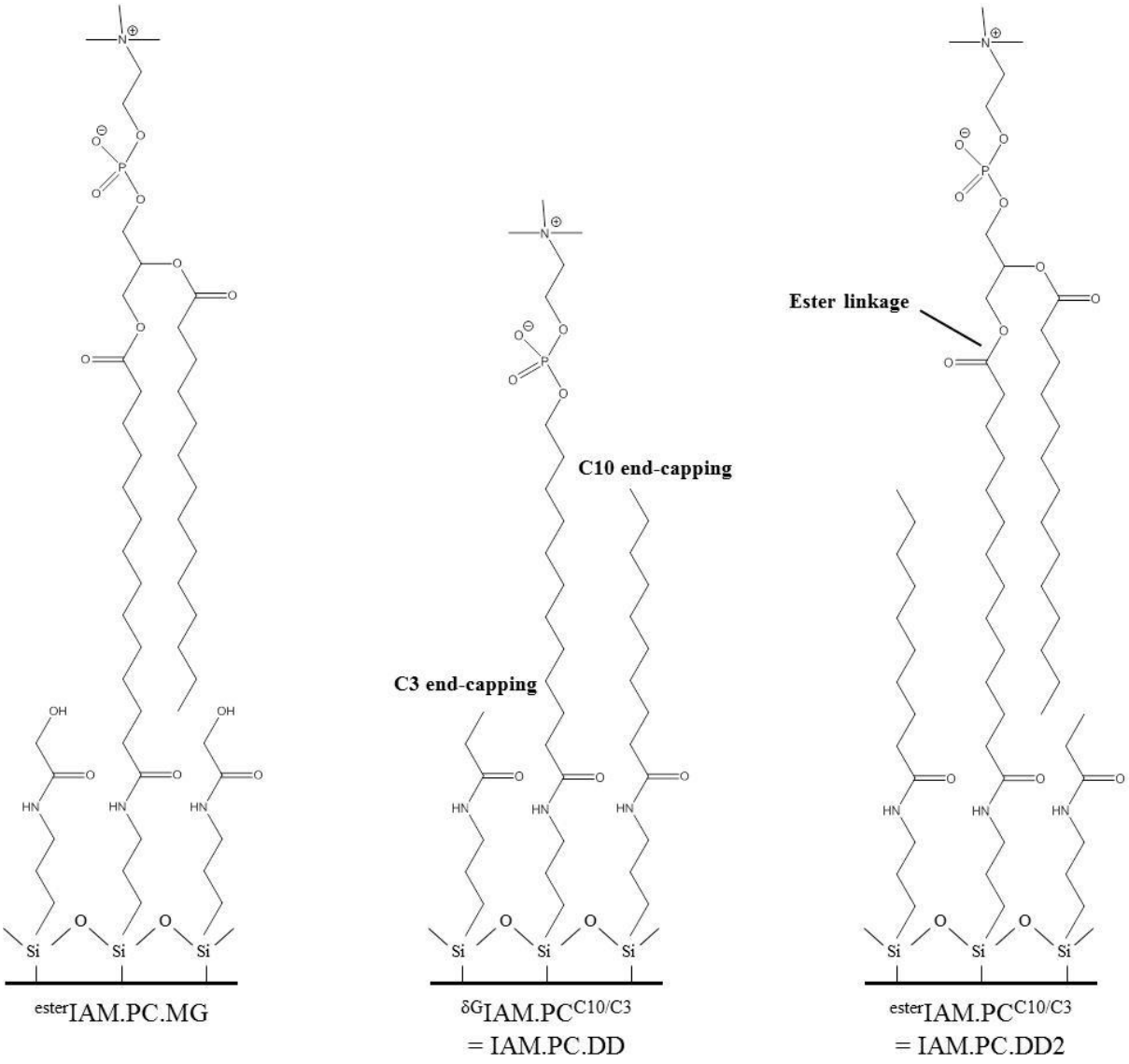

Figure II-11: Structures of commercially available immobilized artificial membranes. Modified from [122].

In 1996, Ong et al. [123] tested the ability of surface hydroxyl and methoxy groups to predict drug membrane interactions. To do this, 12-methoxy dodecanoic acid and 12-hydroxy dodecanoic acid were immobilized on aminopropyl silica. The authors concluded that surface PC headgroups, surface OH groups and surface OCH_3 groups all provide the properties necessary to predict drug membrane interactions better than reversed-phase C_{18} surfaces. However, the IAM.PC column was a much better in vitro screen for predicting drug-membrane interactions compared to the OH and OCH_3 bonded phases. Here, they also compared the double-chain IAM.PC.DD2 and the single-chain IAM.PC.DD stationary phases using 16 compounds from three structurally related series. A good correlation was found

between the two surfaces, and the results indicated that the double-chain IAM.PC.DD2 is more hydrophobic.

Pidgeon et al. [124] also suggested that IAM chromatography, unlike n-octanol:water partitioning, can predict membrane transport of structurally unrelated drugs. Therefore, Salminen et al. compared the IAM retention factor (on a IAM.PC.DD column) with the n-octanol:water partition coefficient as a descriptor in multiple regression models for predicting the brain/blood concentration ratios [125]. They found that carboxylic acids, which were almost completely in the anionic form at pH 7.4, formed a subgroup that behaved differently in IAM chromatography than the n-octanol:water partition coefficients (log K_{oct}). The authors concluded that IAM chromatography seemed a useful method for the prediction of solute distribution in membranes. They did however not consider the log k_{IAM} values to be better performing than the log K_{oct} as a parameter in models predicting brain/blood concentration ratios of drugs.

Reichel et al. [126] also investigated the potential of the IAM technology for the prediction of drug delivery to the brain. Although this study was based on a limited set of compounds, it suggested that IAM columns were suitable for ranking compounds towards entering the brain. They suggested that the predictive potential of log k_{IAM} was comparable to the physico-chemical descriptors log $D_{7.4}$, log P and log k_w for lipid soluble compounds, but was superior for more polar compounds. Therefore, they concluded that IAMLC was a suitable approach to predict drug penetration across the BBB.

Another way to construct IAM stationary phases has been introduced by Krause et al. [127]. They reported on the use of noncovalent IAM surfaces, which are constructed by dynamic coating of a reversed-phase C_{18} column with phospholipids, thereby resulting in a bilayer structure. The column stability was found to be sufficient for multiple column runs in the presence of reasonable eluent concentrations [23].

Until now, research in IAMLC was almost exclusively performed on the commercially available PC-based stationary phases. This is however not completely realistic, since PC is only one of the phospholipids present in membranes. Very recently, Zhao et al. [128] developed a novel mixed phospholipid functionalized monolithic column through an easy one-step co-polymerization approach. They illustrated that is was possible to quantitatively and accurately adjust the phospholipid composition on the monolithic column. A possible advantage of mixed phospholipid functionalized column is that they can better mimic the binding of drugs to a specific biomembrane and better predict corresponding pathophysiological effects. The test results on the columns were reproducible. The

introduction of the negatively charged PS into the stationary phase significantly enhanced the contribution of electrostatic interaction. Acidic analytes were subject to a stronger electrostatic repulsion (resulting in a shorter retention time); while a stronger electrostatic interaction for the basic analytes resulted in a higher retention.

As in all other HPLC-related in vitro techniques, the drug retention factor (k) can be calculated from the retention time (t_r) of drug molecules on IAM chromatography columns according to the equation,

$$k = \frac{t_r - t_0}{t_0} \quad (1)$$

where t_0 corresponds to the column dead time or void volume. The retention factor is linearly related to the equilibrium partition coefficient K:

$$k = \frac{V_s}{V_m} K \quad (2)$$

Where V_m is the total volume of solvent within the IAMLC column and V_s is the volume of the IAM interphase created by the immobilized phospholipids. The phase ratio V_s/V_m is constant for a given IAM column. Therefore, it is not necessary to make the difficult experimental measurement of V_s. By measuring k, the drug partition coefficient into the IAM interphase can be determined [121,123].

For hydrophilic compounds, retention factors can be determined by using a purely aqueous mobile phase. For lipophilic drugs, it is necessary to add an organic modifier (methanol or acetonitrile) to the mobile phase to accelerate the elution, after which an extrapolation to 0 % modifier should be performed. Concerning the obtained log k values, the choice between methanol and acetonitrile causes no significant difference. However, methanol is more appropriate for charged compounds [122]. The obtained log k values can be used for the prediction of drug transport across biological barriers. For most authors, the retention factor derived from IAMLC alone is not sufficient to predict drug intestinal absorption or log BB values, and the addition of other descriptors (e.g. molecular weight, hydrogen-bonding, …) is generally needed to enhance the correlations [129].

II.3.2.1.4 Other HPLC-based techniques

The retention of compounds on RPLC using octadecyl silica (ODS) stationary phases was first used to correlate with biological activity. However, with this stationary phase, electronic

interactions between solutes and the polar lipid head groups of the membranes are not modeled [119].

Immobilized liposomes have been proposed as stationary phases for chromatographic analysis of membrane-solute interactions. Traditionally, drug-liposome studies have been carried out with free liposomes suspended in aqueous solutions. Immobilized liposome chromatography (ILC) uses stationary phases where liposomes are steric, hydrophobic, electrostatic or covalently immobilized into gel beads. The column preparation is simple and they are stable for a long time. These systems seem to be more similar to natural membranes than other, more simplified models. ILC turned out to be a good approach to study drug-membrane interactions since the phospholipid ratios used to prepare the liposomes can be modulated to get liposomes with phospholipid, protein and cholesterol ratios very similar to the composition of the membrane of interest, except for the biological membrane asymmetry [130-132].

Special columns for quantifying the interaction of drugs with serum proteins (bovine serum albumin, human serum albumin (HSA) and α-acid glycoprotein (AGP)-columns), keratin, and collagen [133] have also been developed [22]. The HSA column contains a chemically bonded protein stationary phase. Although HSA binding is mainly related to lipophilicity, some compounds (acidic and neutral) show stronger binding, which can be related to known binding sites [134]. AGP is a serum protein that binds mainly basic drugs. AGP has only one common drug binding site, which binds drugs through hydrophobic and electrostatic interactions [133]. Affinity HPLC on immobilized protein stationary phases can be a convenient tool for studying drug-protein interactions. These interactions are important, since high plasma protein binding can reduce brain penetration [135] as it affects the unbound (free) drug concentration that is available to diffuse from the blood and reach the target tissue [136]. Both HSA binding and IAM partition showed similar octanol/water partition coefficients for neutral compounds. However, it was found that the positively and negatively charged compounds bind differently to HSA and IAM. Negatively charged compounds bind more strongly to albumin, whereas positively charged compounds bind more strongly to the immobilized phosphatidylcholine phase. It has been found that the difference between the IAM binding and HSA binding showed good correlation with the volume of distribution of the compounds. These findings support the general observations that positively charged compounds have a larger volume of distribution [137].

II.3.2.2 The assessment of membrane permeation by capillary electrophoresis

As mentioned before, the concept of biopartitioning chromatography (BPC) also led to the introduction of the use of biomembrane-mimetic structures in capillary electrophoresis (CE). The biomembrane-mimetic structures can be immobilized physically or chemically on the capillary wall, forming a stationary phase for the compounds to partition in. This is called capillary electrochromatography (CEC). They can also be added into the running buffer in CE to form a pseudostationary phase in electrokinetic chromatography (EKC), such as micellar electrokinetic chromatography (MEKC), microemulsion electrokinetic chromatography (MEEKC), liposome electrokinetic chromatography (LEKC), vesicle electrokinetic chromatography (VEKC), and bicelle electrokinetic chromatography (BEKC) [114]. A schematic representation of the corresponding membrane-mimetic structures of these techniques is provided in Figure II-12. So far, the use of CE-based techniques to predict drug penetration across the BBB is scarce (to our knowledge only in LEKC); therefore, this section should be considered rather as an indication of possible future extensions.

CEC can be considered as a combination between HPLC and CE, since there is both electrophoretic migration of the solutes and interaction between the solutes in the mobile phase and the stationary phase. According to Wang et al. [138], the most popular strategy to reduce protein adsorption to the silanol groups on the surface of fused-silica capillaries is to shield the silanols with a coating. The authors proposed a "semipermanent" surfactant coating using the unsaturated phospholipid 1,2-dioleoyl-sn-glycero-3-phosphocholine. The authors demonstrated that the coatings were stable for up to 20 h. The reproducibility was, however, inferior to permanent coatings. Because of the possibilities in phospholipid choice, this technique could provide a good alternative type of in vitro BBB predictions.

Micellar Electrokinetic Chromatography (MEKC), a mode of capillary electrophoresis (CE) that incorporates micelles acting as pseudo-stationary phases has proven to be useful for describing the biological behavior of different kinds of compounds. MEKC can be viewed as a hybrid of MLC and capillary zone electrophoresis (CZE) [22]. MEKC is an excellent tool for the analyses of neutral compounds. In some cases, the use of MEKC is limited because of a poor solubilization capacity of micelles for hydrophilic molecules and large molecules [139]. Recently, Lamalle et al. [140] studied the effective mobilities of neutrals, cations and anions at neutral, basic and acidic pH with the background electrolyte containing increasing SDS concentrations and acetonitrile proportions. At high SDS concentrations and low acetonitrile proportions, the migration order was reversed compared to CZE: electroosmotic

flow (EOF) first, then anions, then neutrals and cations. The analytes-micelles interactions became weaker with decreasing SDS concentration and increasing acetonitrile proportion. Using a high acetonitrile proportion, the migration order is again comparable to that in CZE. Using these considerations in a proper way, MEKC can be an attractive tool not only for the separation of neutral compounds, but also for variously charged analytes.

The possibility of utilizing microemulsions in electrokinetic chromatography of ionic and non-ionic samples has been demonstrated for the first time by Watarai [141]. The microemulsions are similar to micelles in that they can solubilize hydrophobic compounds, but with a much larger capacity because of the larger droplet size. As with MELC, there are two principal types of MEEKC: oil-in-water and water-in-oil. Again, oil-in-water microemulsions are typically employed, which contain oil droplets (e.g. n-octane), suspended in buffered water. Droplet formation is facilitated by addition of a surfactant above its CMC and a short-chain alcohol (e.g. 1-butanol) is added as a cosurfactant, which further lowers surface tension and stabilizes the microemulsion system. As solutes can penetrate the surface of the microemulsion droplets more easily than the more rigid MEKC micelle, MEEKC can be applied to a wider range of solutes. MEEKC has therefore been found to be superior to MEKC regarding separation efficiency, probably due to the improvement in mass transfer between the microemulsion droplet and the aqueous phase, mediated by the cosurfactant [142-144]. In MEEKC, separation of charged analytes occurs based on their charge and relative electrophoretic migration toward the anode or cathode. At high pH values, the EOF is strong and sweeps all solutes (even anions) toward the cathode and through the detector. The microemulsion droplet acts as a pseudo-stationary phase and allows separation of neutral as well as charged analytes. The more hydrophobic the solute is, the more it will partition into the microemulsion droplet and the longer it will take to migrate to the detector [145].

The first report in which LEKC was tested as a tool to profile drug penetration across the BBB was published in 2007 [146]. LEKC has some advantages compared to IAM, such as shorter analysis time and lower cost. The composition of liposomes is also easy to be controlled via adjusting the type and mole fractions of phospholipids [96,147] as well as incorporating cholesterol and even proteins. Some additional info about liposomes can be found in section II.2.2.

Vesicles (in VEKC) are large aggregates of amphiphiles containing a spherical bilayer structure encapsulating an internal cavity of solvent, while liposomes are simple vesicles formed specifically by phospholipids. The bilayer structure of a vesicle makes it attractive as a good membrane-mimetic structure. In contrast to the poor stability and laborious preparation

procedures for liposome, selected amphiphiles can form stable unilamellar vesicles spontaneously by simply mixing different amphiphiles solution in the proper ratio [114,148,149].

In BEKC, a characteristic bicelle structure is introduced in CE. The bicelle has intermediate morphology and properties between lipid vesicles and classical mixed micelles. As micelles, they are non-compartmentalized, optically transparent, uniform and stable dispersion system in a wide pH range and in varying ionic strength. As vesicles, bicelles are readily prepared in aqueous solution by simply mixing the long-chain lipid DMPC and the short-chain lipid DHPC in the proper ratio [114,150]. Additional information about bicelles can be found in section II.2.3.

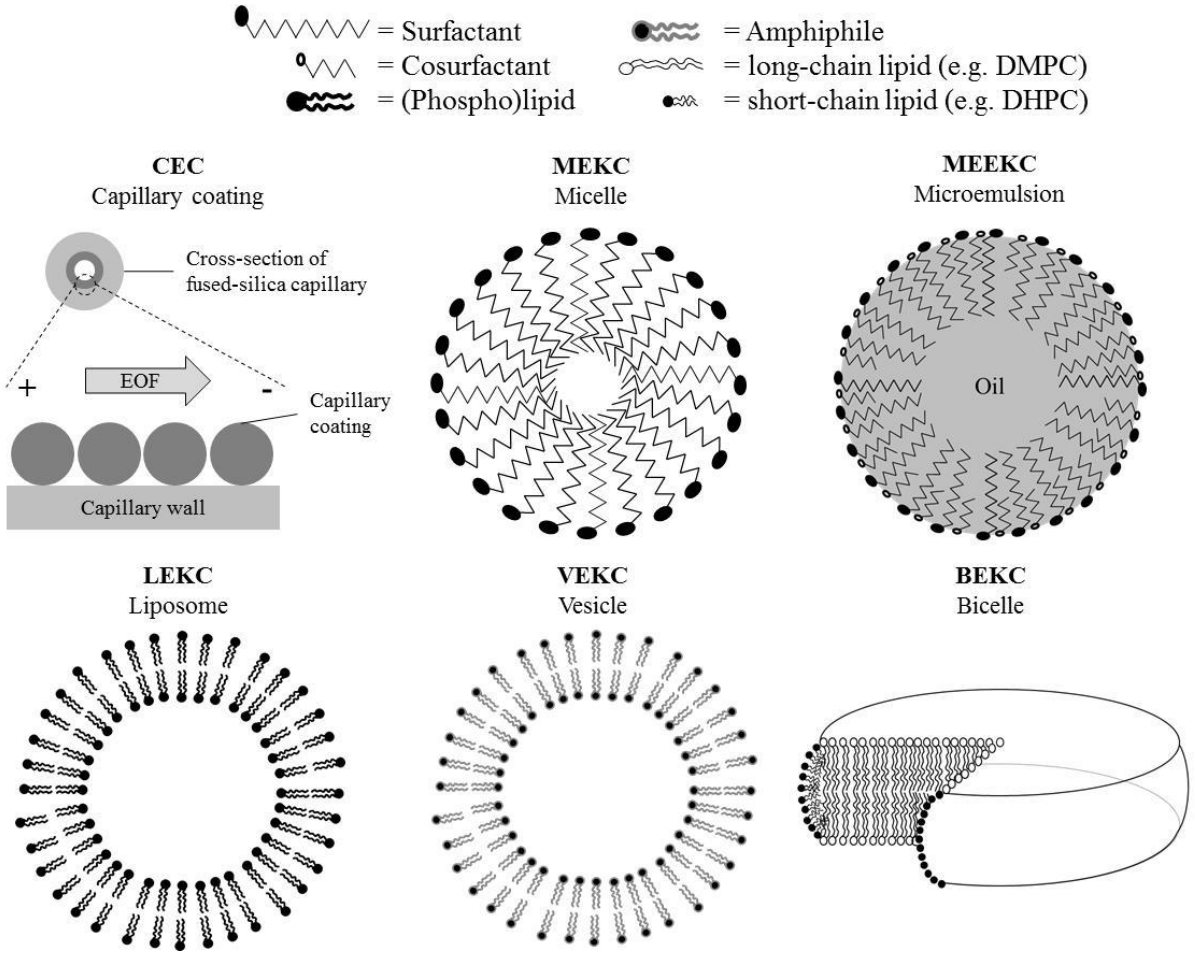

Figure II-12: A schematic representation of immobilized biomembrane-mimetic structures (CEC) and these biomembrane-mimetic structures as pseudo-stationary phase (other techniques). Modified from [151,152,114].

II.3.2.3 Parallel artificial membrane permeation assay to predict drug transport

The main objective of the parallel artificial membrane permeation assay (PAMPA) is the classification of passively absorbed compounds, focusing on the transcellular transport route. PAMPA is based on a 96-well microtiter plate technology. The technique involves a donor compartment and an acceptor compartment separated by a filter supporting a liquid artificial membrane. The artificial membrane can be composed of a variety of phospholipid mixtures. The compound to be tested is placed in the donor compartment and is allowed to permeate between the donor and the acceptor compartments through the artificial membrane [153].

This assay enables measurement of hundreds of compounds per day. The greatest potential lies in the screening of chemical libraries. A PAMPA-BBB study using porcine brain lipids has been suggested as an improvement of the prediction of BBB penetration. Advantages of this assay were the high throughput, accuracy and reproducibility, low cost and low amount of sample required (< 0.5 mg) [154]. Unfortunately, PAMPA is a poorly characterized system which enables only a simple classification of compounds, e.g. low, intermediate and high absorption probability. Also, PAMPA underestimates the absorption of compounds that are actively transported or hydrophilic compounds with a low molecular weight [155].

PAMPA also requires UV absorbance, which many compounds do not exhibit. The long incubation time (up to 15 hours) may present problems with unstable compounds. PAMPA also ignores the role of enzymes, influx and efflux transporters, and the paracellular pathway [93]. A test was also performed by Galinis-Luciani et al. [156] regarding the usefulness of PAMPA. The authors stated that augmenting the alkyl chain length results in an increased PAMPA value, indicating that PAMPA was largely a measure of lipophilicity. After comparing PAMPA values with log $D_{7.4}$ values, the authors concluded that the calculated log $D_{7.4}$ provided almost the same outcome, which indicated the limited asset of PAMPA in drug discovery.

II.3.2.4 Bio-mimetic artificial membrane permeation to predict drug transport

Bio-mimetic artificial membrane permeation (BAMPA) was introduced as an improved version of PAMPA by Sugano et al. [157]. Like PAMPA, BAMPA can be used to predict transcellular pathway permeation. In BAMPA, the composition of the lipid membrane was modified to mimic the intestinal brush border membrane. Based on this composition, only predictions for intestinal drug absorption have been made; not for BBB transport. The effect of the chain length of the organic solvents (alkyldienes) and the effect of modification of the

lipids was studied. Shorter chain alkyldienes showed larger permeability of the compounds. Modification of the lipid composition had a significant effect on the permeability of charged drugs.

Sugano et al. [158] also used the paracellular pathway prediction model in combination with BAMPA. This way, the permeability of both transcellular and paracellular pathway was estimated separately, and combined to predict total passive intestinal absorption. This model was shown to predict the total passive intestinal permeability more adequately than BAMPA alone.

II.3.2.5 The use of cell lines for the prediction of intestinal absorption

The Caco-2 cell line, derived from a human colon adenocarcinoma, has provided an in vitro cellular epithelium model to predict the intestinal permeability of drugs [115]. These cell lines are cultivated as monolayers on permeable filters for studies of the transepithelial transport of drugs. The studies have shown that cell monolayers can be used to identify drugs with potential absorption problems and possibly also to predict in vivo drug absorption [159]. The transport of drugs across the intestinal epithelium may occur by one or more of four different routes: the passive transcellular and paracellular routes, the carrier mediated route and by transcytosis. Caco-2 monolayers have been used to study drug transport by all four routes.

The Caco-2 cell line results can be subjected to some variability. The properties of Caco-2 monolayers vary based on differences in passage number [160], time in culture [161], the extracellular (filter) support [162] and the cell culture medium [163]. All sources of variability should be taken into account when results from different laboratories are compared [159]. The results obtained with Caco-2 monolayers suggest that the best correlation with the in vivo absorbed fraction is obtained for passively transported drugs.

Using Caco-2 cells, false negatives are likely to be generated with actively transported drug candidates. Thus, the Caco-2 cell model can only serve as a one-way screen: compounds with high permeability in the model are typically well absorbed in vivo, while compounds with low permeability cannot be ruled out as poorly absorbed compounds in vivo [71].

Caco-2 cells provide a high throughput in vitro model for the evaluation of a large number of drug candidates for their intestinal absorption potential. Preparing a fully differentiated confluent Caco-2 cell monolayer is, however, very time-consuming and generally requires a 3-week cell culture period with 8-10 laborious cell feedings. Therefore, alternatives for this long preparation were sought and evaluated. Chong et al. [164] reported the use of a 3-day

alternative preparation step. This method also provided a reasonable correlation between the in vitro permeability through the adapted Caco-2 cell monolayer and the in vivo absorption in humans. The authors thus concluded that the new type of monolayer appeared to be a more convenient and productive absorption screening tool compared to the conventional 3-week system. Also, the use of an automatic liquid handling system has been reported to increase capacity and significantly decrease the need for manpower during experiments [165].
Several authors have isolated numerous subclones from the Caco-2 parental cell line, among which the TC-7 clone. Although TC-7 had similar morphological characteristics compared to Caco-2 cell monolayers, the TC-7 clone was more homogenous and its growth rate and cell density were greater. Regarding some parameters, the TC-7 clone would be a more valuable tool for investigating transport characteristics compared to parental Caco-2 cells [166].

II.3.2.6 The use of Madin-Darby canine kidney cells for the prediction of drug transport

Madin-Darby canine kidney (MDCK) cells differentiate into columnar epithelial cells and form tight junctions when cultured on semipermeable membranes. A membrane permeability comparison between MDCK and Caco-2 cells gave a satisfactory correlation to human absorption [167]. Given the fact that Caco-2 cells are derived from human colon carcinoma cells whereas the MDCK cells are derived from dog kidney cells, it is very likely that the expression level of various transporters greatly differs in these two cell lines.
One of the major advantages of MDCK cells over Caco-2 cells is the shorter cultivation period (3 days vs. 3 weeks). This shorter cell culture time becomes a significant advantage considering reduced labor and reduced downtime in case of cell contamination [71]. The MDCK assay has been extended to predict passive BBB permeability. It gave good prediction qualitatively for the extent of brain exposure and reasonable prediction of the rate of brain uptake in vivo for a small set of compounds [79]. However, a study on a large set of CNS drugs with diverse physicochemical properties showed that MDCK had low prediction of passive BBB permeability in vivo based on in situ brain perfusion assay [86].

II.3.2.7 Other methods

Two other in vitro models for the BBB are RBE4 cells and the ECV304 cell line cocultured with C6 glioma cells. RBE4 is an immortalized rat brain microvessel endothelial cell line that expresses several BBB transporters. ECV304 cells have an endothelial phenotype, although

they are a clonal derivative of the bladder carcinoma cell line. The cells show upregulation of BBB features when cocultured with C6 glioma cells [168].

Bovine and porcine brain microvessel endothelial cell (BMEC) cultures have also been developed. Although most research has focused on the development and characterization of bovine BMEC cultures as in vitro models for the BBB, studies have shown that porcine BMECs can also serve as an appropriate model [169]. BMEC monolayers is a carrier-mediated mechanism which can be used for in vitro log BB computation [170,171]. The monolayers are mostly made based on bovine BMECs, which are soaked in a buffer on both sides. BMECs form a complete monolayer after 10-14 days in culture, these monolayers can be used for permeability studies. The model created by Usansky et al. [171] demonstrated a reasonable ability to compute in vivo log BB values, regardless of the involvement or mechanisms of carrier-mediated transport.

Human umbilical endothelial cells have also been used as BBB models [172]. The advantage of these cells is that they are a human cell line, however, not of cerebral origin.

The octanol:water system has been very successful and became the basis of the QSAR methodology. Unfortunately, this system can only explain membrane transport for a homologous series of drugs. The reason is that the bulky n-octanol isn't an ideal model for a biomembrane. A biomembrane consists of ordered hydrophilic and lipophilic regions with anisotropic and interfacial properties, while n-octanol is an isotropic[3], bulky solvent. Also, drug-membrane interactions are the sum of diverse intermolecular forces, including hydrophobic force, electrostatic force, hydrogen bond and steric effect; the octanol:water system only models hydrophobic force and partial hydrogen bond [114]. The conventional shake-flask measurements are time-consuming and tedious to make, and require relatively large amounts of solute. Some solutions to these problems were provided, including microscaling and an automated parallel plate assay [23].

Liquid liposomes possess the most structural similarity to the bilayer biomembranes. It has been shown that solute partitioning into liposomes is virtually identical to solute partitioning into cell plasma membrane [48]. However, the liposome procedure is time-consuming and tedious and includes four steps: (i) preparation of the liposome, (ii) equilibration of the solute in the liposome suspension, (iii) quantitation of the free solute in the presence of liposomes, and (iv) correction for the amount of drug that has partitioned into the aqueous space of the liposomes [121]. Other disadvantages of the liposome method are: difficulty in separating the

[3] Uniform physical properties throughout the system

free drug, sample amount and purity requirement and poor reproducibility. These factors limit the use of liposomes as an in vitro model for the large-scale screening of drug permeability in early drug development [114]. Additional information about liposomes can be found in section II.2.2.

II.3.3 The prediction of drug transport across the blood-brain barrier with in silico systems

Apart from experimental techniques, computational approaches have been developed to predict the BBB permeation of new chemicals. These computational approaches are referred to as in silico systems. In silico systems offer several advantages compared to in vivo and in vitro systems: they are fast and cheap and can be performed even before the compound is synthesized.

Over the years, various authors have attempted to predict BBB transport using parameters such as lipophilicity (log P), solvatochromic parameters, H-bonding capacity, topological indices, polar surface area (PSA), and a variety of descriptors [173]. Since in silico procedures are very fast and fully automated, the prescreening of virtual libraries and other compound sets prior to synthesis or purchase is possible. Therefore, in silico calculations can and should certainly be performed as an initial step in drug discovery projects where BBB penetration is an issue [174].

The lack of reliable data on which to base the development of the models is, however, a point of concern. Large and well-balanced datasets of reliable and structurally diverse data are a prerequisite for the development of computational models that can be implemented as routine screens in the drug development process. Unless the models are derived from such databases, their utility will remain limited to compounds closely related to the training sets used to develop the models [93,23]. Since the amount of in vivo log BB data is limited (only around 350 compounds, of which most are mentioned in Appendix A), the scope of in silico models is also limited.

II.3.3.1 Examples of in silico predictions of log BB values

In 1992, Vandewaterbeemd et al. [175] established a relationship between the calculated polar molecular surface areas of drug molecules and uptake in the BBB. The polar molecular surface area is here defined as the sum of the parts of the surface area associated with polar

atoms, e.g. oxygen, nitrogen and hydrogen attached to polar atoms. It was however demonstrated that the relationship was very poor for compounds outside the training set, suggesting that the training set was insufficient to derive a generally applicable QSAR for predicting log BB [176].

In 1999, Clark [174] published his results for the log BB calculation using only the PSA and calculated log P as variables. Using 55 compounds, a correlation coefficient of 0.887 was obtained. The obtained equation was also applied on two test sets and proved to perform better than other in silico methods. Unfortunately, the use of only two terms introduces an overdependence on consistent log P estimates. Also, for compounds with many rotatable bonds, the PSA term may be influenced by the conformational choice [177].

Liu et al. [178] defined a new hydrophobicity descriptor and developed a simple predictive model of BBB penetration for early screening in drug discovery. The so-called lipoaffinity descriptor was calculated by adding the contributions to the log P values of all but nitrogen and oxygen atoms. The final model used only the molecular weight (MW) and the lipoaffinity descriptor and still provided a correlation coefficient of 0.889 for the training set of 55 compounds used in the study of Clark [174]. Since the calculation time for MW and the lipoaffinity descriptor is very short, the authors concluded that their model was at least as good as other models reported in literature.

In 2003, Subramanian et al. [177] proposed several PLS-based models starting with the assumption that PSA and log P terms are interesting for log BB prediction. The correlation coefficients for the derived models ranged from 0.90 to 0.92 for a training set of 58 compounds using only 7 descriptors. The most effective model was able to classify 90 % of the molecules correctly for qualitative CNS permeation prediction.

In 2004, Fu et al. [179] obtained a simple two-descriptor (molecular volume and PSA) model for a training set of 79 compounds with a correlation coefficient of 0.83. The log BB values predicted for the test set were in good agreement with the experimental ones.

Abraham et al. [77] used the general linear free energy relationship to predict the log BB values. For a set of 302 compounds, a correlation coefficient of 0.87 was obtained. When 138 of these compounds were used as a test set, the correlation coefficient still reached 0.84, a very good correlation based on the large number of compounds. The authors emphasized that the predictive value of the training set was only valid for a restricted chemical space. Therefore, predictions of compounds in the test set are only valid if the compounds occupy the same (or a similar) chemical space as the training set.

In 2006, Garg et al. [180] tried to generate accurate and reliable BBB models able to mimic the in vivo situation closely. Therefore, they tried to take active transport of the molecules into consideration in the form of their probability of becoming a substrate to P-gp. Their results indicated that the P-gp plays a role in BBB permeability for some of the molecules. Seven descriptors were used for model building and a correlation coefficient of 0.90 was achieved for a training set of 132 compounds.

Fu et al. [75] created a predictive model for BBB penetration using only the molecular weight and the number of polar atoms (oxygen, nitrogen and attached hydrogen atoms) as structural descriptors. Using a training set of 86 compounds and a test set of 25 compounds, a correlation coefficient of 0.86 was achieved. From the derived equation, it could be concluded that the log BB of a compound is inversely correlated with its hydrogen-bonding capacity. Because of its simplicity and easy computations, the model was proposed to be suitable for the rapid prediction of the BBB penetration of drug candidates.

Guerra et al. [181] used an artificial neural network for the prediction of BBB permeation. The molecules were defined by the CODES program, for which only the SMILES codes (i.e. the chemical structures) were needed. The developed model had a correlation coefficient of 0.89, the correlation coefficient for the external test set was 0.85.

Shen et al. [182] developed a chemometric method called genetic algorithm based variable selection for modeling the BBB penetration. In this method, each combination of variables was represented as an individual, whose fitness was determined by MLR analysis. The genetic operations were executed so that a "fitter" population could be obtained after several regulations. The best model contained six descriptors with a correlation coefficient of 0.85. The predicted correlation coefficient for an external test set was 0.84.

Yan et al. [183] achieved a correlation coefficient of 0.90 using MLR analysis with 14 descriptors on a training set of 198 compounds. The correlation coefficient of the test set of 122 compounds was still 0.89.

Although log BB values were nicely predicted by these in silico models, we chose to perform predictions based on in vitro chromatographic models. Previously, it was shown that chromatographic descriptors can add valuable information to in silico models based on theoretical descriptors [184]. The use of computational in silico models can help in initial screening and effectively accelerate the drug development process, but in vitro and in vivo studies will remain necessary tools to support clinical studies and advancements in drug discovery [185].

II.3.3.2 Classification systems for the prediction of drug transport

Several rule-based methods for BBB permeation have been published in the literature. Van de Waterbeemd et al. [186] analysed 125 marketed drugs and proposed a limit for the polar surface area (PSA) of 90 Å and for the molecular weight of about 450. On the basis of 776 orally administered potential CNS drugs, Kelder et al.[187] found a lower limit for the PSA (60-70 Å). Norinder et al. [188] proposed a simple system based on two rules: (i) if the number of N + O is five or less in a molecule, it has a high chance of entering the brain, and (ii) if log P – (N + O) > 0, then log BB is positive. Up to 90 % of correct classifications were obtained by testing these classification rules on several data sets. Pardridge [37,189] stated that a drug is probably a poor CNS-penetration molecule if the MW of the drug is > 400 Dalton, if the molecule is a substrate for active efflux transporters and/or the drug forms 8 or more H-bonds.

For classification purposes, very often artificial neural networks (ANN, see next section) are used. They are robust to noise and allow fast and accurate predictions.

II.4 Regression models for the prediction of blood-brain barrier transport

The prediction of the log BB values of compounds can be performed by various computational methods, such as multiple linear regression (MLR), principal components analysis (PCA), partial least squares (PLS), multivariate adaptive regression splines (MARS), ridge regression (RR), Volsurf, genetic algorithms, ANN, k Nearest Neighbor and molecular dynamics [132,153,180,190,184,191]. Most of these computational models are briefly explained in section II.4.1. These models can be used for quantitative structure-retention relationship (QSRR), QSAR, and quantitative retention-activity relationship (QRAR) methods (section II.4.2).

II.4.1 Computational models to establish relationships between descriptors and values of interest.

Linear regression is an approach for modeling the relationship between a dependent variable y and one or more independent variables X. When there is more than one independent variable, and both dependent and independent variables are numerical, the process is called multiple linear regression (MLR). This approach examines relations between the independent variables

and the dependent variable at the same time, which can deliver a prediction model following equation (3).

$$Y = \beta_0 + \beta_1 X_1 + \beta_2 X_2 + \cdots + \beta_n X_n \quad (3)$$

In principle, MLR can be used with very many independent variables. However, if the number of independent variables gets too large (e.g. greater than the number of observations), the model will likely fit the sampled date perfectly but will fail to predict new data well. This phenomenon is called overfitting. In such cases, there may be only a few underlying or latent factors that account for most of the variation in the response. The general idea of PLS is to try to extract these latent factors. The latent variables in PLS are linear combinations of the descriptive variables in the data set, but instead of maximizing the variance in the matrix with descriptive variables, the covariance with the response variable is maximized. The scores on the PLS factors are used as input for MLR after selection of the optimal number of PLS factors to be considered. If the number of extracted factors is greater than or equal to the rank of the sample factor space, PLS is equivalent to MLR [184,192,193].

With PCA, the number of original variables is reduced to a few latent ones called principal components, that still contain the main information from the original data set. The first new variable is chosen in the direction of the largest variance in the data and thus contains the main information. The second principal component is defined so that it is orthogonal to the first one and it represents a maximum of variance that was not explained by the first one, etc [194]. A drawback of the PCA technique is that no importance is given to how each variable may be related to the dependent or target variable. In a way it is an unsupervised dimension reduction technique. Due to the supervised nature of its algorithm, PCA is less efficient than PLS when a dependent variable for a regression is specified [193].

MARS is a local modeling technique dividing the data space in several, possible overlapping regions and fitting truncated spline functions in each region. In general, a MARS analysis consists of three steps. In the first step, the variable for which the selected pair of spline functions gives the best description of the response is selected as starting point for the model. After the selection of this first pair of splines, new spline functions are added stepwise. In each step, the pair of splines is added that gives the best improvement in the description of the training set. In the second step of the analysis, the global MARS-model is pruned using a sequence of general cross-validations alternated with 10-fold cross-validations. In the final step, the optimal model is selected using a cross-validation technique [184].

An artificial neural network is a biologically inspired computer algorithm designed to treat the data in a manner emulating the learning pattern in the brain. The computer-based network

accepts a set of input values, transforms these, and generates an associated set of output values. Through an iterative learning process, the network refines the information derived from the input values (descriptors) in order to reproduce an associated set of property values (e.g. log BB). A potential problem with the use of an ANN is that it may overtrain i.e. derive a relationship which is too specialized. This problem is averted by delegating a portion of the compounds to serve as a validation set. By tracking the validation set error, the optimal set of weights to be used as the final predictive model can be identified [195]. Complex methods like PLS and ANN suffer from the drawback of being hard to interpret, whereas simple methods like MLR often yield less accurate results or even only rough guidelines [196].

The k Nearest Neighbor method is very similar to the local lazy regression. The latter is a modeling approach that utilizes linear models for individual neighborhoods and obtains a prediction for a query molecule using its local neighborhood, rather than considering the whole data set. The neighborhood of a query molecule in the data set is determined on the fly. The k Nearest Neighbor method has been utilized as a classification method, to predict penetrating and nonpenetrating BBB structures, and to estimate log BB values [191].

There are several programs available that are able to perform one or more of the above-mentioned computational models, such as: Microsoft Excel, Matlab, R, Minitab, Codessa Pro, QSAR-BENCH, SAS, SPSS, …

II.4.2 The use of QSRR, QSAR and QRAR

The principal aim of QSRR is to predict retention data from the molecular structure. However, this methodology can also be used for the prediction of physical properties (e.g. log P values) from retention data. QSRR is a technique for relating the variations in one (or rarely several) response variables (Y-variables) to the variations of several descriptors (X-variables), with predictive or at least explanatory purposes. Y-variables are normally called dependent and X-variables are called independent variables. One of the Y- or X-variables should be related to chromatographic retention, the others should comprise the molecular structure. Héberger [197] provided an excellent overview about QSRR, including QSRR examinations performed in micellar liquid chromatography.

QSAR describes the effect of the molecular structure (in terms of lipophilic, electronic and steric descriptors) on the biological activity of a compound. In classical QSAR based on MLR analysis, the number of samples required is preferably more than ten times the number of molecular descriptors needed to obtain both interpretative and predictive equations, which is

the main purpose of QSAR studies. However, most of the time it is almost impossible to collect enough data for the QSAR studies of a family of drugs. This problem can be solved in two ways: (i) the use of latent variables as an alternative to the original descriptors and activities, such as those obtained by PCA or PLS methods; and (ii) the reduction of the number of descriptors. Unfortunately, for most situations several descriptors must be included in order to obtain adequate models [22].

The integration of chromatographic experiments leads to the field of QRAR. QRAR is often used if the retention data are used as independent variables to predict biological activity of the molecules.

II.4.3 Validation of the computational models

Model validation can be performed by cross-validation methods. Both leave-one-out cross-validation (LOOCV) and leave-group-out cross-validation (LGOCV) are often performed. In the LOOCV procedure, each compound is removed once from the dataset, and the remaining compounds are used to develop a new model, with which the left-out compound is then predicted [173]. The LGOCV works according to a similar procedure, with the major difference that a group of compounds is removed from the dataset instead of one compound. LGOCV should actually be preferred over the LOOCV method for assessing the predictive power of MLR models, since it is known to be statistically more valid. However, the number of reports including LGOCV statistics is very small, mainly due to the lack of such a function in common statistical packages [198]. A LGOCV can also be named a leave-many-out cross-validation, leave-k-out cross-validation or a leave-X %-out cross-validation [183].

In this thesis, the LOOCV method is used to obtain a good model, although a lot of other methods and variants thereof could have been used. These methods include the Akaike information criterion (AIC), the Bayesian information criterion (BIC) [199,200], the 'predictive divergence for incomplete observation models criterion' [201], streamwise regression, risk inflation criterion [202], accumulative prediction error, stochastic complexity [199], and 'least absolute shrinkage and selection operator' [203]. Among these methods, the AIC and BIC have been extensively used.

While the AIC was proposed as an approximately unbiased estimator of the 'mean expected log likelihood' of a model [204], the BIC is an approximation of the posterior probability that a model is the best model [205]. The AIC asymptotically selects the model that minimizes the mean squared error of a prediction or estimation. The AIC also minimizes maximum possible

risk in finite sample sizes [200]. The LOOCV error of a linear model has been shown to be asymptotically equivalent to the AIC [206,207]. However, when many different models are being considered (for example, different combinations of features), there is a danger of overfitting when cross-validation is used [202]. The BIC is consistent in model selection: it is guaranteed to select the true model as the sample size grows, as long as the true model is among the candidate models being considered [200].

II.4.4 Model selection

All computational models have certain advantages (e.g. easy to interpret or to program) and disadvantages (e.g. longer calculation time, hard to interpret or to program). PLS was chosen throughout this thesis as computational model. In chapter VIII, MLR is also used and compared to the results of the more sophisticated PLS model. Model validation was performed using the LOOCV technique. PLS and LOOCV were performed with Matlab version 8.1, MLR was performed with RStudio (R version 3.1.0) software.

The emphasis in this thesis was put on the comparison of the results of several chromatographic methods using only one computational model and one cross-validation method. Although the selection of other (even more sophisticated) computational models and cross-validation methods might have led to improved correlations, this was not considered to be the main goal and was therefore not performed.

II.5 References

1. Tontsch U, Bauer HC (1991) Glial-Cells and Neurons Induce Blood-Brain-Barrier Related Enzymes in Cultured Cerebral Endothelial-Cells. Brain research 539 (2):247-253.

2. Kacem K, Lacombe P, Seylaz J, Bonvento G (1998) Structural organization of the perivascular astrocyte endfeet and their relationship with the endothelial glucose transporter: A confocal microscopy study. Glia 23 (1):1-10.

3. Abbott NJ, Ronnback L, Hansson E (2006) Astrocyte-endothelial interactions at the blood-brain barrier. Nat Rev Neurosci 7 (1):41-53.

4. Dore-Duffy P (2008) Pericytes: Pluripotent cells of the blood brain barrier. Curr Pharm Design 14 (16):1581-1593.

5. Wilhelm I, Fazakas C, Krizbai IA (2011) In vitro models of the blood-brain barrier. Acta Neurobiol Exp 71 (1):113-128.

6. Abbott NJ (2013) Blood-brain barrier structure and function and the challenges for CNS drug delivery. J Inherit Metab Dis 36 (3):437-449.

7. Abbott NJ (2004) Prediction of blood-brain barrier permeation in drug discovery from in vivo, in vitro and in silico models. Drug discovery today Technologies 1 (4):407-416.

8. Abbott NJ (2005) Physiology of the blood-brain barrier and its consequences for drug transport to the brain. Int Congr Ser 1277:3-18.

9. Disson O, Lecuit M (2012) Targeting of the central nervous system by Listeria monocytogenes. Virulence 3 (2):213-221.

10. Abbott NJ, Patabendige AAK, Dolman DEM, Yusof SR, Begley DJ (2010) Structure and function of the blood-brain barrier. Neurobiol Dis 37 (1):13-25.

11. Ballabh P, Braun A, Nedergaard M (2004) The blood-brain barrier: an overview - Structure, regulation, and clinical implications. Neurobiol Dis 16 (1):1-13.

12. Wolburg H, Noell S, Mack A, Wolburg-Buchholz K, Fallier-Becker P (2009) Brain endothelial cells and the glio-vascular complex. Cell Tissue Res 335 (1):75-96.

13. Vanbree JBMM, Deboer AG, Danhof M, Breimer DD (1992) Drug Transport across the Blood-Brain-Barrier .1. Anatomical and Physiological-Aspects. Pharm Weekblad 14 (5):305-310.

14. Hirase T, Staddon JM, Saitou M, AndoAkatsuka Y, Itoh M, Furuse M, Fujimoto K, Tsukita S, Rubin LL (1997) Occludin as a possible determinant of tight junction permeability in endothelial cells. J Cell Sci 110:1603-1613.

15. Begley DJ (2004) Delivery of therapeutic agents to the central nervous system: the problems and the possibilities. Pharmacol Therapeut 104 (1):29-45.

16. Bernacki J, Dobrowolska A, Nierwinska K, Malecki A (2008) Physiology and pharmacological role of the blood-brain barrier. Pharmacol Rep 60 (5):600-622.

17. Pagliara A, Reist M, Geinoz S, Carrupt PA, Testa B (1999) Evaluation and prediction of drug permeation. J Pharm Pharmacol 51 (12):1339-1357.

18. Liu XL, Testa B, Fahr A (2011) Lipophilicity and Its Relationship with Passive Drug Permeation. Pharmaceut Res 28 (5):962-977.

19. Lombard J (2014) Once upon a time the cell membranes: 175 years of cell boundary research. Biol Direct 9.

20. Yang CY, Cai SJ, Liu HL, Pidgeon C (1997) Immobilized artificial membranes - Screens for drug membrane interactions. Adv Drug Deliver Rev 23 (1-3):229-256.

21. Gupta SP (1989) Qsar Studies on Drugs Acting at the Central Nervous-System. Chem Rev 89 (8):1765-1800.

22. Quinones-Torrelo C, Martin-Biosca Y, Martinez-Pla JJ, Sagrado S, Villanueva-Camanas RM, Medina-Hernandez MJ (2002) QRAR Models for Central Nervous System Drugs using Biopartitioning Micellar Chromatography. Mini-Rev Med Chem 2 (2):145-161.

23. Malkia A, Murtomaki L, Urtti A, Kontturi K (2004) Drug permeation in biomembranes in vitro and in silico prediction and influence of physicochemical properties. Eur J Pharm Sci 23 (1):13-47.

24. Tsuji A, Tamai I (1996) Carrier-mediated intestinal transport of drugs. Pharmaceut Res 13 (7):963-977.

25. Gangwar S, Pauletti GM, Wang BH, Siahaan TJ, Stella VJ, Borchardt RT (1997) Prodrug strategies to enhance the intestinal absorption of peptides. Drug Discov Today 2 (4):148-155.

26. Chen Y, Liu LH (2012) Modern methods for delivery of drugs across the blood-brain barrier. Adv Drug Deliver Rev 64 (7):640-665.

27. Bradbury MWB (1993) The Blood-Brain-Barrier. Exp Physiol 78 (4):453-472.

28. Liu XR, Chen CP, Smith BJ (2008) Progress in brain penetration evaluation in drug discovery and development. J Pharmacol Exp Ther 325 (2):349-356.

29. Krol S (2012) Challenges in drug delivery to the brain: Nature is against us. J Control Release 164 (2):145-155.

30. Dash AK, Elmquist WF (2003) Separation methods that are capable of revealing blood-brain barrier permeability. Journal of Chromatography B-Analytical Technologies in the Biomedical and Life Sciences 797 (1-2):241-254.

31. Jeffrey P, Summerfield S (2010) Assessment of the blood-brain barrier in CNS drug discovery. Neurobiol Dis 37 (1):33-37.
32. Mehta DC, Short JL, Hilmer SN, Nicolazzo JA (2015) Drug Access to the Central Nervous System in Alzheimer's Disease: Preclinical and Clinical Insights. Pharmaceut Res 32 (3):819-839.
33. Aryal M, Arvanitis CD, Alexander PM, McDannold N (2014) Ultrasound-mediated blood-brain barrier disruption for targeted drug delivery in the central nervous system. Adv Drug Deliver Rev 72:94-109.
34. Blumling JP, Silva GA (2012) Targeting the Brain: Advances in Drug Delivery. Curr Pharm Biotechno 13 (12):2417-2426.
35. Lennernas H (1997) Human jejunal effective permeability and its correlation with preclinical drug absorption models. J Pharm Pharmacol 49 (7):627-638.
36. Bodor N (1994) Drug Targeting and Retrometabolic Drug Design Approaches - Introduction. Adv Drug Deliver Rev 14 (2-3):157-166.
37. Pardridge WM (2007) Blood-brain barrier delivery. Drug Discov Today 12 (1-2):54-61.
38. Begley DJ (2003) Understanding and circumventing the blood-brain barrier. Acta Paediatr 92:83-91.
39. Dyrna F, Hanske S, Krueger M, Bechmann I (2013) The Blood-Brain Barrier. J Neuroimmune Pharm 8 (4):763-773.
40. Jolliet-Riant P, Tillement JP (1999) Drug transfer across the blood-brain barrier and improvement of brain delivery. Fundam Clin Pharm 13 (1):16-26.
41. Azad TD, Pan J, Connolly ID, Remington A, Wilson CM, Grant GA (2015) Therapeutic strategies to improve drug delivery across the blood-brain barrier. Neurosurg Focus 38 (3).
42. Garg P, Dhakne R, Belekar V (2015) Role of breast cancer resistance protein (BCRP) as active efflux transporter on blood-brain barrier (BBB) permeability. Mol Divers 19 (1):163-172.
43. Lai F, Fadda AM, Sinico C (2013) Liposomes for brain delivery. Expert Opin Drug Del 10 (7):1003-1022.
44. Pinzon-Daza ML, Campia I, Kopecka J, Garzon R, Ghigo D, Riganti C (2013) Nanoparticle- and Liposome-carried Drugs: New Strategies for Active Targeting and Drug Delivery Across Blood-brain Barrier. Curr Drug Metab 14 (6):625-640.
45. Betageri GV, Rogers JA (1987) Thermodynamics of Partitioning of Beta-Blockers in the Normal-Octanol-Buffer and Liposome Systems. Int J Pharm 36 (2-3):165-173.

46. Margalit R, Alon R, Linenberg M, Rubin I, Roseman TJ, Wood RW (1991) Liposomal Drug Delivery - Thermodynamic and Chemical Kinetic Considerations. J Control Release 17 (3):285-296.

47. Suntres ZE (2011) Liposomal Antioxidants for Protection against Oxidant-Induced Damage. Journal of toxicology 2011:152474.

48. Choi YW, Rogers JA (1990) The Liposome as a Model Membrane in Correlations of Partitioning with Alpha-Adrenoceptor Agonist Activities. Pharmaceut Res 7 (5):508-512.

49. Pidgeon C, Ong S, Choi HS, Liu HL (1994) Preparation of Mixed-Ligand Immobilized Artificial Membranes for Predicting Drug-Binding to Membranes. Anal Chem 66 (17):2701-2709.

50. Luchette PA, Vetman TN, Prosser RS, Hancock REW, Nieh MP, Glinka CJ, Krueger S, Katsaras J (2001) Morphology of fast-tumbling bicelles: a small angle neutron scattering and NMR study. Bba-Biomembranes 1513 (2):83-94.

51. Sanders CR, Prosser RS (1998) Bicelles: a model membrane system for all seasons? Struct Fold Des 6 (10):1227-1234.

52. Wohlfart S, Gelperina S, Kreuter J (2012) Transport of drugs across the blood-brain barrier by nanoparticles. J Control Release 161 (2):264-273.

53. Gastaldi L, Battaglia L, Peira E, Chirio D, Muntoni E, Solazzi I, Gallarate M, Dosio F (2014) Solid lipid nanoparticles as vehicles of drugs to the brain: Current state of the art. Eur J Pharm Biopharm 87 (3):433-444.

54. Koo YEL, Reddy GR, Bhojani M, Schneider R, Philbert MA, Rehemtulla A, Ross BD, Kopelman R (2006) Brain cancer diagnosis and therapy with nanoplatforms. Adv Drug Deliver Rev 58 (14):1556-1577.

55. Bhaskar S, Tian FR, Stoeger T, Kreyling W, de la Fuente JM, Grazu V, Borm P, Estrada G, Ntziachristos V, Razansky D (2010) Multifunctional Nanocarriers for diagnostics, drug delivery and targeted treatment across blood-brain barrier: perspectives on tracking and neuroimaging. Part Fibre Toxicol 7.

56. Garcia-Garcia E, Andrieux K, Gil S, Couvreur P (2005) Colloidal carriers and blood-brain barrier (BBB) translocation: A way to deliver drugs to the brain? Int J Pharm 298 (2):274-292.

57. Jolesz FA (2014) Science to Practice: Opening the Blood-Brain Barrier with Focused Ultrasound-A Potential Treatment for Alzheimer Disease? Radiology 273 (3):631-633.

58. Downs ME, Buch A, Sierra C, Karakatsani ME, Chen SS, Konofagou EE, Ferrera VP (2015) Long-Term Safety of Repeated Blood-Brain Barrier Opening via Focused Ultrasound with Microbubbles in Non-Human Primates Performing a Cognitive Task. Plos One 10 (5).
59. Illum L (2000) Transport of drugs from the nasal cavity to the central nervous system. Eur J Pharm Sci 11 (1):1-18.
60. Lochhead JJ, Thorne RG (2012) Intranasal delivery of biologics to the central nervous system. Adv Drug Deliver Rev 64 (7):614-628.
61. Kozlovskaya L, Abou-Kaoud M, Stepensky D (2014) Quantitative analysis of drug delivery to the brain via nasal route. J Control Release 189:133-140.
62. Chen H, Chen CC, Acosta C, Wu SY, Sun T, Konofagou EE (2014) A New Brain Drug Delivery Strategy: Focused Ultrasound-Enhanced Intranasal Drug Delivery. Plos One 9 (10).
63. Lemaire M, Desrayaud S (2005) The priorities/needs of the pharmaceutical industry in drug delivery to the brain. Int Congr Ser 1277:32-46.
64. Thorne RG, Frey WH (2001) Delivery of neurotrophic factors to the central nervous system - Pharmacokinetic considerations. Clin Pharmacokinet 40 (12):907-946.
65. Rapoport SI (2001) Advances in osmotic opening of the blood-brain barrier to enhance CNS chemotherapy. Expert Opin Inv Drug 10 (10):1809-1818.
66. Kraemer DF, Fortin D, Neuwelt EA (2002) Chemotherapeutic dose intensification for treatment of malignant brain tumors: recent developments and future directions. Current neurology and neuroscience reports 2 (3):216-224.
67. Hendricks BK, Cohen-Gadol AA, Miller JC (2015) Novel delivery methods bypassing the blood-brain and blood-tumor barriers. Neurosurg Focus 38 (3).
68. Mangas-Sanjuan V, Gonzalez-Alvarez I, Gonzalez-Alvarez M, Casabo VG, Bermejo M (2013) Innovative in Vitro Method To Predict Rate and Extent of Drug Delivery to the Brain across the Blood-Brain Barrier. Mol Pharmaceut 10 (10):3822-3831.
69. Nielsen PA, Andersson O, Hansen SH, Simonsen KB, Andersson G (2011) Models for predicting blood-brain barrier permeation. Drug Discov Today 16 (11-12):472-475.
70. Goodwin JT, Clark DE (2005) In silico predictions of blood-brain barrier penetration: Considerations to "keep in mind". J Pharmacol Exp Ther 315 (2):477-483.
71. Balimane PV, Chong SH, Morrison RA (2000) Current methodologies used for evaluation of intestinal permeability and absorption. J Pharmacol Toxicol 44 (1):301-312.
72. Kararli TT (1995) Comparison of the Gastrointestinal Anatomy, Physiology, and Biochemistry of Humans and Commonly Used Laboratory-Animals. Biopharm Drug Dispos 16 (5):351-380.

73. Lin JH (1995) Species Similarities and Differences in Pharmacokinetics. Drug Metab Dispos 23 (10):1008-1021.

74. Summerfield SG, Dong KC (2013) In vitro, in vivo and in silico models of drug distribution into the brain. J Pharmacokinet Phar 40 (3):301-314.

75. Fu XC, Wang GP, Shan HL, Liang WQ, Gao JQ (2008) Predicting blood-brain barrier penetration from molecular weight and number of polar atoms. Eur J Pharm Biopharm 70 (2):462-466.

76. Ecker GF, Noe CR (2004) In silico prediction models for blood-brain barrier permeation. Curr Med Chem 11 (12):1617-1628.

77. Abraham MH, Ibrahim A, Zhao Y, Acree WE (2006) A data base for partition of volatile organic compounds and drugs from blood/plasma/serum to brain, and an LFER analysis of the data. J Pharm Sci 95 (10):2091-2100.

78. Pardridge WM (2004) Log(BB), PS products and in silico models of drug brain penetration. Drug Discov Today 9 (9):392-393.

79. Di L, Kerns EH, Bezar IF, Petusky SL, Huang YP (2009) Comparison of Blood-Brain Barrier Permeability Assays: In Situ Brain Perfusion, MDR1-MDCKII and PAMPA-BBB. J Pharm Sci 98 (6):1980-1991.

80. Upton RN (2007) Cerebral uptake of drugs in humans. Clin Exp Pharmacol P 34 (8):695-701.

81. Martin I (2004) Prediction of blood-brain barrier penetration: are we missing the point? Drug Discov Today 9 (4):161-162.

82. Summerfield SG, Jeffrey P (2006) In vitro prediction of brain penetration - a case for free thinking? Expert Opin Drug Dis 1 (6):595-607.

83. Mente SR, Lombardo F (2005) A recursive-partitioning model for blood-brain barrier permeation. J Comput Aid Mol Des 19 (7):465-481.

84. Shen DD, Artru AA, Adkison KK (2004) Principles and applicability of CSF sampling for the assessment of CNS drug delivery and pharmacodynamics. Adv Drug Deliver Rev 56 (12):1825-1857.

85. Takasato Y, Rapoport SI, Smith QR (1984) An Insitu Brain Perfusion Technique to Study Cerebrovascular Transport in the Rat. Am J Physiol 247 (3):H484-H493.

86. Summerfield SG, Read K, Begley DJ, Obradovic T, Hidalgo IJ, Coggon S, Lewis AV, Porter RA, Jeffrey P (2007) Central nervous system drug disposition: The relationship between in situ brain permeability and brain free fraction. J Pharmacol Exp Ther 322 (1):205-213.

87. van Rooy I, Cakir-Tascioglu S, Hennink WE, Storm G, Schiffelers RM, Mastrobattista E (2011) In Vivo Methods to Study Uptake of Nanoparticles into the Brain. Pharmaceut Res 28 (3):456-471.
88. Lennernas H (1998) Human intestinal permeability. J Pharm Sci 87 (4):403-410.
89. Fellner S, Bauer B, Miller DS, Schaffrik M, Fankhanel M, Spruss T, Bernhardt G, Graeff C, Farber L, Gschaidmeier H, Buschauer A, Fricker G (2002) Transport of paclitaxel (Taxol) across the blood-brain barrier in vitro and in vivo. J Clin Invest 110 (9):1309-1318.
90. Ohno K, Pettigrew KD, Rapoport SI (1978) Lower Limits of Cerebrovascular Permeability to Non-Electrolytes in Conscious Rat. Am J Physiol 235 (3):H299-H307.
91. Oldendorf WH (1970) Measurement of brain uptake of radiolabeled substances using a tritiated water internal standard. Brain research 24 (2):372-376.
92. Kakee A, Tersaki T, Sugiyama Y (1996) Brain efflux index as a novel method of analyzing efflux transport at the blood-brain barrier. J Pharmacol Exp Ther 277 (3):1550-1559.
93. Hidalgo IJ (2001) Assessing the Intestinal Absorption of New Pharmaceuticals. Curr Top Med Chem 1 (5):385-401.
94. Liu JF, Sun J, Sui XF, Wang YJ, Hou YN, He ZG (2008) Predicting blood-brain barrier penetration of drugs by microemulsion liquid chromatography with corrected retention factor. J Chromatogr A 1198:164-172.
95. Salary M, Ebrahimi P, Hadjmohammadi MR (2013) SDS-Based Biomembrane Mimetic Chromatography for Prediction of Human Drug Transport as an in Vitro Technique. Chromatographia 76 (13-14):757-765.
96. Wiedmer SK, Jussila MS, Riekkola ML (2004) Phospholipids and liposomes in liquid chromatographic and capillary electromigration techniques. Trac-Trend Anal Chem 23 (8):562-582.
97. Mallols JMS, Camanas RMV, Sagrado S, MedinaHernandez MJ (1997) Quantitative retention - Structure and retention - Activity relationship studies of ionic and non-ionic catecholamines by micellar liquid chromatography. Chromatographia 46 (11-12):605-612.
98. Berthod A, Garcia-Alvarez-Coque MC (2000) Micellar Liquid Chromatography. Marcel Dekker Incorporated, New York
99. Cuenca-Benito M, Sagrado S, Villanueva-Camanas RM, Medina-Hernandez MJ (1998) Quantitative retention-structure and retention-activity relationships of barbiturates by micellar liquid chromatography. J Chromatogr A 814 (1-2):121-132.

100. Ruiz-Angel MJ, Carda-Broch S, Torres-Lapasio JR, Garcia-Alvarez-Coque MC (2009) Retention mechanisms in micellar liquid chromatography. J Chromatogr A 1216 (10):1798-1814.

101. Molero-Monfort M, Escuder-Gilabert L, Villaneuva-Camanas RM, Sagrado S, Medina-Hernandez MJ (2001) Biopartitioning micellar chromatography: an in vitro technique for predicting human drug absorption. J Chromatogr B 753 (2):225-236.

102. Escuder-Gilabert L, Molero-Monfort A, Villanueva-Camanas RM, Sagrado S, Medina-Hernandez MJ (2004) Potential of biopartitioning micellar chromatography as an in vitro technique for predicting drug penetration across the blood-brain barrier. Journal of Chromatography B-Analytical Technologies in the Biomedical and Life Sciences 807 (2):193-201.

103. Lu R, Sun J, Wang YJ, Li HY, Liu JF, Fang L, He ZG (2009) Characterization of biopartitioning micellar chromatography system using monolithic column by linear solvation energy relationship and application to predict blood-brain barrier penetration. J Chromatogr A 1216 (27):5190-5198.

104. Khaledi MG (1997) Micelles as separation media in high-performance liquid chromatography and high-performance capillary electrophoresis: overview and perspective. J Chromatogr A 780 (1-2):3-40.

105. Escuder-Gilabert L, Martin-Biosca Y, Sagrado S, Villanueva-Camanas RM, Medina-Hernandez MJ (2002) Quality control of pharmaceuticals containing non-steroidal anti-inflammatory drugs by micellar liquid chromatography. Chromatographia 55 (5-6):283-288.

106. Bermudez-Saldana JM, Quinones-Torrelo C, Sagrado S, Medina-Hernandez MJ, Villanueva-Camanas RM (2002) A micellar liquid chromatographic method for quality control of pharmaceutical preparations containing tricyclic antidepressants. Chromatographia 56 (5-6):299-306.

107. McCormick TJ, Foley JP, Riley CM, Lloyd DK (2000) The effect of stationary-phase pore size on retention behavior in micellar liquid chromatography. Anal Chem 72 (2):294-301.

108. McCormick TJ, Foley JP, Lloyd DK (2003) Chromatographic performance of large-pore versus small-pore columns in micellar liquid chromatography. Journal of Chromatography B-Analytical Technologies in the Biomedical and Life Sciences 785 (1):1-20.

109. Detroyer A, Vander Heyden Y, Reynaert K, Massart DL (2004) Evaluating "fast" micellar monolithic liquid chromatography for high-throughput quantitative structure-retention relationship screening. Anal Chem 76 (7):1903-1908.

110. Mittal KL (1977) Micellization, Solubilization and Microemulsions, vol 1. Plenum Press, New York

111. Lopez-Grio S, Baeza-Baeza JJ, Garcia-Alvarez-Coque MC (1998) Influence of the addition of modifiers on solute-micelle interaction in hybrid micellar liquid chromatography. Chromatographia 48 (9-10):655-663.

112. Marsh A, Clark BJ, Altria KD (2005) A review of the background, operating parameters and applications of microemulsion liquid chromatography (MELC). J Sep Sci 28 (15):2023-2032.

113. Liu JF, Sun J, Wang YJ, Liu XH, Sun YH, Xu H, He ZG (2007) Characterization of microemulsion liquid chromatography systems by solvation parameter model and comparison with other physicochemical and biological processes. J Chromatogr A 1164 (1-2):129-138.

114. Sun J, Wu X, Lu R, Liu JF, Wang YJ, He ZG (2008) Profiling drug membrane permeability and activity via biopartitioning chromatography. Curr Drug Metab 9 (2):152-166.

115. Pidgeon C, Venkataram UV (1989) Immobilized Artificial Membrane Chromatography - Supports Composed of Membrane-Lipids. Anal Biochem 176 (1):36-47.

116. Rhee D, Markovich R, Chae WG, Qiu X, Pidgeon C (1994) Chromatographic Surfaces Prepared from Lyso Phosphatidylcholine Ligands. Anal Chim Acta 297 (3):377-386.

117. Ong SW, Cai SJ, Bernal C, Rhee D, Qiu XX, Pidgeon C (1994) Phospholipid Immobilization on Solid-Surfaces. Anal Chem 66 (6):782-792.

118. Qiu XX, Ong SW, Bernal C, Rhee D, Pidgeon C (1994) A General Synthetic Route for Preparing Ether Phospholipids Suitable for Immobilization - a Phosphotriester Approach. J Org Chem 59 (3):537-543.

119. Ong SW, Liu HL, Qiu XX, Bhat G, Pidgeon C (1995) Membrane Partition-Coefficients Chromatographically Measured Using Immobilized Artificial Membrane Surfaces. Anal Chem 67 (4):755-762.

120. Caldwell GW, Masucci JA, Evangelisto M, White R (1998) Evaluation of the immobilized artificial membrane phosphatidylcholine - Drug discovery column for high-performance liquid chromatographic screening of drug-membrane interactions. J Chromatogr A 800 (2):161-169.

121. Pidgeon C, Ong SW (1995) Predicting Drug Membrane Interactions. Chemtech 25 (6):38-48.

122. Taillardat-Bertschinger A, Carrupt PA, Barbato F, Testa B (2003) Immobilized artificial membrane HPLC in drug research. J Med Chem 46 (5):655-665.

123. Ong SW, Liu HL, Pidgeon C (1996) Immobilized-artificial-membrane chromatography: Measurements of membrane partition coefficient and predicting drug membrane permeability. J Chromatogr A 728 (1-2):113-128.

124. Pidgeon C, Ong SW, Liu HL, Qiu XX, Pidgeon M, Dantzig AH, Munroe J, Hornback WJ, Kasher JS, Glunz L, Szczerba T (1995) Iam Chromatography - an in-Vitro Screen for Predicting Drug Membrane-Permeability. J Med Chem 38 (4):590-594.

125. Salminen T, Pulli A, Taskinen J (1997) Relationship between immobilised artificial membrane chromatographic retention and the brain penetration of structurally diverse drugs. J Pharmaceut Biomed 15 (4):469-477.

126. Reichel A, Begley DJ (1998) Potential of immobilized artificial membranes for predicting drug penetration across the blood-brain barrier. Pharmaceut Res 15 (8):1270-1274.

127. Krause E, Dathe M, Wieprecht T, Bienert M (1999) Noncovalent immobilized artificial membrane chromatography, an improved method for describing peptide-lipid bilayer interactions. J Chromatogr A 849 (1):125-133.

128. Zhao XL, Chen WJ, Liu ZH, Guo JL, Zhou ZY, Crommen J, Moaddel R, Jiang ZJ (2014) A novel mixed phospholipid functionalized monolithic column for early screening of drug induced phospholipidosis risk. J Chromatogr A 1367:99-108.

129. Nicoli R, Martel S, Rudaz S, Wolfender JL, Veuthey JL, Carrupt PA, Guillarme D (2010) Advances in LC platforms for drug discovery. Expert Opin Drug Dis 5 (5):475-489.

130. Zhang YX, Zeng CM, Li YM, Hjerten S, Lundahl P (1996) Immobilized liposome chromatography of drugs on capillary continuous beds for model analysis of drug-membrane interactions. J Chromatogr A 749 (1-2):13-18.

131. Lundahl P, Zeng CM, Hagglund CL, Gottschalk I, Greijer E (1999) Chromatographic approaches to liposomes, proteoliposomes and biomembrane vesicles. J Chromatogr B 722 (1-2):103-120.

132. Escuder-Gilabert L, Martinez-Pla JJ, Sagrado S, Villanueva-Camanas RM, Medina-Hernandez MJ (2003) Biopartitioning micellar separation methods: modelling drug absorption. Journal of Chromatography B-Analytical Technologies in the Biomedical and Life Sciences 797 (1-2):21-35.

133. Kaliszan R (1998) Retention data from affinity high-performance liquid chromatography in view of chemometrics. J Chromatogr B 715 (1):229-244.

134. Valko K, Nunhuck S, Bevan C, Abraham MH, Reyncilds DP (2003) Fast gradient HPLC method to determine compounds binding to human serum albumin. Relationships with

octanol/water and immobilized artificial membrane lipophilicity. J Pharm Sci 92 (11):2236-2248.

135. Rowley M, Kulagowski JJ, Watt AP, Rathbone D, Stevenson GI, Carling RW, Baker R, Marshall GR, Kemp JA, Foster AC, Grimwood S, Hargreaves R, Hurley C, Saywell KL, Tricklebank MD, Leeson PD (1997) Effect of plasma protein binding on in vivo activity and brain penetration of glycine/NMDA receptor antagonists. J Med Chem 40 (25):4053-4068.

136. Valko K (2004) Application of high-performance liquid chromatography based measurements of lipophilicity to model biological distribution. J Chromatogr A 1037 (1-2):299-310.

137. Valko KL, Nunhuck SB, Hill AP (2011) Estimating Unbound Volume of Distribution and Tissue Binding by In Vitro HPLC-Based Human Serum Albumin and Immobilised Artificial Membrane-Binding Measurements. J Pharm Sci 100 (3):849-862.

138. Wang CZ, Lucy CA (2005) Oligomerized phospholipid bilayers as semipermanent coatings in capillary electrophoresis. Anal Chem 77 (7):2015-2021.

139. Watarai H (1997) Microemulsions in separation sciences. J Chromatogr A 780 (1-2):93-102.

140. Lamalle C, Servais AC, Fradi I, Crommen J, Fillet M (2012) Micellar electrokinetic chromatography systems for the separation of mixtures of charged and uncharged compounds. J Sep Sci 35 (15):1933-1939.

141. Watarai H (1991) Microemulsion Capillary Electrophoresis. Chem Lett (3):391-394.

142. Yu LS, Chu KD, Ye HZ, Liu XX, Yu LS, Xu XQ, Chen GN (2012) Recent advances in microemulsion electrokinetic chromatography. Trac-Trend Anal Chem 34:140-151.

143. Szucs R, VanHove E, Sandra P (1996) Micellar and microemulsion electrokinetic chromatography of hop bitter acids. Hrc-J High Res Chrom 19 (4):189-192.

144. Lynen F, Saveedra L, Nickerson B, Sandra P (2011) Evaluation of a multiarray system for pharmaceutical analysis by microemulsion electrokinetic chromatography. Talanta 84 (3):724-729.

145. Ryan R, Altria K, McEvoy E, Donegan S, Power J (2013) A review of developments in the methodology and application of microemulsion electrokinetic chromatography. Electrophoresis 34 (1):159-177.

146. Wang YJ, Sun J, Liu HZ, He ZG (2007) Rapidly profiling blood-brain barrier penetration with liposome EKC. Electrophoresis 28 (14):2391-2395.

147. Wiedmer SK, Kulovesi P, Riekkola ML (2008) Liposome electrokinetic capillary chromatography in the study of analyte-phospholipid membrane interactions. Application to pesticides and related compounds. J Sep Sci 31 (14):2714-2721.
148. Tondre C, Caillet C (2001) Properties of the amphiphilic films in mixed cationic/anionic vesicles: a comprehensive view from a literature analysis. Adv Colloid Interfac 93 (1-3):115-134.
149. Yu WY, Yang YM, Chang CH (2005) Cosolvent effects on the spontaneous formation of vesicles from 1 : 1 anionic and cationic surfactant mixtures. Langmuir 21 (14):6185-6193.
150. Holland LA, Leigh AM (2003) Bilayered phospholipid micelles and capillary electrophoresis: A new additive for electrokinetic chromatography. Electrophoresis 24 (17):2935-2939.
151. Dittmann MM, Rozing GP (1996) Capillary electrochromatography - A high-efficiency micro-separation technique. J Chromatogr A 744 (1-2):63-74.
152. Yang Q, Liu XY, Miyake J, Toyotama H (1998) Self-assembly and immobilization of liposomes in fused-silica capillary by avidin-biotin binding. Supramol Sci 5 (5-6):769-772.
153. Carpenter TS, Kirshner DA, Lau EY, Wong SE, Nilmeier JP, Lightstone FC (2014) A Method to Predict Blood-Brain Barrier Permeability of Drug-Like Compounds Using Molecular Dynamics Simulations. Biophys J 107 (3):630-641.
154. Di L, Kerns EH, Fan K, McConnell OJ, Carter GT (2003) High throughput artificial membrane permeability assay for blood-brain barrier. Eur J Med Chem 38 (3):223-232.
155. Kansy M, Senner F, Gubernator K (1998) Physicochemical high throughput screening: Parallel artificial membrane permeation assay in the description of passive absorption processes. J Med Chem 41 (7):1007-1010.
156. Galinis-Luciani D, Nguyen L, Yazdanian M (2007) Is PAMPA a useful too for discovery? J Pharm Sci 96 (11):2886-2892.
157. Sugano K, Hamada H, Machida M, Ushio H (2001) High throughput prediction of oral absorption: Improvement of the composition of the lipid solution used in parallel artificial membrane permeation assay. J Biomol Screen 6 (3):189-196.
158. Sugano K, Takata N, Machida M, Saitoh K, Terada K (2002) Prediction of passive intestinal absorption using bio-mimetic artificial membrane permeation assay and the paracellular pathway model. Int J Pharm 241 (2):241-251.
159. Artursson P, Palm K, Luthman K (1996) Caco-2 monolayers in experimental and theoretical predictions of drug transport. Adv Drug Deliver Rev 22 (1-2):67-84.

160. Walter E, Kissel T (1995) Heterogeneity in the Human Intestinal-Cell Line Caco-2 Leads to Differences in Transepithelial Transport. Eur J Pharm Sci 3 (4):215-230.
161. Wilson G, Hassan IF, Dix CJ, Williamson I, Shah R, Mackay M, Artursson P (1990) Transport and Permeability Properties of Human Caco-2 Cells - an Invitro Model of the Intestinal Epithelial-Cell Barrier. J Control Release 11 (1-3):25-40.
162. Nicklin P, Irwin B, Hassan I, Williamson I, Mackay M (1992) Permeable Support Type Influences the Transport of Compounds across Caco-2 Cells. Int J Pharm 83 (1-3):197-209.
163. Jumarie C, Malo C (1991) Caco-2 Cells Cultured in Serum-Free Medium as a Model for the Study of Enterocytic Differentiation Invitro. J Cell Physiol 149 (1):24-33.
164. Chong SH, Dando SA, Morrison RA (1997) Evaluation of Biocoat (R) intestinal epithelium differentiation environment (3-day cultured Caco-2 cells) as an absorption screening model with improved productivity. Pharmaceut Res 14 (12):1835-1837.
165. Garberg P, Eriksson P, Schipper N, Sjostrom B (1999) Automated absorption assessment using Caco-2 cells cultured on both sides of polycarbonate membranes. Pharmaceut Res 16 (3):441-445.
166. Gres MC, Julian B, Bourrie M, Meunier V, Roques C, Berger M, Boulenc X, Berger Y, Fabre G (1998) Correlation between oral drug absorption in humans, and apparent drug permeability in TC-7 cells, a human epithelial intestinal cell line: Comparison with the parental Caco-2 cell line. Pharmaceut Res 15 (5):726-733.
167. Irvine JD, Takahashi L, Lockhart K, Cheong J, Tolan JW, Selick HE, Grove JR (1999) MDCK (Madin-Darby canine kidney) cells: A tool for membrane permeability screening. J Pharm Sci 88 (1):28-33.
168. Kramer SD, Schutz YB, Wunderli-Allenspach H, Abbott NJ, Begley DJ (2002) Lipids in blood-brain barrier models in vitro II: Influence of glial cells on lipid classes and lipid fatty acids. In Vitro Cell Dev-An 38 (10):566-571.
169. Nicolazzo JA, Charman SA, Charman WN (2006) Methods to assess drug permeability across the blood-brain barrier. J Pharm Pharmacol 58 (3):281-293.
170. Rim S, Audus KL, Borchardt RT (1986) Relationship of Octanol Buffer and Octanol Water Partition-Coefficients to Trans-Cellular Diffusion across Brain Microvessel Endothelial-Cell Monolayers. Int J Pharm 32 (1):79-84.
171. Usansky HH, Sinko PJ (2003) Computation of log BB values for compounds transported through carrier-mediated mechanisms using in vitro permeability data from brain microvessel endothelial cell (BMEC) monolayers. Pharmaceut Res 20 (3):390-396.

172. Langford D, Hurford R, Hashimoto M, Digicaylioglu M, Masliah E (2005) Signalling crosstalk in FGF2-mediated protection of endothelial cells from HIV-gp120. Bmc Neurosci 6.
173. Ooms F, Weber P, Carrupt PA, Testa B (2002) A simple model to predict blood-brain barrier permeation from 3D molecular fields. Bba-Mol Basis Dis 1587 (2-3):118-125.
174. Clark DE (1999) Rapid calculation of polar molecular surface area and its application to the prediction of transport phenomena. 2. Prediction of blood-brain barrier penetration. J Pharm Sci 88 (8):815-821.
175. Vandewaterbeemd H, Kansy M (1992) Hydrogen-Bonding Capacity and Brain Penetration. Chimia 46 (7-8):299-303.
176. Abraham MH, Chadha HS, Mitchell RC (1994) Hydrogen-Bonding .33. Factors That Influence the Distribution of Solutes between Blood and Brain. J Pharm Sci 83 (9):1257-1268.
177. Subramanian G, Kitchen DB (2003) Computational models to predict blood-brain barrier permeation and CNS activity. J Comput Aid Mol Des 17 (10):643-664.
178. Liu RF, Sun HM, So SS (2001) Development of quantitative structure-property relationship models for early ADME evaluation in drug discovery. 2. Blood-brain barrier penetration. J Chem Inf Comp Sci 41 (6):1623-1632.
179. Fu XC, Song ZF, Fu CY, Liang WQ (2005) A simple predictive model for blood-brain barrier penetration. Pharmazie 60 (5):354-358.
180. Garg P, Verma J (2006) In silico prediction of blood brain barrier permeability: An artificial neural network model. J Chem Inf Model 46 (1):289-297.
181. Guerra A, Paez JA, Campillo NE (2008) Artificial neural networks in ADMET modeling: Prediction of blood-brain barrier permeation. Qsar Comb Sci 27 (5):586-594.
182. Shen J, Du YP, Zhao YX, Liu GX, Tang Y (2008) In silico prediction of blood-brain partitioning using a chemometric method called Genetic Algorithm Based Variable Selection. Qsar Comb Sci 27 (6):704-717.
183. Yan A, Liang H, Chong Y, Nie X, Yu C (2013) In-silico prediction of blood-brain barrier permeability. Sar Qsar Environ Res 24 (1):61-74.
184. Deconinck E, Ates H, Callebaut N, Van Gyseghem E, Vander Heyden Y (2007) Evaluation of chromatographic descriptors for the prediction of gastro-intestinal absorption of drugs. J Chromatogr A 1138 (1-2):190-202.
185. Naik P, Cucullo L (2012) In vitro blood-brain barrier models: Current and perspective technologies. J Pharm Sci 101 (4):1337-1354.

186. van de Waterbeemd H, Camenisch G, Folkers G, Chretien JR, Raevsky OA (1998) Estimation of blood-brain barrier crossing of drugs using molecular size and shape, and H-bonding descriptors. J Drug Target 6 (2):151-165.
187. Kelder J, Grootenhuis PDJ, Bayada DM, Delbressine LPC, Ploemen JP (1999) Polar molecular surface as a dominating determinant for oral absorption and brain penetration of drugs. Pharmaceut Res 16 (10):1514-1519.
188. Norinder U, Haeberlein M (2002) Computational approaches to the prediction of the blood-brain distribution. Adv Drug Deliver Rev 54 (3):291-313.
189. Pardridge WM (2001) Crossing the blood-brain barrier: are we getting it right? Drug Discov Today 6 (1):1-2.
190. Martens H, Naes T (1989) Multivariate Calibration. Wiley, New York
191. Mensch J, Oyarzabal J, Mackie C, Augustijns P (2009) In Vivo, In Vitro and In Silico Methods for Small Molecule Transfer Across the BBB. J Pharm Sci 98 (12):4429-4468.
192. Tobias RD (1995) An introduction to Partial Least Squares Regression. SAS Institute Inc. http://www.ats.ucla.edu/stat/sas/library/pls.pdf.
193. Maitra S, Yan J (2008) Principle component analysis and partial least squares: two dimension reduction techniques for regression. Casualty Actuarial Society, Discussion paper program.
194. Detroyer A, Heyden YV, Cambre I, Massart DL (2003) Chemometric comparison of recent chromatographic and electrophoretic methods in a quantitative structure-retention and retention-activity relationship context. J Chromatogr A 986 (2):227-238.
195. Karelson M, Dobchev D, Tamm T, Tulp I, Janes J, Tamm K, Lomaka A, Savchenko D, Karelsona G (2008) Correlation of blood-brain penetration and human serum albumin binding with theoretical descriptors. Arkivoc:38-60.
196. Muehlbacher M, Spitzer GM, Liedl KR, Kornhuber J (2011) Qualitative prediction of blood-brain barrier permeability on a large and refined dataset. J Comput Aid Mol Des 25 (12):1095-1106.
197. Heberger K (2007) Quantitative structure-(chromatographic) retention relationships. J Chromatogr A 1158 (1-2):273-305.
198. Konovalov DA, Coomans D, Deconinck E, Vander Heyden Y (2007) Benchmarking of QSAR models for blood-brain barrier permeation. J Chem Inf Model 47 (4):1648-1656.
199. Myung JI, Tang Y, Pitt MA (2009) Evaluation and Comparison of Computational Models. Method Enzymol 454:287-304.

200. Vrieze SI (2012) Model Selection and Psychological Theory: A Discussion of the Differences Between the Akaike Information Criterion (AIC) and the Bayesian Information Criterion (BIC). Psychol Methods 17 (2):228-243.
201. Cavanaugh JE, Shumway RH (1998) An Akaike information criterion for model selection in the presence of incomplete data. J Stat Plan Infer 67 (1):45-65.
202. Zhou J, Foster DP, Stine RA, Ungar LH (2006) Streamwise feature selection. J Mach Learn Res 7:1861-1885.
203. Zhang YL, Yang YH (2015) Cross-validation for selecting a model selection procedure. J Econometrics 187 (1):95-112.
204. Bozdogan H, Haughton DMA (1998) Informational complexity criteria for regression models. Comput Stat Data An 28 (1):51-76.
205. Schwarz G (1978) Estimating Dimension of a Model. Ann Stat 6 (2):461-464.
206. Stone M (1977) Asymptotic Equivalence of Choice of Model by Cross-Validation and Akaikes Criterion. J R Stat Soc B 39 (1):44-47.
207. Shao J (1993) Linear-Model Selection by Cross-Validation. J Am Stat Assoc 88 (422):486-494.

Chapter III. Predicting drug penetration across the blood–brain barrier: comparison of micellar liquid chromatography and immobilized artificial membrane liquid chromatography[4]

III.1 Summary

Several in vitro methods have been tested for their ability to predict drug penetration across the blood–brain barrier (BBB) into the central nervous system (CNS). In this chapter, the performance of a variety of micellar liquid chromatographic (MLC) methods and immobilized artificial membrane (IAM) liquid chromatographic approaches were compared for a set of 45 solutes. MLC measurements were performed on a C_{18} column with sodium dodecyl sulfate (SDS), polyoxyethylene (23) lauryl ether (Brij35), or sodium deoxycholate (SDC) as surfactant in the micellar mobile phase. IAM liquid chromatography measurements were performed with Dulbecco's phosphate-buffered saline (DPBS) and methanol as organic modifier in the mobile phase. The corresponding retention and computed descriptor data for each solute were used for construction of models to predict transport across the blood–brain barrier (log BB). All data were correlated with experimental log BB values and the relative performance of the models was studied. SDS-based models proved most suitable for prediction of log BB values, followed closely by a simplified IAM method, in which it could be observed that extrapolation of retention data to 0 % modifier in the mobile phase was unnecessary.

[4] Published as: De Vrieze M, Lynen F, Chen K, Szucs R, Sandra P (2013) Predicting drug penetration across the blood-brain barrier: comparison of micellar liquid chromatography and immobilized artificial membrane liquid chromatography. Anal Bioanal Chem 405 (18):6029-6041

III.2 Introduction

An essential prerequisite for a pharmaceutical compound designed to affect the central nervous system (CNS) is satisfactory transport through the blood–brain barrier (BBB) [1]. As discussed in chapter II, this obstacle severely restricts the diffusion of both small molecules and larger objects (for example bacteria) into the cerebrospinal fluid (CSF). A common measure of the extent of BBB permeation is the ratio of the steady-state concentration of the drug molecule in the brain to the concentration in the blood, usually expressed as log (C_{brain}/C_{blood}) or log BB [2]. In the last decade, emphasis has been set on modeling of BBB permeation to avoid in vivo measurements. Both in silico and in vitro models have been proposed for this [3-5].

In vitro chromatographic models mimic the lipid environment of the barrier by dynamically or covalently immobilizing lipids on a column. The affinity of the solutes for the immobilized phase is then combined with physicochemical data or molecular descriptors for optimum model construction.

Micellar liquid chromatography (MLC) uses a surfactant solution above the critical micellar concentration (CMC) as mobile phase [6]. Neutral polyoxyethylene (23) lauryl ether (Brij35) is the most widely used surfactant for BBB permeation modeling, but anionic sodium dodecyl sulfate (SDS) and cationic cetyltrimethylammonium bromide (CTAB) have also been used [7]. MLC is a fascinating example of the benefits of secondary equilibrium in RPLC. The primary equilibrium is solute partitioning between bulk solvent and the stationary phase. A secondary equilibrium is established with the micelles in the mobile phase. Both equilibria are affected by a variety of factors, for example the nature and concentration of the surfactant and additives (e.g. salts), temperature, ionic strength, and pH. This allows for improved mimicking of the BBB environment.

In contrast with MLC, immobilized artificial membranes (IAMs) mimic the lipid environment of a cell membrane by anchoring synthetic phospholipid analogues to silica particles, which are subsequently used as HPLC column packing material [8-11]. This type of column is particularly interesting for prediction of drug partitioning into biological membranes, because it avoids the use of micellar solutions, enabling more conventional gradient HPLC operation and MS detection with volatile buffers. The MLC eluents used in this chapter contained no organic solvent, although the solutes had a broad hydrophobicity range. However, for IAMs, addition of an organic modifier is required for solute elution. According to Taillardat-Bertschinger et al. [10], extrapolation to 100 % aqueous phase is required to enable

comparison of retention factors, irrespective of the amount and type of organic co-solvent and to avoid the use of fictitious interaction scales because of the differences in the order of elution which occur at different percentages of co-solvent.

To enable comparison of chromatographic IAM and MLC methods, the quality of the model achievable with input from different experimental setups was compared in this work, in which 45 pharmaceutical drugs with known log BB values were used. The drugs were analyzed by MLC with SDS, Brij35, and sodium deoxycholate (SDC) as surfactants, and on a PC.DD2 phosphatidylcholine IAM column. The corresponding models were constructed by use of partial least-squares regression (PLS).

III.3 Materials and methods

III.3.1 Chemicals

Solutes were obtained from several sources: 2,2,2-trifluoroethyl vinyl ether, 2,6-diisopropylphenol, acetaminophen, acetylsalicylic acid, aminopyrine, amitriptyline, amobarbital, antipyrine, atenolol, caffeine, carbamazepine, chlorambucil, cimetidine, clonidine, cotinine, desipramine, domperidone, eserine, ethylbenzene, fluphenazine, hexobarbital, hydroxyzine, ibuprofen, imipramine, mianserin, N-methyl-2-pyridineethanamine, omeprazole, oxazepam, pentobarbital, phenylbutazone, phenytoin, propranolol, pyrilamine, quinidine, ranitidine, ropinirole, salicylic acid, theobromine, theophylline, toluene, valproic acid, verapamil and zidovudine (Sigma–Aldrich, St Louis, MO, USA or Steinheim, Germany); indomethacin (Fluka, St Louis, MO, USA), and benzene (Acros, Geel, Belgium).

III.3.2 Apparatus

MLC and IAM retention analysis was performed on an Alliance, Waters 2690 chromatograph (Milford, MA, USA) with a quaternary pump and an automatic injector. A Waters 2487 dual-wavelength absorbance detector was used. The detection wavelength was set between 210 nm and 300 nm, depending on the compound analyzed (the exact wavelengths are presented in Table C-1; Appendix C). Data acquisition and processing were performed with a PeakSimple Chromatography Data System (model 202) and PeakSimple software (SRI Instruments,

Torrance, CA, USA). MLC and IAM experiments were performed on Grace GraceSmart C_{18} (3 μm, 150 mm×2.1 mm; Deerfield, IL, USA) and Regis IAM.PC.DD2 (10 μm, 150 mm×4.6 mm; Morton Grove, IL, USA) columns, respectively. For MLC experiments, analysis was performed at 37 °C with a flow rate of 0.2 mL min^{-1}. For IAM experiments, analysis was performed at 25 °C with a flow rate of 1 mL min^{-1}.

III.3.3 Mobile phase and sample preparation

Two MLC mobile phases were composed of aqueous solutions of 0.05 mol L^{-1} polyoxyethylene (23) lauryl ether (Brij35) (Sigma–Aldrich) or 0.05 mol L^{-1} sodium dodecyl sulfate (SDS) (Acros). pH was adjusted with pH 7.4 phosphate buffer, prepared with 0.05 mol L^{-1} disodium hydrogen phosphate (Sigma–Aldrich) and potassium dihydrogen phosphate (Sigma–Aldrich). To reproduce the osmotic pressure of biological fluids, NaCl (9.20 g L^{-1}) (Sigma –Aldrich) was added to the micellar mobile phase. The 0.05 mol L^{-1} sodium deoxycholate (SDC) (Sigma–Aldrich, BioXtra, ≥98.0 %) MLC phase was prepared in 0.05 mol L^{-1} borate buffer, obtained by dissolving 12.5 mmol L^{-1} sodium tetraborate decahydrate (Sigma–Aldrich) and adjusting to pH 7.5 with boric acid (Sigma–Aldrich). IAM mobile phases consisted of different ratios of methanol (HPLC-grade; Biosolve, Valkenswaard, The Netherlands) and Dulbecco's phosphate buffered saline (DPBS) (20:80, 30:70, or 40:60 v/v). The latter was composed of 2.7 mmol L^{-1} KCl, 1.5 mmol L^{-1} potassium dihydrogenphosphate, 137 mmol L^{-1} NaCl, and 8.1 mmol L^{-1} disodium hydrogenphosphate (Sigma–Aldrich). The pH of the mobile phase, which was altered by addition of methanol, was adjusted to 7.4 by use of phosphoric acid (Sigma–Aldrich). Before use, all mobile phases were vacuum-filtered through 0.20 μm nylon membranes (Grace, Lokeren, Belgium).

Stock solutions of all drugs were prepared by dissolving 10 mg in 1 mL methanol except for quinidine and theobromine, for which stock concentrations of 1 mg mL^{-1} and 200 μg mL^{-1} were used, caffeine and theophylline, which were dissolved in water (10 mg mL^{-1}), and domperidone, which was dissolved in dimethyl sulfoxide (10 mg mL^{-1}). Stock solutions were stored at 5 °C, except for atenolol and zidovudine, which were stored at −20 °C. Working solutions were prepared by dilution of the stock solutions (to 50 μg mL^{-1}) with mobile phase.

III.3.4 Data sources, software, and processing

A total of 45 values of the logarithm of brain–blood distribution coefficients (log BB) were collected [1,12,13]. The experimental values of log BB (Table C-1) ranged between −1.70 and 1.51. Values of acidity constants (not shown in Table C-1) were obtained from Refs. [14,15] or were calculated. The acidity constants were used to calculate the total molar charge (α) values at pH 7.4. Structural data (molar refractivity (MR), molar volume (MV), parachor (Pr), and polarizability) were calculated by use of ACD/Chemsketch software. Other data (log P, log D7.4, intrinsic aqueous solubility (log WSo), pH solubility profile (WS7.4), plasma protein binding (PB), Ames test mutagenic index (MI and MIA), and human intestinal absorption (HIA)) were predicted by use of Chemsilico prediction software (Chemsilico free trial version). The values for these are presented in Table C-1. The experimental logarithms of the retention factors (log k) are listed in Table III-1 for the MLC and IAM experiments. All retention data are averages from triplicate determination. Microsoft Excel (Microsoft Corporation, v. 2007) and Matlab (version 7.12) were used to perform statistical analysis of the results.

III.4 Rationale

The accuracy of prediction of a model depends on the type of model selected, the relevance, diversity, and orthogonality (independence) of the input variables used therein and on the shortlist of those which have been retained after model optimization, the size of the training set, and the similarity of the test molecules to those in the training set.

Next to in silico strategies, applying only mathematically processed descriptors [1,4,16,17], the approach whereby chromatographic retention data are used as additional input in these models is labeled by the terminology quantitative retention–activity relationships (QRAR) or quantitative structure–retention relationships (QSRR). The latter have been well reviewed by Héberger [18]. This type of multivariate problem is typically solved by the multivariate calibration family of algorithms, for example multiple linear regression (MLR), principle-component regression (PCR), and partial least-squares (PLS) methodology. There are also reports on the application of artificial neural networks (ANN) in combination with pure in silico strategies [19,17]. The implementation of ANN strategy is nevertheless more sophisticated and the optimized mathematical model cannot be expressed with explicit functions or equations.

Table III-1: Log k values of compounds measured by MLC and IAM liquid chromatography[a,b].

Nr.	Compound	log k_{Brij35} 0.05 M	log k_{SDC} 0.05 M	log k_{SDS} 0.05 M	log k_{IAM} 40% MeOH	log k_{IAM} 30% MeOH	log k_{IAM} 20% MeOH	log k_{IAM} 0 % MeOH extrapolation
1	2,2,2-trifluoroethyl vinyl ether	0.928	0.694	1.080	-0.089	0.095	0.207	0.5142
2	2,6-diisopropylphenol	1.254	1.598	1.750	1.156	1.544	1.866	2.5867
3	acetaminophen	0.261	-0.231	-0.095	-0.657	-0.372	-0.160	0.3479
4	acetylsalicylic acid	-0.498	-1.004	-0.688	-0.964	-0.664	-0.413	0.1455
5	aminopyrine	0.474	1.438	1.527	-0.547	-0.206	0.100	0.7528
6	amitriptyline	2.386		2.123	1.519	1.975		3.3437
7	amobarbital	0.936	0.693	1.249	0.112	0.457	0.755	1.4066
8	antipyrine	0.268	0.964	1.053	-0.694	-0.368	-0.077	0.5458
9	atenolol	-0.093	1.253	1.189	-0.436	-0.206	0.007	0.4525
10	benzene	1.039	1.120	1.207	0.155	0.338	0.485	0.8218
11	caffeine	0.073	0.485	0.767	-0.948	-0.590	-0.313	0.3344
12	carbamazepine	0.799	1.236	1.226	0.202	0.593	1.075	1.9334
13	chlorambucil	1.530	0.261	-0.889	0.397	0.793	1.096	1.8106
14	cimetidine	0.301	0.934	1.031	-0.491	-0.145	0.214	0.9157
15	clonidine	0.584	1.877	1.500	0.227	0.458	0.713	1.1948
16	cotinine	0.194	1.100	1.110	-1.139	-0.711	-0.404	0.3524
17	desipramine	1.704		1.991	1.462	1.864		3.0696
18	domperidone	0.984	1.891	1.924	1.461	2.042		3.7854
19	eserine	0.987	2.074	1.547	0.014	0.355	0.691	1.3682
20	ethylbenzene	1.233	1.476	1.636	0.718	0.994	1.211	1.7127
21	fluphenazine	1.553		2.046	2.022	2.596		4.3172
22	hexobarbital	0.789	0.769	1.260	-0.064	0.253	0.516	1.1044
23	hydroxyzine	1.271		2.010	1.276	1.800	2.240	3.2172
24	ibuprofen	0.693	0.194	0.565	0.123	0.499	0.780	1.4527
25	imipramine			2.096	1.409	1.838		3.1229
26	indomethacin	0.730	0.291	0.738	0.541	1.061	1.577	2.6142
27	mianserin	1.940		2.173	1.439	1.843		3.0535
28	N-methyl-2-pyridineethanamine	0.454	1.977	1.560	-0.419	-0.249	-0.120	0.1845
29	omeprazole	0.974	1.562	1.764	0.223	0.713	1.206	2.1888
30	oxazepam	0.945	1.244	1.439	0.702	1.118	1.491	2.2866
31	pentobarbital	0.932	0.739	1.274	0.150	0.489	0.800	1.4558
32	phenylbutazone	0.701	-0.179	0.594	0.041	0.477	0.829	1.6306
33	phenytoin	0.933	0.898	1.349	0.392	0.761	1.220	2.0319
34	propranolol	1.326	2.270	1.936	1.119	1.474	1.860	2.5955
35	pyrilamine			2.001	0.747	1.132	1.516	2.2850
36	quinidine	1.282	1.408	1.590	0.937	1.346	1.810	2.6738
37	ranitidine	0.283	1.756	1.191	-0.331	-0.045	0.207	0.7514
38	ropinirole	0.936	1.938	1.636	0.102	0.385	0.692	1.2789
39	salicylic acid	0.179	-0.998	-0.672	-1.057	-0.656	-0.427	0.2313
40	theobromine	-0.191	-0.076	0.275	-1.334	-0.932	-0.670	0.0177
41	theophylline	0.011	-0.091	0.312	-0.945	-0.621	-0.368	0.2202
42	toluene	1.260	1.395	1.511	0.450	0.683	0.858	1.2767
43	valproic acid	-0.098		-0.135	-0.689	-0.546	-0.430	-0.1656
44	verapamil	1.652		2.197	1.055	1.663	2.295	3.5322
45	zidovudine	0.085	-0.252	0.303	-0.670	-0.482	-0.185	0.2817

[a] All log k data are averages from three analyses
[b] Empty boxes in the table indicate that log k values were not obtained, mostly because of too long elution times

Within the multivariate calibration family of algorithms, both MLR and PLS models have thus far been proposed for prediction of drug absorption whereby mathematically generated

descriptors are combined with retention data [19,14,20]. MLR achieves maximum correlation between the variable matrix X and the log BB vector y. However, the performance of MLR is significantly affected by the variables selected, especially as there is strong correlation among these variables. PCR is one means of dealing with ill-conditioned problems by capturing the maximum variance in X. A weak point of PCR is that it does not make use of the information in y, with the result that some principal components are not relevant for prediction but only relevant for describing variance in X. To overcome these problems, PLS tries to do both by maximizing the covariance between X and y [21]. Instead of finding hyperplanes of minimum variance between y and X, PLS finds a linear regression model by projecting y and X to a new space, where the projected original variables are transformed as latent variables in nomenclature. PLS regression is particularly suitable for problems when the number of samples is fewer than the number of independent variables and where there is probably a large correlation among X values. All the above-mentioned methods from the multivariate calibration family can provide an equation of the type $y = b_0 + b_1 x_1 + b_2 x_2 + \ldots + b_n x_n$, where y is the predicted (log BB) value, b_0–b_n are constants and x_1–x_n are variables (descriptors). Obtaining a suitable equation of this type is important for this type of work.

As the accuracy of the response (in this case log BB) of the model depends on both the choice and relevance of the descriptors used, the use of solute retention data in the model is particularly attractive, because they represent the affinity of a compound in a column environment emulating the blood-brain barrier. Such chromatographic strategies are compared and evaluated in this work. The following mathematically processed descriptors were used, by analogy with a previous MLC study [14]: total molar charge (α), molecular weight (MW), molar refractivity (MR), molar volume (MV), parachor (Pr), polarizability, and the logarithm of the octanol–water partition coefficient (log P). This set was expanded by inclusion of the logarithm of the octanol–water distribution coefficient at pH 7.4 (log D7.4), intrinsic aqueous solubility (log WSo), solubility profile at pH 7.4 (WS7.4), plasma protein binding (PB), Ames test mutagenic index (MI and MIA), and human intestinal absorption (HIA). The α values, which can be positive of negative, were calculated as in Ref. [22].

All descriptors are listed in Table C-1. In this work, PLS models were constructed by use of retention data for 45 solutes for which experimental log BB data are available together with the set of molecular descriptors mentioned above. The merits of each model were then compared.

III.5 Results and discussion

The set of previously used SDS and Brij35 type of micelles in MLC for log BB prediction was expanded by addition of micelles of sodium deoxycholate (SDC), a natural bile acid which possibly better emulates lipids in the blood–brain barrier. Because one of the functions of bile acids is the processing of fat by the formation of micelles, and because they are essentially UV transparent, they were directly applicable as an MLC surfactant in this chapter. Because of deoxycholate precipitation in the phosphate-buffered solution, the phosphate buffer was replaced by a borate buffer. The retention factors measured with the three MLC conditions are given in the left part of Table III-1. It is apparent that some solutes could not be detected if Brij35 and, especially, SDC buffer, were used. This could be related to increased background absorbance of the SDC buffer combined with loss of sensitivity at high retention (except for valproic acid). Note that although MLC is a powerful technique in terms of selectivity optimization and for complete elution under aqueous conditions, it is inherently hindered by peak-broadening phenomena because of the thick layer of surfactant that covers the stationary phase [23] and therefore rarely allows one to achieve theoretical plate heights within reasonable analysis times, with reduced S/N ratios and sensitivity as a consequence.

The logarithms of the retention factors measured by use of DPBS containing 40, 30, or 20 % methanol as mobile phase with an IAM.PC.DD2 column are listed in the right part of Table III-1. Some solutes were excessively retained when 20 % methanol was used and were, therefore, no longer detected under those conditions. As an example, the chromatograms obtained for ethylbenzene are shown in Figure III-1. The disadvantages of the SDC buffer, namely increased background absorbance and loss of sensitivity, are notable (Figure III-1b). The retention data in Table III-1 was also extrapolated to 100 % aqueous phases. The rationale was that this enables comparison irrespective of the amount of organic co-solvent and avoids fictitious interaction scales because of differences in the order of elution which occur for different percentages of co-solvent.

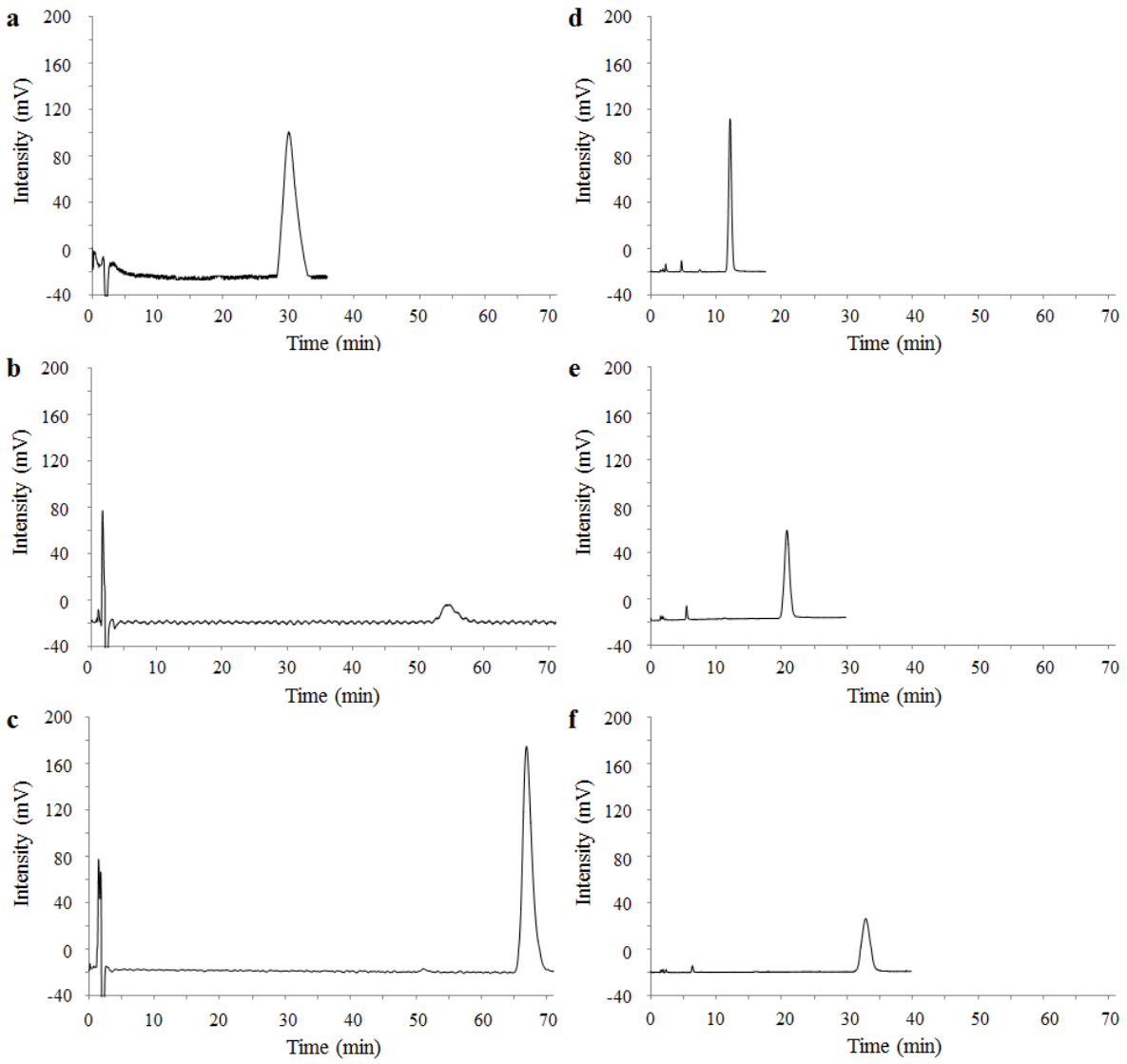

Figure III-1: Chromatograms obtained for ethylbenzene by use of MLC (**a**, **b**, and **c**) and IAM liquid chromatography (**d**, **e**, and **f**). Chromatogram **a** was obtained with Brij35 in the mobile phase, **b** with SDC, and **c** with SDS. Chromatograms **d**, **e**, and **f** were obtained by use of 40 %, 30 %, and 20 % methanol, respectively.

III.5.1 Prediction of log BB

Partial least-squares (PLS) regression was subsequently performed in Matlab to determine the correlation coefficients (R) between experimental log BB values (Table C-1) and log BB values predicted by use of log k values together with the other descriptors mentioned in Table C-1. The correlation coefficients in Table III-2 enable comparison of the merits of the different models. The lowest correlation coefficient was obtained when Brij35 was used as surfactant. The highest correlation coefficient (R= 0.9159) was obtained with SDC as surfactant, but this micellar mobile phase enabled measurement for 36 out of the 45 compounds only. This demonstrates the potential of SDC-type micelles but, because the final

objective in this type of research is accurate prediction of the log BB value for any drug, not only for those drugs that are easy to measure, those conditions which enabled measurement for all 45 compounds were considered most interesting.

Table III-2: Correlation coefficients between predicted and experimentally determined log BB values when using normal partial least-squares regression (PLS) or using leave-one-out cross-validation (LOOCV).

	Brij35 0.05 M	SDC 0.05 M	SDS 0.05 M	IAM 40 % MeOH	IAM 30 % MeOH	IAM 20 % MeOH	IAM 0 % MeOH	SDS + IAM 40 % MeOH	SDS + IAM 30 % MeOH
# compounds	43	36	45	45	45	39	45	45	45
R (PLS)	0.8387	0.9159	0.8866	0.8707	0.8737	0.8646	0.8744	0.8972	0.8981
R (LOOCV)	0.5069	0.6846	0.6962	0.6159	0.6303	0.5837	0.6500	0.6926	0.6933

Measurement for all 45 compounds was possible by use of SDS as surfactant on a C_{18} column or by use of the IAM.PC.DD2 column with DPBS buffer containing 30 or 40 % methanol. When using the IAM column, the correlation between experimental and predicted log BB values was somewhat higher when the mobile phase contained 30% methanol (R= 0.8737) in comparison with 40 % methanol (R= 0.8707). Use of PLS models built on extrapolation to 100 % aqueous somewhat improved the accuracy of prediction (R= 0.8744). These data therefore illustrate there is little benefit in retention factor extrapolation to 100 % aqueous mobile phase, which is a time-consuming procedure. Direct use of the 30 % or 40 % MeOH data enables construction of a suitable model when working with the IAM.PC.DD2 column. The highest applicable correlation measured was observed when using SDS as surfactant (R= 0.8866). The correlation between predicted and experimental log BB values with SDS as surfactant for the 45 solutes is shown in Figure III-2a. With the exception of a few outliers, the predicted log BB values for most compounds appear satisfactorily close to the experimentally determined values. The correlation improved even further when the results of MLC with SDS were combined with the IAM results obtained by use of 30 % or 40 % MeOH. This is logical, because the more variables available to work with, the better the PLS correlation that can be obtained.

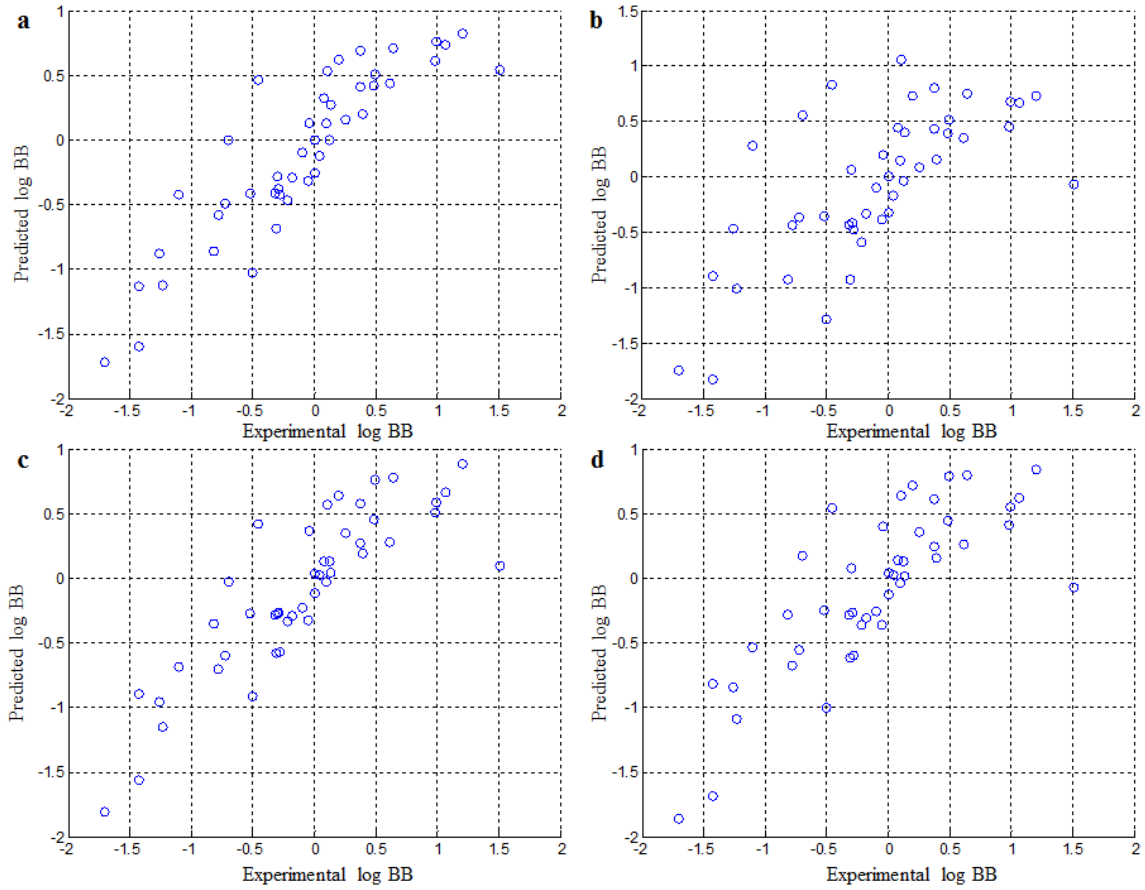

Figure III-2: Scatter plots comparing predicted log BB values with values determined experimentally by use of SDS as surfactant. Predicted log BB values are based on partial-least squares regression (**a**, **c**) or leave-one-out cross-validation (**b**, **d**). **C** and **d** were obtained after elimination of several variables from Table C-1.

Overfitting is an inevitable problem when the performance of multivariate calibration models is evaluated. An overfitted model usually has much a better regression performance on the training data set than on the test data set or the validation data set. To avoid overfitted models, crossvalidation methods are often used to detect the robustness of models. These methods include k-fold CV, twofold CV, random sub-sampling validation, and leave-one-out crossvalidation (LOOCV).

In this chapter, LOOCV was applied to the dataset. Fortyfour compounds were used as the training set and one compound as test sample. This procedure was repeated for each compound, enabling the construction of a new scatter plot; this is presented for SDS in Figure III-2b. The approach was repeated for each MLC and IAM method; the corresponding correlation coefficients are listed in Table III-2.

A relative large decrease of 0.2407, on average, in regression coefficients R is observed for all models when they are assessed in that way. In other words, the equations constructed for log BB prediction when the solutes are included, fit the training set in a much better way than is

the case when they are not included, which is typically regarded as indicative of overfitting. There are at least two major sources of overfitting. The first is related to use of a model which is too complex and has inferred too much (e.g. too many variables or other data) from the available training samples. Variable selection is one solutions used to solve this problem – unrelated variables are removed from the training data set, making the model more generalized for both training and test data sets. The second source is related to undersampling of the underlying distribution. In other words, the samples presented do not cover the major range of the underlying native distribution of samples. In this case, there is little that can be done unless more representative data or samples can be added to the model.

Therefore, variable selection was performed by systematic removal and/or reinsertion of all descriptors from the models while monitoring the effect on the LOOCV regression coefficients. This process was iteratively improved until maximum correlation was obtained for the LOOCV results. The maximum correlation was obtained when eight of the 15 descriptors, i.e. MW, MR, MV, Pr, log P, log D7.4, MI, and MIA, were removed from the model. The correlation coefficients for the simplified models are listed in Table III-3. Further descriptor removal led to a decrease in regression coefficients. For instance, when the log k descriptor was removed, regression coefficients for Brij35, SDC, and IAM with 20 % MeOH dropped to 0.6066, 0.6011, and 0.6494, respectively; for all other models (in which all 45 compounds were detected) the correlation coefficient dropped to 0.6378. This huge drop in regression coefficient illustrates why in vitro measurement of log k has a positive effect on experimental log BB prediction.

Table III-3: Correlation coefficients between predicted and experimentally determined log BB values when using normal partial least-squares regression (PLS) or using leave-one-out cross-validation (LOOCV) after elimination of eight variables (MW, MR, MV, Pr, log P, log D7.4, MI and MIA) from the model.

	Brij35 0.05 M	SDC 0.05 M	SDS 0.05 M	IAM 40 % MeOH	IAM 30 % MeOH	IAM 20 % MeOH	IAM 0 % MeOH	SDS + IAM 40 % MeOH	SDS + IAM 30 % MeOH
# compounds	43	36	45	45	45	39	45	45	45
R (PLS)	0.787	0.8862	0.8564	0.8602	0.8659	0.8389	0.8621	0.8825	0.8848
R (LOOCV)	0.662	0.7842	0.7993	0.7533	0.7724	0.7451	0.7831	0.7916	0.7982

On study of Table III-2 and III-3, two important differences can be noticed. On the one hand, the correlation coefficient of the PLS regression has dropped for each type of analysis. This is logical, because the PLS regression tries to fit the data as well as possible to an equation. The more variables available to work with, the better the correlations that can be obtained, though

this is mainly overfitting. On the other hand, the correlation coefficient after the leave-one-out cross-validation has significantly increased, demonstrating that the predictive capabilities of the different models have, indeed, been improved by applying this strategy.

As a result, the average difference between the PLS and LOOCV R values has dropped to 0.0928 in Table III-3. Compared with the average value of 0.2407 in Table III-2, this indicates that the model after variable selection is more generalized across the data sets and, therefore, enables more robust prediction. For analysis with IAM liquid chromatography (with 30 % or 40 % MeOH), the correlation increased from ±0.62 to ±0.76. A consequence is that the improved IAM model is now performing almost as well as the SDS-based model, illustrating that both approaches are commendable and applicable.

Note that the correlation coefficients for the other types of analysis (Brij35, SDC, and IAM with 20 and 0 % MeOH) are also substantially improved by applying this strategy. The correlation coefficient after leave-one-out cross-validation for 0 % MeOH IAM was even higher than for 30 % MeOH IAM. The values for 0 % MeOH were, however, obtained by extrapolation of the values for IAM with 20, 30, and 40 % MeOH, which means many measurements had to be taken to obtain a relatively small increase in the correlation coefficient. This is why emphasis in this work was set on the methods enabling straightforward detection of all 45 solutes (i.e. SDS MLC and 30 and 40 % MeOH IAM). In Figure III-2c, d, the SDS-based correlations between predicted and experimental log BB values are presented as scatter plots for the optimized models. Comparison of Figure III-2a, c (PLS) with Figure III-2b, d (LOOCV) enables visual assessment of the improvements in correlation achieved with the new SDS-based model. Analogous conclusions can be made for analysis with Brij35, SDC, or IAM liquid chromatography.

The coefficients of the equations obtained from PLS regressions that lead to the R values listed in Table III-3, are listed in Table III-4. The general equation for Table III-4 is: $predicted\ log\ BB = a + b \times \alpha + c \times Polarizability + d \times log\ WSo + e \times WS7.4 + f \times PB + g \times HIA + h \times log\ k_1\ (+ i \times log\ k_2)$.

As is apparent from Figure III-3, there are, inherently, various differences between MLC and IAM retention mechanisms. Both approaches emulate the blood–brain barrier in an interesting but different way. When a C_{18} column is used with a surfactant solution above the critical micellar concentration, retention of a compound depends both on its interactions with the modified reversed stationary phase and with the micelles present in the mobile phase (Figure III-3a).

Table III-4: Coefficients generated by PLS regression after elimination of several descriptors. The general equation for the predicted log BB values is: *log BB = a + b × α + c × Polarizability + d × log WSo + e × WS7.4 + f × PB + g × HIA + h × log k_1 (+ i × log k_2).*

	Brij35 0.05 M	SDC 0.05 M	SDS 0.05 M	IAM 40 % MeOH	IAM 30 % MeOH	IAM 20 % MeOH	IAM 0 % MeOH	SDS + IAM 40 % MeOH	SDS + IAM 30 % MeOH
a	-3.666	-3.800	-3.911	-3.039	-2.995	-2.809	-2.859	-3.350	-3.302
b	0.589	0.241	0.397	0.455	0.495	0.437	0.600	0.324	0.358
c	-0.039	-0.053	-0.050	-0.044	-0.051	-0.053	-0.069	-0.046	-0.051
d	0.099	0.063	0.080	0.155	0.152	0.146	0.133	0.146	0.144
e	-0.002	-0.003	-0.003	-0.003	-0.002	-0.002	-0.002	-0.003	-0.003
f	0.007	0.007	0.011	0.003	0.002	0.003	0.004	0.005	0.005
g	0.044	0.048	0.044	0.047	0.046	0.042	0.042	0.045	0.045
h	0.530	0.439	0.571	0.709	0.705	0.517	0.604	0.453	0.466
i	-	-	-	-	-	-	-	0.344	0.323

In addition, dynamic adsorption of a time-averaged fixed amount of surfactant monomers on the stationary phase also occurs, in this way giving rise to a stable modified column and regular retention behavior [24]. By contrast, when the IAM.PC.DD2 column is used, no micelles are present in the mobile phase, which means that interactions of compounds can only occur with the stationary phase (Figure III-3b). On the IAM.PC.DD2 column, phosphatidylcholine is covalently bonded to aminopropyl silica and endcapped with C_{10} and C_3 amides [8].

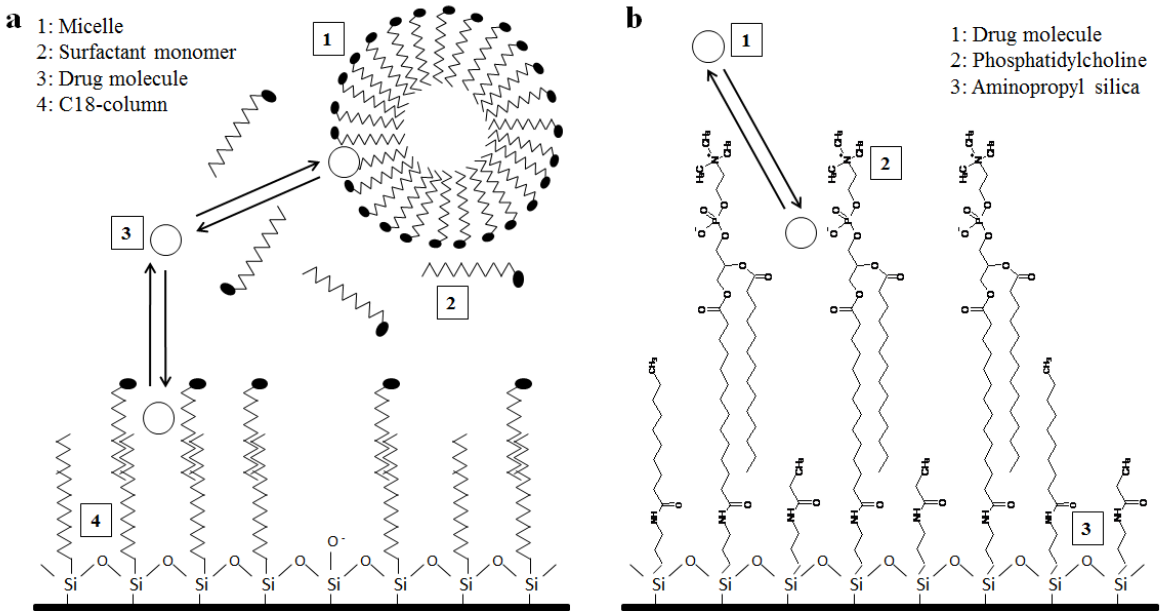

Figure III-3: Schematic representation of drug interactions in MLC (**a**) and in IAM liquid chromatography (**b**).

Because interactions on the C_{18} column and the IAM column are different, the corresponding solute retention factors also seem to be significantly different (Table III-1). Because of the

acceptable models which could be constructed by use of the individual MLC and IAM data, it was interesting to construct a model based on both datasets. Therefore, two extra PLS regressions were performed in which the log k values obtained by IAM liquid chromatography (with 40 and 30 % methanol) were added to the dataset obtained from MLC analysis with SDS.

It seemed that the corresponding correlation coefficients increased from 0.8564 (SDS, Table III-3) to 0.8825 (SDS + 40 % MeOH) and 0.8848 (SDS + 30 % MeOH), respectively, demonstrating the interesting potential of combining chromatographic data from orthogonal approaches for experimental data prediction. This was, however, not confirmed by leave-one-out cross-validation, in which correlation coefficients of these combinations decreased from 0.7993 (SDS, Table III-3) to 0.7916 and 0.7982, respectively. An obvious extra practical drawback of this strategy is that the combined approach increases the number of measurements required.

III.6 Conclusion

In this chapter, several in vitro methods for predicting the logarithm of blood–brain distribution coefficient (log BB) values were compared. MLC was performed on a C_{18} column with Brij35, SDC, and SDS as surfactants. IAM liquid chromatography was performed with methanol as organic modifier. SDS as a surfactant resulted in the best correlation coefficient between experimental and predicted log BB values (R = 0.7993), followed closely by IAM measurements using 30 % methanol (R = 0.7724). Combination of results from use of immobilized artificial membrane LC phases and micellar LC did not improve the accuracy of log BB prediction.

III.7 References

1. Katritzky AR, Kuanar M, Slavov S, Dobchev DA, Fara DC, Karelson M, Acree WE, Solov'ev VP, Varnek A (2006) Correlation of blood-brain penetration using structural descriptors. Bioorgan Med Chem 14 (14):4888-4917.

2. Fu XC, Wang GP, Shan HL, Liang WQ, Gao JQ (2008) Predicting blood-brain barrier penetration from molecular weight and number of polar atoms. Eur J Pharm Biopharm 70 (2):462-466.

3. Ruiz-Angel MJ, Garcia-Alvarez-Coque MC, Berthod A (2009) New Insights and Recent Developments in Micellar Liquid Chromatography. Sep Purif Rev 38 (1):45-96.

4. Mensch J, Oyarzabal J, Mackie C, Augustijns P (2009) In Vivo, In Vitro and In Silico Methods for Small Molecule Transfer Across the BBB. J Pharm Sci 98 (12):4429-4468.

5. Naik P, Cucullo L (2012) In vitro blood-brain barrier models: Current and perspective technologies. J Pharm Sci 101 (4):1337-1354.

6. Berthod A, Garcia-Alvarez-Coque MC (2000) Micellar Liquid Chromatography. Marcel Dekker Incorporated, New York

7. Cuenca-Benito M, Sagrado S, Villanueva-Camanas RM, Medina-Hernandez MJ (1998) Quantitative retention-structure and retention-activity relationships of barbiturates by micellar liquid chromatography. J Chromatogr A 814 (1-2):121-132.

8. Ong SW, Liu HL, Pidgeon C (1996) Immobilized-artificial-membrane chromatography: Measurements of membrane partition coefficient and predicting drug membrane permeability. J Chromatogr A 728 (1-2):113-128.

9. Yang CY, Cai SJ, Liu HL, Pidgeon C (1997) Immobilized artificial membranes - Screens for drug membrane interactions. Adv Drug Deliver Rev 23 (1-3):229-256.

10. Taillardat-Bertschinger A, Galland A, Carrupt PA, Testa B (2002) Immobilized artificial membrane liquid chromatography: proposed guidelines for technical optimization of retention measurements. J Chromatogr A 953 (1-2):39-53.

11. Verzele D, Lynen F, De Vrieze M, Wright AG, Hanna-Brown M, Sandra P (2012) Development of the first sphingomyelin biomimetic stationary phase for immobilized artificial membrane (IAM) chromatography. Chem Commun 48 (8):1162-1164.

12. Abraham MH, Chadha HS, Mitchell RC (1994) Hydrogen-Bonding .33. Factors That Influence the Distribution of Solutes between Blood and Brain. J Pharm Sci 83 (9):1257-1268.

13. Platts JA, Abraham MH, Zhao YH, Hersey A, Ijaz L, Butina D (2001) Correlation and prediction of a large blood-brain distribution data set - an LFER study. Eur J Med Chem 36 (9):719-730.

14. Escuder-Gilabert L, Molero-Monfort A, Villanueva-Camanas RM, Sagrado S, Medina-Hernandez MJ (2004) Potential of biopartitioning micellar chromatography as an in vitro technique for predicting drug penetration across the blood-brain barrier. Journal of Chromatography B-Analytical Technologies in the Biomedical and Life Sciences 807 (2):193-201.

15. Interactive PhysProp Database Demo. (2013) SRC Inc, Syracuse, N.Y. http://www.syrres.com/what-we-do/databaseforms.aspx?id=386. Accessed 31 Jan 2013

16. Ecker GF, Noe CR (2004) In silico prediction models for blood-brain barrier permeation. Curr Med Chem 11 (12):1617-1628.

17. Yan A, Liang H, Chong Y, Nie X, Yu C (2013) In-silico prediction of blood-brain barrier permeability. Sar Qsar Environ Res 24 (1):61-74.

18. Heberger K (2007) Quantitative structure-(chromatographic) retention relationships. J Chromatogr A 1158 (1-2):273-305.

19. Escuder-Gilabert L, Martinez-Pla JJ, Sagrado S, Villanueva-Camanas RM, Medina-Hernandez MJ (2003) Biopartitioning micellar separation methods: modelling drug absorption. Journal of Chromatography B-Analytical Technologies in the Biomedical and Life Sciences 797 (1-2):21-35.

20. Winiwarter S, Ax F, Lennernas H, Hallberg A, Pettersson C, Karlen A (2003) Hydrogen bonding descriptors in the prediction of human in vivo intestinal permeability. J Mol Graph Model 21 (4):273-287.

21. Borga M, Landelius T, Knutsson H (1997) A unified approach to PCA, PLS, MLR and CCA. Tech Rep, Number LiTH-ISY-R-1992, ISY, SE-581 83 Linköping, Sweden.

22. Escuder-Gilabert L, Sanchis-Mallols JM, Sagrado S, Medina-Hernandez MJ, Villanueva-Camanas RM (1998) Chromatographic quantitation of the hydrophobicity of ionic compounds by the use of micellar mobile phases. J Chromatogr A 823 (1-2):549-559.

23. Ruiz-Angel MJ, Carda-Broch S, Garcia-Alvarez-Coque MC (2013) Chromatographic Efficiency in Micellar Liquid Chromatography: Should it Be Still a Topic of Concern? Sep Purif Rev 42 (1):1-27.

24. Ruiz-Angel MJ, Carda-Broch S, Torres-Lapasio JR, Garcia-Alvarez-Coque MC (2009) Retention mechanisms in micellar liquid chromatography. J Chromatogr A 1216 (10):1798-1814.

Chapter IV. Development of the first Sphingomyelin biomimetic stationary phase for Immobilized Artificial Membrane Liquid Chromatography[5]

IV.1 Summary

A prototype sphingomyelin stationary phase for Immobilized Artificial Membrane (IAM) chromatography was synthesized by an ultra-short, solid-phase inspired methodology, in which an oxidative release monitoring strategy played a vital role. Evaluated in a proof-of-concept model for blood–brain barrier passage, partial least squares regression demonstrated its potential as an in vitro prediction tool.

IV.2 Introduction

As an innovative approach to liquid chromatography in which the stationary phase emulates the lipid environment of a cell membrane, the so-called Immobilized Artificial Membrane (IAM) technology offers an in vitro HPLC model of in vivo drug partitioning [1,2]. High-throughput and simple, the practical advantages of this chemical technique over more traditional biological methods are, however, affected by oversimplification and structural ambiguities in the small range of commercial, 'phosphatidylcholine-only' IAM columns such as **1** (Figure IV-1). Considering the mechanistic complexity of the in vivo uptake process [3],

[5] Published as: Verzele D, Lynen F, De Vrieze M, Wright AG, Hanna-Brown M, Sandra P (2012) Development of the first sphingomyelin biomimetic stationary phase for immobilized artificial membrane (IAM) chromatography. Chem Commun 48 (8):1162-1164.

alternative and more sophisticated IAM stationary phases are desired, the synthetic aspects need up-to-date revision, and assay correlations [4] should accordingly be improved.

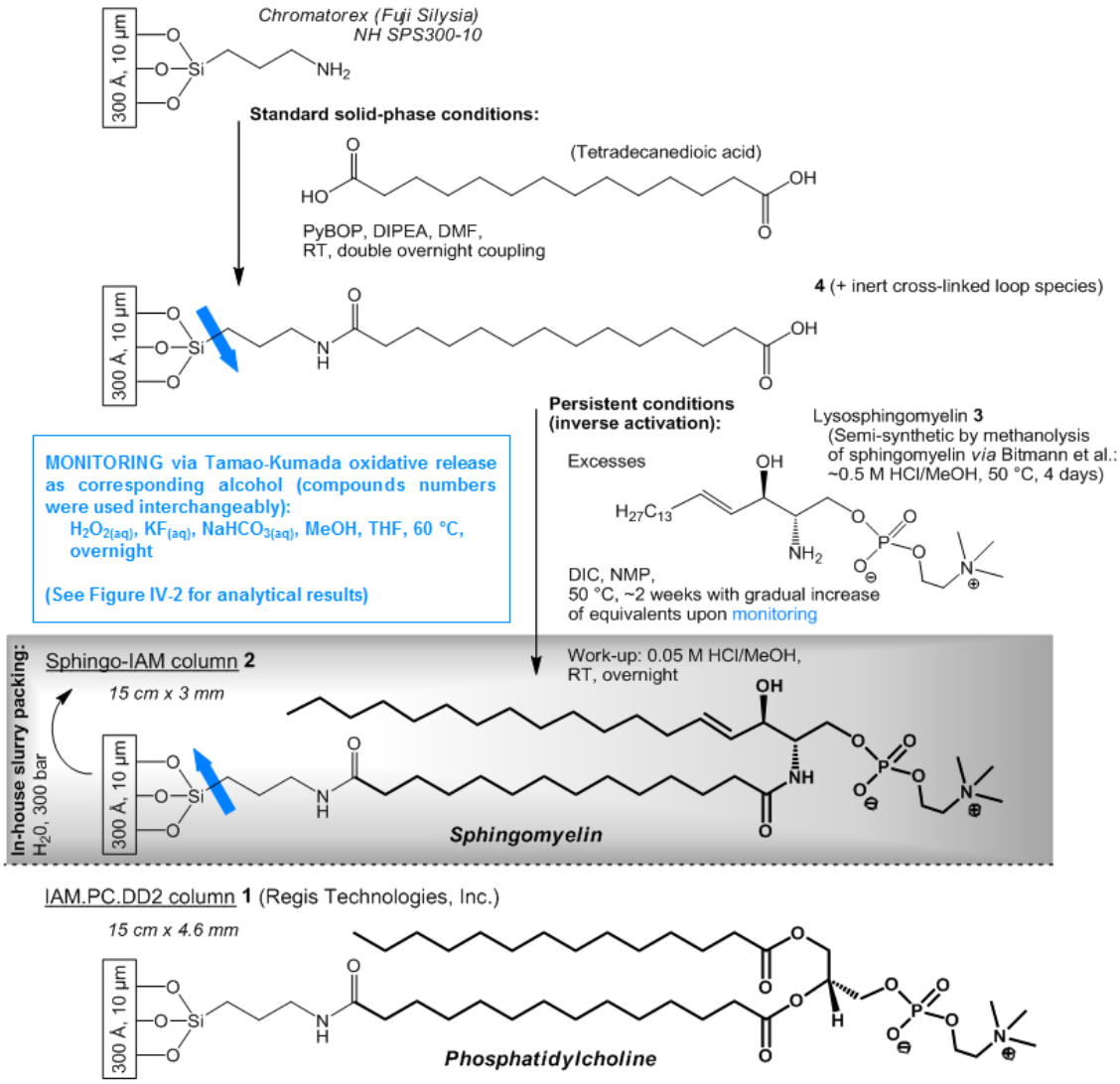

Figure IV-1: Synthesis and structure of Sphingo-IAM silica **2**, as counterpart of the commercial IAM.PC.DD2 reference **1** (Phosphatidylcholine.Drug Discovery 2nd generation).

The focus in this chapter is the development of a sphingomyelin [5,6] counterpart **2** (Figure IV-1) of the columns that are available so far. Useful as such in a broader synthetic context, an oxidative release monitoring strategy proved to be essential to achieve a straightforward, ultra-short synthesis of the desired silica material, while minimizing the aforementioned ambiguities. As such, this chapter provides the development and proof-of-concept evaluation of a prototype sphingomyelin stationary phase manufactured through an unprecedented, solid-phase inspired methodology, susceptible to mixed-phase approaches towards more genuine membrane mimics. To the best of our knowledge, neither such material for IAM

chromatography in particular nor such methodology for synthesis of dedicated stationary phases in general was previously reported.

IV.3 Materials and methods

IV.3.1 Chemicals

Test compounds were obtained from several sources: acetaminophen, acetylsalicylic acid, aminopyrine, amobarbital, antipyrine, carbamazepine, cimetidine, eserine, ethylbenzene, hexobarbital, ibuprofen, N-methyl-2-pyridineethanamine, omeprazole, oxazepam, pentobarbital, phenylbutazone, phenytoin, ranitidine, ropinirole, salicylic acid and toluene (Sigma–Aldrich, St Louis, MO, USA or Steinheim, Germany); indomethacin (Fluka, St Louis, MO, USA), and benzene (Acros, Geel, Belgium).

Products and solvents used for synthesis (Figure IV-1) were obtained from Sigma-Aldrich, except for the silica gel (Chromatorex NH SPS300-10; Fuji Silysia, Tokio, Japan) and sphingomyelin (egg source; Avanti Polar Lipids, Alabaster, AL, USA).

IV.3.2 Apparatus

IAM retention analysis was performed on an Alliance, Waters 2690 chromatograph (Milford, MA, USA) with a quaternary pump and an automatic injector. A Waters 2487 dual-wavelength absorbance detector was used. The detection wavelength was set between 210 nm and 300 nm, depending on the compound analyzed. Data acquisition and processing were performed with a PeakSimple Chromatography Data System (model 202) and PeakSimple software (SRI Instruments, Torrance, CA, USA). For IAM experiments, analysis was performed at 25 °C with a flow rate of 1 mL min^{-1} for the Regis IAM.PC.DD2 (10 µm, 150 mm×4.6 mm; Morton Grove, IL, USA) column, and a flow rate of 0.5 mL min^{-1} for the new Sphingo-IAM (150mm×3mm) column.

LC-MS runs were performed on an Agilent 1100 series HPLC (Agilent Technologies, Waldbronn, Germany) connected to an Agilent G1956B single quad Mass Spectrometer with ESI-ionization source. Data acquisition and processing were performed with Agilent B.01.03.SR2 chemstation software. A Phenomenex Luna C_{18} column (5 µm, 250 mm × 4.6 mm; Utrecht, The Netherlands) was used with a flow rate of 1 mL min^{-1} at 35 °C using a

gradient run going from 0 to 100 % ACN in 15 minutes and a 5 mM $NH_4OAc_{(aq)}$ solution. The injection volume was 5 µL.

IV.3.3 Experimental conditions

In this section, the detailed procedure for the preparation of the Sphingo-IAM column **2** is described, which involves coupling of lysosphingomyelin **3** to intermediate material **4**, and packing of the resulting silica **2** into a column. The intermediate silica material **4** (2.34 g, 0.137 mmol g^{-1}, 0.32 mmol) was weighed into a round-bottomed flask (100 mL), followed by the addition of lysosphingomyelin **3** (297.2 mg, 0.64 mmol, 2 eq.) and anhydrous NMP (16 mL). After complete dissolution of **3** and homogeneity of the silica suspension, the flask was flushed with argon and DIC (59.6 µL, 0.385 mmol, 1.2 eq.) was added. The resulting orange/yellowish opaque mixture was gently agitated overnight at 50 °C. By successively adding reagents and solvent upon evaluation of several Tamao–Kumada samples (see next paragraph), a total of 38 equivalents DIC and 6 equivalents lysosphingomyelin were eventually reacted in 23 mL of total NMP volume over a period of 2 weeks, yielding complete conversion as shown in LC-MS results (Figure IV-2). The resulting silica was isolated and purified by filtration over a nylon-66 membrane (0.45 µm pores) under reduced pressure and washed with NMP, MeOH and Et_2O to give an orange/brownish filtrate. The off-white silica was dried for 3 hours at 70 °C and carefully transferred to a round-bottomed flask (100 mL). Finally, the material was gently treated overnight at room temperature with a methanolic HCl solution (20 mL, 50 mM, pH 2) under an argon atmosphere as described. The above filtration, washing (MeOH, ACN, THF, $CHCl_3$ and Et_2O) and transfer procedure was repeated to yield the white Sphingo-silica **2** (1.8325 g) upon careful drying under high vacuum. This material (1.5037 g) was suspended in water (7 mL) and the resulting slurry packed (300 bar) in an HPLC column (15 cm × 3 mm) for subsequent proof-of-concept IAM-evaluation (Figure IV-3).

Monitoring via Tamao–Kumada oxidative release of silica samples: by means of a glass pipette, an aliquot (500 µL) of the above silica suspension was withdrawn from the reaction flask. The above filtration, washing (NMP, MeOH, ACN, $CHCl_3$ and Et_2O) and transfer procedure was repeated to obtain a silica sample in a small pressure tube. Upon adding equal volumes (215 µL) of THF, MeOH, $NaHCO_3$ (aq,sat), KF (aq,sat) and H_2O_2 (35% aq), the resulting white, heterogeneous mixture was gently stirred overnight at 60 °C. The tube was cautiously opened, followed by the above filtration and washing (MeOH, THF and EtOH)

procedure to its content. Collected in a roundbottomed flask (250 mL), the colourless filtrate was concentrated under reduced pressure at 40 °C, and the wax-like, opaque/whitish residue dried under high vacuum. Upon redissolution in MeOH, a sample was prepared for analysis.

IV.3.4 Data Sources, software, and processing

A total of 23 values of the logarithm of brain–blood distribution coefficients (log BB) were collected [7-9]. The experimental values of log BB ranged between −1.42 and 0.61. Values of acidity constants were obtained from Refs. [10,11] or were calculated. The acidity constants were used to calculate the total molar charge (α) values at pH 7.4. Structural data (molecular weight (MW), molar refractivity (MR), molar volume (MV), parachor (Pr), and polarizability) were calculated by use of ACD/Chemsketch software. Other data (log P, log D7.4, intrinsic aqueous solubility (log WSo), pH solubility profile (WS7.4), plasma protein binding (PB), Ames test mutagenic index (MI and MIA), and human intestinal absorption (HIA)) were predicted by use of Chemsilico prediction software (Chemsilico free trial version). The values for these can be found in Table C-1 (Appendix C). The experimental retention factors (k) are listed in Appendix D. All retention data are averages from triplicate determination. Microsoft Excel (Microsoft Corporation, v. 2007) and Matlab (version 7.12) were used to perform statistical analysis of the results.

IV.4 Results and discussion

As depicted in Figure IV-1, target material **2** was assembled on a similar carrier and through the same linker chemistry in order to allow direct comparison to state-of-the-art IAM.PC.DD2 (reference) column **1**, pioneered by Pidgeon et al. already more than two decades ago [1,12]. In this approach, gram quantities of the precious [13] lysosphingomyelin (D-erythro-sphingosylphosphorylcholine) building block **3** could be semi-synthetically prepared by chemical means through methanolysis of sphingomyelin, adapted from Bittman et al. [14]. Through merger of the lysosphingomyelin amine functionality and the immobilized fatty acid linker **4** in this N-deacylation/reacylation strategy, the complete sphingomyelin molecule is reconstituted while being anchored to the silica particles.

As such, the aminopropyl silica carrier is regarded from a solid-phase point of view, with its typical merits. However, the so-called black-box character of this approach challenged the

aim to ensure proper stationary phase integrity, and possible cross-link formation by reacting a symmetrical C_{14}-diacid linker prompted a critical evaluation of the coupling outcome. Neither qualitative efforts by malachite green colour testing [15] or infrared (HATR, DRIFT, 2D mapping) measurements, nor quantitative HR-MASNMR experiments provided consistent clues [16], let alone conclusive data on the amount of available COOH moieties and/or cross-linked species. Yet fortunately, Tamao–Kumada (TK) oxidative release of the attached molecules from a silica sample, recently disclosed by Komba et al. [17], solved this issue. By mild oxidation of the Si–C bond (Figure IV-1), analytical aliquots are readily available for standard solution phase evaluation of the generated alcohols, which conveniently increase the compatibility of the hydrophobic lipid species with reversed-phase and mass spectrometry techniques. This procedure provides reaction monitoring without the need for interfering cleavage handles.

A 42/58 COOH/cross-link ratio was derived from LC-MS data (Figure IV-2a) after standard PyBOP-mediated coupling (equimolar, double treatment overnight), with an apparently negligible/inconsistent influence of equivalent ratios during further attempts. As N-cap moieties with fatty acid character, these inert cross-links resemble features of the IAM.PC.DD2 column **1**, and allow steps to follow, direct and optimize reaction progress of the subsequent coupling as a reference LC-MS signal.

Demanding because of its inverse nature (activated COOH species on support instead of in solution) yet delicate because of its straightforwardness, proper introduction of unprotected lysosphingomyelin **3** onto silica intermediate **4** (Figure IV-1) indeed succeeded due to the LC-MS monitoring, possible through the Tamao–Kumada protocol. Prior stability testing confirmed the resistance of the sphingomyelin amide over a phosphatidylcholine ester to Tamao-Kumada conditions, the latter one being completely hydrolyzed overnight. Further agreeing with the (lyso)sphingomyelin and strategic choice, N-acylation is likewise favoured over O-acylation upon proper activation, and quantitative DIC-mediated [18,19] conversion was achieved by gradual increase of reagent equivalents upon careful monitoring, as confirmed in Figure IV-2b (see section IV.3.3). NMP proved thereby mandatory for dissolution of building block **3**, despite literature precedents and an initial preference for $CHCl_3$ in regard to supposed sidereactions and selectivity [19,20]. Neither the cross-links (which are dimensionally expected to form loops) nor the silica carrier prevented diffusion or reaction, provided 300 Å material is used, which is in line with the above choices and the commercial IAM.PC.DD2 column **1**.

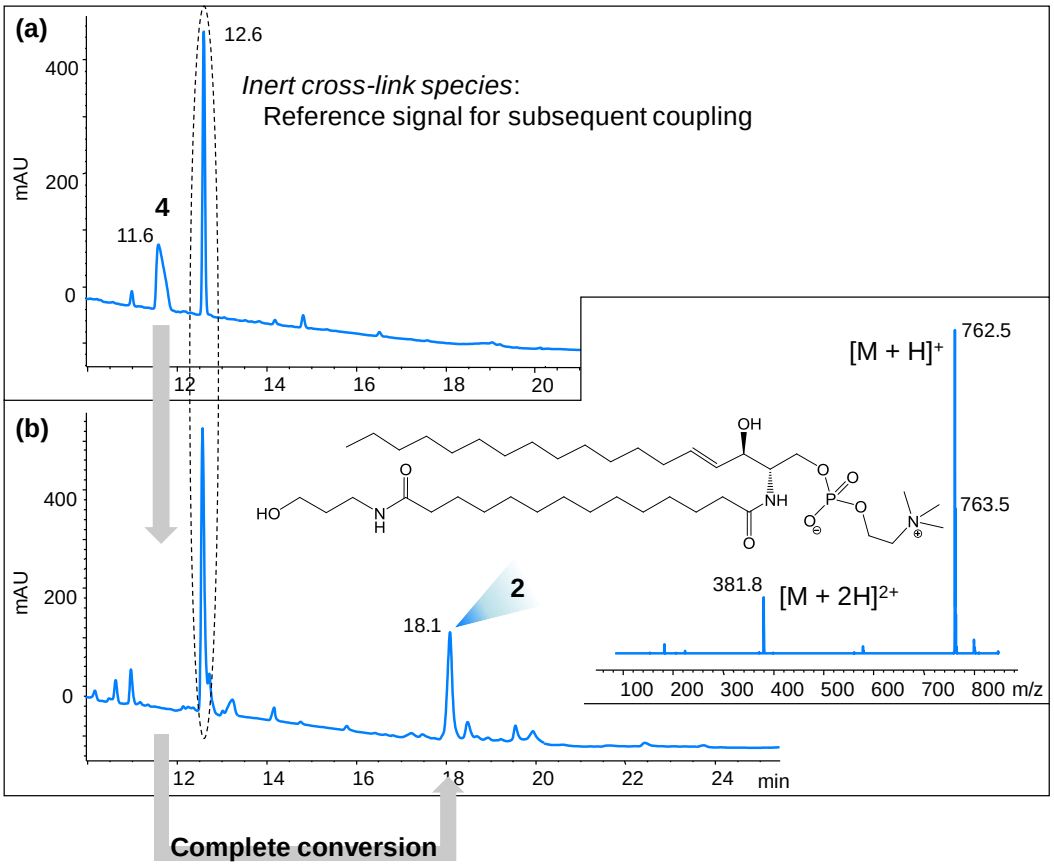

Figure IV-2: LC-MS (0 – 100 % ACN vs. 5 mM $NH_4OAc_{(aq)}$ in 15 min 1 mL/min; C_{18}-100 Å, 25 cm × 4.6 mm; 214 nm) results for the Tamao–Kumada sample of (a) intermediate material **4**, and (b) final Sphingo-IAM silica **2** (ESI+, Exact mass 761.6 Da).

To correct for remaining traces of unreacted COOH intermediate **4** and the presence of labile or miscoupled species, a finishing methylation/methanolysis under mild conditions was felt worthwhile in order to further strive for minimal ambiguities. As such, free, O-acylated, activated or anhydride linker species are all capped/converted to the corresponding methyl ester, whereas possible esters formed during linker coupling are discarded from residual silanol groups. Attention should be paid to the shielding effect of such species during subsequent lysosphingomyelin reaction, which should conveniently serve as protecting group for potentially interfering silanol moieties. The presence of free silanols in the ester-based phosphatidylcholine reference column **1** [21], with apparently no further end-capping efforts, should be noted. However, both these silanol functionalities and residual aminopropyl groups are buried in the bulky surrounding of the immobilized lipids, which tends to minimize retention biases as stated in the literature [1,2]. A ninhydrin, TNBS and chloranil [22] negative result for the amine moieties after linker/cross-link introduction must thereby further be noted. The methylation/methanolysis step should enhance the stability of the sphingomyelin amide, column lifetime and reliability.

In a proof-of-concept evaluation through comparative assessment with IAM.PC.DD2 column **1**, the new stationary phase **2** passed exploratory correlation studies as an in vitro prediction tool (Figure IV-3; see Appendix D for details). As mentioned above, structural similarities between both phases allow for direct comparison and facilitate the investigation of the role of the lipid component in the observed tendencies. After in-house slurry packing of the synthesized material into an HPLC column, a selection of 23 small molecules relevant in drug discovery was eluted under typical isocratic IAM conditions [23], and flow rates adjusted to compensate for varying column diameters. The covalently fixed IAM monolayer thereby mimicked the phospholipid bilayer to be crossed for uptake, so that chromatographic partitioning (expressed by partition coefficient K_{IAM}) corresponded to cellular diffusion. Experimental retention factors k_{IAM} were calculated from retention time measurements and included as a parameter in a prediction model for in vivo Blood–Brain (BB) passage [10]. Similar PLS regression results between the novel Sphingo-IAM prototype **2** and reference column **1** form the basis for the profound study in chapter V.

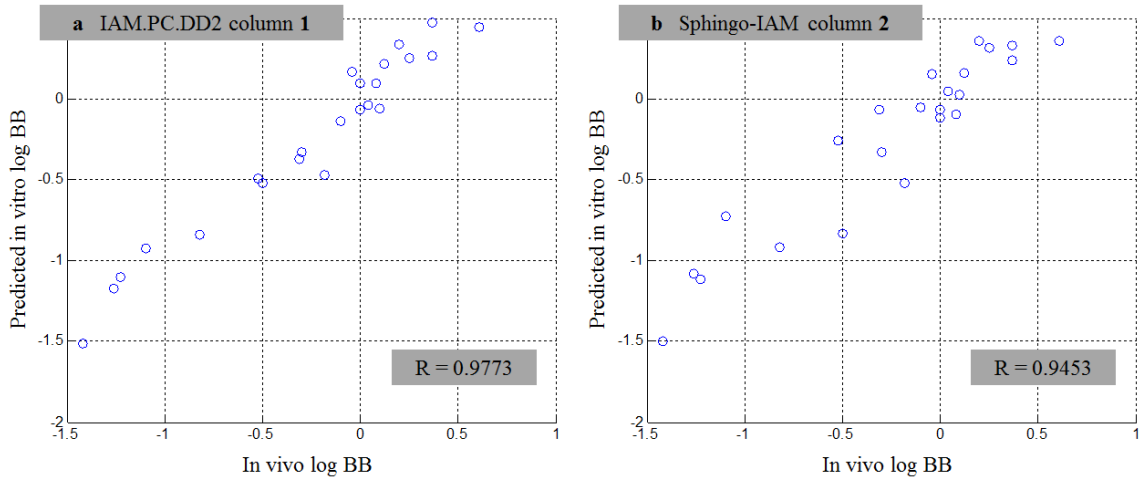

Figure IV-3: Proof-of-concept evaluation by PLS regression (see Appendix D for details), correlating in vivo log BB data of 23 small molecules with predicted in vitro model values involving experimental retention factors k_{IAM} from (**a**) IAM.PC.DD2 column **1** and (**b**) Sphingo-IAM column **2**.

IV.5 Conclusion

In this chapter, a new sphingomyelin-based IAM stationary phase was created for which proof-of-concept correlation studies were performed; extended correlation studies are presented in the next chapter. As an important constituent of eukaryotic plasma membranes [5,6] in general, interesting behavior is anticipated for the sphingomyelin lipid. Tuning of the

synthetic route should give access to a repertoire of further IAM silicas, combinations thereof and mixed-phase materials [24] with enhanced integrity. With some additional effort, throughput, reliability and predictability [25] of IAM chromatography could be improved.

IV.6 References

1. Yang CY, Cai SJ, Liu HL, Pidgeon C (1997) Immobilized artificial membranes - Screens for drug membrane interactions. Adv Drug Deliver Rev 23 (1-3):229-256.

2. Taillardat-Bertschinger A, Carrupt PA, Barbato F, Testa B (2003) Immobilized artificial membrane HPLC in drug research. J Med Chem 46 (5):655-665.

3. Sugano K, Kansy M, Artursson P, Avdeef A, Bendels S, Di L, Ecker GF, Faller B, Fischer H, Gerebtzoff G, Lennernaes H, Senner F (2010) Coexistence of passive and carrier-mediated processes in drug transport. Nat Rev Drug Discov 9 (8):597-614.

4. Valko K (2004) Application of high-performance liquid chromatography based measurements of lipophilicity to model biological distribution. J Chromatogr A 1037 (1-2):299-310.

5. Ramstedt B, Slotte JP (2002) Membrane properties of sphingomyelins. Febs Lett 531 (1):33-37.

6. Futerman AH, Hannun YA (2004) The complex life of simple sphingolipids. Embo Rep 5 (8):777-782.

7. Katritzky AR, Kuanar M, Slavov S, Dobchev DA, Fara DC, Karelson M, Acree WE, Solov'ev VP, Varnek A (2006) Correlation of blood-brain penetration using structural descriptors. Bioorgan Med Chem 14 (14):4888-4917.

8. Abraham MH, Chadha HS, Mitchell RC (1994) Hydrogen-Bonding .33. Factors That Influence the Distribution of Solutes between Blood and Brain. J Pharm Sci 83 (9):1257-1268.

9. Platts JA, Abraham MH, Zhao YH, Hersey A, Ijaz L, Butina D (2001) Correlation and prediction of a large blood-brain distribution data set - an LFER study. Eur J Med Chem 36 (9):719-730.

10. Escuder-Gilabert L, Molero-Monfort A, Villanueva-Camanas RM, Sagrado S, Medina-Hernandez MJ (2004) Potential of biopartitioning micellar chromatography as an in vitro technique for predicting drug penetration across the blood-brain barrier. Journal of Chromatography B-Analytical Technologies in the Biomedical and Life Sciences 807 (2):193-201.

11. Interactive PhysProp Database Demo. (2013) SRC Inc, Syracuse, N.Y. http://www.syrres.com/what-we-do/databaseforms.aspx?id=386. Accessed 31 Jan 2013

12. Pidgeon C, Venkataram UV (1989) Immobilized Artificial Membrane Chromatography - Supports Composed of Membrane-Lipids. Anal Biochem 176 (1):36-47.

13. Sigma-Aldrich [S4257]: € 504/25 mg. Compared to Sphingomyelin from Avanti Polar Lipids, Inc. [860061P]: 400 USD/1 g.

14. Bittman R, Verbicky CA (2000) Methanolysis of sphingomyelin: toward an epimerization-free methodology for the preparation of D-erythro-sphingosylphosphocholine. J Lipid Res 41 (12):2089-2093.

15. Attardi ME, Porcu G, Taddei M (2000) Malachite green, a valuable reagent to monitor the presence of free COOH on the solid-phase. Tetrahedron Lett 41 (38):7391-7394.

16. Kohler J, Chase DB, Farlee RD, Vega AJ, Kirkland JJ (1986) Comprehensive Characterization of Some Silica-Based Stationary Phases for High-Performance Liquid-Chromatography. J Chromatogr 352:275-305.

17. Terauchi T, Machida S, Komba S (2010) A new method for cleavage of silicon-carbon linkers on glass plate supports with applications to solid-phase syntheses on silica resins. Tetrahedron Lett 51 (11):1497-1499.

18. Morigaki E, Nagao M, Miura Y, Takahata K, Tada M, Nakajima S, Baba N, Shimizu S (1998) Syntheses of sphingomyelins and ceramides bearing a docosahexaenoyl or arachidonoyl group. Biosci Biotech Bioch 62 (10):2070-2072.

19. Sripada PK, Maulik PR, Hamilton JA, Shipley GG (1987) Partial Synthesis and Properties of a Series of N-Acyl Sphingomyelins. J Lipid Res 28 (6):710-718.

20. Balcom BJ, Petersen NO (1989) Solvent Dependence of Carboxylic-Acid Condensations with Dicyclohexylcarbodiimide. J Org Chem 54 (8):1922-1927.

21. Lazaro E, Rafols C, Roses M (2008) Characterization of the acidity of residual silanol groups in immobilized artificial membranes. J Chromatogr A 1182 (2):233-236.

22. Gaggini F, Porcheddu A, Reginato G, Rodriquez M, Taddei M (2004) Colorimetric tools for solid-phase organic synthesis. J Comb Chem 6 (5):805-810.

23. Braddy AC, Janaky T, Prokai L (2002) Immobilized artificial membrane chromatography coupled with atmospheric pressure ionization mass spectrometry. J Chromatogr A 966 (1-2):81-87.

24. Pidgeon C, Ong S, Choi HS, Liu HL (1994) Preparation of Mixed-Ligand Immobilized Artificial Membranes for Predicting Drug-Binding to Membranes. Anal Chem 66 (17):2701-2709.

25. Sprunger L, Blake-Taylor BH, Wairegi A, Acree WE, Abraham MH (2007) Characterization of the retention behavior of organic and pharmaceutical drug molecules on an immobilized artificial membrane column with the Abraham model. J Chromatogr A 1160 (1-2):235-245.

Chapter V. Evaluation of sphingomyelin, cholester and phosphatidylcholine based immobilized artificial membrane liquid chromatography to predict drug penetration across the blood-brain barrier[6]

V.1 Summary

In this chapter, the sphingomyelin column created in chapter IV and a cholester column are tested towards their ability to predict drug penetration across the blood-brain barrier. Upon comparison with the phosphatidylcholine stationary phase, the sphingomyelin and cholester based columns depict similar predictive performance. Combining data from the different stationary phases did not lead to improvements of the models.

V.2 Introduction

In general, the BBB restricts the diffusion of both small molecules and larger objects (for example bacteria) into the cerebrospinal fluid (CSF). When the blood-brain barrier is studied, the extent of BBB-permeation is expressed as the ratio of the steady-state concentration of the substance in the brain to the concentration in blood, usually called log (C_{brain}/C_{blood}) or log BB [1,2].

In vitro chromatographic models have been suggested for modeling of BBB-permeation, since they mimic the lipid environment of the barrier by dynamically or covalently immobilizing

[6] Published as: De Vrieze M, Verzele D, Szucs R, Sandra P, Lynen F (2014) Evaluation of sphingomyelin, cholester, and phosphatidylcholine-based immobilized artificial membrane liquid chromatography to predict drug penetration across the blood-brain barrier. Anal Bioanal Chem 406 (25):6179-6188

structures on a column. The affinity of the solutes for the immobilized phase is then combined with physicochemical data or molecular descriptors for optimal model construction.

IAMLC is one of the most commonly used in vitro chromatographic models for the prediction of log BB values [3,4]. IAMLC follows an approach whereby the lipid environment of a cell membrane is mimicked by anchoring synthetic phospholipid analogues at monolayer density to silica particles. These particles are subsequently used as column packing material for HPLC [3,5,6]. Thanks to the work of Pidgeon et al. [7], this type of stationary phase was introduced about 20 years ago. Although some research was conducted towards the use of mixed ligands [8], this methodology never really gained foothold. Eventually, only PC-coated particles became available in commercial columns. Usually, IAMLC is combined with UV detection, analyzing a single compound each run. Therefore, throughput for drug discovery applications is not very high. However, the use of a volatile buffer (e.g. ammonium acetate) allows coupling with atmospheric pressure ionization mass spectrometry, which provides the possibility for simultaneous determination of retention factors and, therefore, an increased throughput.

Methanol and acetonitrile are the most popular co-solvents in HPLC. Their use in the extrapolation of log k_{IAM} values has been studied with an IAM.PC.DD2 column [6]. The conclusion was that methanol is more appropriate for obtaining the log k_{IAM} values of charged compounds, since its solvent properties are closer to the properties of water. Furthermore, when acetonitrile is used, mobile phases containing more than 30 % (w/w) must be avoided since their microheterogeneity disrupts the structure of water [9].

IAMs are interesting because of their capacities for the prediction of drug partitioning into biological membranes. Next to a comparative study between MLC and IAMLC [10] (chapter III), a new sphingomyelin stationary phase for IAMLC was recently developed [11] (chapter IV). In this chapter, a total of 49 compounds with known log BB values were selected for comparative in vitro IAMLC measurements. The compounds were analyzed on three different lipid-like IAM-columns, namely the commercial IAM.PC.DD2-column (DD2 = drug discovery 2nd generation), the in-house synthesized Sphingo-IAM-column [11] (Sphingo = sphingomyelin; chapter IV), and an alternative commercial Cholester-column. To the best of our knowledge, the last two types of columns have not yet been tested as alternatives for the IAM.PC.DD2-column. The aim of this chapter is to obtain a full comparison regarding the potential of these IAM phases to predict log BB values.

V.3 Materials and methods

V.3.1 Chemicals

The analytes were obtained from several sources: 2,2,2-trifluoroethyl vinyl ether, 2,6-diisopropylphenol, acetaminophen, acetylsalicylic acid, aminopyrine, amitriptyline, amobarbital, antipyrine, atenolol, caffeine, carbamazepine, chlorambucil, chlorpromazine, cimetidine, clonidine, cotinine, desipramine, domperidone, eserine, ethylbenzene, fluphenazine, haloperidol, halothane, hexobarbital, hydroxyzine, ibuprofen, imipramine, mianserin, N-methyl-2-pyridineethanamine, omeprazole, oxazepam, pentobarbital, phenylbutazone, phenytoin, promazine, propranolol, pyrilamine, quinidine, ranitidine, ropinirole, salicylic acid, theobromine, theophylline, toluene, valproic acid, verapamil and zidovudine were obtained from Sigma–Aldrich (Steinheim, Germany); indomethacin was purchased from Fluka (St Louis, MO, USA), and benzene came from Acros (Geel, Belgium).

V.3.2 Apparatus

The IAM retention analysis was performed on an Alliance, Waters 2690 chromatograph (Milford, MA, USA) with a quaternary pump and an automatic injector. A Waters 2487 dual-wavelength absorbance detector was used, for which the detection wavelength was set between 210 nm and 300 nm, depending on the analyzed compound (the exact wavelengths are presented in Table C-2; Appendix C). The data acquisition and processing were performed with a PeakSimple Chromatography Data System (model 202) and PeakSimple software (SRI Instruments, Torrance, CA, USA). IAM experiments were respectively performed on an IAM.PC.DD2 (10 μm, 150 mm×4.6 mm; Regis Technologies, Morton Grove, IL, USA), a Cosmosil Cholester (5 μm, 250 mm×4.6 mm; Nacalai Tesque, San Diego, CA, USA) and a Sphingo-IAM (150 mm×3.0 mm; [11]) column. Analysis was performed at 25 °C with a flow rate of 1 mL min^{-1}, except for the Sphingo-IAM-column, where the flow rate was set to 0.5 mL min^{-1}.

V.3.3 Mobile phase and sample preparation

The IAM mobile phases consisted of different ratios of methanol (HPLC-grade; Biosolve, Valkenswaard, The Netherlands) and Dulbecco’s phosphate-buffered saline (DPBS). 30

volume% of methanol was added to the mobile phase when the IAM.PC.DD2- or the Sphingo-column was used; the methanol content was increased to 50 volume% using the Cholester-column. The DPBS consisted of 2.7 mmol L^{-1} KCl, 1.5 mmol L^{-1} KH_2PO_4, 137 mmol L^{-1} NaCl, and 8.1 mmol L^{-1} Na_2HPO_4 (Sigma-Aldrich). The pH of the mobile phase, which was altered by addition of methanol, was adjusted to 7.4 by use of H_3PO_4 (Sigma-Aldrich). Before use, all mobile phases were vacuum-filtered through 0.20 μm nylon membranes (Grace Davison, Lokeren, Belgium).

Stock solutions of all drugs were prepared by dissolving 10 mg in 1 mL methanol, except for quinidine and theobromine, for which stock concentrations of 1 mg mL^{-1} and 200 μg mL^{-1} were used; caffeine and theophylline, which were dissolved in water (10 mg mL^{-1}); and domperidone, which was dissolved in dimethyl sulfoxide (10 mg mL^{-1}). Working solutions were prepared by dilution of the stock solutions (to 50 μg mL^{-1}) with mobile phase.

V.3.4 Data sources, software, and processing

A total of 49 actual (= in vivo determined) log BB values were collected from literature [12-14]. The actual values of log BB (Table C-2) ranged between −1.70 and 1.51. Values of acidity constants (not shown in Table C-2) were obtained from Refs. [15,16] or were calculated by ChemSilico prediction software (ChemSilico free trial version). The acidity constants were used to calculate the total molar charge (α) values at pH 7.4. These α values, which can be positive or negative, were calculated as in Ref. [17]. Structural data (molecular weight (MW), molar refractivity (MR), molar volume (MV), parachor (Pr), and polarizability) were calculated by use of ACD/Chemsketch software. Other data (log P, log D7.4, intrinsic aqueous solubility (log WSo), pH solubility profile (WS7.4), plasma protein binding (PB), Ames test mutagenic index (MI and MIA), and human intestinal absorption (HIA)) were predicted by use of ChemSilico prediction software. The experimental logarithms of the retention factors (log k) are listed in Table V-1. All retention data are averages from triplicate determinations. Matlab (version 7.13) was used to perform statistical analysis of the results.

Table V-1: Log k values of compounds measured on different IAM columns.[a]

No.	Compound	IAM.PC.DD2 30 % MeOH	Sphingo-IAM 30 % MeOH	Cholester 50 % MeOH
1	2,2,2-trifluoroethyl vinyl ether	0.095	0.210	0.573
2	2,6-diisopropylphenol	1.544	1.681	1.785
3	acetaminophen	-0.372	-0.261	-0.519
4	acetylsalicylic acid	-0.664	-0.131	-0.476
5	aminopyrine	-0.206	-0.082	0.011
6	amitriptyline	1.975	1.657	1.510
7	amobarbital	0.457	0.617	0.653
8	antipyrine	-0.368	-0.329	-0.273
9	atenolol	-0.206	-0.539	-0.767
10	benzene	0.338	0.530	0.834
11	caffeine	-0.590	-0.477	-0.262
12	carbamazepine	0.593	0.772	0.630
13	chlorambucil	0.793	1.000	1.947
14	chloropromazine	2.404	2.110	1.946
15	cimetidine	-0.145	-0.091	-0.221
16	clonidine	0.458	0.135	-0.061
17	cotinine	-0.711	-0.647	-0.644
18	desipramine	1.864	1.564	1.291
19	domperidone	2.042	1.837	1.468
20	eserine	0.355	0.238	0.096
21	ethylbenzene	0.994	1.139	1.462
22	fluphenazine	2.596	2.445	2.238
23	haloperidol	1.844	1.466	1.379
24	halothane	0.487	0.618	0.956
25	hexobarbital	0.253	0.433	0.518
26	hydroxyzine	1.800	1.741	1.693
27	ibuprofen	0.499	0.884	0.993
28	imipramine	1.838	1.524	1.403
29	indomethacin	1.061	1.462	1.372
30	mianserin	1.843	1.776	1.727
31	N-methyl-2-pyridineethanamine	-0.249	-0.373	-0.773
32	omeprazole	0.713	0.806	0.723
33	oxazepam	1.118	1.182	1.307
34	pentobarbital	0.489	0.647	0.668
35	phenylbutazone	0.477	0.931	0.678
36	phenytoin	0.761	0.981	0.635
37	promazine	2.035	1.708	1.465
38	propranolol	1.474	1.348	0.857
39	pyrilamine	1.132	0.974	0.652
40	quinidine	1.346	1.045	0.909
41	ranitidine	-0.045	-0.204	-0.386
42	ropinirole	0.385	0.166	0.180
43	salicylic acid	-0.656	-0.086	-0.490
44	theobromine	-0.932	-0.819	-0.744
45	theophylline	-0.621	-0.511	-0.355
46	toluene	0.683	0.942	1.171
47	valproic acid	-0.546	-0.112	0.319
48	verapamil	1.663	1.400	1.208
49	zidovudine	-0.482	-0.325	-0.155

[a] All log k data are averages from three analyses

V.4 Rationale

The accuracy of prediction of a model depends on the type of model selected, the relevance, diversity, orthogonality (independence) of the input variables and on the shortlist of those which have been retained after model optimization, the size of the training set, and the similarity of the test molecules to those in the training set.

The processing of QRAR and QSRR studies (whereby chromatographic retention data is used as an additional input in a model using mathematically processed descriptors) can be done with MLR, PCR, PLS and ANN methodologies.

Within the multivariate calibration family of algorithms, both MLR and PLS models have thus far been proposed for prediction of drug absorption for which mathematically generated descriptors are combined with retention data [18,15,19]. The performance of MLR is, however, significantly affected by the selected variables when they are strongly correlated. This problem is avoided in the PLS method, which finds a linear regression model by projecting y and X to a new space, where the projected original variables are transformed as latent variables in nomenclature. PLS regression is particularly suitable for problems when the number of samples is fewer than the number of independent variables and where there is probably a large correlation among X-values. Eventually, an equation of the type $y = b_0 + b_1 x_1 + b_2 x_2 + \ldots + b_n x_n$ is created, where y is the predicted (log BB) value, b_0−b_n are constants and x_1-x_n are variables (descriptors). Obtaining a suitable equation of this type is important for this type of work.

As the accuracy of the response (in this case log BB) of the model depends on both the choice and relevance of the used descriptors, use of solute retention data in the model is particularly attractive, because this represents the affinity of a compound in a column environment emulating the blood-brain barrier. Such chromatographic strategies are compared and evaluated in this chapter. All descriptors used in this chapter are listed in Table C-2. PLS models were constructed by use of retention data for 49 solutes for which actual log BB data are available together with the set of molecular descriptors mentioned above. The merits of each model were then compared.

V.5 Results and discussion

When an IAM-column is used, an organic modifier is usually added to the mobile phase since this is a requisite for solute elution. The logarithms of the retention factors (log k) measured

on the different columns by use of DPBS and methanol in the mobile phase are listed in Table V-1. On the Cholester-column, some solutes were excessively retained when 30 % methanol was used and were no longer detected under those conditions. Therefore, measurements were made with 50 % methanol on this column. According to Taillardat-Bertschinger et al. [6], an extrapolation to 100 % aqueous phase is required to enable comparison of retention factors irrespective of the amount and type of organic co-solvent. Extrapolation also avoids the use of fictitious interaction scales because of the differences in the elution order which occur at different percentages of co-solvent. However, extrapolations were not performed here since Detroyer et al. [20] indicated that extrapolation is not necessary when measurable k-values can be obtained for all investigated compounds using only one mobile phase for each column. Furthermore, improvement towards log BB prediction that can be achieved when using extrapolations to 0 % organic co-solvent have been shown to be close to negligible [10].

Figure V-1 illustrates the dissimilarity in retention behavior of compounds on the different stationary phases by comparing the chromatograms obtained for clonidine (a, b and c), halothane (d, e and f) and ibuprofen (g, h and i).

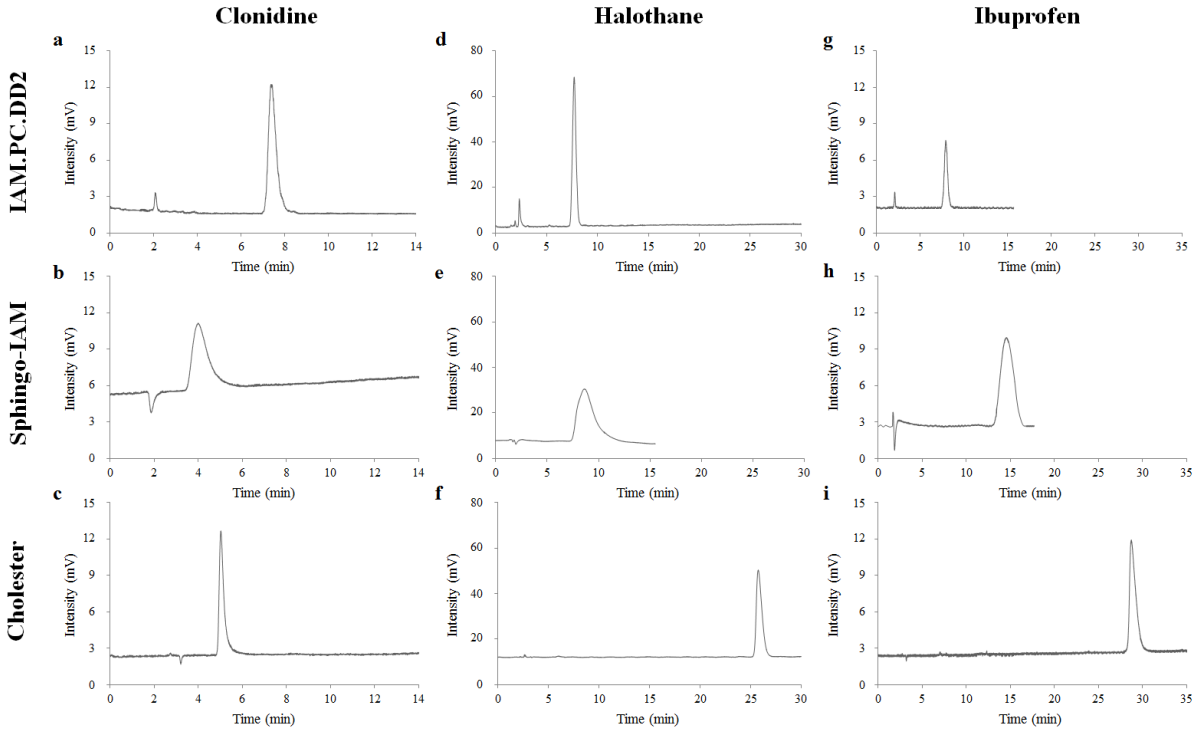

Figure V-1: Chromatograms obtained for clonidine (**a**, **b**, and **c**), halothane (**d**, **e**, and **f**), and ibuprofen (**g**, **h**, and **i**). Chromatograms (**a**, **d**, and **g**), (**b**, **e**, and **h**), and (**c**, **f**, and **i**) were, respectively, obtained on the IAM.PC.DD2-, Sphingo-IAM-, and Cholester-column.

The upper chromatograms (a, d and g) were obtained on the IAM.PC.DD2-column, the central chromatograms (b, e and h) originate from the Sphingo-IAM-column, and the lower chromatograms (c, f and i) were obtained on the Cholester-column. The elution order of the compounds varies, indicating the effect of the different stationary phases.

V.5.1 Prediction of log BB

Partial least-squares (PLS) regression was subsequently performed to determine the correlation coefficients (R) between actual log BB values (Table C-2) and log BB values predicted by use of log k values together with the other descriptors mentioned in Table C-2. The correlation coefficients in Table V-2a enable comparison of the merits of the different columns. The lowest correlation coefficient (R = 0.8604) was obtained when the Cholester-column was used. The highest correlation coefficient (R = 0.8772) was obtained with the IAM.PC.DD2-column. The correlation between predicted and actual log BB values on the IAM.PC.DD2-column is illustrated in Figure V-2a. Except for a few outliers, the predicted log BB values appear sufficiently close to the actually determined values for most compounds.

Table V-2: Correlation coefficients between predicted and experimentally determined log BB values when using normal partial least-squares regression (PLS) or using leave-one-out cross-validation (LOOCV) (**a**) and these correlation coefficients after elimination of 11 variables (MW, MR, MV, Polarizability, Log P, Log D7.4, Log WSo, WS7.4, PB, MI, and MIA) from the model (**b**)

		IAM.PC.DD2	Sphingo-IAM	Cholester
a				
	R(PLS)	0.8772	0.8701	0.8604
	R(LOOCV)	0.6231	0.6064	0.5620
b				
	R(PLS)	0.8542	0.8429	0.8303
	R(LOOCV)	0.8129	0.7994	0.7750

Overfitting is an inevitable problem when the performance of multivariate calibration models is evaluated. To avoid overfitted models, crossvalidation (CV) methods are often used to detect the robustness of models. These methods include k-fold CV, twofold CV, random sub-sampling validation, and leave-one-out crossvalidation (LOOCV) [21].

In this chapter, LOOCV was applied to the dataset. In this method, 48 compounds were used as the training set and one compound as test sample. This procedure was repeated for each

compound, enabling the construction of a new scatter plot; this is presented for the IAM.PC.DD2-column in Figure V-2b. The approach was repeated for the two other columns; the corresponding correlation coefficients are listed in Table V-2a.

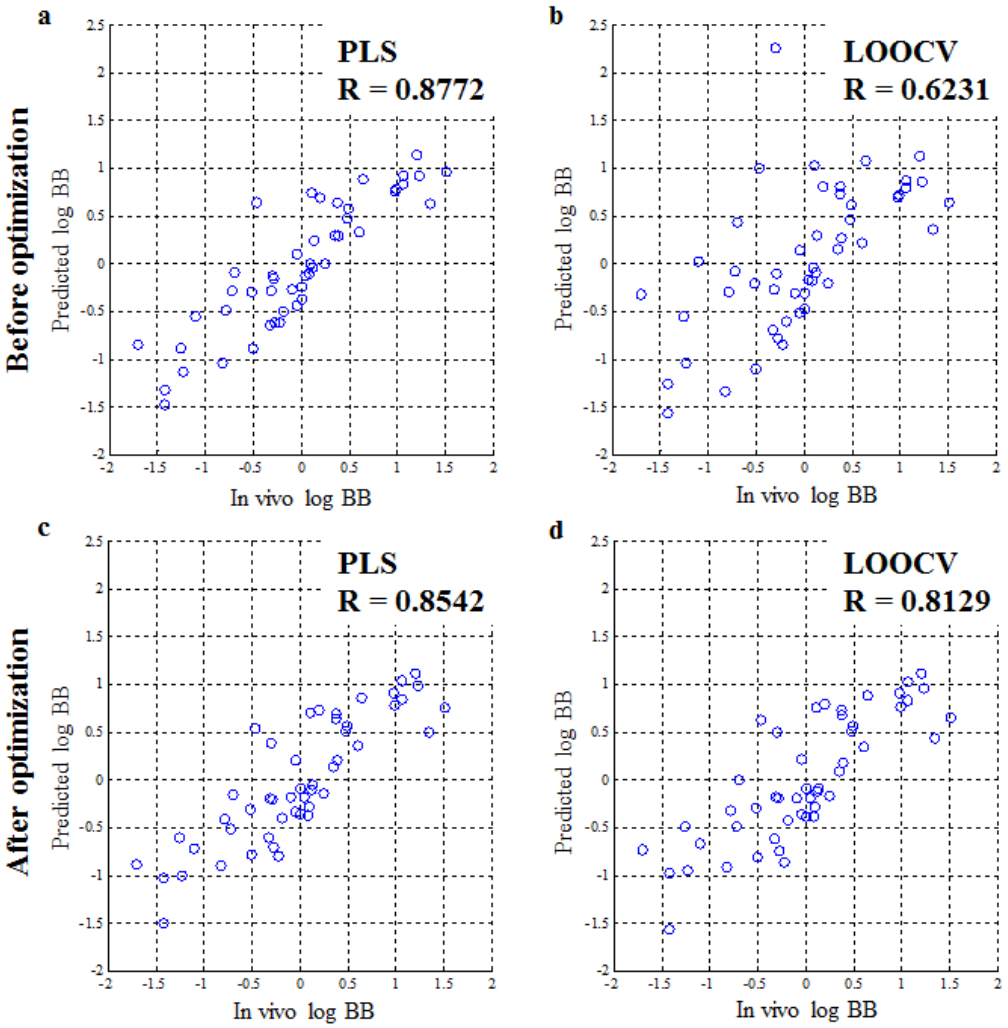

Figure V-2: Scatter plots comparing predicted log BB values with in vivo determined values based on retention factor measurements with an IAM.PC.DD2-column. Predicted log BB values are based on partial least-squares regression (**a** and **c**) or leave-one-out cross-validation (**b** and **d**); **c** and **d** were obtained after elimination of eleven descriptors from Table C-2.

A relatively large average decrease of 0.2721 in regression coefficient R is observed for all columns when they are assessed in that way. In other words, the equations constructed for log BB prediction when the solutes are included, fit the training set in a much better way than is the case when they are not included, which is typically regarded as an indication of overfitting. There are at least two major sources of overfitting. The first one is related to the use of a too complex model (e.g. too many variables or other data). Variable selection is one solution used to solve this problem, in which unrelated variables are removed from the

training data set. The second source is related to undersampling of the underlying distribution. In other words, the samples presented do not cover the major range of the underlying native distribution of samples. In this case, more representative data or samples should be added to the model.

In this chapter, variable selection was performed by systematic removal and/or reinsertion of all descriptors from the models while monitoring the effect on the LOOCV regression coefficients. This process was iteratively improved until maximum correlation was obtained for the LOOCV results. The maximum correlation was obtained when eleven out of fifteen descriptors, i.e. MW, MR, MV, Polarizability, Log P, Log D7.4, Log WS_o, WS7.4, PB, MI and MIA were removed from the model. The correlation coefficients for the simplified models are listed in Table V-2b. Further descriptor removal led to a decrease in regression coefficients. In Figure V-2c, d, the IAM.PC.DD2-based correlations between predicted and actual log BB values are presented as scatter plots for the optimized models. Comparison of Figure V-2a, c (PLS) with Figure V-2b, d (LOOCV) enables visual assessment of the improvements in correlation achieved with the new IAM.PC.DD2-based model. Analogous conclusions can be made for analysis on the two other columns.

To illustrate the importance of the in vitro measurements of log k values by IAMLC, variable selection was performed on the same set of descriptors except log k. Eventually, ten out of fourteen descriptors were removed from the model; only α, Pr, log P and HIA were retained. The obtained regression coefficients (identical for all three columns) dropped to 0.8053 (PLS) and 0.7508 (LOOCV). This drop in regression coefficient clearly illustrates that in vitro measurement of log k has a positive effect on the prediction of actual log BB values.

The coefficients of the equations obtained from PLS regressions that lead to the R values listed in Table V-2b, are listed in Table V-3. The general equation for Table V-3 is: $predicted\ log\ BB = a + b \times \alpha + c \times Pr + d \times HIA + e \times log\ k$. The coefficients obtained for the IAM.PC.DD2- and the Sphingo-IAM-column are similar, while these coefficients are somewhat different for the Cholester-column. This is an indication that the adsorption of compounds to the stationary phase is somewhat comparable for the IAM.PC.DD2- and the Sphingo-IAM-column. This makes sense, since both sphingomyelin and phosphatidylcholine have a polar phosphocholine headgroup and two apolar alkyl chains. The cholesterol bound at the cholester column has a completely different structure, which allows for another adsorption profile of the compounds and consequently other coefficients in Table V-3.

Table V-3: Coefficients generated by PLS regression after elimination of eleven variables. The general equation for the predicted log BB values is: $log\ BB = a + b \times \alpha + c \times Pr + d \times HIA + e \times log\ k$.

	IAM.PC.DD2	Sphingo-IAM	Cholester
a	-2.831	-2.750	-3.374
b	0.444	0.653	0.735
c	-0.003	-0.003	-0.002
d	0.042	0.039	0.044
e	0.703	0.706	0.629

When Tables V-2a and V-2b are compared, two important differences can be noticed. On the one hand, the correlation coefficient of the PLS regression has dropped for each type of analysis. This is logical, because the PLS regression tries to fit the data as well as possible to an equation. The more variables available to work with, the better the correlations that can be obtained, though this is mainly overfitting. On the other hand, the correlation coefficient of the leave-one-out cross-validation has significantly increased, demonstrating that the predictive capabilities of the different models have, indeed, been improved a lot by applying this strategy. As a result, the average difference between the PLS and LOOCV R values has dropped to 0.0467 in Table V-2b. Compared with the average difference of 0.2721 in Table V-2a, this indicates that the model after variable selection is more generalized across the data sets and, therefore, enables more robust prediction.

The final correlation coefficients range from 0.7750 to 0.8129 (Table V-2b). These are excellent values, taking into account that in vitro HPLC methods only allow for prediction of passive permeation of compounds across the BBB. Consequently, all three optimized models are now performing very good, illustrating that all three columns are appropriate for this kind of measurements.

Since all measured log k values contributed positively to the final correlation coefficients, the question also arose whether the combination of k or log k values could lead to an improved correlation coefficient. Therefore, several extra regressions were performed in which the obtained k or log k values for all column types (Table V-1) were combined into one new model with log k' values. The results of the PLS- and LOOCV-analyses are presented in Table V-4. In Table V-4a, log k' values were calculated by combining log k values; in Table V-4b, log k' values were calculated by taking the logarithm of combined k values. All obtained correlation coefficients are smaller than these of IAM.PC.DD2 in Table V-2b. Also, values in Table V-4 increase when the impact of IAM.PC.DD2 is increased and decrease

when the impact of Cholester is increased. For this set of columns, no improvement in correlation coefficients could be achieved through a combination of (log) k values.

Table V-4: Correlation coefficients between predicted and experimentally determined log BB values when using normal partial least-squares regression (PLS) or using leave-one-out cross-validation (LOOCV) after elimination of eleven variables from the model. Log k′ values were generated by combining log k values (**a**) or k values (**b**) as indicated.

a

	log k' = I+II+III	log k' = 2×I+II+III	log k' = I+2×II+III	log k' = I+II+2×III
R(PLS)	0.8485	0.8509	0.8479	0.8457
R(LOOCV)	0.8043	0.8077	0.8041	0.7994

I = log k values IAM.PC.DD2, II = log k values Sphingo-IAM, III = log k values Cholester

b

	log k' = log(IV+V+VI)	log k' = log(2×IV+V+VI)	log k' = log(IV+2×V+VI)	log k' = log(IV+V+2×VI)
R(PLS)	0.8393	0.8418	0.8396	0.8368
R(LOOCV)	0.7911	0.7947	0.7925	0.7865

IV = k values IAM.PC.DD2, V = k values Sphingo-IAM, VI = k values Cholester

V.6 Conclusion

As illustrated in chapter III, the IAM.PC.DD2 column is interesting for the prediction of drug partitioning into biological membranes. In this chapter, three IAM-columns were tested and their abilities towards prediction of log BB values were compared. The correlation coefficients between actual and predicted log BB values of the three corresponding models were very good; all three columns proved to be useful for this kind of prediction. The results obtained with the Sphingo-IAM-column proved to be similar to the commercial IAM.PC.DD2-column (this was also the case for the proof-of-concept correlation studies in chapter IV). As such, the Sphingo-IAM-column is a useful alternative for this kind of measurements. The Sphingo-IAM-column might also perform well at other application areas for which the IAM.PC.DD2-column is used, but this is a subject for other studies.

.

V.7 References

1. Fu XC, Wang GP, Shan HL, Liang WQ, Gao JQ (2008) Predicting blood-brain barrier penetration from molecular weight and number of polar atoms. Eur J Pharm Biopharm 70 (2):462-466.

2. Mensch J, Oyarzabal J, Mackie C, Augustijns P (2009) In Vivo, In Vitro and In Silico Methods for Small Molecule Transfer Across the BBB. J Pharm Sci 98 (12):4429-4468.

3. Yang CY, Cai SJ, Liu HL, Pidgeon C (1997) Immobilized artificial membranes - Screens for drug membrane interactions. Adv Drug Deliver Rev 23 (1-3):229-256.

4. Stewart BH, Chan OH (1998) Use of immobilized artificial membrane chromatography for drug transport applications. J Pharm Sci 87 (12):1471-1478.

5. Ong SW, Liu HL, Pidgeon C (1996) Immobilized-artificial-membrane chromatography: Measurements of membrane partition coefficient and predicting drug membrane permeability. J Chromatogr A 728 (1-2):113-128.

6. Taillardat-Bertschinger A, Galland A, Carrupt PA, Testa B (2002) Immobilized artificial membrane liquid chromatography: proposed guidelines for technical optimization of retention measurements. J Chromatogr A 953 (1-2):39-53.

7. Pidgeon C, Venkataram UV (1989) Immobilized Artificial Membrane Chromatography - Supports Composed of Membrane-Lipids. Anal Biochem 176 (1):36-47.

8. Pidgeon C, Ong S, Choi HS, Liu HL (1994) Preparation of Mixed-Ligand Immobilized Artificial Membranes for Predicting Drug-Binding to Membranes. Anal Chem 66 (17):2701-2709.

9. Marcus Y, Migron Y (1991) Polarity, Hydrogen-Bonding, and Structure of Mixtures of Water and Cyanomethane. J Phys Chem-Us 95 (1):400-406.

10. De Vrieze M, Lynen F, Chen K, Szucs R, Sandra P (2013) Predicting drug penetration across the blood-brain barrier: comparison of micellar liquid chromatography and immobilized artificial membrane liquid chromatography. Anal Bioanal Chem 405 (18):6029-6041.

11. Verzele D, Lynen F, De Vrieze M, Wright AG, Hanna-Brown M, Sandra P (2012) Development of the first sphingomyelin biomimetic stationary phase for immobilized artificial membrane (IAM) chromatography. Chem Commun 48 (8):1162-1164.

12. Platts JA, Abraham MH, Zhao YH, Hersey A, Ijaz L, Butina D (2001) Correlation and prediction of a large blood-brain distribution data set - an LFER study. Eur J Med Chem 36 (9):719-730.

13. Katritzky AR, Kuanar M, Slavov S, Dobchev DA, Fara DC, Karelson M, Acree WE, Solov'ev VP, Varnek A (2006) Correlation of blood-brain penetration using structural descriptors. Bioorgan Med Chem 14 (14):4888-4917.

14. Grumetto L, Carpentiero C, Barbato F (2012) Lipophilic and electrostatic forces encoded in IAM-HPLC indexes of basic drugs: Their role in membrane partition and their relationships with BBB passage data. Eur J Pharm Sci 45 (5):685-692.

15. Escuder-Gilabert L, Molero-Monfort A, Villanueva-Camanas RM, Sagrado S, Medina-Hernandez MJ (2004) Potential of biopartitioning micellar chromatography as an in vitro technique for predicting drug penetration across the blood-brain barrier. Journal of Chromatography B-Analytical Technologies in the Biomedical and Life Sciences 807 (2):193-201.

16. Interactive PhysProp Database Demo. (2013) SRC Inc, Syracuse, N.Y. http://www.syrres.com/what-we-do/databaseforms.aspx?id=386. Accessed 31 Jan 2013

17. Escuder-Gilabert L, Sanchis-Mallols JM, Sagrado S, Medina-Hernandez MJ, Villanueva-Camanas RM (1998) Chromatographic quantitation of the hydrophobicity of ionic compounds by the use of micellar mobile phases. J Chromatogr A 823 (1-2):549-559.

18. Escuder-Gilabert L, Martinez-Pla JJ, Sagrado S, Villanueva-Camanas RM, Medina-Hernandez MJ (2003) Biopartitioning micellar separation methods: modelling drug absorption. Journal of Chromatography B-Analytical Technologies in the Biomedical and Life Sciences 797 (1-2):21-35.

19. Winiwarter S, Ax F, Lennernas H, Hallberg A, Pettersson C, Karlen A (2003) Hydrogen bonding descriptors in the prediction of human in vivo intestinal permeability. J Mol Graph Model 21 (4):273-287.

20. Detroyer A, Heyden YV, Carda-Broch S, Garcia-Alvarez-Coque MC, Massart DL (2001) Quantitative structure-retention and retention-activity relationships of beta-blocking agents by micellar liquid chromatography. J Chromatogr A 912 (2):211-221.

21. Hawkins DM, Basak SC, Mills D (2003) Assessing model fit by cross-validation. J Chem Inf Comp Sci 43 (2):579-586.

Chapter VI. Investigation of the lipid composition of brain tissue

VI.1 Introduction

A striking difference regarding the in vitro research with IAM columns and MLC is the choice of the molecules used for emulation of the in vivo conditions. On IAM columns, phosphatidylcholine, cholesterol and sphingomyelin have been used (as described in chapter V) for the mimicking of the biological environment. Note that all these solutes are part of what is traditionally considered as the lipid family of molecules. With the MLC approach, surfactants – such as SDS, Brij35, CTAB and SDC – proved suitable to allow the prediction of in vivo log BB behavior, although they do not belong to the family of lipids. An overview of the lipid classes is given in Figure VI-1.

Although all IAM columns and MLC surfactants described in the previous chapters can be used for in vitro log BB prediction, their biological relevance might be disputable. It is well known that phospholipids are the main constituents of membranes, but they are certainly not the only constituents (e.g. proteins; see Figure II-3). This chapter will focus on the measurement of the actual composition of (phospho)lipids in (brain) membranes, which will allow a better choice of future MLC and IAM conditions for in vitro log BB prediction.

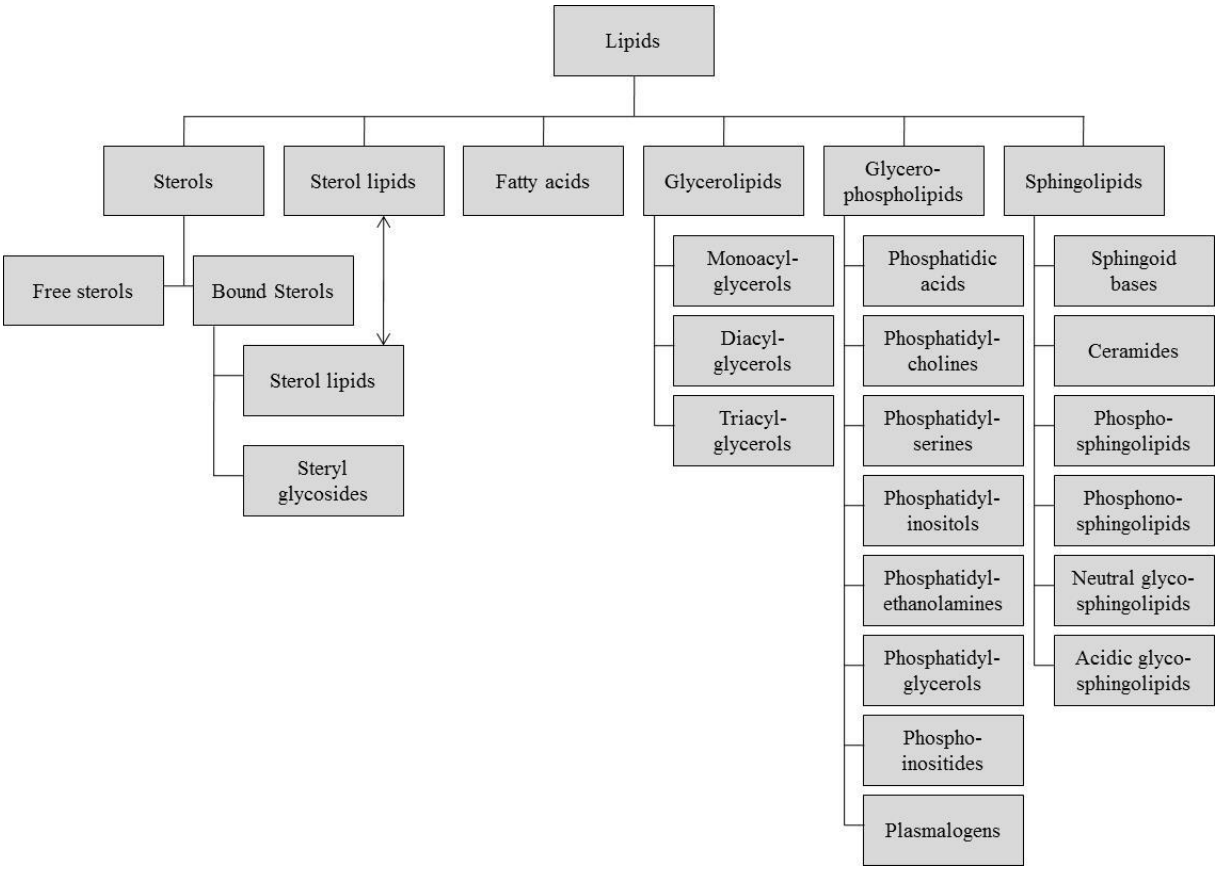

Figure VI-1: Overview of the different lipid classes. Based on [1].

Practically every class of lipids has its own specific functions, independent of participation in membrane formation or use as an energy source. For example, they are involved in the control of transcription and translation, cell signaling, and intercellular interactions. The largest number of lipids and their greatest diversity are commonly found in the most organized part of the body, the brain. This indicates the exceptional importance of these compounds for the specific functions of nervous tissue. The total mass of lipids accounts for 45-50 % of the dry weight of the adult brain [2,3]. Previous investigations have demonstrated that the total lipid content of human brain (on a wet weight basis) increases after birth up to an age of 30-40 years and slowly decreases in older individuals [4].

Membranes of the CNS are characterized by the greatest structural diversity relative to the lipid membranes of other organs, which consist primarily of a large number of molecular types of phospholipids. In addition to glycerophospholipids, which form the basis of biological membranes in all tissues, there are several types of specific lipids in the brain: cerebrosides, sulfocerebrosides, globosides, and gangliosides (all types of glycosphingolipids), whose quantity and structural diversity are typical only of this tissue. Different brain structures may be quite different from each other in their lipid compositions.

For example, the content of cholesterol in neuronal membranes is unusually high. The level of cholesterol is strictly regulated in the brain; cholesterol participates in the formation of lipid rafts and in the synthesis of important signaling molecules [2].

VI.2 Available extraction and identification protocols for the analysis of biological tissues

Based on the need to present a total overview of the lipid composition in membranes, several authors have presented methods for the extraction and/or quantification of (brain) lipids. Folch et al. [5] provided the first general method for the isolation and purification of lipids from animal tissues. In this method, a chloroform-methanol mixture was added to the tissue in order to dissolve the lipids. After filtering, water was added and a biphasic system was obtained. The lower phase (chloroform) contained almost all lipids and could subsequently be analysed.

Holčapek et al. [6-8] used a modified Folch procedure for the lipidomic profiling of biological tissues. A lot of effort was put in the optimization of the separation and quantification of lipid classes. Therefore, a comprehensive lipidomic analysis was created which enabled the quantification of all lipid classes by separation of the lipid classes in the first dimension – using hydrophilic interaction liquid chromatography (HILIC)-HPLC – and identification of the individual lipids in the second dimension – using RP-HPLC/MS.

Matyash et al. [9] developed a methyl-tert-butyl ether (MTBE) protocol and demonstrated that it provided similar or better recoveries for all major lipid classes compared to the Folch-method. In the lipid extraction protocol, methanol, MTBE and water were used. The extraction procedure used later in this chapter was based on this method. Since lipids dissolved in the upper phase (MTBE), pipetting became easier compared to the traditional Folch extraction. After lipid extraction, the lipid profiling was performed by quadrupole time-of-flight mass spectrometry (TOF-MS).

Abbott et al. [10] developed a high-throughput lipidomic analysis of human brain samples. MTBE was used for extraction with mechanical homogenization using ceramic beads. The easy pipetting of the MTBE phase allowed automation of the collection step. Most lipids were analyzed via electrospray ionization MS, sterols were analyzed using gas chromatography mass spectrometry. This high throughput method was considered to be an improved version

of the traditional Folch-method, since the same lipid species were found using the high throughput method. MTBE is also less toxic than chloroform.

VI.3 Literature overview of the lipid classes in brain tissue

The most frequently measured lipid classes in brain tissue are mentioned together with their structure in Table VI-1.

Table VI-1: Overview of the most frequently measured lipid classes in brain tissue and their structures. The fatty acid composition is not fixed, therefore, alkyl chains are indicated by R_1 and R_2.

Lipid class	Abbreviation	Structure
Cholesterol	C	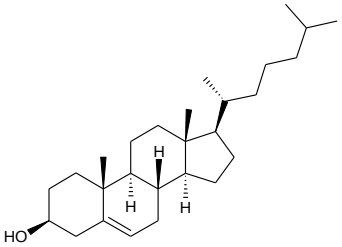
Phosphatidic acid	PA	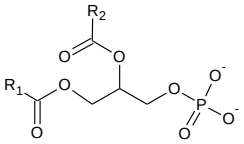
Phosphatidylcholine	PC	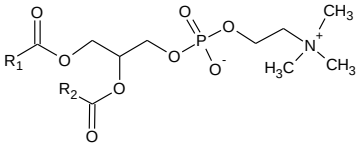
Lysophosphatidylcholine	LPC	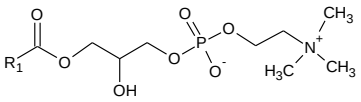
Phosphatidylethanolamine	PE	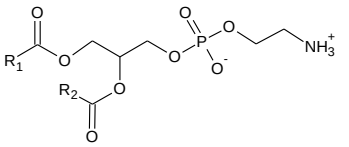
Lysophosphatidylethanolamine	LPE	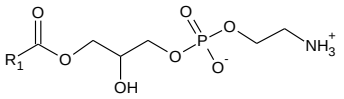
Phosphatidylglycerol	PG	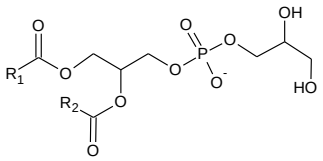
Phosphatidylinositol	PI	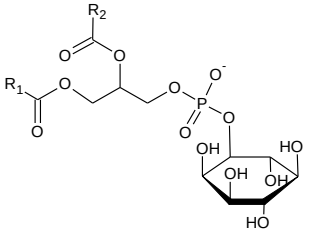
Phosphatidylserine	PS	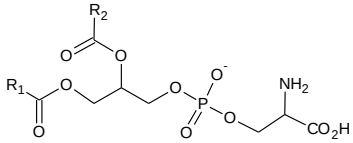
Sphingomyelin	SPM	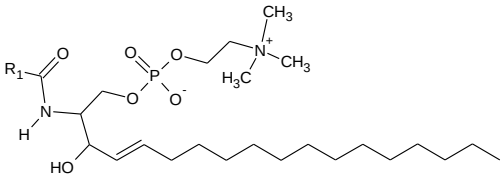

Table VI-2 shows a comparison of the abundances of different lipid classes in porcine, human and rat brain. Despite the differences in analytical methods and brain samples, the abundances are similar. According to this table, the two major lipid classes – PE and PC – account for more than 70 % of the total lipid fraction. When all porcine organs were compared [8], the relative abundance of PC is in the range 32-40 %, PE 26-35 %, SPM 5-19 %, PI up to 20 %, PS up to 13 %, LPE up to 8 %, LPC up to 7 %, and PG up to 5 %.

Table VI-2: Comparison of relative abundances (%) of individual lipid classes in the brain (porcine [8], human or rat [11]). Based on [8].

Lipid class	**Porcine** Relative abundance (%)	**Human** Relative abundance (%)	**Rat** Relative abundance (%)
PI	5.0	5.3	3.3
PE	34.3	37.6	37.6
LPE	2.3	0.0	1.4
PS	13.1	12.5	12.7
PC	37.1	37.6	36.9
SPM	7.3	1.9	4.8
LPC	0.9	0.0	1.5
Others	0.0	5.1	1.8

Table VI-3 shows a comparison of lipids present in porcine, mouse, rat, bovine and human brain endothelial cells (see Figure II-1).

Table VI-3: Comparison of lipid composition of brain endothelial cells (porcine [12], mouse [13], rat [14], bovine and human [15]). Based on [16].

Lipid class	**Porcine** (wt%)[a]	**Mouse** (wt%)[a]	**Rat** (wt%)[a]	**Bovine** (wt%)[a]	**Human** (wt%)[a]
PC	31.7	36.8	31.9	32.1	32.1
PE	25.2	23.4	24.4	23.9	24.5
PS	7.5	12.9	9.8	10.6	10.3
SPM	14.8	18.3	18.1	20.9	17.8
PI	6.1	8.4	[b]	4.5	4.9
PA	NA	NA	0.9	0.7	0.2
C	12.7	NA	NA	NA	NA
Others	2.0	0.2	14.9	7.3	10.2

[a] An average MW of 700 for phospholipids was used to convert mol% to wt%

[b] Included in SPM

Comparison of Table VI-3 with Table VI-2 is not straightforward, since some other lipid classes were measured and the values are expressed in wt%. It is, however, notable that the PC/PE ratio is different in these two tables; the SPM-content also seems to be strikingly different.

From the values presented in this Table VI-2 and VI-3, it can be concluded that it is very difficult to come up with an exact overview of lipid classes and their concentrations present in brain membranes. Differences between different species are obvious, but it is seldom taken into account that differences also arise in various sections of the brain (which will be illustrated in the next section of this chapter), between individuals and related to age [17].

Most authors are not only interested in the lipid classes present in biological tissue; also the carbon chain length of the fatty acids bound to these lipids (e.g. to the glycerol backbone in phospholipids) is very interesting [6-8,18,9,10]. One of the popular techniques to determine this, is a derivatization from the fatty acids to their corresponding fatty acid methyl esters (FAMEs), which easily allows their measurement. The obtained fatty acid composition is strongly dependent on the source of the lipids. A lot of variation can be found between different organs [8]. One general remark however, is that the fatty acids with 16 and 18 carbon atoms usually represent 70 % or more of the total fatty acid content.

VI.4 Determination of lipid classes in white and grey matter of newborn piglets

As mentioned in the section VI.3, the presence and concentration of lipid classes in various parts of the brain is divergent. Research of this type is normally performed on animals, since experimental use of human brain is strictly regulated. Because of the size of the brain, porcine and bovine brain tissue are the most convenient to work with.

The brain can be divided into areas of grey matter and areas of white matter, where grey matter has a darker color. Grey matter is involved in muscle control, and sensory perception such as seeing and hearing, memory, emotions, speech, decision making, and self-control, while white matter provides communication between different areas of grey matter within the CNS [19]. In this section, the lipid fractions of porcine white and grey matter are briefly re-analyzed and discussed. In-house available protocols were used for analysis to assess the scope and variability of the published data and to ascertain the relative order of the natural prevalence of brain lipid solutes in an experimental way. Only porcine tissue was used during experiments due to obvious ethical and availability issues.

VI.4.1 Experimental

VI.4.1.1 Chemicals

All solvents used were HPLC grade. Hexane was purchased at VWR (Leuven, Belgium). Isopropanol, dichloromethane, methanol, MTBE, acetic acid, formic acid, ammoniumacetate, triolein, oleic acid, cholesterol, dioleoylglycerol, 1-oleoyl-rac-glycerol, 1,2-dioleoyl-glycero-3-phosphoethanolamine, L-α-phosphatidylinositol, 1,2-diacyl-glycero-3-phospho-L-serine, 1,2-dioleoyl-glycero-3-phosphocholine and sphingomyelin were purchased from Sigma-Aldrich (St. Louis, MO, USA or Steinheim, Germany). Cholesteryloleate and L-α-lysophosphatidylcholine were respectively from Janssen (Beerse, Belgium) and Avantipolar Lipids (Alabaster, AL, USA).

VI.4.1.2 Sample preparation

Grey and white matter was dissected from the cerebrum of newly born piglets (< 24h). They were separately collected in cryotubes and frozen by liquid nitrogen, after which they were freeze-dried. Lipids were extracted using a procedure mainly based on Matyash et al. [9].

Extraction procedure: to a vial with 100 mg of sample, 1.5 mL of methanol was added after which the vial was put in an ultrasonic bath for 5 min. Then, 5 mL of MTBE was added and the mixture was incubated for 1 h at room temperature in a shaker. Phase separation was induced by adding 1.25 mL of water. Upon 10 min of incubation at room temperature, the sample was centrifuged at 1000 rpm for 10 min. The upper (organic) phase was collected and the lower phase was re-extracted with 3.3 mL MTBE/methanol (10:1, v/v). The combined organic phases were dried in an oven at 80 °C. The extracted lipids were dissolved in 8 mL of hexane/dichloromethane (3:1, v/v).

Different standards – including the most prominent lipids in membranes – were dissolved at a concentration of 100 µg/mL and subsequently used in the comparative study. Fatty acids (FA) were represented by oleic acid. Cholesterol (C) and cholesteryloleate (CO) were chosen as sterol lipids. Triolein, dioleoylglycerol, and 1-oleoyl-rac-glycerol represented respectively the triacylglycerols (TGs), diacylglycerols (DGs) and monoacylglycerols (MGs). Phosphatidylcholines (PCs) were represented by 1,2-dioleoyl-glycero-3-phosphocholine and L-α-lysophosphatidylcholine (LPC). Sphingomyelin (SPM) represented the phosphosphingolipids. Phosphatidylethanolamines (PEs), phosphatidylinositols (PI) and

phosphatidylserines (PSs) were respectively represented by 1,2-dioleoyl-glycero-3-phosphoethanolamine, L-α-phosphatidylinositol, and 1,2-diacyl-glycero-3-phospho-L-serine.

VI.4.1.3 HPLC conditions

Analyses were performed on an Alliance, Waters 2690 chromatograph. A Corona CAD-detector (ESA Analytical, Aylsbury, Buckinghamshire, England) was used for detection using a pressure of 35 psi and a detection range of 500 pA. Data acquisition and processing were performed with a PeakSimple Chromatography Data System (model 202) and PeakSimple software. A Princeton SFC diol column (5 µm, 250 * 4.6 mm) (Princeton, Cranbury, NJ, USA) was used for separation. Experiments were performed at room temperature with a flow rate of 0.5 mL/min. Injection volume was 20 µL. The mobile phase gradient is presented in Table VI-4.

Table VI-4: gradient used for lipid separation. Here, A is hexane/acetic acid (99.5:0.5, v/v); B is dichloromethane/isopropanol/acetic acid (49.75:49.75:0.5, v/v/v); C is isopropanol/buffer (20 mM ammoniumacetate at pH 3.5) (50:50, v/v); and D is isopropanol.

Time (min)	A	B	C	D
0	97	3	0	0
4	97	3	0	0
29	0	100	0	0
30	0	80	20	0
50	0	80	20	0
65	0	65	35	0
66	0	0	0	100
80	0	0	0	100
81	97	3	0	0
110	97	3	0	0

VI.4.2 Results and discussion

Results obtained by analysis of grey and white matter are presented in Figure VI-2. The method allows for separation of both ‘neutral’ (until 29 min in Table VI-4) and ‘polar’ (from 30 till 65 min in Table VI-4) lipid fractions. Although baseline separation was achieved for most compounds, PI and PS fractions could not be separated using this method.

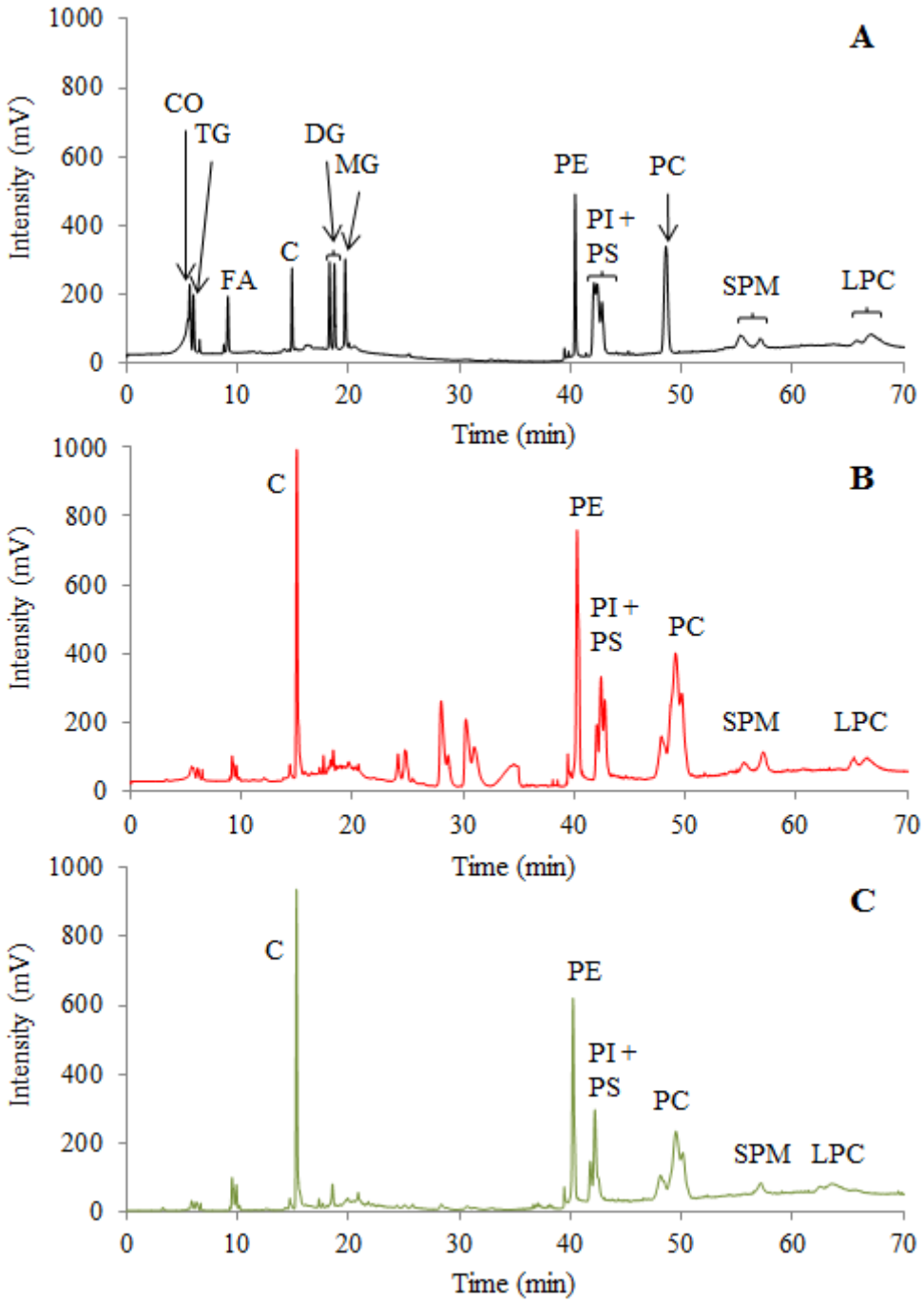

Figure VI-2: Analysis of white and grey matter using HPLC-CAD. Standards were injected to obtain chromatogram A, while B and C were respectively obtained after lipid extraction of the white and grey matter of the cerebrum. Experimental conditions, sample preparation and abbreviations are mentioned in section VI.4.1.

Several lipid standards (mainly DG, SPM and LPC, to a minor extent PI and PS) exhibit several peaks. For dioleoylglycerol (DG), this is explained by a slightly different retention profile of 1,2- and 1,3-substituted diglycerides. The other fractions – PI, PS, SPM and LPC – can show multiple peaks based on differences in fatty acid carbon chain length. As mentioned

in section VI.3, carbon chain lengths with 16 or 18 carbon atoms are the most abundant, although minor fractions of longer (and shorter) chains are also present.

In Figure VI-2 B and C, all the 'polar' lipid fractions (PE, PI, PS, PC, SPM and LPC) are clearly visible, although peak shapes and heights are not completely similar. This is already a first visual indication of differences in various sections of the brain. The PC fraction shows several peaks, which illustrates the different fatty acid carbon chain lengths in biological samples. The 'neutral' lipid fraction (until 29 min) is almost exclusively limited to cholesterol in the analysis of grey matter (Figure VI-2 C). The clearest visual indication of differences in Figure VI-2 B and C is the number of peaks from 23 to 35 min in Figure VI-2 B (white matter). Although peak identification could not be performed due to time constraints, these solutes appear in the zone where glycolipids (such as cerebrosides) are expected.

Next to the peak shapes, the relative peak areas (Table VI-5) were also somewhat divergent for lipid fractions of white and grey matter. Of course, this is mainly due to the high abundance of lipids between 23 and 35 minutes in the white matter of the brain (probably glycolipids; 28.1 %). However, even without considering these lipids, the relative peak areas of cholesterol, phosphatidylcholine, sphingomyelin and lysophosphatidylcholine in white matter (respectively 15.0, 41.1, 5.0 and 5.7 %) show quite some differences, which also illustrates the difference based on sampling area in the brain. In Table VI-5, the relative peak areas measured in this section are compared to the relative abundance of lipids in porcine brain. Peak areas can, however, not be translated into abundances without performing a quantification procedure (not performed due to time constraints), so comparison of the results is difficult here.

Table VI-5: Relative abundances (%) of individual lipid classes in porcine brain [8] and relative peak areas (%) of individual lipid classes in the white and grey matter of newborn piglets.

Lipid class	**Porcine**	**Porcine** White matter	**Porcine** Grey matter
	Relative abundance (%)	Relative peak area (%)	Relative peak area (%)
C	NA	10.8	19.5
PE	34.3	12.3	17.5
PI + PS	18.1	11.5	15.5
PC	37.1	29.6	36.9
SPM	7.3	3.6	2.7
LPC	0.9	4.1	7.9
Others	2.3	28.1	0.0

VI.5 Conclusion

In this chapter, a limited comparative study was performed with HPLC-CAD to visualize differences in the lipid composition of white and grey matter in newborn piglets in order to provide a better insight into the local lipid composition of the brain. Although the lipid profiles were comparable, several differences (e.g. the assumed presence of glycolipids) were found. It is challenging to create an exact overview of lipid classes and their concentrations in brain membranes, since differences arise not only between various sections of the brain, but also between species, individuals, and related to age.

Like the lipid classes, the carbon chain lengths of the fatty acid groups in lipids are not fixed. Fatty acids with 16 or 18 carbon atoms usually represent 70 % or more of the total fatty acid content. Therefore, the most representative examples of natural lipids depict a carbon chain length of 16 or 18 carbon atoms.

When the present lipid classes are compared to the use of MLC and IAMLC for in vitro log BB prediction, IAMLC (chapter V: stationary phases with phosphatidylcholine, sphingomyelin and cholesterol) is clearly based on a more realistic biomimicking system than MLC (chapter III: SDS, Brij35, CTAB, SDC, … as surfactants). The use of lipids in MLC would create a more realistic simulation of drug interactions in brain membranes. Therefore, this field is explored in more detail in chapter VII.

VI.6 References

1. Wenk MR (2005) The emerging field of lipidomics. Nat Rev Drug Discov 4 (7):594-610.

2. Galkina OV, Putilina FE, Eshchenko ND (2014) Changes in the lipid composition of the brain during early onthogenesis. Neurochem J 8 (2):83-88.

3. Summerfield SG, Dong KC (2013) In vitro, in vivo and in silico models of drug distribution into the brain. J Pharmacokinet Phar 40 (3):301-314.

4. Zhang YY, Appelkvist EL, Kristensson K, Dallner G (1996) The lipid compositions of different regions of rat brain during development and aging. Neurobiol Aging 17 (6):869-875.

5. Folch J, Lees M, Stanley GHS (1957) A Simple Method for the Isolation and Purification of Total Lipides from Animal Tissues. J Biol Chem 226 (1):497-509.

6. Lisa M, Cifkova E, Holcapek M (2011) Lipidomic profiling of biological tissues using off-line two-dimensional high-performance liquid chromatography mass spectrometry. J Chromatogr A 1218 (31):5146-5156.

7. Cifkova E, Holcapek M, Lisa M, Ovcacikova M, Lycka A, Lynen F, Sandra P (2012) Nontargeted Quantitation of Lipid Classes Using Hydrophilic Interaction Liquid Chromatography-Electrospray Ionization Mass Spectrometry with Single Internal Standard and Response Factor Approach. Anal Chem 84 (22):10064-10070.

8. Cifkova E, Holcapek M, Lisa M (2013) Nontargeted Lipidomic Characterization of Porcine Organs Using Hydrophilic Interaction Liquid Chromatography and Off-Line Two-Dimensional Liquid Chromatography-Electrospray Ionization Mass Spectrometry. Lipids 48 (9):915-928.

9. Matyash V, Liebisch G, Kurzchalia TV, Shevchenko A, Schwudke D (2008) Lipid extraction by methyl-tert-butyl ether for high-throughput lipidomics. J Lipid Res 49 (5):1137-1146.

10. Abbott SK, Jenner AM, Mitchell TW, Brown SHJ, Halliday GM, Garner B (2013) An Improved High-Throughput Lipid Extraction Method for the Analysis of Human Brain Lipids. Lipids 48 (3):307-318.

11. Pearce JM, Komoroski RA (2000) Analysis of phospholipid molecular species in brain by P-31 NMR spectroscopy. Magnet Reson Med 44 (2):215-223.

12. Tewes BJ, Galla HJ (2001) Lipid polarity in brain capillary endothelial cells. Endothelium-New York 8 (3):207-220.

13. Williams WM, Reichman M, Mcneill TH (1988) Cerebral Microvascular and Parenchymal Phospholipid-Composition in the Mouse. Neurochem Res 13 (8):743-747.

14. Selivonchick DP, Roots BI (1977) Lipid and Fatty Acyl Composition of Rat-Brain Capillary Endothelia Isolated by a New Technique. Lipids 12 (2):165-169.
15. Siakotos AN, Rouser G, Fleische.S (1969) Isolation of Highly Purified Human and Bovine Brain Endothelial Cells and Nuclei and Their Phospholipid Composition. Lipids 4 (3):234-239.
16. Di L, Kerns EH, Bezar IF, Petusky SL, Huang YP (2009) Comparison of Blood-Brain Barrier Permeability Assays: In Situ Brain Perfusion, MDR1-MDCKII and PAMPA-BBB. J Pharm Sci 98 (6):1980-1991.
17. Obrien JS, Sampson EL (1965) Lipid Composition of Normal Human Brain - Gray Matter White Matter and Myelin. J Lipid Res 6 (4):537-544.
18. Lofgren L, Stahlman M, Forsberg GB, Saarinen S, Nilsson R, Hansson GI (2012) The BUME method: a novel automated chloroform-free 96-well total lipid extraction method for blood plasma. J Lipid Res 53 (8):1690-1700.
19. Miller AKH, Alston RL, Corsellis JAN (1980) Variation with Age in the Volumes of Grey and White Matter in the Cerebral Hemispheres of Man - Measurements with an Image Analyzer. Neuropath Appl Neuro 6 (2):119-132.

Chapter VII. In vitro prediction of human intestinal absorption and blood–brain barrier partitioning: development of a lipid analog for micellar liquid chromatography[7]

VII.1 Summary

Over the past decades, several in vitro methods have been tested for their ability to predict either human intestinal absorption (HIA) or penetration across the blood–brain barrier (BBB) of drugs. Micellar liquid chromatography (MLC) has been a successful approach for retention time measurements of drugs to establish models together with other molecular descriptors. Thus far, MLC approaches have only made use of commercial surfactants such as sodium dodecyl sulfate (SDS) and polyoxyethylene (23) lauryl ether (Brij35), which are not representative for the phospholipids present in human membranes. Miltefosine, a phosphocholine-based lipid, is presented in this chapter as an alternative surfactant for MLC measurements. By using the obtained retention factors and several computed descriptors for a set of 48 compounds, two models were constructed: one for the prediction of HIA and another for the prediction of penetration across the BBB expressed as log BB. All data were correlated to experimental HIA and log BB values, and the performance of the models was evaluated. Log BB prediction performed better than HIA prediction, although HIA prediction was also improved a lot (from 0.5530 to 0.7175) compared to in silico predicted HIA values.

[7] Published as: De Vrieze M, Janssens P, Szucs R, Van der Eycken J, Lynen F (2015) In vitro prediction of human intestinal absorption and blood-brain barrier partitioning: development of a lipid analog for micellar liquid chromatography. Anal Bioanal Chem 407 (24):7453-7466

VII.2 Introduction

In modern drug design, the failure of many compounds in the development stage is caused by unfavourable absorption, distribution, metabolism, excretion, and toxicity (ADMET) properties. Therefore, a lot of effort is put into the field of ADMET predictions. Among these properties, good oral bioavailability is one of the most desirable aspects of a new drug. Significant effort is put in the prediction of HIA because the first step for obtaining a high oral bioavailability is to achieve a good oral absorption [1].

VII.3 In vivo behavior and in vitro prediction of human intestinal absorption

Unfavourable absorption, distribution, metabolism and excretion (ADME) properties have been identified as a major cause of failure for candidate molecules in the later stages of drug development. Therefore, there is significant interest in the early prediction of ADME properties, with the objective of increasing the success rate of compounds reaching the development stage [2]. ADME properties are difficult to model for several reasons. The quality of experimental data varies enormously and is often limited in quantity and chemical diversity. In addition, ADME properties such as oral bioavailability, human intestinal absorption (HIA) and metabolic stability arise from multiple physiological mechanisms, which make them difficult to model with traditional quantitative structure-activity relationship (QSAR) approaches [2].

A widely known ADME 'model' is Lipinski's 'rule of 5', which is used in the pharmaceutical industry to filter out compounds likely to be purely absorbed through the human intestine, based on four simple rules related to molecular properties [3]. The 'rule of 5' states that – except for compound classes that are substrates for biological transporters – poor absorption or permeation is more likely when:

- There are more than 5 H-bond donors (expressed as the sum of OHs and NHs)
- There are more than 10 H-bond acceptors (expressed as the sum of Ns and Os)
- The MW is over 500
- The Log P is over 5 (or MLogP is over 4.15)

Oral intake is the most commonly used route of drug administration and the most convenient for patients resulting in high therapy compliance. Orally administered drug compounds should possess biopharmaceutical properties that enable them to achieve therapeutic concentrations at their site of action. The absorption of orally administered drugs is complex and depends not

only on drug properties (e.g. aqueous solubility, molecular size, charge, dosage form, absorption enhancers, …), but also on physiological aspects (e.g. intestinal pH, disease state) and biochemical parameters (e.g. metabolism, efflux/uptake transporters) of the gastrointestinal tract [4]. Based on the fact that the majority of drugs are administered via the oral route, and that the first step for obtaining a high oral bioavailability is to achieve a good oral absorption, HIA is the most studied form of biological permeation, and significant effort is put in its prediction [1].

It is well known that the major absorption barrier to drugs taken orally is the intestinal mucosa membrane [5]. Some of the most important intestinal drug absorption processes are depicted in Figure VII-1. Molecules cross the intestinal epithelium by four main pathways. Firstly, by passive (transcellular) diffusion across the cell membranes, which involves mainly lipophilic compounds. Diffusion across the cell membranes and transcellular permeation through the cells constitute the most important mechanisms by which drugs cross biological membranes. Secondly, by carrier mediated transcellular transport (e.g. of ions, glucose, and amino acids). This is known as active transport and requires two sets of transport proteins in the plasma membrane. One on the apical side of the cells to transport molecules from the gut into the cell. The other in the basolateral surfaces of the cells to facilitate diffusion into the extracellular fluid. Active transport processes require specific binding of the drug to the transporter protein; some proteins (e.g. P-glycoprotein [6]) can cause efflux of a drug. The third mode of transport is a transcytosis (of high-molecular-weight substances, such as proteins), which could be apically taken into the cell by endocytosis, intracellularly transported to the other side of the cell via the transcytotic vesicles and then released to the basolateral space by exocytosis. Finally, the fourth mode of absorption is passive diffusion between adjacent cells, also called paracellular transport, mainly applicable to water-soluble low molecular weight compounds. Paracellular permeation is mainly governed by the size and the number of the pores between the cells, as well as the size and charge of the drug [7,8].

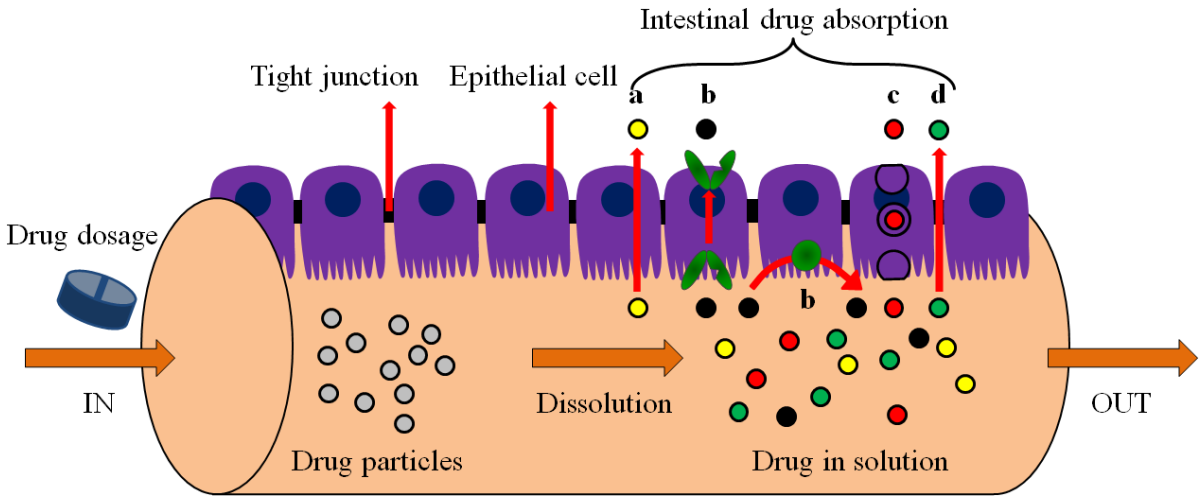

Figure VII-1: Schematic representation of the four main transport mechanisms of intestinal drug absorption. Hydrophobic substances can penetrate cell membranes and might be transported via the cells interior by **passive (transcellular) diffusion** (**a**); specific transporters mediate the transport of specific nutrients (= **carrier-mediated transport**) (**b**); macromolecules can be transported across the cells by **transcytosis** (**c**); and **paracellular transport** is associated with passive diffusion through the space between neighbouring cells of water soluble lowmolecular substances (**d**) (based on [4,8]).

The most important strategy of pharmaceutical industry to overcome its productivity crisis in drug discovery is to integrate early ADME profiling with toxicity (T) optimization in parallel with efficacy. Drug candidates with high potency at a single target and good ADMET profiles are widely recognised as having further opportunity for enhanced success in clinical trials [9].

To improve the prediction of human intestinal absorption, several in vivo [10,11], ex vivo (e.g. intestinal perfusion; everted gut sac experiments) and in situ (e.g. Loc-I-Gut, intestinal perfusion) approaches have been created [12,13]. Research towards factors that govern the intestinal absorption of compounds has been conducted for a long time, since understanding this would provide a useful guideline for the prediction of the degree and speed of absorption of a new drug. Schanker et al. [14] tested the absorption of a large number of acidic and basic compounds by the rat small intestine (in situ). Their results supported the concept that drugs are passively absorbed in the unionized form. Cheaper and faster (in silico and in vitro) methods were also created and are nowadays used for the prediction of HIA.

An important remark is that HIA prediction models are in essence supported by in vivo absorption in rats. However, it has been shown that evaluation of in vivo absorption in rats can be used as an alternative method (because of strong correlation between the values) to predict the extent of HIA following oral administration [15].

Although the in silico approach is very attractive, its accuracy is not overwhelming [16]. Nevertheless, in silico models provide an inexpensive and fast way to assess the ADME

properties of a molecule before synthesis and they enable prioritization of molecules for in vitro and in vivo studies. Therefore, these models are also very interesting [17-19].

A variety of cellular and noncellular in vitro permeability models have been developed and are available for use during the preclinical ADME phase. The created models include PAMPA [16,20]; BAMPA [21]; RPLC, MLC, ILC and IAM [22-24]; MDCK, HT29 and Caco-2 cell line [9,25-28]. There is however no consensus with respect to the better model choice.

VII.4 Limitations of current log BB predictive approaches

Furthermore, an important question is whether or not a new pharmaceutical compound will have an effect on the central nervous system (CNS). This effect can be desired or can be an (un)fortunate side effect of a drug targeting another place in the human body. Barriers at three interfaces separate the blood from the brain interstitial fluid. The BBB, with the largest surface area (12– 18 m^2 for the average human adult) and shortest diffusion distances (typically < 10–15 μm) to neurons, is the most important in regulating drug permeability to the brain. Therefore, a high degree of transportation across the BBB is often used as a measure for effect on the CNS [29,30].

Endothelial cells provide a crucial interface between blood and tissue environments. The free diffusion of chemicals across endothelia is prevented by endothelial tight junctions, of which the permeability varies considerably depending on tissue and conditions. In peripheral tissues (e.g., intestine, kidney, and salivary gland), these cell barriers depict fenestration enabling almost free exchange of water and solutes. The endothelial barrier separating the blood from the CNS is, however, characterized by tight junctions of severely limited permeability (excluding molecules with a diameter larger than 10–15 Å), no fenestrae, and an attenuated pinocytosis. The tight junctions significantly reduce permeation of polar (hydrophilic) solutes through paracellular diffusional pathways between the endothelial cells from the blood plasma to the brain extracellular fluid [31]. This forces molecular traffic to take a largely transcellular route across the brain endothelium [32-34]. The transcellular routes include passive diffusion, carrier-mediated, and vesicular transport mechanisms. A schematic representation of the various pathways involved in the BBB permeability is shown in Figure II-5.

Most of the currently used active drug substances cross cells by passive permeation. In this process, a substance dissolved in the membrane lipid bilayer permeates through the membrane

and enters into the cytoplasm of the cell. To establish an adequate concentration gradient for passive permeation, the substance must not only be soluble in lipids but it must also be sufficiently soluble in water due to the aqueous nature of the extracellular and intracellular spaces. Therefore, lipid/water partitioning is an important factor governing a substance's ability to diffuse through cell membranes [23]. A common measure of the degree of BBB permeation is the ratio of the steady-state concentration of the drug molecule in the brain to concentration in the blood, usually expressed as log (C_{brain}/C_{blood}) or log BB [35,36].

In an attempt to avoid the time-consuming and expensive in vivo log BB determinations, the modeling of BBB permeation has gained in popularity. Both in silico and in vitro models have been proposed for this [36-38]. Contrary to the in silico models whereby no experiments are performed, in the in vitro chromatographic models, the lipid environment of the barrier is mimicked by dynamically or covalently immobilizing lipids on a column. The affinity of the solutes for the immobilized phase is then combined with physicochemical parameters or molecular descriptors for optimal model construction.

In quantitative structure-activity relationship (QSAR) methods, the biological activity of solutes or their ability to penetrate the different hydrophobic barriers (membranes) is related to their physicochemical properties. One of the main drawbacks is that many biologically active compounds of interest in QSAR studies are ionic at physiological pH, and ionic organic compounds are not or only weakly retained in reversed-phase liquid chromatography (RPLC) [39].

A possible way to circumvent this problem is the use of MLC, which has been a popular technique in high-performance liquid chromatography (HPLC) to model drug behavior. MLC is a mode of RPLC which uses a surfactant solution above the critical micellar concentration (CMC) as mobile phase [37,40]. Neutral polyoxyethylene (23) lauryl ether is the most widely used surfactant for BBB permeation modeling, but anionic sodium dodecyl sulfate and cationic cetyltrimethylammonium bromide have also been used frequently [37,41]. Above the CMC, a change in surfactant concentration is translated in an increase in the concentration of micelles in the solution, whereas the number of monomers of surfactant in the mobile phase remains constant. Adsorption of an approximately fixed amount of surfactant monomers on the stationary phase is also produced, giving rise to a stable modified column and regular retention behavior. MLC is a fascinating example of the benefits of secondary equilibrium in RPLC (see Figure VII-2). The primary equilibrium is solute partitioning between bulk solvent and the stationary phase. A secondary equilibrium is established with the micelles in the mobile phase. Both equilibria are affected by a variety of factors, such as the nature and

concentration of the surfactant and additives (e.g., salts), temperature, ionic strength, and pH. This added complexity of MLC compared to conventional RPLC [41,42] also allows improved mimicking of the BBB environment.

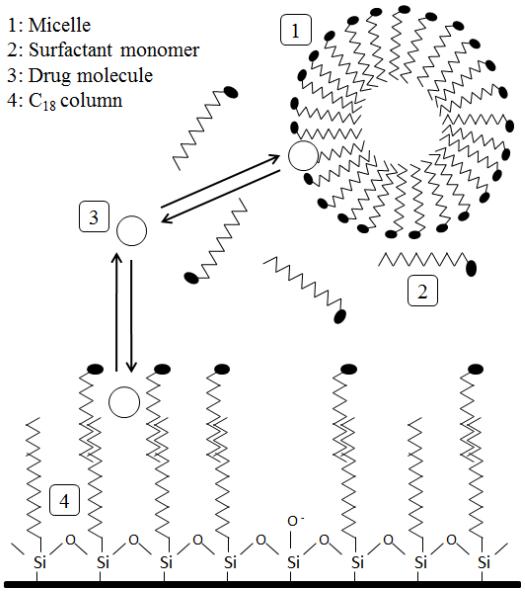

Figure VII-2: Schematic representation of drug interactions in MLC. When a surfactant is used above the CMC, retention depends on interactions with the modified stationary phase and with the micelles present in the mobile phase. A regular retention behavior is achieved based on a fixed amount of surfactant monomers bound to the stationary phase. Modified from [43].

The main chromatographic advantages of MLC are: (i) simultaneous separation of charged and uncharged compounds, (ii) direct on-column injection of physiological fluids, (iii) unique separation selectivity (Figure VII-2; different types of surfactants are possible), (iv) low cost and toxicity, (v) enhanced luminescence detection, and (vi) the biodegradability of the solvents used [44-46]. However, MLC is not a very popular technique due to poor column efficiency and the weak solvent strength of micellar eluents. The two main approaches that have been used to enhance efficiency in MLC are to increase the temperature and to add low amounts of organic modifier to the mobile phase, although some caution should be taken concerning the compounds for which to use an additional organic modifier and the total percentage of modifier [39,42].

Micellar mobile phases have been used for all kinds of purposes in RPLC. The surfactants can be charged positive or negative or can be neutral. The retention of a compound in MLC depends on the type of interaction (electrostatic and/or hydrophobic) with the micelles and with the surfactant-modified stationary phase. Non-ionic solutes are supposed to be only affected by hydrophobic interactions, and charged solutes can be subject to hydrophobic

and/or electrostatic interactions [39]. When the net charge is the same for structurally related compounds, differences in retention arise from differences in hydrophobicity.

A general disadvantage of MLC is that only passive diffusion (see Figure II-5) can be accounted for when using this technique. MLC does not consider the potential role of paracellular transport, carrier-mediated transport, vesicular transport, or drug metabolism on permeability. Although passive diffusion is assumed to be the major factor in drug absorption, overlooking the possible influence of all these other factors can be dangerous and may provide a very limited view of the true absorption potential of a compound [27]. Therefore, it is relevant to mimick the biological structure of cell membranes as much as possible via the use of micelles with high biosimilarity.

VII.5 Miltefosine as a new lipid-like surfactant for improved HIA and log BB prediction

Phospholipids are the major components of cell membranes. These structures – with a hydrophilic 'head' and a hydrophobic 'tail' – could therefore serve as good surfactants for MLC. Thus far, they have not been used as surfactants in MLC, probably as a consequence of cost and solubility issues of many natural phospholipids. However, various synthesis routes have been described for phospholipids [47-49], lysophospholipids [50], and alkylphosphocholines [51-57]. Miltefosine, an alkylphosphocholine, is an antitumor drug [48,52,55,58] which has also been tested for the oral treatment of visceral leishmaniasis [49,59] and for its antifungal and antimicrobial activity [53-57].

Considering the chemical analogy with the other linear synthetic micelformers, and the relatively simple composition allowing bulk synthesis and cheap MLC, it is highly relevant to investigate the use of miltefosine (and of its structural variants) as surfactant in MLC for the prediction of biological behavior. The achievable model quality with input from various descriptors is evaluated in this contribution using 48 pharmaceutical drugs with known log BB values and a subset of 36 drugs with known HIA values. The corresponding models were constructed by partial least squares regressions (PLS) and the added value of the retention factor was investigated.

VII.6 Materials and methods

VII.6.1 Chemicals

The solutes were obtained from several sources: 2,2,2- trifluoroethyl vinyl ether, 2,6-diisopropylphenol, acetaminophen, acetylsalicylic acid, aminopyrine, amitriptyline, amobarbital, antipyrine, atenolol, caffeine, carbamazepine, chlorambucil, chlorpromazine, cimetidine, clonidine, cotinine, desipramine, domperidone, eserine, ethylbenzene, fluphenazine, halothane, haloperidol, hexobarbital, hydroxyzine, ibuprofen, imipramine, mianserin, N-methyl-2-pyridineethanamine, omeprazole, oxazepam, pentobarbital, phenylbutazone, phenytoin, promazine, propranolol, pyrilamine, quinidine, ranitidine, ropinirole, salicylic acid, theobromine, theophylline, toluene, valproic acid, verapamil (Sigma-Aldrich, St. Louis, MO, USA or Steinheim, Germany), indomethacin (Fluka, St. Louis, MO, USA), and benzene (Acros, Geel, Belgium).

VII.6.2 Apparatus

Compound structure verification was achieved using NMR. NMR measurements were performed on a Bruker Avance 300 MHz Ultrashield spectrometer. Synthesis products were dissolved in CD_3OD before analysis. Data was processed with ACDLABS 12.0 1 D NMR processor software.

An Agilent HPLC 1290 system (Agilent Technologies, Waldbronn, Germany) consisting of a binary pump, a diode array detector with a micro flow cell (volume: 1 μL, pathlength: 10 mm), and a 6230 time-of-flight mass spectrometer (TOF-MS) equipped with a Jetstream Electrospray Ionization source was used for the mass determination during synthesis. The system was operated with the Agilent Masshunter software for instrument control and data acquisition. The injection volume was 2 μL, and all experiments were conducted at a temperature of 20 °C. TOF-MS detection was performed in the positive ionization mode. Mass was scanned in the range from 100 to 1000 amu.

Fluorescence spectra and intensities were obtained at room temperature with waters 474 scanning fluorescence detector coupled to an Alliance, Waters 2690 chromatograph (Milford, MA, USA) with a quaternary pump and an automatic injector. The flow rate was set at 0.5 mL/min, and 20 μL was injected for each run. The excitation and emission wavelengths for 8-anilino-1-naphthalenesulfonic acid magnesium salt (ANS, TCI Europe, Zwijndrecht,

Belgium) were, respectively, set at 370 and 470 nm. Data acquisition and processing were performed with a PeakSimple Chromatography Data System (model 202) and PeakSimple software (SRI Instruments, Torrance, CA, USA).

MLC retention analyses were performed on an Alliance, Waters 2690 chromatograph. A Waters 2487 dual wavelength absorbance detector (Milford, MA, USA) was used. The detection wavelength was set between 210 and 300 nm, depending on the analyzed compound (the exact wavelengths are presented in Table VII-1). Data acquisition and processing were performed with a PeakSimple Chromatography Data System (model 202) and PeakSimple software. MLC experiments were performed on a Grace GraceSmart C_{18} (3 μm, 150×2.1 mm) (Deerfield, IL, USA) column at 37 °C with a flow rate of 0.2 mL/min.

VII.6.3 Synthesis

For the synthesis of hexadecylphosphocholine, the following products were used: cetyl alcohol and triethylamine (Acros, Geel, Belgium), toluene (Sigma-Aldrich, St. Louis, MO, USA or Steinheim, Germany), trimethylamine, and 2-chloro-1,3,2-dioxaphospholane-2-oxide (TCI Europe, Zwijndrecht, Belgium).

VII.6.4 Testing of the critical micellar concentration

A stock solution of 450 μM ANS (= 8-Anilino-1-naphthalenesulfonic acid) in water was prepared for the fluorescent tests. During fluorescence measurements, the ANS concentration was diluted to 15 μM. Fluorescence tests were performed by several additions of small aliquots of the surfactant to the solution of ANS. Reported values are averages of triplicate injections. The emission intensity was recorded 2 h after preparation of the samples to allow them to reach an equilibrium.

VII.6.5 Mobile phase and sample preparation

The mobile phase used in MLC was composed of an aqueous solution of 0.01 M miltefosine. The pH was adjusted with a phosphate buffer at pH 7.4, prepared with 0.05 M disodium hydrogen phosphate (Sigma-Aldrich) and potassium dihydrogen phosphate (Sigma-Aldrich). In order to reproduce the osmotic pressure of biological fluids, NaCl (9.20 g/L) (Sigma-

Aldrich) was added to the micellar mobile phase. The mobile phase was vacuum-filtered before use through a 0.45-µm nylon membrane (Grace, Lokeren, Belgium).

Table VII-1: List of selected compounds and their detection wavelengths. Experimentally determined log BB and HIA[a] values are presented, as well as the log k values of these compounds measured by MLC.

No.	Compound	UV (nm)	log BB	HIA (%)	log k
1	2,2,2-trifluoroethyl vinyl ether	210	0.13		1.75
2	2,6-diisopropylphenol	210	0.48		2.30
3	acetaminophen	254	-0.31	83	0.55
4	acetylsalicylic acid	230	-0.50	88	0.41
5	aminopyrine	254	0.00	100	0.64
6	amitriptyline	254	0.98	72	2.67
7	amobarbital	210	0.04		1.47
8	antipyrine	240	-0.10	98	0.39
9	atenolol	270	-1.42	51	0.76
10	benzene	210	0.37	97	1.49
11	caffeine	210	-0.05	100	0.21
12	carbamazepine	210	0.00	89	1.75
13	chlorambucil	254	-1.70	94	1.87
14	chloropromazine	254	1.06	87	2.57
15	cimetidine	210	-1.42	75	0.74
16	clonidine	270	0.11	96	1.21
17	cotinine	260	-0.32		1.90
18	desipramine	254	1.20	99	2.29
19	domperidone	270	-0.78	93	2.43
20	eserine	240	0.08		1.23
21	ethylbenzene	210	0.20	82	1.61
22	fluphenazine	263	1.51		2.54
23	haloperidol	254	1.34	70	2.11
24	halothane	210	0.35		1.53
25	hexobarbital	254	0.10	95	1.28
26	hydroxyzine	210	0.39		1.88
27	ibuprofen	270	-0.18	97	1.68
28	imipramine	240	1.06	99	2.42
29	indomethacin	210	-1.26	100	1.69
30	mianserin	280	0.99		2.81
31	N-methyl-2-pyridineethanamine	254	-0.30	100	0.81
32	omeprazole	300	-0.82	80	1.99
33	oxazepam	230	0.61	92	1.96
34	pentobarbital	210	0.12		1.55
35	phenylbutazone	240	-0.52	94	1.45
36	phenytoin	210	-0.04	90	2.17
37	promazine	254	1.23	40	2.37
38	propranolol	290	0.64	94	2.46
39	pyrilamine	300	0.49		2.22
40	quinidine	254	-0.46	81	1.92
41	ranitidine	230	-1.23	55	0.42
42	ropinirole	254	0.25	100	1.44
43	salicylic acid	300	-1.10	100	0.16
44	theobromine	270	-0.28		-0.10
45	theophylline	270	-0.29	99	0.13
46	toluene	210	0.37	100	1.60
47	valproic acid	210	-0.22	100	0.18
48	verapamil	210	-0.70	90	2.34

[a] Empty boxes in the table indicate that in vivo HIA values were not available

The stock solutions of all drugs were prepared by dissolving 10 mg in 1 ml of methanol except for quinidine and theobromine where stock concentrations of 1 mg/ml and 200 μg/ml were used, caffeine and theophylline which were dissolved in water (10 mg/ml), and domperidone which was dissolved in dimethyl sulfoxide (10 mg/ml). Stock solutions were stored at 5 °C, except for atenolol, which was stored at -20 °C. Working solutions were prepared by dilution of the stock solutions (to 50 μg/ml) with mobile phase.

VII.6.6 Data sources, software, and processing

A total of 48 values of logarithm of brain–blood distribution coefficients (= log BB) were collected from a number of sources [60-62]. Also, for 36 of these compounds, experimental HIA values (ranging between 40 and 100 %, see Table VII-1) were found in literature [1,63-73,19,74-76]. The experimental values of log BB (Table VII-1) range between -1.70 and 1.51. The values of the acidity constants (not shown in Table C-3; Appendix C) were obtained from references [77,78] or were calculated. The acidity constants were used to calculate the total molar charge (α) values at pH 7.4. Structural parameters (molar refractivity (MR), molar volume (MV), parachor (Pr), and polarizability) were calculated using the ACD/Chemsketch software. Other parameters (log P, log D7.4, intrinsic aqueous solubility (log WSo), pH solubility profile (WS7.4), plasma protein binding (PB), Ames test mutagenic index (MI and MIA), and human intestinal absorption (HIA)) were predicted with Chemsilico prediction software (Chemsilico free trial version). The values for polar surface area (PSA) and molecular surface area (MSA) were collected from Chemicalize.org [79]. Hydrogen bond donor (HBD) and hydrogen bond acceptor (HBA) values were achieved from Chemspider [80]. The values for these parameters are presented in Table C-3. The experimental logarithms of the retention factors (log k) are listed in Table VII-1. All retention data are averages of minimally duplicate determinations. Relative standard deviations ranged between 0.01 and 17.82 %; the largest (>10 %) deviations were found for compounds with low retention (log k < 0.6) and were partially caused by fluctuations in t_0. Microsoft Excel (Microsoft Corporation, v. 2007) and Matlab (version 8.1) were used to perform statistical analysis of the results.

VII.7 Rationale

VII.7.1 Synthesis

Synthesis of alkylphosphocholines has been described by several authors [51-59,81,82]. Our synthesis route was slightly modified from a previously reported procedure by Zhang et al. [54]. A mixture of cetyl alcohol (100 mg, 0.41 mmol) and Et_3N (288 µL, 2.06 mmol) in anhydrous toluene (8.25 mL, 77.90 mmol) was cooled to 0 °C. To this solution, 100 µL (1.08 mmol) of 2-chloro-1,3,2-dioxaphospholane-2-oxide was added dropwise while stirring. The solution was kept at 0 °C for 15 min, warmed to room temperature, and stirred for an additional 4 h. The precipitation formed during the reaction was removed through filtration, and the filtrate was concentrated in vacuo yielding an oily residue 1 (Figure VII-3).

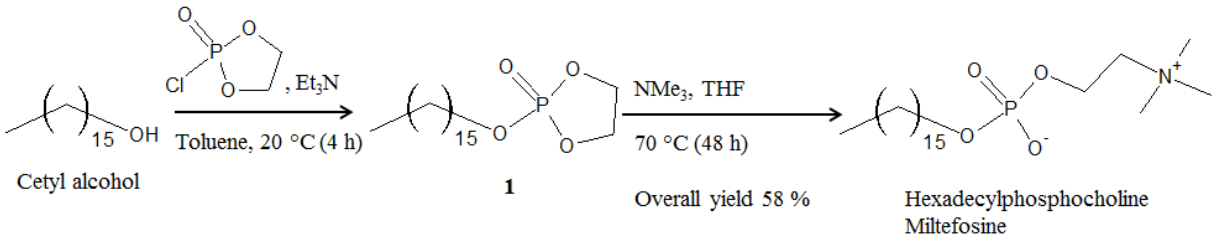

Figure VII-3: Synthesis route for hexadecylphosphocholine (miltefosine). The individual steps are described in the text.

For the synthesis of hexadecylphosphocholine, NMe_3 (9 mL, 18 mmol, 2 M in anhydrous THF) was added to the oily residue in a pressure tube. The mixture was heated to 70 °C for 48 h, subsequently quenched with MeOH and concentrated in vacuo. MeOH/CH_3CN (1.3 mL, 10/90, v/v) was added, and all solids were removed through filtration. A final recrystallization from acetone of the concentrated filtrate afforded the target compound.

VII.7.2 Testing of the critical micellar concentration

After obtaining the target compound, its CMC was determined. Several methods exist for the estimation of the CMC of surfactants. These methods include the use of fluorimetric titrations of ANS or rhodamine 6G [54,83,84] and the variation of surface tension [56,85-87].

Fluorescent probes are particularly useful to detect changes in physicochemical properties of the compounds kept in solution even at very low concentrations. Mast and Haynes [88] reported that an enhancement of fluorescence of the anionic ANS was observed with

nonionic, anionic, and zwitterionic surfactants. The anionic dye, ANS, is almost nonfluorescent in water, but becomes highly fluorescent in organic solvents or when bound to most macromolecules. Rhodamine 6G has also proven to be effective with either zwitterionic, cationic, or nonionic surfactants. This dye is strongly fluorescent in water, and its fluorescence is usually quenched upon binding. The use of ANS or rhodamine 6G with a surfactant of opposite charge may lead to interactions when the surfactant is at concentrations below the CMC, leading to less reliable results. When considering a zwitterionic surfactant, both ANS and rhodamine 6G show a good response [83].

VII.7.3 Prediction of HIA and log BB

The accuracy of prediction of a model is dependent on the type of model which is selected, the relevance, diversity, and orthogonality (independency) of the input variables used therein and on the shortlist of those which have been retained after model optimization, the size of the training set, and on the similarity of the test molecules versus the training set.

Next to in silico strategies, applying only mathematically processed descriptors [36,60,89,90], the approach whereby chromatographic retention data is used as additional in vitro input in these models is labeled by the terminology quantitative retention activity relationships (QRAR) or quantitative structure retention relationships (QSRR). The latter have been well reviewed by Héberger [91]. This type of multivariate problem is typically solved by the algorithm family of multivariate calibrations, such as the multiple linear regression (MLR), principle component regression (PCR), and partial least squares (PLS) methodology.

Considering multivariate calibrations, both MLR and PLS models have been proposed for drug absorption predictions whereby mathematically generated descriptors are combined with retention data [23,77,18]. In this chapter, PLS was chosen as regression model. All the above mentioned methods from the family of multivariate calibrations can provide an equation of the type $y = b_0 + b_1 x_1 + b_2 x_2 + \ldots + b_n x_n$, where y is the predicted (HIA or log BB) value, b_0 until b_n are constants, and x_1 until x_n are variables (descriptors). Obtaining a suitable (and preferably simple) equation of this type is one of the main goals in this chapter.

As the accuracy of the response (in this case HIA or log BB) of the model depends both on the choice and on the relevance of the used descriptors, the use of solute retention data in the model is particularly attractive since it represents the affinity of a compound in a column environment emulating the physiology of a membrane.

Following mathematically processed descriptors were used in analogy with a previous MLC study [77]: total molar charge (α), molecular weight (MW), molar refractivity (MR), molar volume (MV), parachor (Pr), polarizability, and the logarithm of octanol-water partition coefficients (log P). This set was expanded by inclusion of the logarithm of octanol–water distribution coefficients at pH 7.4 (log D7.4), intrinsic aqueous solubility (log WSo), solubility profile at pH 7.4 (WS7.4), plasma protein binding (PB), Ames test mutagenic index (MI and MIA), human intestinal absorption (HIA), polar surface area (PSA), hydrogen bond acceptor and donor (HBA and HBD), and molecular surface area (MSA). The α values, which can be positive of negative, were calculated as in reference [92].

All calculated descriptors are presented in Table C-3. In this chapter, PLS models are constructed based on the retention data of 36 (or 48) solutes for which experimental HIA (or log BB) data are available together with the set of molecular descriptors mentioned above. The merits of the models are evaluated.

VII.8 Results and discussion

In this section, the results for the synthesis of miltefosine are presented. Afterwards, the CMC of miltefosine is determined, providing a good base for its use as a surfactant in MLC. Finally, the results of the chromatographic runs with miltefosine as surfactant are used together with other descriptors for the prediction of HIA and log BB values.

VII.8.1 Synthesis of hexadecylphosphocholine (= miltefosine).

The synthesis procedure can be found in the "Rationale". After the first step of the synthesis, HPLC-TOF-MS was used to check the oily residue (1 in Figure VII-3). This molecule, with a molecular weight of 348.2429 Da, provided the major m/z peak of 349.2463 (Figure VII-4a). The peaks with m/z 697.4892 and 719.4757 are the $(2M+H)^+$ and the $(2M+Na)^+$ fragments. Miltefosine (= hexadecylphosphocholine), a white-brownish solid with a molecular weight of 407.3164 Da, was evaluated with HPLC-TOF-MS (Figure VII-4b), and with ^{1}H- and ^{13}C-NMR (results at end of this paragraph). In Figure VII-4b, the peaks at m/z 408.3198 and 815.6362 are provided by miltefosine, clearly illustrating a good purity of the product. The overall yield of the reaction was 58 %. ^{1}H-NMR (300 MHz, MeOD-d_4) δ ppm 4.25–4.36 (m, 2 H), 3.85–3.95 (m, 2 H), 3.64–3.73 (m, 2 H), 3.21–3.29 (m, 9 H), 1.64 (m, J= 7.00 Hz, 2 H),

1.17–1.47 (m, 26 H), 0.83–0.97 (m, 3 H). ^{13}C-NMR (75 MHz, MeOD-d_4) δ ppm 67.59 (CH_2), 67.48 (CH_2), 60.74 (CH_2), 54.84 (CH_3), 33.22 (CH_2), 32.02 (CH_2), 30.95 (CH_2), 30.63 (CH_2), 27.04 (CH_2), 23.88 (CH_2), 14.63 (CH_3).

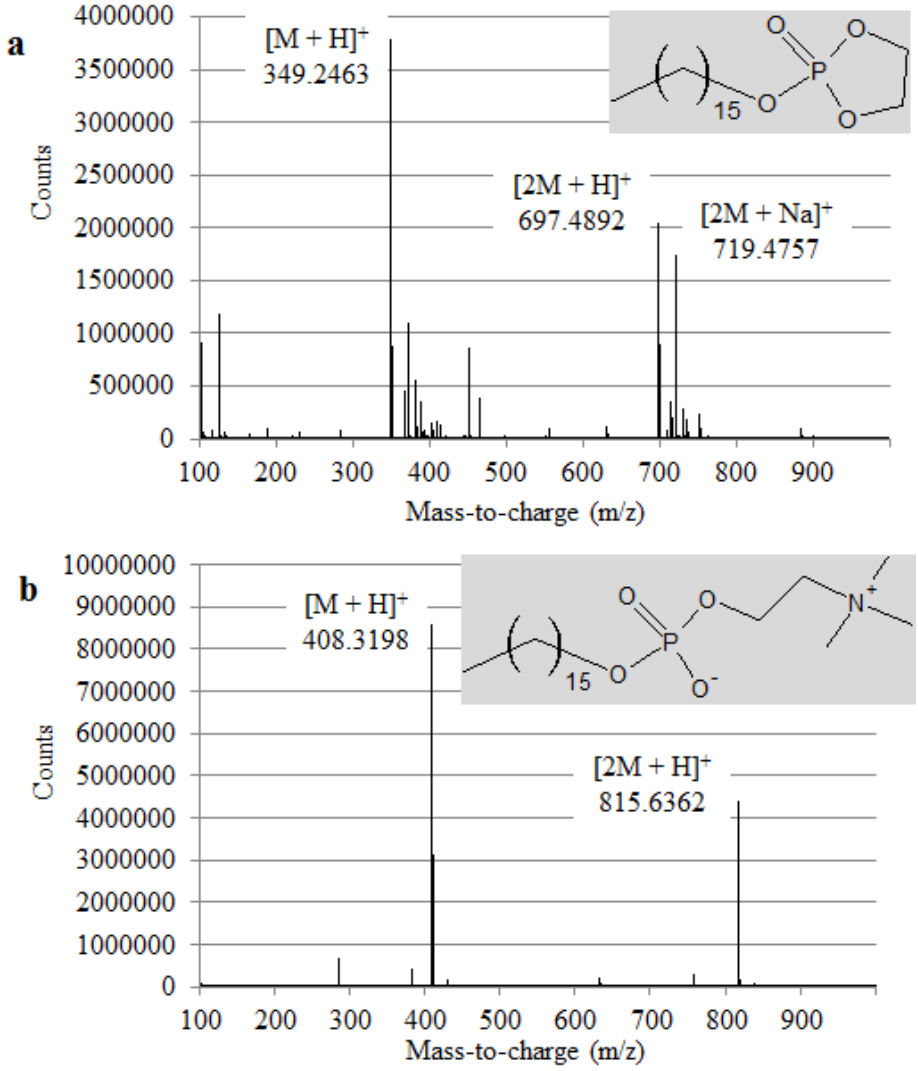

Figure VII-4: TOF-MS spectra, conditions as mentioned in "Materials and methods". The molecular weight of the molecule in **a** is 348.2429 Da. In **b**, the mass spectrum of miltefosine is shown. This molecule has a molecular weight of 407.3164 Da.

VII.8.2 Testing of the CMC

Since the choice of appropriate MLC conditions is important, initial knowledge of the CMC of miltefosine was crucial. After miltefosine was obtained, its CMC was determined using an online flow injection system with a fluorescence detector. According to literature [56,86,87], miltefosine has a CMC of around 0.012 mM. Based on the report of De Vendittis [83], this

should be measurable by fluorescence with both the anionic ANS and the cationic rhodamine 6G since both fluorescent molecules were proven to be effective with zwitterionic surfactants. Here, tests were performed with 15 µM ANS solutions and miltefosine concentrations ranging from 3 to 45 µM. The average areas (after subtracting the blank peak areas) obtained with miltefosine concentrations of 3, 6, 9, 12, 15, 21, 30, and 45 µM were, respectively, 12, 11, 18, 17, 20, 39, 61 and 93. These values are represented in Figure VII-5. The CMC is defined as the breakpoint in the plot of peak area vs concentration. As can be seen in Figure VII-5, two separate trendlines can be drawn, giving rise to an intersection somewhere between 12 and 15 µM, very close to the imposed CMC of 12 µM.

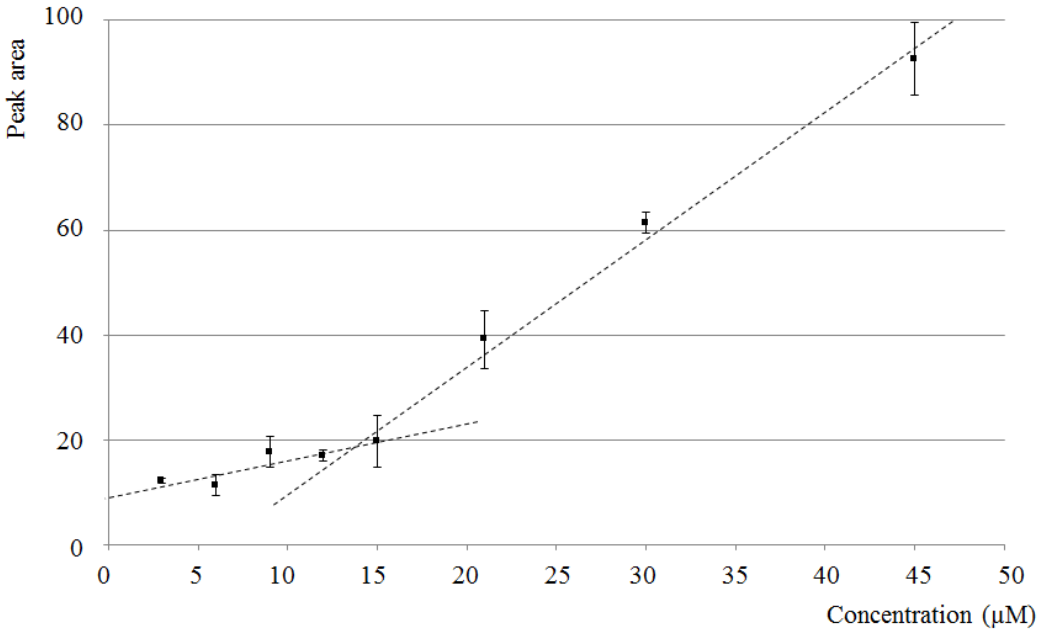

Figure VII-5: Critical micellar concentration of miltefosine in H_2O with 15 µM ANS. Results based on 20 µL injections with a flow rate of 0.5 mL/min at 25 °C. The excitation and the emission wavelengths were, respectively, 370 and 470 nm. All values are averages of triplicate injections. Standard deviations of each point are indicated in the figure.

Compared to more common surfactants, like sodium dodecyl sulfate (8.2 mM), cetyltrimethylammonium bromide (0.92 to 1 mM), and polyoxyethylene (23) lauryl ether (91 µM), the CMC of miltefosine is very low. This implies that MLC could be performed with miltefosine at lower concentrations than when other surfactants are used. A rather high surfactant concentration is however pleasant since retention time decreases when the micelle concentration increases.

VII.8.3 The use of miltefosine as surfactant

A concentration of 10 mM miltefosine was chosen for MLC. One of the major advantages of MLC is the possibility to use a purely aqueous mobile phase. Although organic solvents can be used, they are preferentially avoided since a high concentration can lead to a change or a disruption of the micelles. Elution times can be decreased by increasing the temperature, the surfactant concentration, or the amount of organic solvent. In Figure VII-6, the obtained chromatograms for some of the measured compounds are given. The peak shapes were usually nice, although the efficiency for this type of runs was not very high (quite broad peaks), and some compounds (e.g., atenolol) were subject to some tailing. The chromatographic efficiency is, however, comparable to what is obtained in conventional MLC on this type of column.

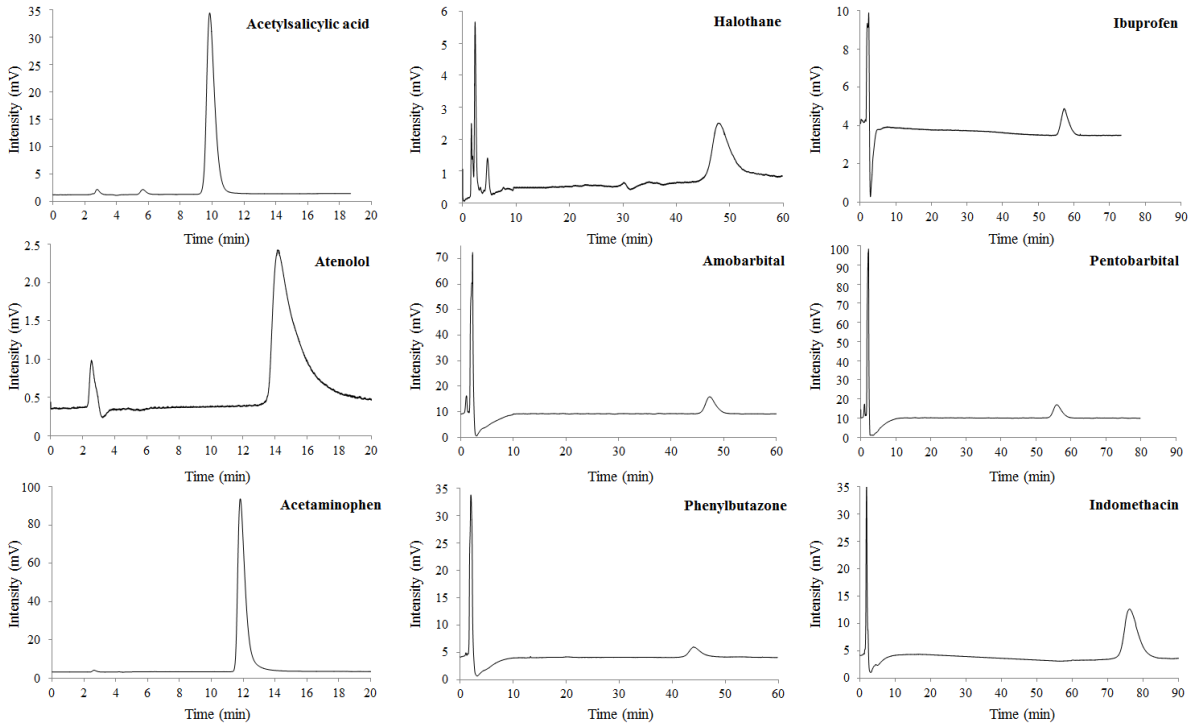

Figure VII-6: Chromatograms obtained for acetaminophen, acetylsalicylic acid, amobarbital, atenolol, halothane, ibuprofen, indomethacin, pentobarbital, and phenylbutazone. HPLC and solvent conditions can be found under "Materials and methods".

The logarithms of the retention factors (log k) measured in this chapter using 10 mM of miltefosine as surfactant in a purely aqueous buffer are listed in Table VII-1. As can be seen, 14 out of the 48 compounds have a log k value > 2, indicating a very long elution time. However, in this case, there would only be one interesting option to decrease these elution times. Increasing the temperature is no option since 37 °C is the most relevant for mimicking

the body temperature. Since it was not easy to solubilize miltefosine in a phosphate buffer at a concentration of 10 mM, increasing the surfactant concentration does not seem to be the best choice. The final option, i.e., the addition of organic modifier (methanol or acetonitrile), would therefore be the most promising alternative to reduce the log k values, providing the amount of modifier is limited.

VII.8.4 Prediction of HIA and log BB

Partial least-squares (PLS) regression was performed to determine the correlation coefficients (R) between actual HIA or log BB values (Table VII-1) and those values predicted by use of log k (Table VII-1) values together with the descriptors mentioned in Table C-3. The correlation coefficients in Table VII-2a give an indication of the performance of the model. The correlation coefficient for the 36 compounds with experimental HIA values (R = 0.8237) was substantially lower than for the 48 compounds with experimental log BB values (R = 0.8827).

Table VII-2: Correlation coefficients between predicted and actual HIA and log BB values when using partial least-squares regression (PLS) or using leave-one-out cross-validation (LOOCV) (a) and these correlation coefficients after elimination of 12 (for HIA) or 11 (for log BB) variables from the model (b).

		HIA	log BB
a			
	R(PLS)	0.8237	0.8827
	R(LOOCV)	0.3666	0.5298
b			
	R(PLS)	0.7991	0.8484
	R(LOOCV)	0.7175	0.7849

Overfitting is an inevitable problem when the performance of multivariate calibration models is evaluated. To avoid overfitted models, cross-validation (CV) methods are often used to detect the robustness of models. These methods include k-fold CV, 2-fold CV, random subsampling validation, and leave-one-out cross-validation (LOOCV) [93].

In this chapter, LOOCV was applied to the data set. In this method, 35 (or 47 for log BB) compounds were used as the training set and one compound as test sample. This procedure was repeated for each compound. The correlations between predicted and actual values by LOOCV are illustrated by a scatter plot in Figure VII-7a (HIA values) and VII-7b (log BB values). The corresponding correlation coefficients (0.3666 and 0.5298) can also be found in Table VII-2a. A large difference between R values from PLS and LOOCV regressions is

observed, which is a clear indication for overfitting. In other words, the equations constructed for HIA and log BB prediction, when the test sample is included, fit the training set in a much better way than is the case when it is not included, which is typically regarded as an indication of overfitting.

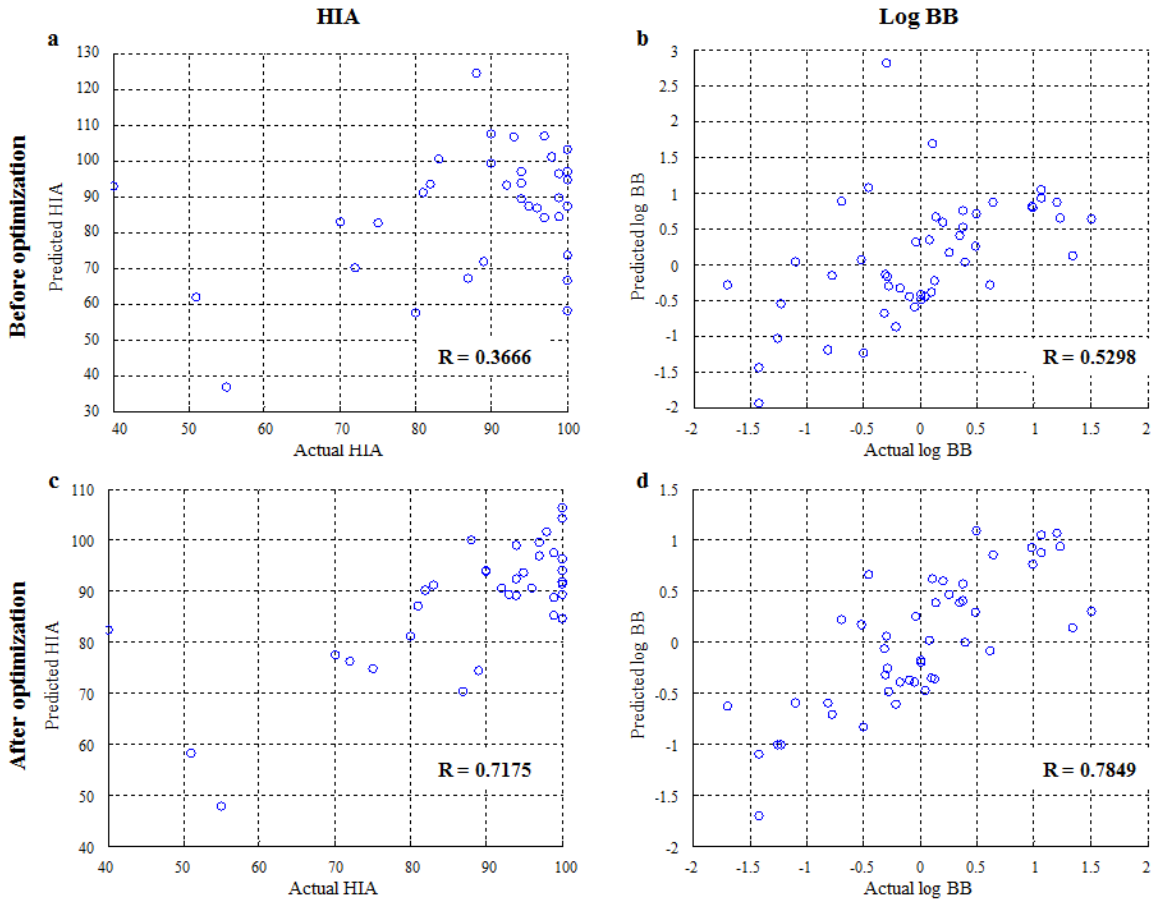

Figure VII-7: Scatter plots comparing predicted leave-one-out cross-validation HIA values (**a** and **c**) or log BB values (**b** and **d**) with actual values. Predicted values are calculated using several descriptors and log k values from MLC with 10 mM miltefosine. Predicted R values based on LOOCV were calculated before (**a** and **b**) and after (**c** and **d**) optimization (elimination) of several descriptors from Table C-3.

There are two major sources of overfitting. The first source is related to the use of a too complex model (e.g., too many variables or other data). This problem can be solved by variable selection – unrelated variables are removed from the training data set, making the model more generalized for both training and test data sets. The second source is related to undersampling of the underlying distribution. In other words, the samples presented do not cover the major range of the underlying native distribution of samples. In this case, there is little that can be done unless more representative data or samples can be added to the model. Therefore, variable selection was performed by systematic removal and/or reinsertion of all

descriptors from the models while monitoring the effect on the LOOCV regression coefficients. This process was iteratively improved until maximum correlation was obtained for the LOOCV results.

The maximum correlation was obtained when 12 (for HIA) or 11 (for log BB) out of 19 descriptors were removed from the model. The correlation coefficients for the simplified models are listed in Table VII-2b. Further descriptor removal led to a decrease in LOOCV regression coefficients. In Figure VII-7c, d, the correlations between the predicted and actual values are presented as scatter plots for the optimized LOOCV models. Comparison of Figure VII-7a, b with c and d enables visual assessment of the improvements in correlation achieved by optimizing the model.

The coefficients of the equations obtained from PLS regressions that lead to the R values listed in Table VII-2b are listed in Table VII-3. The equations indicated by Table VII-3 are:

- $Predicted\ HIA = a + b \times log\ k + c \times \alpha + d \times MW + e \times Pr + g \times log\ WSo + j \times HIA + m \times MSA$
- $Predicted\ log\ BB = a + b \times log\ k + c \times \alpha + f \times polarizability + h \times WS7.4 + i \times PB + j \times HIA + k \times PSA + l \times HBA$

Table VII-3: Coefficients generated by PLS regression after elimination of variables. The general equation for the predicted values is: $x = a + b \times log\ k + c \times \alpha + d \times MW + e \times Pr + f \times polarizability + g \times log\ WSo + h \times WS7.4 + i \times PB + j \times HIA + k \times PSA + l \times HBA + m \times MSA$

	HIA	log BB
a	-5.350	-2.669
b	12.349	0.234
c	-8.390	0.699
d	0.115	-
e	-0.243	-
f	-	-0.048
g	6.532	-
h	-	-0.002
i	-	0.009
j	1.117	0.034
k	-	-0.017
l	-	0.167
m	0.267	-

The descriptors that are withheld in the final models are almost completely different for both models. This is nice since there is a large difference in the physiology of the intestinal membranes and the BBB. These two models thus indicate that descriptor selection cannot be generalized and should be performed for each case separately. In both models, log k is retained, which indicates that this experimentally measured value gives additional input that is

not provided by the selected descriptors. For the prediction of HIA values, one of the retained descriptors is HIA, which was predicted by the Chemsilico prediction software. Although this descriptor provides quite some information on its own (R(PLS) = 0.5992 and R(LOOCV) = 0.5530), these values are not sufficient. The increase for R(LOOCV) to 0.7175 in Table VII-2b indicates that the other descriptors also contribute to a large extent in providing a better prediction model.

When Table VII-2a, b is compared, two important differences can be noticed. On the one hand, the correlation coefficient of the PLS regression has dropped for each type of analysis. This is logical because the PLS regression tries to fit the data as well as possible to an equation. The more variables available to work with, the better the correlations which can be obtained, though this is mainly overfitting. On the other hand, the correlation coefficient of the leave-one-out cross-validation has significantly increased, demonstrating that the predictive capabilities of the different models have, indeed, been improved a lot by applying this strategy. As a result, the average difference between the PLS and LOOCV R values has dropped to 0.0725 in Table VII-2b. Compared with the average difference of 0.4050 in Table VII-2a, this indicates that the model after variable selection is more generalized across the data sets and, therefore, enables more robust prediction.

The final correlation coefficients in Table VII-2b, 0.7175 and 0.7849, indicate that the log BB values are predicted in a better way than what is possible for the HIA values. The comparatively lower correlation observed for the HIA prediction can probably partially be attributed to the choice of sample set. As can be seen in Table VII-1, 23 compounds (out of 36) have a HIA value $\geq$ 90, and 30 compounds have a HIA value $\geq$ 80. Since the chosen compounds do not homogeniously cover the range from 0 to 100 %, and the focus is placed on compounds with high HIA values, it is more difficult to model for compounds with a low HIA value, as can be seen clearly for promazine (HIA = 40 %). Nevertheless, the final correlation coefficient for log BB (0.7849) is a satisfactory value, taking into account that in vitro HPLC methods only allow for prediction of passive permeation (b in Figure II-5) of compounds across the BBB. Miltefosine can thus be considered to be an alternative surfactant for MLC in predicting log BB values. The prediction of HIA values could probably be improved if a more diverse set of compounds and descriptors would be selected, but the approach shows potential as an alternative or complementary MLC strategy for the prediction of in vivo behavior.

VII.9 Conclusion

In this chapter, miltefosine was synthesized and evaluated as a possible surfactant in MLC. Retention of compounds proved to be shorter compared to a purely aqueous mobile phase, indicating that the principle of MLC also works with miltefosine-based micelles. Since a phosphocholine-based lipid is structurally more similar to biological membranes than common surfactants, retention data was used for in vitro predictions of HIA and log BB values. The optimized model for HIA prediction on a compound set of 36 compounds provided a correlation coefficient of 0.7175, while a value of 0.7849 was reached for log BB prediction with 48 compounds. For both predictions, data provided by MLC with miltefosine proved to contribute in a positive way.

Since biological membranes are composed of several types of (phospho)lipids, additional research, in which a variety of (phospho)lipids are combined as surfactants for MLC, might prove to be very interesting for this type of work.

VII.10 Acknowledgments

The authors would like to thank T. Courtin for recording the ^{13}C NMR-spectra and P. Surmont for providing the TOF-MS data.

VII.11 References

1. Hou TJ, Wang JM, Zhang W, Xu XJ (2007) ADME evaluation in drug discovery. 7. Prediction of oral absorption by correlation and classification. J Chem Inf Model 47 (1):208-218.

2. Butina D, Segall MD, Frankcombe K (2002) Predicting ADME properties in silico: methods and models. Drug Discov Today 7 (11):S83-S88.

3. Lipinski CA, Lombardo F, Dominy BW, Feeney PJ (1997) Experimental and computational approaches to estimate solubility and permeability in drug discovery and development settings. Adv Drug Deliver Rev 23 (1-3):3-25.

4. Macheras P, Karalis V, Valsami G (2013) Keeping a Critical Eye on the Science and the Regulation of Oral Drug Absorption: A Review. J Pharm Sci 102 (9):3018-3036.

5. Wang SM, Yang GL, Zhang H, Liu HY, Li ZW (2007) QRAR models for cardiovascular system drugs using biopartitioning micellar chromatography. Journal of Chromatography B-Analytical Technologies in the Biomedical and Life Sciences 846 (1-2):329-333.

6. del Amo EM, Heikkinen AT, Monkkonen J (2009) In vitro-in vivo correlation in p-glycoprotein mediated transport in intestinal absorption. Eur J Pharm Sci 36 (2-3):200-211.

7. Malkia A, Murtomaki L, Urtti A, Kontturi K (2004) Drug permeation in biomembranes in vitro and in silico prediction and influence of physicochemical properties. Eur J Pharm Sci 23 (1):13-47.

8. Kosinska A, Andlauer W (2013) Modulation of tight junction integrity by food components. Food Res Int 54 (1):951-960.

9. Hai PT, Gonzalez-Alvarez I, Bermejo M, Garrigues T, Huong LTT, Cabrera-Perez MA (2013) The Use of Rule-Based and QSPR Approaches in ADME Profiling: A Case Study on Caco-2 Permeability. Mol Inform 32 (5-6):459-479.

10. Lennernas H (1998) Human intestinal permeability. J Pharm Sci 87 (4):403-410.

11. Sjogren E, Dahlgren D, Roos C, Lennernas H (2015) Human in Vivo Regional Intestinal Permeability: Quantitation Using Site-Specific Drug Absorption Data. Mol Pharmaceut 12 (6):2026-2039.

12. Luo ZQ, Liu Y, Zhao BS, Tang MM, Dong HH, Zhang L, Lv BR, Wei L (2013) Ex vivo and in situ approaches used to study intestinal absorption. J Pharmacol Toxicol 68 (2):208-216.

13. Stappaerts J, Brouwers J, Annaert P, Augustijns P (2015) In situ perfusion in rodents to explore intestinal drug absorption: Challenges and opportunities. Int J Pharm 478 (2):665-681.

14. Schanker LS, Tocco DJ, Brodie BB, Hogben CAM (1958) Absorption of Drugs from the Rat Small Intestine. J Pharmacol Exp Ther 123 (1):81-88.

15. Zhao YH, Abraham MH, Le J, Hersey A, Luscombe CN, Beck G, Sherborne B, Cooper I (2003) Evaluation of rat intestinal absorption data and correlation with human intestinal absorption. Eur J Med Chem 38 (3):233-243.

16. Verma RP, Hansch C, Selassie CD (2007) Comparative QSAR studies on PAMPA/modified PAMPA for high throughput profiling of drug absorption potential with respect to Caco-2 cells and human intestinal absorption. J Comput Aid Mol Des 21 (1-3):3-22.

17. Balimane PV, Chong SH, Morrison RA (2000) Current methodologies used for evaluation of intestinal permeability and absorption. J Pharmacol Toxicol 44 (1):301-312.

18. Winiwarter S, Ax F, Lennernas H, Hallberg A, Pettersson C, Karlen A (2003) Hydrogen bonding descriptors in the prediction of human in vivo intestinal permeability. J Mol Graph Model 21 (4):273-287.

19. Perez PAC, Sanz MB, Torres LR, Avalos RC, Gonzalez MP, Diaz HG (2004) A topological sub-structural approach for predicting human intestinal absorption of drugs. Eur J Med Chem 39 (11):905-916.

20. Kansy M, Senner F, Gubernator K (1998) Physicochemical high throughput screening: Parallel artificial membrane permeation assay in the description of passive absorption processes. J Med Chem 41 (7):1007-1010.

21. Sugano K, Takata N, Machida M, Saitoh K, Terada K (2002) Prediction of passive intestinal absorption using bio-mimetic artificial membrane permeation assay and the paracellular pathway model. Int J Pharm 241 (2):241-251.

22. Pidgeon C, Ong SW (1995) Predicting Drug Membrane Interactions. Chemtech 25 (6):38-48.

23. Escuder-Gilabert L, Martinez-Pla JJ, Sagrado S, Villanueva-Camanas RM, Medina-Hernandez MJ (2003) Biopartitioning micellar separation methods: modelling drug absorption. Journal of Chromatography B-Analytical Technologies in the Biomedical and Life Sciences 797 (1-2):21-35.

24. Deconinck E, Ates H, Callebaut N, Van Gyseghem E, Vander Heyden Y (2007) Evaluation of chromatographic descriptors for the prediction of gastro-intestinal absorption of drugs. J Chromatogr A 1138 (1-2):190-202.

25. Wilson G, Hassan IF, Dix CJ, Williamson I, Shah R, Mackay M, Artursson P (1990) Transport and Permeability Properties of Human Caco-2 Cells - an Invitro Model of the Intestinal Epithelial-Cell Barrier. J Control Release 11 (1-3):25-40.
26. Yamashita S, Furubayashi T, Kataoka M, Sakane T, Sezaki H, Tokuda H (2000) Optimized conditions for prediction of intestinal drug permeability using Caco-2 cells. Eur J Pharm Sci 10 (3):195-204.
27. Hidalgo IJ (2001) Assessing the Intestinal Absorption of New Pharmaceuticals. Curr Top Med Chem 1 (5):385-401.
28. Markowska M, Oberle R, Juzwin S, Hsu CP, Gryszkiewicz M, Streeter AJ (2001) Optimizing Caco-2 cell monolayers to increase throughput in drug intestinal absorption analysis. J Pharmacol Toxicol 46 (1):51-55.
29. Abbott NJ (2004) Prediction of blood-brain barrier permeation in drug discovery from in vivo, in vitro and in silico models. Drug discovery today Technologies 1 (4):407-416.
30. Abbott NJ (2005) Physiology of the blood-brain barrier and its consequences for drug transport to the brain. Int Congr Ser 1277:3-18.
31. Wolburg H, Noell S, Mack A, Wolburg-Buchholz K, Fallier-Becker P (2009) Brain endothelial cells and the glio-vascular complex. Cell Tissue Res 335 (1):75-96.
32. Vanbree JBMM, Deboer AG, Danhof M, Breimer DD (1992) Drug Transport across the Blood-Brain-Barrier .1. Anatomical and Physiological-Aspects. Pharm Weekblad 14 (5):305-310.
33. Hirase T, Staddon JM, Saitou M, AndoAkatsuka Y, Itoh M, Furuse M, Fujimoto K, Tsukita S, Rubin LL (1997) Occludin as a possible determinant of tight junction permeability in endothelial cells. J Cell Sci 110:1603-1613.
34. Begley DJ (2004) Delivery of therapeutic agents to the central nervous system: the problems and the possibilities. Pharmacol Therapeut 104 (1):29-45.
35. Fu XC, Wang GP, Shan HL, Liang WQ, Gao JQ (2008) Predicting blood-brain barrier penetration from molecular weight and number of polar atoms. Eur J Pharm Biopharm 70 (2):462-466.
36. Mensch J, Oyarzabal J, Mackie C, Augustijns P (2009) In Vivo, In Vitro and In Silico Methods for Small Molecule Transfer Across the BBB. J Pharm Sci 98 (12):4429-4468.
37. Ruiz-Angel MJ, Garcia-Alvarez-Coque MC, Berthod A (2009) New Insights and Recent Developments in Micellar Liquid Chromatography. Sep Purif Rev 38 (1):45-96.
38. Naik P, Cucullo L (2012) In vitro blood-brain barrier models: Current and perspective technologies. J Pharm Sci 101 (4):1337-1354.

39. Mallols JMS, Camanas RMV, Sagrado S, MedinaHernandez MJ (1997) Quantitative retention - Structure and retention - Activity relationship studies of ionic and non-ionic catecholamines by micellar liquid chromatography. Chromatographia 46 (11-12):605-612.

40. Berthod A, Garcia-Alvarez-Coque MC (2000) Micellar Liquid Chromatography. Marcel Dekker Incorporated, New York

41. Cuenca-Benito M, Sagrado S, Villanueva-Camanas RM, Medina-Hernandez MJ (1998) Quantitative retention-structure and retention-activity relationships of barbiturates by micellar liquid chromatography. J Chromatogr A 814 (1-2):121-132.

42. Ruiz-Angel MJ, Carda-Broch S, Torres-Lapasio JR, Garcia-Alvarez-Coque MC (2009) Retention mechanisms in micellar liquid chromatography. J Chromatogr A 1216 (10):1798-1814.

43. Quinones-Torrelo C, Martin-Biosca Y, Martinez-Pla JJ, Sagrado S, Villanueva-Camanas RM, Medina-Hernandez MJ (2002) QRAR Models for Central Nervous System Drugs using Biopartitioning Micellar Chromatography. Mini-Rev Med Chem 2 (2):145-161.

44. Khaledi MG (1997) Micelles as separation media in high-performance liquid chromatography and high-performance capillary electrophoresis: overview and perspective. J Chromatogr A 780 (1-2):3-40.

45. El-Shaheny RN, El-Maghrabey MH, Belal FF (2015) Micellar Liquid Chromatography from Green Analysis Perspective. Open Chem 13 (1):877-892.

46. Escuder-Gilabert L, Martin-Biosca Y, Sagrado S, Villanueva-Camanas RM, Medina-Hernandez MJ (2002) Quality control of pharmaceuticals containing non-steroidal anti-inflammatory drugs by micellar liquid chromatography. Chromatographia 55 (5-6):283-288.

47. Woolley P, Eibl H (1988) Synthesis of Enantiomerically Pure Phospholipids Including Phosphatidylserine and Phosphatidylglycerol. Chem Phys Lipids 47 (1):55-62.

48. Pinchuk AN, Rampy MA, Longino MA, Skinner RWS, Gross MD, Weichert JP, Counsell RE (2006) Synthesis and structure - Activity relationship effects on the tumor avidity of radioiodinated phospholipid ether analogues. J Med Chem 49 (7):2155-2165.

49. Coghi P, Vaiana N, Pezzano MG, Rizzi L, Kaiser M, Brun R, Romeo S (2008) Parallel synthesis and antileishmanial activity of ether-linked phospholipids. Bioorg Med Chem Lett 18 (16):4658-4660.

50. Eibl H, Woolley P (1988) A General Synthetic Method for Enantiomerically Pure Ester and Ether Lysophospholipids. Chem Phys Lipids 47 (1):63-68.

51. Geilen CC, Samson A, Wieder T, Wild H, Reutter W (1992) Synthesis of Hexadecylphospho[Methyl-C-14]-Choline. J Labelled Compd Rad 31 (12):1071-1076.

52. Agresta M, D'Arrigo P, Fasoli E, Losi D, Pedrocchi-Fantoni G, Riva S, Servi S, Tessaro D (2003) Synthesis and antiproliferative activity of alkylphosphocholines. Chem Phys Lipids 126 (2):201-210.
53. Obando D, Widmer F, Wright LC, Sorrell TC, Jolliffe KA (2007) Synthesis, antifungal and antimicrobial activity of alkylphospholipids. Bioorgan Med Chem 15 (15):5158-5165.
54. Zhang QH, Horst R, Geralt M, Ma XQ, Hong WX, Finn MG, Stevens RC, Wuthrich K (2008) Microscale NMR screening of new detergents for membrane protein structural biology. J Am Chem Soc 130 (23):7357-7363.
55. Markoulides MS, Regan AC (2011) Synthesis of phosphinate analogues of the phospholipid anti-tumour agent hexadecylphosphocholine (miltefosine). Tetrahedron Lett 52 (23):2954-2956.
56. Lukac M, Mrva M, Garajova M, Mojzisova G, Varinska L, Mojzis J, Sabol M, Kubincova J, Haragova H, Ondriska F, Devinsky F (2013) Synthesis, self-aggregation and biological properties of alkylphosphocholine and alkylphosphohomocholine derivatives of cetyltrimethylammonium bromide, cetylpyridinium bromide, benzalkonium bromide (C16) and benzethonium chloride. Eur J Med Chem 66:46-55.
57. Ravu RR, Chen YL, Jacob MR, Pan XW, Agarwal AK, Khan SI, Heitman J, Clark AM, Li XC (2013) Synthesis and antifungal activities of miltefosine analogs. Bioorg Med Chem Lett 23 (17):4828-4831.
58. Eibl H, Unger C (1990) Hexadecylphosphocholine - a New and Selective Antitumor Drug. Cancer Treat Rev 17 (2-3):233-242.
59. Kuhlencord A, Maniera T, Eibl H, Unger C (1992) Hexadecylphosphocholine - Oral Treatment of Visceral Leishmaniasis in Mice. Antimicrob Agents Ch 36 (8):1630-1634.
60. Katritzky AR, Kuanar M, Slavov S, Dobchev DA, Fara DC, Karelson M, Acree WE, Solov'ev VP, Varnek A (2006) Correlation of blood-brain penetration using structural descriptors. Bioorgan Med Chem 14 (14):4888-4917.
61. Abraham MH, Chadha HS, Mitchell RC (1994) Hydrogen-Bonding .33. Factors That Influence the Distribution of Solutes between Blood and Brain. J Pharm Sci 83 (9):1257-1268.
62. Platts JA, Abraham MH, Zhao YH, Hersey A, Ijaz L, Butina D (2001) Correlation and prediction of a large blood-brain distribution data set - an LFER study. Eur J Med Chem 36 (9):719-730.

63. Sabourin PJ, Chen BT, Lucier G, Birnbaum LS, Fisher E, Henderson RF (1987) Effect of Dose on the Absorption and Excretion of [C-14] Benzene Administered Orally or by Inhalation in Rats and Mice. Toxicol Appl Pharm 87 (2):325-336.

64. Owen BA (1990) Literature-Derived Absorption-Coefficients for 39 Chemicals Via Oral and Inhalation Routes of Exposure. Regul Toxicol Pharm 11 (3):237-252.

65. Baelum J, Molhave L, Hansen SH, Dossing M (1993) Hepatic-Metabolism of Toluene after Gastrointestinal Uptake in Humans. Scand J Work Env Hea 19 (1):55-62.

66. Yee SY (1997) In vitro permeability across Caco3 cells (colonic) can predict in vivo (small intestinal) absorption in man - Fact or myth. Pharmaceut Res 14 (6):763-766.

67. Chiou WL, Barve A (1998) Linear correlation of the fraction of oral dose absorbed of 64 drugs between humans and rats. Pharmaceut Res 15 (11):1792-1795.

68. Wessel MD, Jurs PC, Tolan JW, Muskal SM (1998) Prediction of human intestinal absorption of drug compounds from molecular structure. J Chem Inf Comp Sci 38 (4):726-735.

69. Yazdanian M, Glynn SL, Wright JL, Hawi A (1998) Correlating partitioning and Caco-2 cell permeability of structurally diverse small molecular weight compounds. Pharmaceut Res 15 (9):1490-1494.

70. Clark DE (1999) Rapid calculation of polar molecular surface area and its application to the prediction of transport phenomena. 1. Prediction of intestinal absorption. J Pharm Sci 88 (8):807-814.

71. Zhao YH, Le J, Abraham MH, Hersey A, Eddershaw PJ, Luscombe CN, Boutina D, Beck G, Sherborne B, Cooper I, Platts JA (2001) Evaluation of human intestinal absorption data and subsequent derivation of a quantitative structure-activity relationship (QSAR) with the Abraham descriptors. J Pharm Sci 90 (6):749-784.

72. Deretcy E, Feher M, Schmidt JM (2002) Rapid prediction of human intestinal absorption. Quant Struct-Act Rel 21 (5):493-506.

73. Klopman G, Stefan LR, Saiakhov RD (2002) ADME evaluation 2. A computer model for the prediction of intestinal absorption in humans. Eur J Pharm Sci 17 (4-5):253-263.

74. Varma MVS, Sateesh K, Panchagnula R (2005) Functional role of P-glycoprotein in limiting intestinal absorption of drugs: Contribution of passive permeability to P-glycoprotein mediated efflux transport. Mol Pharmaceut 2 (1):12-21.

75. Gunturi SB, Narayanan R (2007) In silico ADME modeling 3: Computational models to predict human intestinal absorption using sphere exclusion and kNN QSAR methods. Qsar Comb Sci 26 (5):653-668.

76. Hou TJ, Wang JM, Zhang W, Xu XJ (2007) ADME evaluation in drug discovery. 6. Can oral bioavailability in humans be effectively predicted by simple molecular property-based rules? J Chem Inf Model 47 (2):460-463.
77. Escuder-Gilabert L, Molero-Monfort A, Villanueva-Camanas RM, Sagrado S, Medina-Hernandez MJ (2004) Potential of biopartitioning micellar chromatography as an in vitro technique for predicting drug penetration across the blood-brain barrier. Journal of Chromatography B-Analytical Technologies in the Biomedical and Life Sciences 807 (2):193-201.
78. Interactive PhysProp Database Demo. (2013) SRC Inc, Syracuse, N.Y. http://www.syrres.com/what-we-do/databaseforms.aspx?id=386. Accessed 31 Jan 2013
79. Chemicalize.org beta. (2015) ChemAxon. http://www.chemicalize.org/. Accessed 11 Feb 2015
80. ChemSpider. (2015) Royal Society of Chemistry. http://www.chemspider.com/. Accessed 12 Feb 2015
81. Geilen CC, Haase A, Wieder T, Arndt D, Zeisig R, Reutter W (1994) Phospholipid Analogs - Side Chain-Dependent and Polar Head Group-Dependent Effects on Phosphatidylcholine Biosynthesis. J Lipid Res 35 (4):625-632.
82. Xu FM, Wang HB, Zhao J, Liu XS, Li DD, Chen CJ, Ji J (2013) Chiral Packing of Cholesteryl Group as an Effective Strategy To Get Low Molecular Weight Supramolecular Hydrogels in the Absence of Intermolecular Hydrogen Bond. Macromolecules 46 (11):4235-4246.
83. Devendittis E, Palumbo G, Parlato G, Bocchini V (1981) A Fluorimetric Method for the Estimation of the Critical Micelle Concentration of Surfactants. Anal Biochem 115 (2):278-286.
84. Palladino P, Rossi F, Ragone R (2010) Effective Critical Micellar Concentration of a Zwitterionic Detergent: A Fluorimetric Study on n-Dodecyl Phosphocholine. J Fluoresc 20 (1):191-196.
85. Rakotomanga M, Loiseau PM, Saint-Pierre-Chazalet M (2004) Hexadecylphosphocholine interaction with lipid monolayers. Bba-Biomembranes 1661 (2):212-218.
86. Yaseen A, Lu JR, Webster JRP, Penfold J (2005) Adsorption of single chain Zwitterionic phosphocholine surfactants: Effects of length of alkyl chain and head group linker. Biophys Chem 117 (3):263-273.

87. Menez C, Legrand P, Rosilio V, Lesieur S, Barratt G (2007) Physicochemical characterization of molecular assemblies of miltefosine and amphotericin B. Mol Pharmaceut 4 (2):281-288.

88. Mast RC, Haynes LV (1975) Use of Fluorescent-Probes Perylene and Magnesium 8-Anilinonaphthalene-1-Sulfonate to Determine Critical Micelle Concentration of Surfactants in Aqueous-Solution. J Colloid Interf Sci 53 (1):35-41.

89. Ecker GF, Noe CR (2004) In silico prediction models for blood-brain barrier permeation. Curr Med Chem 11 (12):1617-1628.

90. Yan A, Liang H, Chong Y, Nie X, Yu C (2013) In-silico prediction of blood-brain barrier permeability. Sar Qsar Environ Res 24 (1):61-74.

91. Heberger K (2007) Quantitative structure-(chromatographic) retention relationships. J Chromatogr A 1158 (1-2):273-305.

92. Escuder-Gilabert L, Sanchis-Mallols JM, Sagrado S, Medina-Hernandez MJ, Villanueva-Camanas RM (1998) Chromatographic quantitation of the hydrophobicity of ionic compounds by the use of micellar mobile phases. J Chromatogr A 823 (1-2):549-559.

93. Hawkins DM, Basak SC, Mills D (2003) Assessing model fit by cross-validation. J Chem Inf Comp Sci 43 (2):579-586.

Chapter VIII. Critical assessment of the developed, existing and combined MLC and IAMLC methods

In the previous chapters, several MLC and IAMLC methods were presented. Several points of concern have, however, not been addressed so far. Firstly, although combinations of MLC and IAMLC methods were performed in chapters III and V, the combination of a micellar phase in an IAM-column has not been tested. This setup could lead to a significant difference in retention times, since surfactant interactions with the stationary phase should be totally different compared to MLC. Secondly, the results of all different methods were not compared yet, although this type of comparison would allow the selection of the most appropriate method. Thirdly, no additional information has been provided so far concerning the effect of performing another regression method or the usefulness of the descriptors, while these points are actually critical to obtain a good overall in vitro correlation. These issues are treated in this chapter.

VIII.1 Investigation of the use of MLC conditions on an IAM column for the prediction of log BB and HIA values

VIII.1.1 Introduction

Historically, MLC has mostly been performed on C_{18} columns, although C_8 and cyanopropyl columns have also been used [1,2]. C_{18} stationary phases are particularly interesting, since the long C_{18} carbon chains of the stationary phase can interact with the hydrophobic part of a surfactant molecule. This results in the adsorption of an approximately fixed amount of surfactant monomers on the stationary phase, and therefore a stable modified column and regular retention behavior [2,3]. The use of MLC allows for the presence of micelles in the

mobile phase and creates a secondary equilibrium in RPLC (explained in section VII-4 and illustrated in Figure VII-2). One of the advantages of this technique is that the use of an organic modifier can be avoided.

This is not the case in IAMLC, where the use of an organic modifier is necessary for lipophilic drugs. The types of stationary phases in IAM columns are, however, mimicking the biological conditions in a better way than MLC with C_{18}, C_8 and cyanopropyl columns. Since the evaluation of several IAM columns in chapter V indicated that these column types are also interesting for in vitro predictions of log BB values, the question arose whether the use of a mobile phase similar to those used in MLC would have a positive effect on retention in IAMLC. This was investigated in section VIII.1.

VIII.1.2 Materials and methods

VIII.1.2.1 Chemicals

Except for indomethacin (Fluka, St. Louis, MO, USA) and benzene (Acros, Geel, Belgium), all analytes were obtained from Sigma-Aldrich (Steinheim, Germany).

VIII.1.2.2 Apparatus

The IAM retention analysis was performed on an Alliance, Waters 2690 chromatograph (Milford, MA, USA) with a quaternary pump and an automatic injector. A Waters 2487 dual wavelength absorbance detector was used, for which the detection wavelength was set between 210 and 300 nm, depending on the analyzed compound (the exact wavelengths are presented in Table VIII-1). Experiments were performed on an IAM.PC.DD2 (10 μm, 150 mm× 4.6 mm; Regis Technologies, Morton Grove, IL, USA) column. Data acquisition and processing were performed with a PeakSimple Chromatography Data System (model 202) and PeakSimple software (SRI Instruments, Torrance, CA, USA). Analysis was performed at 25 °C with a flow rate of 1 mL min^{-1}.

Table VIII-1: Complete set of compounds with their corresponding in vivo log BB and HIA[a] values, together with their log k values measured on an IAM.PC.DD2 column with a DPBS buffer and 20 mmol L^{-1} SDS in the mobile phase.[b]

No.	Compound	UV (nm)	log BB	HIA (%)	log k
1	2,2,2-trifluoroethyl vinyl ether	210	0.13		0.72
2	2,6-diisopropylphenol	210	0.48		1.79
3	acetaminophen	254	-0.31	83	0.20
4	acetylsalicylic acid	230	-0.50	88	-0.44
5	aminopyrine	254	0.00	100	0.83
6	amitriptyline	254	0.98	72	1.75
7	amobarbital	210	0.04		1.01
8	antipyrine	240	-0.10	98	0.58
9	atenolol	270	-1.42	51	0.92
10	benzene	210	0.37	97	0.99
11	caffeine	210	-0.05	100	0.21
12	carbamazepine	210	0.00	89	0.98
13	chlorambucil	254	-1.70	94	1.62
14	chloropromazine	254	1.06	87	1.80
15	cimetidine	210	-1.42	75	0.99
16	clonidine	270	0.11	96	1.80
17	cotinine	260	-0.32		0.34
18	desipramine	254	1.20	99	1.69
19	domperidone	270	-0.78	93	1.56
20	eserine	240	0.08		1.30
21	ethylbenzene	210	0.20	82	1.40
22	fluphenazine	263	1.51		1.73
23	haloperidol	254	1.34	70	2.05
24	halothane	210	0.35		1.14
25	hexobarbital	254	0.10	95	0.87
26	hydroxyzine	210	0.39		1.73
27	ibuprofen	270	-0.18	97	0.39
28	imipramine	240	1.06	99	1.76
29	indomethacin	210	-1.26	100	0.76
30	mianserin	280	0.99		1.62
31	N-methyl-2-pyridineethanamine	254	-0.30	100	1.24
32	omeprazole	300	-0.82	80	1.18
33	oxazepam	230	0.61	92	1.12
34	pentobarbital	210	0.12		1.05
35	phenylbutazone	240	-0.52	94	0.30
36	phenytoin	210	-0.04	90	1.38
37	promazine	254	1.23	40	1.75
38	propranolol	290	0.64	94	1.65
39	pyrilamine	300	0.49		1.56
40	quinidine	254	-0.46	81	1.91
41	ranitidine	230	-1.23	55	1.05
42	ropinirole	254	0.25	100	1.38
43	salicylic acid	300	-1.10	100	-0.45
44	theobromine	270	-0.28		-0.10
45	theophylline	270	-0.29	99	0.02
46	toluene	210	0.37	100	1.27
47	valproic acid	210	-0.22	100	-0.28
48	verapamil	210	-0.70	90	1.79
49	zidovudine	270	-0.72	100	0.17

[a] Empty boxes in the table indicate that in vivo HIA values were not available
[b] All log k data are averages from three analyses

VIII.1.2.3 Mobile phase and sample preparation

The mobile phase was prepared similar to mobile phases in chapter V, only replacing methanol with sodium dodecyl sulfate (SDS). The mobile phase was again based on the Dulbecco's phosphate-buffered saline (DPBS). The DPBS consisted of 2.7 mmol L^{-1} KCl, 1.5 mmol L^{-1} KH_2PO_4, 137 mmol L^{-1} NaCl, and 8.1 mmol L^{-1} Na_2HPO_4 (Sigma-Aldrich). After addition of 20 mmol L^{-1} SDS, the pH of the mobile phase was adjusted to 7.4 by use of acetic acid (Sigma-Aldrich). Before use, the mobile phase was vacuum-filtered through a 0.20 μm nylon membrane (Grace Davison, Lokeren, Belgium).

Stock solutions of all drugs were prepared by dissolving 10 mg in 1 mL methanol, except for quinidine and theobromine, for which stock concentrations of 1 mg mL^{-1} and 200 μg mL^{-1} were used; caffeine and theophylline, which were dissolved in water (10 mg mL^{-1}); and domperidone, which was dissolved in dimethyl sulfoxide (10 mg mL^{-1}). Working solutions were prepared by dilution of the stock solutions (to 50 μg mL^{-1}) with mobile phase.

VIII.1.2.4 Data sources, software, and processing

The descriptors in Table C-4 (Appendix C) are the same as those mentioned in section VII.4.6; only zidovudine was added to the dataset. The experimental logarithms of the retention factors (log k) are listed in Table VIII-1. All retention data are averages from triplicate determinations. Matlab (ver. 8.1) was used to perform statistical analysis of the results.

VIII.1.3 Results and discussion

As can be seen in Table VIII-1, all compounds eluted without the use of an organic modifier in a reasonable amount of time (average t_0 = 1.32 min). This indicates that the micelles formed by the addition of SDS give rise to a secondary equilibrium. Similar to MLC, a solute in the bulk solvent can now interact both with the stationary phase (phosphatidylcholine) and the micelles (SDS). Because of the interaction with SDS micelles, compounds are retained for a shorter amount of time on the stationary phase and elution is expedited. Therefore, organic solvents are no longer required when micellar mobile phases are used with this type of columns.

PLS regression was subsequently performed to determine the correlation coefficients between actual HIA or log BB values (Table VIII-1) and their values predicted by use of log k values

together with the descriptors mentioned in Table C-4. The correlation coefficients are presented in Table VIII-2a. As in the previous chapters, overfitting can cause problems, and cross-validation (CV) methods can be used to detect the robustness of the model. Therefore, LOOCV was applied to the dataset. The correlation coefficients are presented in Table VIII-2a and illustrated in Figure VIII-1a,b.

Table VIII-2: Correlation coefficients between predicted and actual HIA and log BB values when using partial least-squares regression (PLS) or using leave-one-out cross-validation (LOOCV) (a) and these correlation coefficients after elimination of 11 (for HIA) or 13 (for log BB) variables from the models (b).

	HIA	Log BB
Number of compounds	37	49
a		
R(PLS)	0.7987	0.8873
R(LOOCV)	-0.0747	0.4189
b		
R(PLS)	0.7706	0.8452
R(LOOCV)	0.6694	0.7863

In Table VIII-2a, a very large average decrease of 0.6709 is found when the difference between R(PLS) and R(LOOCV) is calculated. This is again a typical indication for overfitting.

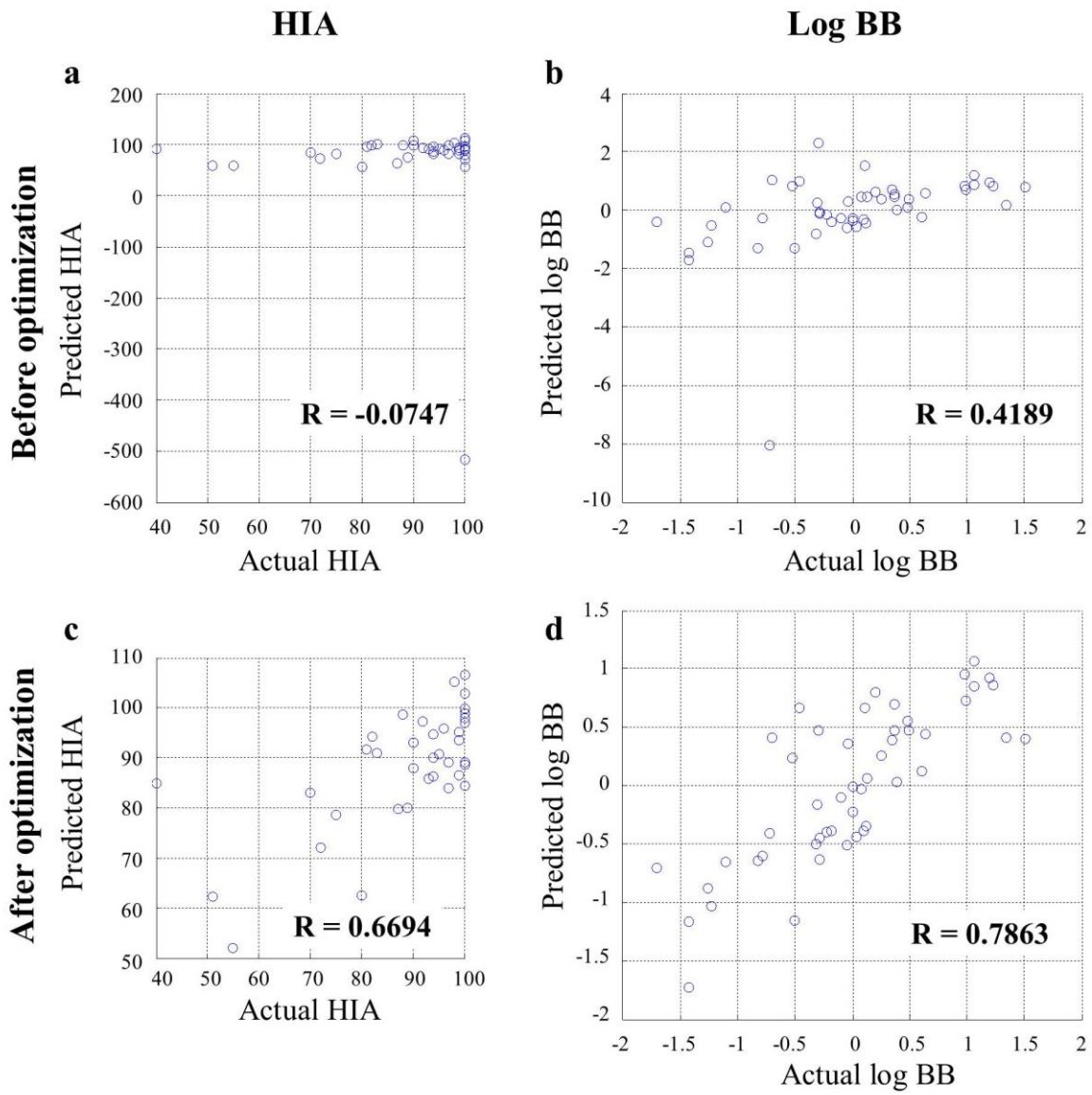

Figure VIII-1: Scatter plots comparing predicted leave-one-out cross-validation HIA values (a and c) or log BB values (b and d) with actual values. Predicted values are calculated using several descriptors and log k values. Predicted R-values based on LOOCV were calculated before (a and b) and after (c and d) optimization (elimination) of superfluous descriptors.

If the overfitting is caused by the use of a too complex model, the model should perform much better after variable selection, in which the unrelated variables are removed from the training set. If the overfitting is related to undersampling of the sample distribution, more representative samples should be added to the model to overcome this problem, which is sometimes very difficult. Therefore, variable selection was performed by systematic removal and/or reinsertion of all descriptors from the models while monitoring the effect on the LOOCV regression coefficients. This process was iteratively improved until maximum correlation was obtained for the LOOCV results.

For the HIA model, 12 out of 19 descriptors were removed this way, while for the log BB model 13 descriptors were removed. The correlation coefficients for the simplified models are listed in Table VIII-2b. After optimization of the models, the difference in correlation coefficients between the PLS and the LOOCV values for HIA and log BB prediction have respectively dropped to 0.1012 and 0.0589. The difference for the HIA model is still significant, which means that undersampling might be a problem here. Since 24 (out of 37) compounds have a HIA value ≥ 90, and 31 compounds have a HIA value ≥ 80, it is safe to assume that this is not an optimal sample distribution. Therefore, the use of an additional set of compounds with in vivo HIA values ranging between 0 and 80 would lead to a better sample distribution and would eliminate the problem of undersampling. This was, however, not tested due to time limitations.

In Figure VIII-1c,d, the correlations between predicted and in vivo values are presented as scatter plots for the optimized models. Since HIA-values of the chosen compounds do not homogeniously cover the range from 0 to 100 %, and the focus is placed on compounds with high HIA-values, it is more difficult to model for compounds with a low HIA value, as can be seen clearly for promazine (HIA = 40 %). Also, as can be seen from the initial models (Figure VIII-1a,b), one compound is not fitting the model at all and might be an outlier. Based on the log BB value (-0.72), this compound was easily identified as zidovudine. There are two possible reasons for this compound to be wrongly predicted: (i) the predicted value of one or more descriptors is causing a problem; (ii) the azide functionality of this compound causes diverging characteristics or retention behavior, which leads to a wrong prediction. All structural formulas are presented in Appendix B; zidovudine is the only compound with an azide-group. As can be seen in Figure VIII-1c,d, zidovudine is no longer causing a problem after optimization of the model. Therefore, zidovudine was not deleted from the model. Also, correlation coefficients for the optimized models without using zidovudine (HIA R(LOOCV) = 0.6704; Log BB R(LOOCV) = 0.7841) are not so different compared to the correlation coefficients in Table VIII-2, which indicates that zidovudine itself may not really be an outlier.

The coefficients of the equations obtained from PLS regressions that lead to the R values listed in Table VIII-2b, are listed in Table VIII-3. The equations indicated by Table VIII-3 are:

- $Predicted\ HIA = a + c \times MW + d \times MV + e \times Pr + f \times log\ D7.4 + g \times log\ WSo + h \times PB + i \times HIA$
- $Predicted\ log\ BB = a + b \times \alpha + e \times Pr + f \times log\ D7.4 + h \times PB + i \times HIA + j \times PSA$

The descriptors that are withheld in the final models are almost completely different for both models. This appears relevant, since there is a large difference in the physiology of the intestinal membranes and the BBB. A very important remark here, is that log k has not been retained for the construction of the final log BB and HIA model. This means that the experimentally measured values did not provide additional input compared to the selected descriptors for the construction of the log BB and HIA model.

Table VIII-3: Coefficients generated by PLS regression after elimination of variables. The general equation for the predicted values is: $x = a + b \times \alpha + c \times MW + d \times MV + e \times Pr + f \times log\ D7.4 + g \times log\ WSo + h \times PB + i \times HIA + j \times PSA$.

	HIA	log BB
a	22.5956	-2.8602
b	-	0.6132
c	0.1887	-
d	0.4710	-
e	-0.2689	-0.0016
f	1.8587	0.1723
g	8.8444	-
h	0.2670	0.0072
i	0.8159	0.0357
j	-	-0.0069

Although the log k values were not retained for both models – illustrating that the chromatographic runs did not provide additional prediction power compared to a pure in silico method – the conclusion that can be drawn from this experimental work is very important, since the use of MLC conditions with SDS on an IAM.PC.DD2 column was – to our knowledge – not yet documented. The use of MLC conditions provided the ability to avoid the use of organic modifiers on the IAM column, which was previously not possible.

An enhanced prediction of HIA values is probably possible by the selection of a more diverse set of compounds and descriptors, which could also allow the log k values to gain in importance. The correlation coefficient of 0.6694 is however substantially lower than what was obtained in chapter VII (R(LOOCV) = 0.7175), which indicates that the use of surfactants in the mobile phase on an IAM column may not be an improvement compared to the use of conventional MLC for the prediction of in vivo behavior.

VIII.1.4 Conclusion

In this section, the use of MLC conditions on an IAM column has been studied for the prediction of log BB and HIA values. SDS was selected as surfactant, since this provided the

best results in chapter III. Based on the performance of the different IAM columns (chapter V), the IAM.PC.DD2 column was selected.

The correlation coefficients based on LOOCV in this section (both for log BB and HIA) were created without the log k values and were lower than the values obtained in the previous chapters. Also, since IAM columns are more expensive than conventional C_{18}-columns and the mobile phase described in this section could facilitate column blockage, it can be concluded that conventional C_{18}-columns are more appropriate for MLC studies.

VIII.2 Extended comparison of MLC and IAMLC methods

A qualitative comparison of the performance of MLC and IAMLC methods towards the prediction of in vivo behavior based on results in literature is nearly impossible because of the discrepancy between different studies. Differences between studies can be due to the selected compounds, the column type and dimensions, the mobile phase composition, the selected descriptors, computational processing, etc. These differences impede the selection of the best suited in vitro method.

Since comparison of the selected methods has been one of the goals throughout this thesis, differences have been eliminated as much as possible by using identical compounds, columns (for MLC), equipment, descriptors and data treatment. Based on these similarities, methods that were studied in chapters III, V, VII and VIII.1 are compared in this section in terms of their capability to predict both log BB and HIA behavior.

VIII.2.1 Overview of the methods

An overview of the log k values for the selected methods is given in Table VIII-4. As in chapter III, MLC methods with Brij35, SDC and SDS were selected. The models were created based on 43 log k values for Brij35 and 36 values for SDC out of 45 compounds measured (see chapter III). For SDS, an additional 4 compounds (chloropromazine, haloperidol, halothane and promazine) were measured (extension of chapter III). As mentioned in chapter III, the IAM.PC.DD2-column provided better results when more (30 or 40 % MeOH) organic modifier was used in the mobile phase. Therefore, the method with only 20 % MeOH and the extrapolation to 0 % were not selected for additional research towards HIA-prediction. Log k values for the sphingomyelin and cholester columns were taken from chapter V.

Table VIII-4: Overview of the selected methods and the log k values obtained for these methods[a].

N°	Brij35 0.05 M	SDC 0.05 M	SDS 0.05 M	IAM 40% MeOH	IAM 30% MeOH	SM-IAM 30% MeOH	Cholester 50% MeOH	Miltefosine 0.01 M	IAM.PC + SDS 0.02 M
1	0.928	0.694	1.080	-0.089	0.095	0.210	0.573	1.746	0.725
2	1.254	1.598	1.750	1.156	1.544	1.681	1.785	2.305	1.785
3	0.261	-0.231	-0.095	-0.657	-0.372	-0.261	-0.519	0.550	0.197
4	-0.498	-1.004	-0.688	-0.964	-0.664	-0.131	-0.476	0.407	-0.445
5	0.474	1.438	1.527	-0.547	-0.206	-0.082	0.011	0.636	0.832
6	2.386		2.123	1.519	1.975	1.657	1.510	2.669	1.754
7	0.936	0.693	1.249	0.112	0.457	0.617	0.653	1.468	1.008
8	0.268	0.964	1.053	-0.694	-0.368	-0.329	-0.273	0.386	0.576
9	-0.093	1.253	1.189	-0.436	-0.206	-0.539	-0.767	0.756	0.917
10	1.039	1.120	1.207	0.155	0.338	0.530	0.834	1.490	0.990
11	0.073	0.485	0.767	-0.948	-0.590	-0.477	-0.262	0.208	0.207
12	0.799	1.236	1.226	0.202	0.593	0.772	0.630	1.752	0.979
13	1.530	0.261	-0.889	0.397	0.793	1.000	1.947	1.870	1.622
14	NA	NA	2.069	1.851	2.404	2.110	1.946	2.566	1.800
15	0.301	0.934	1.031	-0.491	-0.145	-0.091	-0.221	0.739	0.986
16	0.584	1.877	1.500	0.227	0.458	0.135	-0.061	1.212	1.798
17	0.194	1.100	1.110	-1.139	-0.711	-0.647	-0.644	1.902	0.340
18	1.704		1.991	1.462	1.864	1.564	1.291	2.290	1.691
19	0.984	1.891	1.924	1.461	2.042	1.837	1.468	2.432	1.560
20	0.987	2.074	1.547	0.014	0.355	0.238	0.096	1.229	1.301
21	1.233	1.476	1.636	0.718	0.994	1.139	1.462	1.605	1.401
22	1.553		2.046	2.022	2.596	2.445	2.238	2.541	1.727
23	NA	NA	2.188	1.330	1.844	1.466	1.379	2.107	2.048
24	NA	NA	1.237	0.247	0.487	0.618	0.956	1.527	1.143
25	0.789	0.769	1.260	-0.064	0.253	0.433	0.518	1.276	0.866
26	1.271		2.010	1.276	1.800	1.741	1.693	1.881	1.729
27	0.693	0.194	0.565	0.123	0.499	0.884	0.993	1.685	0.392
28			2.096	1.409	1.838	1.524	1.403	2.422	1.755
29	0.730	0.291	0.738	0.541	1.061	1.462	1.372	1.693	0.759
30	1.940		2.173	1.439	1.843	1.776	1.727	2.811	1.625
31	0.454	1.977	1.560	-0.419	-0.249	-0.373	-0.773	0.808	1.239
32	0.974	1.562	1.764	0.223	0.713	0.806	0.723	1.989	1.178
33	0.945	1.244	1.439	0.702	1.118	1.182	1.307	1.962	1.120
34	0.932	0.739	1.274	0.150	0.489	0.647	0.668	1.548	1.054
35	0.701	-0.179	0.594	0.041	0.477	0.931	0.678	1.446	0.297
36	0.933	0.898	1.349	0.392	0.761	0.981	0.635	2.172	1.378
37	NA	NA	1.964	1.490	2.035	1.708	1.465	2.373	1.754
38	1.326	2.270	1.936	1.119	1.474	1.348	0.857	2.460	1.645
39			2.001	0.747	1.132	0.974	0.652	2.221	1.563
40	1.282	1.408	1.590	0.937	1.346	1.045	0.909	1.925	1.909
41	0.283	1.756	1.191	-0.331	-0.045	-0.204	-0.386	0.424	1.045
42	0.936	1.938	1.636	0.102	0.385	0.166	0.180	1.438	1.379
43	0.179	-0.998	-0.672	-1.057	-0.656	-0.086	-0.490	0.159	-0.453
44	-0.191	-0.076	0.275	-1.334	-0.932	-0.819	-0.744	-0.103	-0.103
45	0.011	-0.091	0.312	-0.945	-0.621	-0.511	-0.355	0.131	0.017
46	1.260	1.395	1.511	0.450	0.683	0.942	1.171	1.601	1.267
47	-0.098		-0.135	-0.689	-0.546	-0.112	0.319	0.177	-0.279
48	1.652		2.197	1.055	1.663	1.400	1.208	2.340	1.791
49	0.085	-0.252	0.303	-0.670	-0.482	-0.325	-0.155	0.221	0.166

[a] Empty boxes in the table indicate that log k values were not obtained, mostly because of too long elution times

The log k values based on the MLC runs with miltefosine on a normal C_{18} column and with SDS on the IAM column were respectively taken from chapters VII and VIII. Except for Brij35 and SDC, all methods presented in Table VIII-4 provide log k values for 49 compounds.

VIII.2.2 Results and discussion

As in chapter VII and in section VIII.1, the log k values were used in combination with a set of descriptors (Table C-4) to predict log BB and HIA values (for which in vivo values are presented in Table VIII-1). The data was processed as in chapter VII using a PLS regression in Matlab, and LOOCV was performed to check the robustness of the models. The correlation coefficients of the initial models and the optimized models (after elimination of superfluous descriptors) are presented in Table VIII-5.

Table VIII-5: Correlation coefficients between predicted and actual HIA and log BB values when using partial least-squares regression (PLS) and leave-one-out cross-validation (LOOCV) and the optimized coefficients after elimination of superfluous variables from the models. Values indicated in orange indicate that log k values were not selected in the optimized model.

Log BB prediction	Brij35 0.05 M	SDC 0.05 M	SDS 0.05 M	IAM.PC 40 % MeOH	IAM.PC 30 % MeOH	SM-IAM 30 % MeOH	Cholester 50 % MeOH	Miltefosine 0.01 M	IAM.PC + SDS 0.02 M
# compounds	43	36	49	49	49	49	49	49	49
Initial model									
R(PLS)	0.8668	0.9222	0.9026	0.8865	0.8905	0.8900	0.8832	0.8830	0.8873
R(LOOCV)	0.2279	0.4097	0.2598	0.3659	0.4334	0.4800	0.3304	0.3107	0.4189
Optimized model									
R(PLS)	0.8358	0.8970	0.8886	0.8470	0.8543	0.8509	0.8452	0.8487	0.8452
R(LOOCV)	0.7409	0.8200	0.8228	0.8036	0.8131	0.8032	0.7863	0.7879	0.7863
HIA prediction	**Brij35 0.05 M**	**SDC 0.05 M**	**SDS 0.05 M**	**IAM.PC 40 % MeOH**	**IAM.PC 30 % MeOH**	**SM-IAM 30 % MeOH**	**Cholester 50 % MeOH**	**Miltefosine 0.01 M**	**IAM.PC + SDS 0.02 M**
# compounds	33	29	37	37	37	37	37	37	37
Initial model									
R(PLS)	0.9202	0.9274	0.8027	0.7994	0.7967	0.8025	0.8063	0.8165	0.7987
R(LOOCV)	0.2270	0.1873	-0.0838	-0.0650	-0.0672	-0.0540	-0.0676	-0.0598	-0.0747
Optimized model									
R(PLS)	0.9093	0.9014	0.7706	0.7706	0.7706	0.7746	0.7811	0.7821	0.7706
R(LOOCV)	0.8216	0.7756	0.6694	0.6694	0.6694	0.6727	0.6987	0.7002	0.6694

As mentioned in VIII.2.1, log BB prediction was performed on a set of 49 compounds for all methods except those with Brij35 (43 compounds) and SDC (36 compounds). For HIA

prediction, the amount of compounds for the Brij35 and SDC model was again lower than for the other models.

Concerning log BB prediction, several conclusions can be made. For some of the models (Brij35, Cholester and IAM.PC+SDS), the log BB prediction was only ameliorated to some extent or not ameliorated at all when the log k values were added to the model, leading to the elimination of log k values (together with other descriptors) in the optimized model. These values are presented in orange in Table VIII-5. The R(LOOCV) value of 0.7863 is also quite close to the value for the miltefosine-model (0.7879), which indicates that the use of miltefosine as a surfactant in MLC does not provide a much better model compared to the model without log k values. All other R(LOOCV)-values are > 0.80, which illustrates that the log k values of these models contribute much more to the log BB prediction. The SDS, SDC and IAM.PC 30 % MeOH models provided the highest predictive values, favouring these setups. The SDC model was, however, created using only 36 compounds, while 49 compounds were used for the other models. Therefore, the two other models may be considered as more reliable. The R(PLS) values are all around 0.85, except for the higher values for the SDS (0.88) and SDC (0.89) models. The difference between R(PLS) and R(LOOCV) values in the log BB prediction is always < 0.10, indicating that the models are quite robust and that overfitting is limited.

Several conclusions can also be drawn from the HIA prediction in Table VIII-5. Most of the models (SDC, SDS, IAM.PC (30 an 40 % MeOH) and IAM.PC+SDS) were not improved towards HIA prediction when the log k values were added to the model. Therefore, the log k values were not retained in the optimized models. The orange values in Table VIII-5 indicate the models for which the log k values were not selected in the final model. The R(LOOCV) value of 0.6694 is also quite close to the value for the sphingomyelin-IAM-model (0.6727), which indicates that the sphingomyelin column does not provide a much better model compared to the model without log k values (even though the results of the sphingomyelin column were good for log BB prediction). The other R(LOOCV)-values are higher, which illustrates that the log k values of these models contribute much more to the HIA prediction. The correlation coefficients of the cholester and miltefosine model are similar, although these two models are based on a completely different method. The Brij35 model provides very high PLS and LOOCV correlation coefficients (0.9093 and 0.8216), but these high values are mainly caused by the advantage that only 33 compounds were used to create the model. When the same 33 compounds and the same descriptors were selected for the cholester and miltefosine models, their PLS correlation coefficients respectively increased to 0.9046 and

0.9122 and their LOOCV correlation coefficients to 0.8005 and 0.8229. This indicates that the choice of compounds in the data set is also important and that a rather small change in selection (e.g. elimination of 4 compounds) may lead to a phenomenal increase in correlation coefficients. In contrast to what might be expected from Table VIII-5, the Brij35 model is not better than the miltefosine model (value of 0.8229 in adapted model). This indicates that the miltefosine model is actually the best choice of the presented models towards the prediction of HIA values.

When the log BB and HIA predictions are compared in Table VIII-5, one might conclude that the techniques that lead to a good log BB prediction are not really interesting for HIA prediction and vice versa. None of the presented models was able to perform really well for both types of predictions. This indicates that method selection is sometimes crucial for in vitro prediction studies.

Table VIII-6 shows the coefficients that were obtained based on the log BB and HIA predictions for all optimized models presented in Table VIII-5. In the optimized models for log BB prediction, the descriptors MW, log WSo, MI and MSA were not relevant for any of the models; for HIA prediction, α, MR, log P, HBD and MSA were not retained in the final models. Both for log BB and HIA prediction, several descriptors are (almost) always present in the optimized models; while the descriptors of the log BB models are to a great extent different than those of the HIA models.

VIII.2.3 Conclusion

In section VIII.2, most previously used methods were compared towards both log BB and HIA prediction. Methods with a relatively good log BB prediction generally showed a rather poor (no improvement based on the log k values) HIA prediction capability and vice versa. Therefore, the type of in vitro method that should be selected actually depends on the type of in vivo behavior that should be modeled. There was no clear indication that any of the MLC or IAMLC methods could be claimed as ‘the best’ general method. The SDS model provided the highest LOOCV value for log BB prediction, whereas the miltefosine model provided the highest LOOCV value for HIA prediction (even compared to Brij35 in an adapted model). The model in which the IAM.PC.DD2 column was used with the addition of 20 mM of SDS in the mobile phase was – based on the LOOCV values – the least relevant model presented here.

Table VIII-6: Coefficients for log BB and HIA prediction generated by PLS regression after elimination of variables.

Log BB	Brij35 0.05 M	SDC 0.05 M	SDS 0.05 M	IAM 40% MeOH	IAM 30% MeOH	SM-IAM 30% MeOH	Cholester 50% MeOH	Miltefosine 0.01 M	IAM.PC + SDS 0.02 M
Constant	-2.784	-3.584	-4.437	-2.849	-2.831	-2.626	-2.860	-2.657	-2.860
α	0.573		0.284	0.413	0.444	0.590	0.613	0.640	0.613
MR	-0.017		-0.013			-0.015			
MV		0.014							
Pr		-0.008		-0.002	-0.003		-0.002		-0.002
Polarizability								-0.043	
Log P		-0.228	0.155						
Log D7.4		0.127					0.172		0.172
WS7.4	-0.003	-0.002	-0.002					-0.002	
PB	0.010	0.008					0.007	0.008	0.007
MIA			0.376						
HIA	0.038	0.043	0.051	0.043	0.042	0.037	0.036	0.034	0.036
PSA	-0.034		-0.007			-0.005	-0.007	-0.017	-0.007
HBA	0.293							0.147	
HBD	0.225								
Log k		0.413	0.467	0.719	0.702	0.583		0.237	
HIA	**Brij35 0.05 M**	**SDC 0.05 M**	**SDS 0.05 M**	**IAM 40% MeOH**	**IAM 30% MeOH**	**SM-IAM 30% MeOH**	**Cholester 50% MeOH**	**Miltefosine 0.01 M**	**IAM.PC + SDS 0.02 M**
Constant	26.172	56.711	22.596	22.596	22.596	19.922	10.413	6.607	22.596
MW	0.314	0.204	0.189	0.189	0.189	0.190			0.189
MV	0.421	0.348	0.471	0.471	0.471	0.186	0.336	0.446	0.471
Pr	-0.214	-0.186	-0.269	-0.269	-0.269		-0.152	-0.209	-0.269
Polarizability	-1.909	-1.713				-3.227			
Log D7.4			1.859	1.859	1.859				1.859
Log WSo	7.385		8.844	8.844	8.844	8.193	7.507	7.932	8.844
WS7.4		0.044							
PB	0.231	0.265	0.267	0.267	0.267	0.149	0.195	0.248	0.267
MI		3.431							
MIA	-4.291					-3.840			
HIA	0.757	0.430	0.816	0.816	0.816	0.910	0.955	0.933	0.816
PSA		-0.620							
HBA		8.454					2.768	3.633	
Log k	8.715					8.692	7.631	8.944	

VIII.3 Study of the correlation of the used descriptors

Based on the previously obtained results, overfitting seems to be a recurring issue. A major improvement is obtained when the complexity of the model is reduced by variable selection. During variable selection, most parameters that are irrelevant for the requested prediction or very similar to other parameters, are deleted from the model. In this section, the documented descriptors are analyzed and are compared to each other and to the log BB and HIA values. Based on the analysis and comparison of the descriptors, it is – to some extent – possible to evaluate how important a descriptor is and, therefore, some conclusions can be drawn. All figures and tables in this section were created based on calculations with RStudio (R version 3.1.0) software.

VIII.3.1 Analysis and comparison of the descriptors

VIII.3.1.1 Individual descriptors

First, all descriptors used for model construction were analyzed. A histogram was made for each descriptor (Figure VIII-2), illustrating that for some descriptors (e.g. log D7.4 and log WSo), the distribution along the x-axis follows roughly a normal distribution. Then, a histogram was also created for the experimental log k values and the in vivo log BB and HIA values (Figure VIII-2).

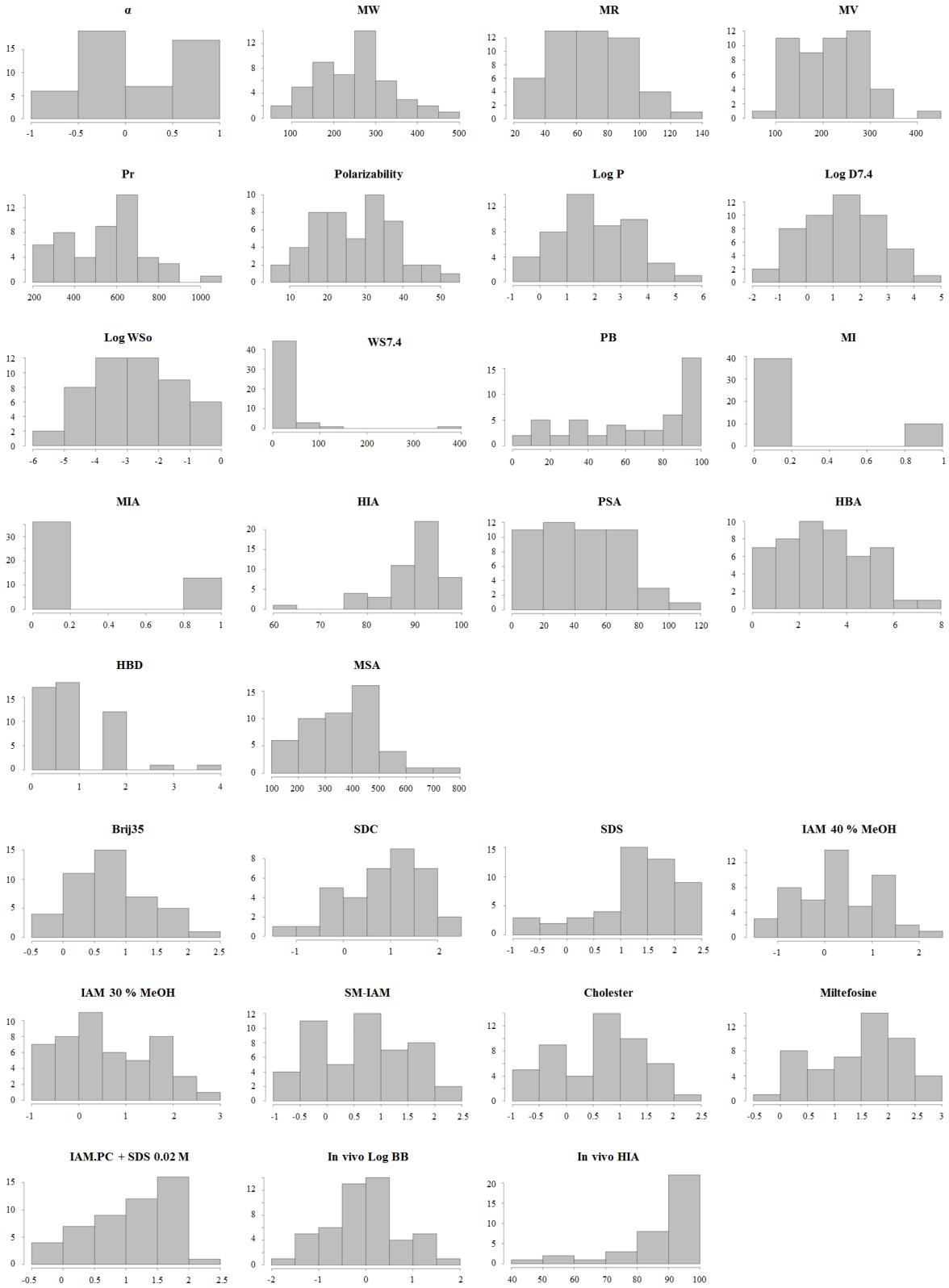

Figure VIII-2: Histograms for all descriptors (exact values are presented in Table C-4; Appendix C), log k values (Table VIII-4) and in vivo values (Table VIII-1) used for model constructions.

Also, for each of these possibilities, the minimum, maximum, 1st and 3rd quartile, median and mean were calculated. These values are presented in Table VIII-7. It should be noted that – aside from 'log k Brij35', 'log k SDC' and 'in vivo HIA' – all histograms and statistics were based on the compound set with 49 compounds.

Table VIII-7: Statistical overview of all descriptors, log k values and in vivo values used for model constructions.

	α	MW	MR	MV	Pr	Polarizabil.	Log P	Log D7.4	LogWSo	WS7.4
Min.	-1.00	78.11	22.50	89.40	207.20	8.92	-0.50	-1.93	-5.19	0.02
1st Qu.	-0.05	180.16	49.38	153.10	370.90	19.57	1.11	0.25	-3.68	0.24
Median	0.00	252.34	69.68	209.10	531.30	27.62	1.99	1.83	-2.92	1.92
Mean	0.20	248.17	69.07	209.00	540.70	27.36	2.11	1.39	-2.79	18.89
3rd Qu.	0.95	286.71	87.85	257.70	677.30	34.82	3.18	2.49	-1.93	10.20
Max.	1.00	454.60	131.86	429.30	1063.90	52.27	5.01	4.17	-0.17	377.00
	PB	MI	MIA	HIA	PSA	HBA	HBD	MSA	Log k Brij35	Log k SDC
Min.	7.66	0.00	0.00	64.30	0.00	0.00	0.00	135.90	-0.50	-1.00
1st Qu.	34.75	0.00	0.00	87.60	23.55	2.00	0.00	272.90	0.28	0.28
Median	72.02	0.00	0.00	91.00	40.54	3.00	1.00	367.90	0.93	1.03
Mean	64.54	0.20	0.27	89.49	42.15	3.51	1.00	373.60	0.79	0.91
3rd Qu.	92.66	0.00	1.00	93.10	63.95	5.00	2.00	459.70	1.24	1.50
Max.	99.93	1.00	1.00	96.70	108.30	8.00	4.00	782.00	2.39	2.27
NA's									6	13
	Log k SDS	Log k IAM 40	Log k IAM 30	Log k SM-IAM	Log k Cholester	Log k Milt	Log k IAM.PC + SDS 0.02 M	In vivo Log BB	In vivo HIA	
Min.	-0.89	-1.33	-0.93	-0.82	-0.77	-0.10	-0.45	-1.70	40.00	
1st Qu.	1.03	-0.44	-0.21	-0.09	-0.16	0.76	0.73	-0.46	83.00	
Median	1.35	0.20	0.49	0.77	0.67	1.61	1.14	0.00	94.00	
Mean	1.24	0.28	0.65	0.67	0.64	1.50	1.06	-0.01	88.65	
3rd Qu.	1.92	1.06	1.47	1.40	1.37	2.17	1.65	0.39	99.00	
Max.	2.20	2.02	2.60	2.45	2.24	2.81	2.05	1.51	100.00	

Some conclusions can be drawn from Figure VIII-2 and Table VIII-7. Concerning WS7.4, there is clearly an outlier in the dataset (N-methyl-2-pyridineethanamine). For MI and MIA, far more compounds have value 0 (= not mutagenic); PB and in vivo HIA values between 90 and 100 are abundantly present (which explains why PB was always retained in the optimized HIA models in Table VIII-6). When the median is compared to the mean in Table VIII-7, these values are mostly similar. However, for log D7.4, the median (1.83) is rather high compared to the mean (1.39); for WS7.4, the mean (18.89) is much higher than the median (1.92), which is partially explained by the outlier in this dataset.

VIII.3.1.2 Correlations between the descriptors

During model optimization, similar parameters are deleted from the model. Figure VIII-3 illustrates the correlation between different descriptors and the log k values based on MLC with SDS. Although the scatter plots are quite small, it is still easy to see that the correlation between some of the descriptors is very high (e.g. between MR and polarizability; MV and Pr; Pr and MSA); while other correlations are very low (e.g. between HBA and log WSo; PB and HIA; MI and log k SDS). A visual confirmation of (in)dependence of descriptors is nice, but it is easier to check the actual correlation coefficients. These are presented in Table VIII-8. High values (e.g. > 0.80) indicate that the descriptors are highly correlated, meaning that it's probable that one of them will be eliminated during model optimization. For example, MW, MR, MV, Pr and Polarizability are clearly highly correlated. In Table VIII-6, only one model uses two of these descriptors after log BB model optimization. This is not the case for HIA model optimization because Table VIII-8 is based on the dataset with 49 compounds, not the limited dataset of 37 compounds used for HIA prediction.

When the correlation coefficient between the descriptors and the log k values of MLC with SDS as surfactant are evaluated, the highest correlations are found with α (R = 0.70) and log D7.4 (R = 0.68). This indicates that these descriptors show (to a certain extent) similar behavior to the experimental data of SDS. Similar scatter plots and tables can be obtained for all other MLC and IAMLC setups, but this is not illustrated here.

Figure VIII-3: Scatter plots of correlations between all descriptors and log k values for MLC with SDS.

Table VIII-8: Correlation coefficients between all descriptors and log k values for MLC with SDS.

	α	MW	MR	MV	Pr	Polar.	Log P	Log D7.4	Log WSo	WS 7.4	PB	MI	MIA	HIA	PSA	HBA	HBD	MSA	log k SDS
α	1.00	0.34	0.42	0.43	0.41	0.42	0.13	0.26	-0.25	0.07	-0.05	0.06	0.06	-0.09	-0.17	0.00	-0.04	0.41	0.70
MW	0.34	1.00	0.96	0.94	0.96	0.96	0.45	0.41	-0.65	-0.29	0.57	0.17	0.13	-0.01	0.28	0.49	0.12	0.94	0.43
MR	0.42	0.96	1.00	0.97	0.99	1.00	0.52	0.44	-0.70	-0.26	0.62	0.14	0.03	0.07	0.16	0.39	0.05	0.98	0.52
MV	0.43	0.94	0.97	1.00	0.99	0.97	0.54	0.45	-0.69	-0.25	0.60	0.12	0.06	0.04	0.17	0.36	0.04	0.99	0.52
Pr	0.41	0.96	0.99	0.99	1.00	0.99	0.51	0.42	-0.68	-0.25	0.60	0.15	0.05	0.05	0.21	0.41	0.07	0.99	0.50
Polar.	0.42	0.96	1.00	0.97	0.99	1.00	0.52	0.44	-0.70	-0.25	0.62	0.13	0.02	0.07	0.16	0.38	0.05	0.98	0.53
Log P	0.13	0.45	0.52	0.54	0.51	0.52	1.00	0.78	-0.81	-0.37	0.84	-0.03	-0.19	0.02	-0.45	-0.39	-0.27	0.49	0.48
Log D7.4	0.26	0.41	0.44	0.45	0.42	0.44	0.78	1.00	-0.66	-0.37	0.57	0.02	-0.18	0.00	-0.43	-0.30	-0.30	0.40	0.68
Log WSo	-0.25	-0.65	-0.70	-0.69	-0.68	-0.70	-0.81	-0.66	1.00	0.52	-0.79	-0.10	0.00	0.04	0.10	0.07	0.02	-0.66	-0.47
WS7.4	0.07	-0.29	-0.26	-0.25	-0.25	-0.25	-0.37	-0.37	0.52	1.00	-0.43	-0.13	-0.11	0.14	-0.06	-0.07	-0.05	-0.24	-0.08
PB	-0.05	0.57	0.62	0.60	0.60	0.62	0.84	0.57	-0.79	-0.43	1.00	0.17	-0.07	0.16	-0.17	-0.12	-0.10	0.58	0.28
MI	0.06	0.17	0.14	0.12	0.15	0.13	-0.03	0.02	-0.10	-0.13	0.17	1.00	0.38	0.01	0.25	0.18	0.27	0.13	-0.08
MIA	0.06	0.13	0.03	0.06	0.05	0.02	-0.19	-0.18	0.00	-0.11	-0.07	0.38	1.00	-0.31	0.32	0.25	0.35	0.05	-0.19
HIA	-0.09	-0.01	0.07	0.04	0.05	0.07	0.02	0.00	0.04	0.14	0.16	0.01	-0.31	1.00	-0.14	-0.01	-0.38	0.04	-0.02
PSA	-0.17	0.28	0.16	0.17	0.21	0.16	-0.45	-0.43	0.10	-0.06	-0.17	0.25	0.32	-0.14	1.00	0.90	0.71	0.20	-0.37
HBA	0.00	0.49	0.39	0.36	0.41	0.38	-0.39	-0.30	0.07	-0.07	-0.12	0.18	0.25	-0.01	0.90	1.00	0.47	0.41	-0.16
HBD	-0.04	0.12	0.05	0.04	0.07	0.05	-0.27	-0.30	0.02	-0.05	-0.10	0.27	0.35	-0.38	0.71	0.47	1.00	0.06	-0.23
MSA	0.41	0.94	0.98	0.99	0.99	0.98	0.49	0.40	-0.66	-0.24	0.58	0.13	0.05	0.04	0.20	0.41	0.06	1.00	0.50
log k SDS	0.70	0.43	0.52	0.52	0.50	0.53	0.48	0.68	-0.47	-0.08	0.28	-0.08	-0.19	-0.02	-0.37	-0.16	-0.23	0.50	1.00

VIII.3.2 Specific relations with log BB and HIA

In this section, the correlation coefficients of the individual descriptors and the experimental log k values are compared to the log BB and HIA values (Table VIII-9). Correlations with HIA were calculated based on the compound set of 37 compounds. Both for log BB and HIA, the number of compounds was lower (see Table VIII-5) for Brij35 and SDC correlations. As can be seen in Table VIII-9, the correlation coefficients compared to log BB are mostly positive. Also, most of the correlations with log k values are > 0.50; while only few descriptors can reach this value. This indicates that the performed experiments show some potential towards log BB prediction.

Table VIII-9: Correlation coefficients of all descriptors and the experimental log k values compared to the log BB and HIA values.

	Log BB	HIA		Log BB	HIA		Log BB	HIA
α	0.432	-0.377	WS7.4	-0.147	0.202	Brij35	0.520	0.002
MW	0.027	-0.282	PB	0.291	-0.002	SDC	0.339	-0.198
MR	0.109	-0.318	MI	-0.036	0.022	SDS	0.621	-0.251
MV	0.103	-0.292	MIA	-0.115	-0.202	IAM 40 % MeOH	0.609	-0.226
Pr	0.069	-0.311	HIA	0.305	0.586	IAM 30 % MeOH	0.587	-0.234
Polarizability	0.110	-0.319	PSA	-0.656	-0.099	SM-IAM	0.543	-0.117
Log P	0.477	-0.130	HBA	-0.505	-0.056	Cholester	0.506	-0.029
Log D7.4	0.563	-0.099	HBD	-0.446	-0.249	Miltefosine	0.539	-0.163
Log WSo	-0.307	0.378	MSA	0.065	-0.304	IAM.PC + SDS 0.02 M	0.471	-0.295

When we look into the correlations with HIA, it is obvious that most of the correlation coefficients are negative. There is only one descriptor with a correlation coefficient > 0.40. Also in absolute values, all correlation coefficients comparing HIA with log k values are (a lot) lower. Generally, we could conclude here that the experimental log k values are initially (not eventually; see section VIII.2.2) more relevant towards log BB prediction.

The scatter plots in Figure VIII-4 show the correlations between log BB and log k values as presented in Table VIII-9. Due to the poor correlation coefficients, the scatter plots of correlations between HIA and log k values are not shown.

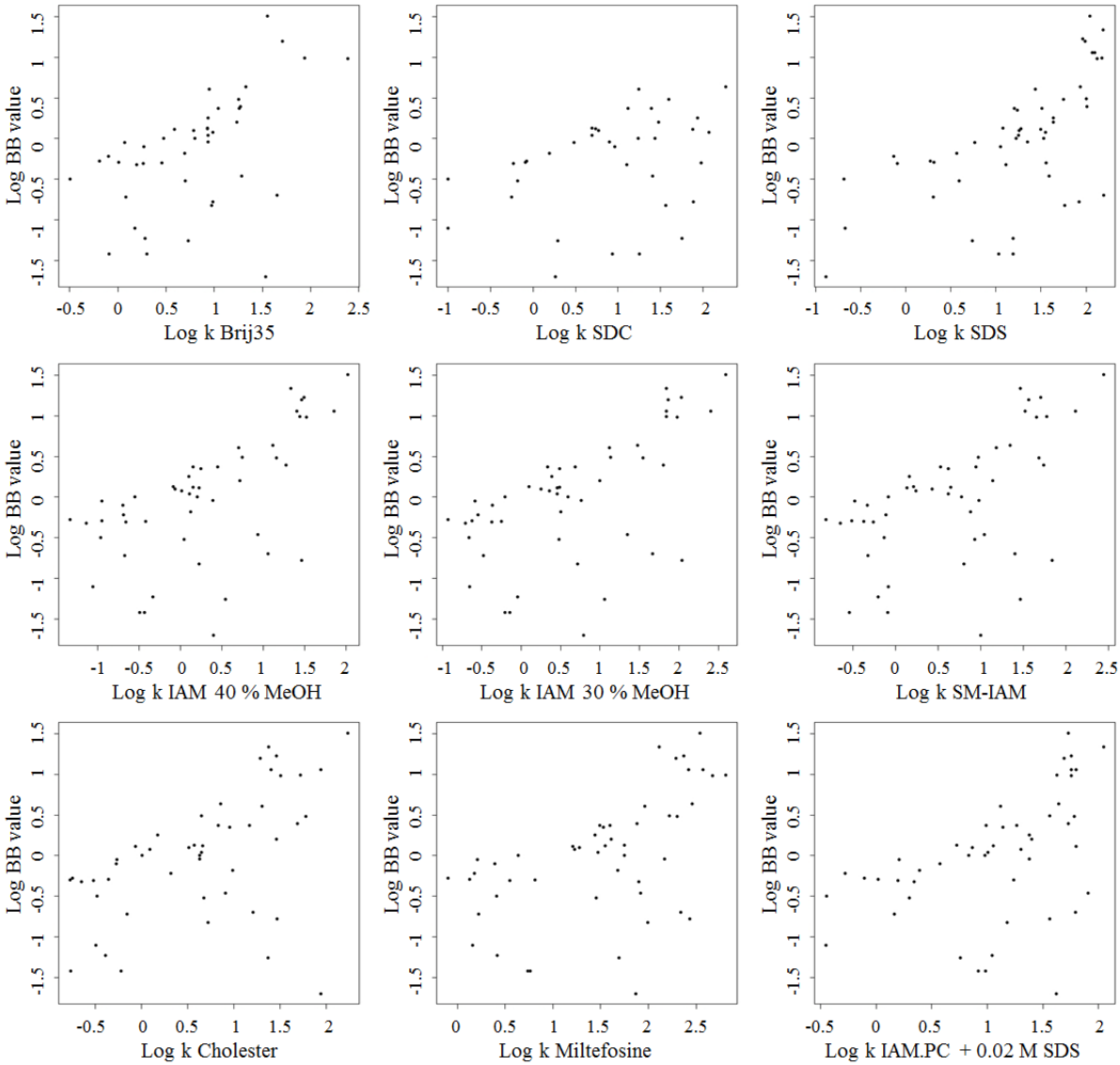

Figure VIII-4: Scatter plots illustrating the correlations between log BB and log k values.

As can be seen in Figure VIII-4, for most compounds a low log k value was obtained for a low log BB value and vice versa. However, for some compounds a low log BB value resulted in a high log k value, which would allow to create a parabolic correlation for a subset of compounds (when high log BB / high log k compounds are not taken into account).

VIII.4 Choice of the computational model

As mentioned in section II.4, several computational models can be applied for the intended purposes. In this work, emphasis has been set on the partial least squares (PLS) regression approach. Multiple linear regression (MLR) can, however, offer quite equivalent results as can be obtained by PLS (see II.4). In order to assess the performance of both approaches, the results of the PLS regression using Matlab are compared to the results of MLR performed with RStudio (R version 3.1.0) software in this section.
Correlation coefficients for log BB and HIA prediction using MLR are calculated as in Table VIII-5 and are displayed in Table VIII-10. Model optimization was not again performed here; the same descriptors as in section VIII.2 were kept in the optimized model.

Table VIII-10: Correlation coefficients between predicted and actual HIA and log BB values when using multiple linear regression (MLR) and the optimized coefficients after elimination of superfluous variables from the models. Values indicated in orange indicate that log k values were not selected in the optimized model.

Log BB prediction	Brij35 0.05 M	SDC 0.05 M	SDS 0.05 M	IAM.PC 40 % MeOH	IAM.PC 30 % MeOH	SM-IAM 30 % MeOH	Cholester 50 % MeOH	Miltefosine 0.01 M	IAM.PC + SDS 0.02 M
# compounds	43	36	49	49	49	49	49	49	49
Initial model									
R(MLR)	0.8668	0.9222	0.9027	0.8865	0.8905	0.8900	0.8832	0.8829	0.8873
Optimized model									
R(MLR)	0.8358	0.8970	0.8886	0.8471	0.8543	0.8509	0.8452	0.8486	0.8452
HIA prediction	**Brij35 0.05 M**	**SDC 0.05 M**	**SDS 0.05 M**	**IAM.PC 40 % MeOH**	**IAM.PC 30 % MeOH**	**SM-IAM 30 % MeOH**	**Cholester 50 % MeOH**	**Miltefosine 0.01 M**	**IAM.PC + SDS 0.02 M**
# compounds	33	29	37	37	37	37	37	37	37
Initial model									
R(MLR)	0.9202	0.9274	0.8027	0.7994	0.7967	0.8024	0.8063	0.8165	0.7987
Optimized model									
R(MLR)	0.9093	0.9014	0.7706	0.7706	0.7706	0.7747	0.7811	0.7820	0.7706

When the values from Tables VIII-5 and VIII-10 are compared, it can be seen that the results of MLR and PLS regression are almost identical for this (limited) dataset. The coefficients for the corresponding equations are also identical to those in Table VIII-6 and are not displayed

here. Therefore, it can be concluded that the choice between PLS and MLR as computational model was not relevant in this work.

VIII.5 References

1. McCormick TJ, Foley JP, Riley CM, Lloyd DK (2000) The effect of stationary-phase pore size on retention behavior in micellar liquid chromatography. Anal Chem 72 (2):294-301.

2. Ruiz-Angel MJ, Carda-Broch S, Torres-Lapasio JR, Garcia-Alvarez-Coque MC (2009) Retention mechanisms in micellar liquid chromatography. J Chromatogr A 1216 (10):1798-1814.

3. Quinones-Torrelo C, Martin-Biosca Y, Martinez-Pla JJ, Sagrado S, Villanueva-Camanas RM, Medina-Hernandez MJ (2002) QRAR Models for Central Nervous System Drugs using Biopartitioning Micellar Chromatography. Mini-Rev Med Chem 2 (2):145-161.

Chapter IX. Summary and general conclusions

IX.1 Summary

In contemporary drug design, significant effort is put in the prediction of drug delivery at the biological location of interest. The rationale behind this, is that the sooner one can establish if drug leads pose problems in terms of drug delivery, the sooner they can be eliminated from the expensive development process. Therefore, a broad variety of methods have been created to establish approaches for predictive modeling. Since all of these in silico or in vitro methods possess certain advantages and drawbacks, so far no golden standard has been developed to accomplish this task. This work focused on the development of in vitro HPLC methods using micellar liquid chromatography and immobilized artificial membrane liquid chromatography for the prediction of drug delivery in the brain and also through the intestinal system. A comparison of existing techniques and several extensions on available approaches are provided.

In **chapter II**, an overview of the typical methods used for the prediction of transport across the BBB is provided. The functions, structure and transport across the BBB are thereby illustrated. Subsequently, the most relevant known delivery systems across the BBB are mentioned, followed by an overview of existing in vivo, in vitro and in silico methods for the prediction of transport across the BBB. Finally, information is provided concerning the possible computational methods which can be used in this type of predictions.

In **chapter III**, several in vitro methods for the prediction of the logarithm of blood–brain distribution coefficient (log BB) values were compared. MLC was performed on a C_{18} column with Brij35, SDC, and SDS as surfactants. IAMLC was performed with methanol as organic

modifier. SDS as a surfactant resulted in the best correlation coefficient between experimental and predicted log BB values (R = 0.7993), followed closely by IAM measurements using 30 % methanol (R = 0.7724). During data treatment, the combination of the results from IAMLC phases and MLC appeared not to improve the accuracy of log BB predictions.

In **chapter IV**, a novel type of stationary phase was manufactured as an alternative to the commercially available immobilized artificial membrane columns. Sphingomyelin was chosen to be processed into the new stationary phase because interesting behavior was anticipated for this lipid, since it is an important constituent of eukaryotic plasma membranes in general. Based on the provided proof-of-concept correlation studies, the sphingomyelin phase was considered to be a promising alternative phase in IAMLC. Scalable, short and modular tuning of the synthetic route should give access to the development of a further repertoire of the novel IAM phases.

In **chapter V**, the abilities of three different types of IAM-columns towards predicting log BB values were compared. The correlation coefficients between actual and predicted log BB values of the three corresponding models appeared very good as all three columns proved useful for this kind of prediction. The results obtained with the sphingomyelin column proved similar to the commercial phosphatidylcholine column. As such, the sphingomyelin column was considered to be a useful alternative for this type of measurements. Since the correlation coefficients based on the results with the cholester column were slightly less promising than those of the other two columns, this column was considered to be a somewhat less interesting option for this type of work.

Methods for extraction, identification and quantification of the main lipid classes (in brain membranes) were presented in **chapter VI**. Phosphatidylcholine and –ethanolamine are the most prominent lipids in brain membranes, while the relative concentrations of other lipid classes have been reported to be divergent in literature. It is therefore challenging to create an exact overview of lipid classes and their concentrations in brain membranes. Differences arise not only between species, but also between individuals, in various sections of the brain, and related to age. A limited comparative study was performed to visualize differences in the lipid composition of white and grey matter in newborn piglets. Although the major lipid classes provided a similar lipid profile, several differences were observable, confirming that significant differences in lipid composition exist between various sections of the brain.

Based on the results in chapter VI, the suggestion was made that the use of lipids in MLC would create a more realistic simulation of drug interactions in brain membranes. Therefore, this field has been explored in **chapter VII**. Based on the findings that phosphatidylcholine and phosphatidylethanolamine are the two most prominent phospholipids in membranes, and the fatty acid groups in lipids typically have a carbon chain length of 16 or 18 carbon atoms, miltefosine was selected for evaluation as a possible surfactant in MLC. Retention of compounds proved to be shorter compared to a purely aqueous mobile phase, indicating that the principle of MLC also works with miltefosine-based micelles. Since this phosphocholine-based lipid is structurally more similar to biological membranes than common surfactants, retention data was used for in vitro predictions of HIA and log BB values. The optimized model for HIA prediction on a compound set of 36 compounds provided a correlation coefficient of 0.7175, while a value of 0.7849 was reached for log BB prediction with 48 compounds.

In the first part of **chapter VIII**, the use of MLC conditions on an IAM column has been studied for the prediction of log BB and HIA values. SDS was chosen as a surfactant for analyses on the IAM.PC.DD2 column, in this way combining experimentally the principles of MLC and IAMLC. However, the correlation coefficients based on LOOCV (both for log BB and HIA) were lower than the values obtained in the previous chapters, proving that the prediction capability of the approach is limited. Also, since the IAM columns are expensive and as the micellar mobile phase could more easily lead to column blockage, the conclusion was made that conventional C_{18}-columns are more appropriate for MLC studies.
In the second part of chapter VIII, the most interesting previously developed methods were compared in an unambiguous way for their capability to predict log BB and HIA values. It appeared that methods with a relatively good log BB prediction generally showed a rather bad HIA prediction and vice versa. Therefore, the type of in vitro method that should be selected actually depends on the type of in vivo behavior that should be modeled. Both for log BB and HIA prediction, several MLC and IAMLC methods could be selected for prediction purposes.
In the third section of chapter VIII, the degree of correlation of the used descriptors is shown in more detail. First, the individual descriptors were statistically processed, then the correlation between all descriptors was evaluated. Finally, the relations with log BB and HIA values were also shown. The results indicated that the correlation between some of the

descriptors is very high, which increases their probability towards elimination during model optimization.

In the final section of chapter VIII, results of the partial least squares regression were compared to those of multiple linear regression. For this limited set of compounds and descriptors, the results of the two methods appeared to be identical. Therefore, the specific choice of regression model was considered to be less important in this work.

IX.2 General conclusions

Introducing a new therapeutic agent on the market is a time-consuming (typically 10 – 15 years) and expensive (ranging from hundreds of millions to several billion euro) process. The overall attrition rate in drug development is very high (> 99%), since most new compounds do not pass the broad range of tests during the consecutive stages of the development process. In contemporary drug design, significant effort is put in the prediction of drug delivery at the biological location of interest, since a faster assessment of lead compounds (or problematic compounds) allows to reduce the total cost of drug development.

In vitro and in silico methods have been developed for the prediction of drug delivery. HPLC-based methods are an important subset of in vitro-based assays to predict drug penetration. This thesis focused on the development and use of micellar liquid chromatography and immobilized artificial membrane liquid chromatography methods in an attempt to improve the prediction of drug delivery.

A problem related to micellar liquid chromatography, is that, although classical surfactants – such as sodium dodecyl sulfate – provide a reasonable prediction of drug delivery, they do not present a realistic mimic of membranes. Therefore, a phosphocholine-based lipid was used as a surfactant in an attempt to create a better simulation of the interaction with membranes. Since biological membranes are composed of several types of (phospho)lipids, additional research, in which a variety of (phospho)lipids are combined as surfactants for MLC, might prove to be very interesting. However, the solubility of phospholipids in water might create problems for this type of mixed micelles.

For immobilized artificial membrane liquid chromatography, research was until now only performed on phosphatidylcholine-coated particles (which allowed proper prediction of drug delivery). Here, the synthesis of sphingomyelin-coated particles was presented and this new type of column was evaluated. Based on the results obtained with this column, we could

assume that other IAM-phases provide alternative interactions with compounds. Therefore, the creation of a mixed stationary phase (which could be created by the coupling of different column segments, by mixing several stationary phases into one column, or by linking several lipids to aminopropyl silica particles) with a selected composition, should in principal provide the best possible mimic of the biological membrane of interest and could therefore provide an improvement of the prediction of drug delivery. However, as mentioned in chapter II, technical limitations with concerns about column consistency and quality control might cause problems for mixed stationary phases.

Throughput is a major issue for in vitro predictions. Although no attention was paid to this point in the thesis, it should be mentioned that throughput could be increased at least by factor 10 when shorter columns should be selected and higher flow rates would be used. The only drawback here is that the efficiency of the chromatographic runs would decrease. Another way to increase throughput would be to use an MS-compatible buffer. MS measurements would allow to measure multiple components simultaneously, which would greatly benefit the total analysis time for a set of compounds.

Samenvatting en algemene conclusies

Samenvatting

Bij de hedendaagse ontwikkeling van geneesmiddelen wordt er veel aandacht besteed aan het voorspellen van het afleveren van die geneesmiddelen op de daarvoor bedoelde plaats in het lichaam. De reden hiervoor is dat geneesmiddelen sneller verwijderd kunnen worden uit het dure ontwikkelingsproces als men sneller te weten komt dat de aflevering in het lichaam problemen met zich meebrengt. Daarom is er een brede waaier aan methodes ontwikkeld om voorspellingen te kunnen maken. Aangezien al deze in silico en in vitro methodes bepaalde voor- en nadelen hebben, is er voorlopig nog geen gulden regel om voorspellingen te maken. In dit werk is de focus gelegd op het ontwikkelen van in vitro hoge performantie vloeistofchromatografie (HPLC) methodes waarbij gebruik gemaakt wordt van micellaire vloeistofchromatografie (MLC) en geïmmobilizeerd artificiëel membraan vloeistofchromatografie (IAMLC) voor het voorspellen van het afleveren van geneesmiddelen in de hersenen alsook doorheen het darmsysteem. Een vergelijking van bestaande technieken en verschillende uitbreidingen op de beschikbare methodes worden besproken.

In **hoofdstuk II** werd een overzicht gegeven van de typische methodes die gebruikt worden voor het voorspellen van transport doorheen de bloed-hersenbarrière (BBB). De functies, structuur en transport doorheen de BBB werden hierbij toegelicht. Vervolgens werden de belangrijkste gekende afleveringssystemen doorheen de BBB opgelijst, gevolgd door een overzicht van bestaande in vivo, in vitro en in silico methodes voor het voorspellen van transport doorheen de BBB. Tenslotte werden enkele mogelijke computationele methodes aangehaald die gebruikt kunnen worden bij dit type voorspellingen.

In **hoofdstuk III** werden enkele in vitro systemen voor het voorspellen van het logaritme van de bloed-hersen verdelingscoëfficiënt (log BB) vergeleken. MLC werd uitgevoerd op een C_{18} kolom met Brij35, natrium deoxycholaat (SDC) en natriumdodecylsulfaat (SDS) als

surfactanten. IAMLC werd uitgevoerd met methanol als organisch solvent. SDS leverde de beste correlatiecoëfficiënt tussen experimentele en voorspelde log BB waarden (R = 0,7993), gevolgd door de geïmmobilizeerd artificiëel membraan (IAM) metingen met 30 % methanol (R = 0,7724). Bij het verwerken van de data leverde het combineren van de resultaten van IAMLC en MLC geen verbetering voor het voorspellen van log BB waarden.

In **hoofdstuk IV** werd een nieuw type stationaire fase aangemaakt, dat als een alternatief kan gebruikt worden voor de commercieel beschikbare IAM kolommen. Sfingomyeline werd gekozen om in de nieuwe stationaire fase te verwerken aangezien interessante kenmerken voorzien werden voor dit lipide omdat het een belangrijk bestanddeel is van het plasmamembraan bij eukaryoten. Afgaande op de initiële correlatiestudies werd de sfingomyeline fase beschouwd als een veelbelovende alternatieve IAMLC fase. De synthesemethode, die opschaalbaar, kort en modulair is, zou toegang moeten geven tot het ontwikkelen van een nieuwe set IAM fases.

In **hoofdstuk V** werden de mogelijkheden van drie verschillende types IAM kolommen vergeleken op vlak van het voorspellen van log BB waarden. De correlatiecoëfficiënten tussen de actuele en voorspelde log BB waarden van de drie overeenkomstige modellen bleken zeer goed, de drie kolommen werden dus allen geschikt bevonden voor dit type voorspellingen. De resultaten die bekomen werden met de sfingomyeline kolom waren gelijkaardig aan die van de commerciële fosfatidylcholine kolom. Zodoende werd de sfingomyeline kolom beschouwd als een goed alternatief voor dit type metingen. Aangezien de correlatiecoëfficiënten gebaseerd op de resultaten met de cholester kolom minder goed waren dan deze van de andere twee kolommen, werd deze kolom beschouwd als een minder interessante optie voor dit type metingen.

Methodes voor extractie, identificatie en kwantificatie van de belangrijkste lipidenklassen (in hersenmembranen) werden voorgesteld in **hoofdstuk VI**. Fosfatidylcholine en –ethanolamine zijn de meest voorkomende lipiden in hersenmembranen; de relatieve concentraties van andere lipidenklassen zijn volgens de literatuur uiteenlopend. Daarom is het zeer moeilijk om een exact overzicht te geven van lipidenklassen en hun concentraties in hersenmembranen. Verschillen ontstaan niet enkel tussen soorten, maar ook tussen individuen, in verschillende delen van de hersenen en afhankelijk van de leeftijd. Een beperkte vergelijkende studie werd uitgevoerd om verschillen in lipidensamenstelling te visualiseren tussen witte en grijze stof in

pasgeboren biggetjes. Alhoewel de belangrijkste lipidenklassen een gelijkaardig lipidenprofiel vertoonden, waren er ook enkele duidelijke verschillen, hetgeen bevestigde dat er significante verschillen zijn op vlak van lipidensamenstelling in verschillende secties van de hersenen.

Afgaande op de resultaten van hoofdstuk VI, werd er gesuggereerd dat het gebruik van lipiden in MLC zou leiden tot een meer realistische simulatie van interacties van geneesmiddelen in hersenmembranen. Bijgevolg werd dit studiegebied verkend in **hoofdstuk VII**. Gebaseerd op de bevindingen dat fosfatidylcholine en –ethanolamine de twee meest prominente fosfolipiden in membranen zijn, en dat de vetzuurgroepen in lipiden typisch een koolstofketen met 16 of 18 koolstofatomen hebben, werd miltefosine geselecteerd voor evaluatie als een mogelijk surfactant in MLC. De retentie van componenten was korter in vergelijking met een puur waterig systeem, wat aangeeft dat het principe van MLC ook werkt met micellen gebaseerd op miltefosine. Aangezien dit fosfocholine-gebaseerd lipide qua structuur beter aanleunt bij biologische membranen in vergelijking met gewone surfactanten, werd de retentiedata gebruikt voor in vitro voorspellingen van menselijke intestinale absorptie (HIA) en log BB waarden. Het geöptimaliseerde model voor HIA voorspellingen met een set van 36 componenten leverde een correlatiecoëfficiënt van 0,7175; een waarde van 0,7849 werd bereikt voor log BB voorspellingen op basis van 48 componenten.

In het eerste gedeelte van **hoofdstuk VIII** werd het gebruik van MLC condities op een IAM kolom bestudeerd voor het voorspellen van log BB en HIA waarden. SDS werd gekozen als surfactant voor metingen op een IAM.PC.DD2 kolom; zodat de principes van MLC en IAMLC op deze manier experimenteel gecombineerd werden. Niettemin waren de correlatiecoëfficiënten zowel voor de predictie van log BB als van HIA lager dan de waarden die in de vorige hoofdstukken bereikt werden, wat aangeeft dat de mogelijkheden op vlak van voorspellen via deze methode beperkt zijn. Aangezien het ook zo is dat IAM kolommen duur zijn en een micellaire mobiele fase gemakkelijker kan zorgen voor blokkage van de kolom, was de conclusie dat conventionele C_{18} kolommen meer geschikt zijn voor MLC studies.
In het tweede gedeelte van hoofdstuk VIII werden de meest interessante methodes uit deze thesis vergeleken naar hun mogelijkheden om log BB en HIA waarden te voorspellen. Het leek er op dat methodes met een relatief goede log BB voorspelling algemeen gezien eerder slecht presteerden op vlak van HIA-voorspelling (en omgekeerd). Daarom lijkt het belangrijk om te weten welk type in vivo gedrag gemodelleerd moet worden vooraleer het type in vitro

methode gekozen wordt. Zowel voor log BB als voor HIA voorspelling zijn er enkele MLC en IAMLC methodes die geselecteerd kunnen worden om voorspellingen te maken.
In de derde sectie van hoofdstuk VIII werd de correlatie van de gebruikte descriptoren in meer detail getoond. Eerst werden de individuele descriptoren statistisch verwerkt, waarna de correlatie tussen alle descriptoren werd geëvalueerd. Tenslotte werden de verbanden met log BB en HIA ook getoond. De resultaten gaven aan dat de correlatie tussen enkele van descriptoren zeer hoog is, wat de kans op eliminatie tijdens het optimaliseren van een model doet toenemen.
In het laatste deel van hoofdstuk VIII werden de resulaten van de PLS regressie vergeleken met deze van meervoudige lineaire regressie (MLR). Voor deze beperkte set van componenten en descriptoren bleken de resultaten van de twee methodes identiek. Hierdoor konden we stellen dat de keuze van regressiemodel minder relevant was in dit werk.

Algemene conclusies

De invoering van een nieuw geneesmiddel is een tijdrovend (typisch 10 tot 15 jaar) en duur (enkele honderden miljoenen to enkele miljarden euro) proces. Bij het ontwikkelingsproces gaat gewoonlijk meer dan 99 % van de geneesmiddelen verloren aangezien de meeste nieuwe componenten niet slagen voor de grote waaier aan testen tijdens de opeenvolgende stappen in de ontwikkeling. Bij het huidige ontwikkelingsproces van geneesmiddelen wordt er veel aandacht besteed aan het voorspellen van het afleveren van die geneesmiddelen op de daarvoor bedoelde plaats in het lichaam, aangezien een snellere toewijzing van interessante (of problematische) componenten toelaat om de totale kost van de geneesmiddelenontwikkeling te verminderen.
In vitro en in silico methodes werden ontwikkeld voor het voorspellen van het afleveren van geneesmiddelen. HPLC-gebaseerde methodes omvatten een belangrijk deel van de in vitro onderzoeken om de doorlaatbaarheid van geneesmiddelen te voorspellen. In deze thesis werd de nadruk gelegd op de ontwikkeling en het gebruik van micellaire vloeistofchromatografie (MLC) en geïmmobilizeerd artificiëel membraan vloeistofchromatografie (IAMLC) methodes, met als doel om de aflevering van geneesmiddelen beter te kunnen voorspellen.
Een probleem met betrekking tot MLC is dat, alhoewel klassieke surfactanten – zoals natriumdodecylsulfaat – een redelijke voorspelling bewerkstelligen, ze geen realistisch beeld van membranen geven. Daarom werd een fosfocholine-gebaseerd lipide gebruikt als

surfactant in een poging om een betere simulatie van de interactie met membranen te bekomen. Aangezien biologische membranen bestaan uit meerdere types (fosfo)lipiden, zou extra onderzoek, waarbij meerdere (fosfo)lipiden gecombineerd worden als surfactanten bij MLC, zeer interessant kunnen zijn. De oplosbaarheid van fosfolipiden in water zou echter voor problemen kunnen zorgen bij dit type van gemengde micellen.

Voor IAMLC werd onderzoek tot nog toe enkel uitgevoerd op deeltjes gecoat met fosfatidylcholine (die een redelijke voorspelling van het afleveren van geneesmiddelen toelieten). Hier werd de synthese van deeltjes gecoat met sfingomyeline voorgesteld en dit nieuw type kolom werd geëvalueerd. Gebaseerd op de resultaten die met deze kolom bekomen werden, konden we aannemen dat andere IAM fases andere interacties met de componenten aan zouden kunnen gaan. Daarom zou de ontwikkeling van een gemengde stationaire fase (die bekomen zou kunnen worden door het aaneenkoppelen van verschillende kolomsegmenten, door het mengen van verschillende stationaire fases in één kolom, of door het linken van verschillende lipiden op aminopropyl silica deeltjes) met een gekozen samenstelling in principe de best mogelijke nabootsing van het biologisch membraan van interesse kunnen leveren en bijgevolg ook een verbetering van de voorspelling van het afleveren van geneesmiddelen. Zoals reeds werd aangehaald in hoofdstuk II zouden technische limitaties en zorgen om kolom consistentie en kwaliteitscontrole problemen kunnen veroorzaken bij gemengde stationaire fases.

Snelheid is een belangrijk aspect bij in vitro voorspellingen. Alhoewel er in deze thesis geen aandacht werd besteed aan dit punt, is het belangrijk om te vermelden dat de snelheid van de metingen ten minste met een factor 10 verhoogd kan worden door het gebruik van kortere kolommen en hogere vloeistofdebieten. Het enige nadeel hierbij is dat de efficiëntie van de chromatografische metingen zou afnemen. Een andere manier om de snelheid te verhogen is het gebruik van een massaspectrometrie (MS)-compatibele buffer. MS metingen zouden toelaten om meerdere componenten tegelijkertijd te meten, wat de totale analysetijd voor een reeks componenten enorm zou verminderen.

Appendix A. Overview of experimental log BB values

The Table in this section gives an overview of compounds with in vivo determined log BB values present in literature [1-24]. When multiple log BB values were found, the average value was calculated. Compounds indicated in grey were experimentally used in this thesis; the structural formula of these compounds is presented in Appendix B. The Table also provides a limited overview of drug usage for these compounds.

As can be seen in the Table below, various drug applications are mentioned, of which most are recurrent. The discussion of all applications lies beyond the scope of this research. However, a brief explanation is provided here for some of the more frequently used applications:

- Analgesic: this type of drug is used to relieve the pain (= painkiller).
- Anesthetic: a drug that causes a temporal loss of sensation.
- Anticonvulsant: mainly used in the treatment of epileptic seizures (= antiepileptic).
- Antiemetic: an effective drug against vomiting and nausea.
- Antihistamine: can be used to treat gastric acid conditions or to suppress allergic reactions.
- Antipsychotic: a drug used primarily to manage psychosis, particularly schizophrenia and bipolar disorder (= neuroleptic).
- Anxiolytic: reduces or inhibits anxiety.
- Benzodiazepine: enhances the effect of a neurotransmitter, which results in sedative, muscle relaxant, hypnotic, anxiolytic and anticonvulsant properties.
- Beta-blocker: a drug particularly used to manage cardiac arrhythmias, to protect the heart from a second heart attack, and sometimes for hypertension.
- Stimulant: induce temporary improvements in mental and/or physical functions (e.g. caffeine and nicotine).
- Some other drugs are specifically used for the treatment of diseases like Alzheimer's and Parkinson's.

Overview of experimental log BB values

	CAS	Name	Possible drug use	Log BB	References
1	630-20-6	1,1,1,2-Tetrachloroethane	-	0.33	14,15
2	71-55-6	1,1,1-Trichloroethane	Insecticide	0.28	1,6,8,10,11,14,15,16,20,21,22,23,24
3	75-88-7	1,1,1-Trifluoro-2-chloroethane	-	-0.12	1,6,8,16,24
4	79-00-5	1,1,2-Trichloroethane	-	-0.10	14,15
5	75-34-3	1,1-Dichloroethane	Inhalational anesthetic	-0.28	14,15
6	635-46-1	1,2,3,4-Tetrahydroquinoline	-	0.65	16
7	95-63-6	1,2,4-Trimethylbenzene (Pseudocumene)	-	0.16	14,15
8	2234-75-5	1,2,4-Trimethylcyclohexane	-	1.02	14,15
9	107-06-2	1,2-Dichloroethane	-	-0.14	14,15
10	583-57-3	1,2-Dimethylcyclohexane	-	1.07	14,15
11	106-99-0	1,3-Butadiene	-	-0.17	14,15
12	92817-10-2	16a-Fluoroestradiol (estradiol-16a-fluoro)	PET imaging agent	-0.30	14,15
13	106-94-5	1-Bromopropane	-	0.31	14,15
14	71-36-3	1-Butanol	-	-0.02	14,15
15	6336-01-2	1-Butyl-3-phenylthiourea	-	0.04	6,12
16	872-05-9	1-Decene	-	0.96	14,15
17	59468-90-5	1-Hydroxymidazolam	Benzodiazepine	-0.07	1,6,10,12,14,15,16,17
18	124-11-8	1-Nonene	-	0.86	14,15
19	111-66-0	1-Octene	-	0.74	14,15
20	71-41-0	1-Pentanol	-	0.20	14,15
21	71-23-8	1-Propanol	-	-0.13	1,6,8,10,11,12,14,15,16,19,20,21,22,23,24
22	406-90-6	2,2,2-Trifluoroethyl vinyl ether (Fluroxene)	Inhalational anesthetic	0.13	1,6,8,10,11,14,15,16,20,21,23,24
23	75-83-2	2,2-Dimethylbutane	-	1.04	1,6,8,10,11,12,14,15,16,20,21,22,23,24
24	132235-73-5	2',3'-Dideoxy-3'-hydroxymethylcytidine	Antiviral	-0.79	17
25	2078-54-8	2,6-diisopropylphenol (Propofol)	Anesthetic	0.59	6,12,14,15
26	75-26-3	2-Bromopropane	-	0.56	14,15
27	78-93-3	2-Butanone (Methyl ethyl ketone)	-	-0.10	1,6,8,10,11,12,14,15,16,20,21,22,23,24
28	592-27-8	2-Methyl heptane	-	0.86	14,15
29	871-83-0	2-Methyl nonane	-	1.05	14,15
30	3221-61-2	2-Methyl octane	-	0.98	14,15
31	78-83-1	2-Methyl-1-propanol (Isobutanol)	-	-0.16	6,8,10,11,12,14,15,16,20,21,22,23,24
32	43133-95-5	2-Methylpentane	-	0.97	1,6,8,10,11,12,14,15,16,20,21,22,23,24
33	107-87-9	2-Pentanone	-	-0.01	14,15
34	67-63-0	2-Propanol (Isopropanol)	Antiseptic	-0.14	1,6,8,10,11,12,14,15,16,20,21,22,23,24
35	6304-27-4	2-Pyridine-ethanamine-n-n-dimethyl	Antihistamine	-0.61	12,14,15,16,17,18,20,21,23

	CAS	Name	Possible drug use	Log BB	References
36	123-51-3	3-Methyl-1-butanol (Isopentanol)	-	0.04	14,15
37	589-34-4	3-Methylhexane	-	0.90	1,6,8,10,11,12,14,15,16,20,21,23,24
38	96-14-0	3-Methylpentane	-	1.01	1,6,8,10,11,12,14,15,16,20,21,22,23,24
39	98-56-6	4-Chlorobenzotrifluoride	-	0.17	14,15
40	5400-60-2	4-Fluoroantipyrine	Blood flow tracer	-0.05	14,15
41	30896-57-2	4-Hydroxyalprazolam	Benzodiazepine	-1.48	16
42	59468-85-8	4-Hydroxymidazolam	Benzodiazepine	-0.20	1,6,10,12,14,15,16,17
43	201-019-9	5-Butyl-5-ethyl barbituric acid (Butethal)	Barbiturate	0.19	14,15
44	27653-63-0	5-Methyl-5-ethyl barbituric acid	Barbiturate	0.00	14,15
45	144598-75-4	9-Hydroxy-Risperidone	Antipsychotic	-0.67	1,4,10,12,14,15,16,18
46	37517-30-9	Acebutolol	Beta-blocker	-0.15	17
47	103-90-2	Acetaminophen (paracetamol)	Analgesic	-0.37	1,2,5,7,8,9,10,11,12,13,14,15,16,17,19,20,21,24
48	67-64-1	Acetone (Propanone)	-	-0.16	1,6,8,10,11,12,14,15,16,20,21,22,23,24
49	50-78-2	Acetylsalicylic Acid (aspirin)	Analgesic/ NSAID	-0.59	1,2,5,6,8,9,10,11,12,13,16,17,18,19,20,21,24
50	107-13-1	Acrylonitrile	-	-0.40	14,15
51	59277-89-3	Acyclovir	Antiviral	-0.84	22
52	178307-42-1	AI-9 (Revaprazan hydrochloride)	Anticancer drugs	0.21	14,15
53	52-43-7	Allobarbital	Barbiturate	-0.22	17
54	25526-93-6	Alovudine	Antiviral	-0.59	1,14,15
55	28981-97-7	Alprazolam	Benzodiazepine/ Anxiolytic	0.03	1,5,6,7,8,9,10,11,12,13,14,15,16,17,18,19,20,21,24
56	13655-52-2	Alprenolol	Beta-blocker	-0.23	17
57	58-15-1	Aminopyrine	Analgesic	0.00	1,5,6,7,10,12,13,14,15,16
58	50-48-6	Amitriptyline (Triptanol)	Antidepressant	0.90	4,5,6,7,12,13,14,15,16,17,18,19,20,21,23
59	57-43-2	Amobarbital	Barbiturate/ Hypnotic	0.04	1,5,6,7,10,12,13,14,15,16,19
60	300-62-9	Amphetamine	Stimulant	0.93	16
61	161814-49-9	Amprenavir	Antiviral	-0.56	17
62	75-85-4	Amylene-hydrate (tertiary-amyl alcohol)	Anesthetic	0.07	14,15
63	60-80-0	Antipyrine (Phenazone)	Analgesic	-0.11	1,2,5,6,8,9,10,11,12,13,14,15,16,18,19,20,21,22,24
64	151581-23-6	Apaxifylline	Neuroprotective agent	-1.40	17
65	7440-37-1	Argon	-	0.03	10,11,15,16
66	29122-68-7	Atenolol	Beta-blocker	-1.12	1,3,5,7,10,12,13,14,15,16,17,19
67	51-55-8	Atropine	Anticholinergic	-0.06	5,13,16
68	57-44-3	Barbital (5-Ethyl-5-ethyl barbituric acid)	Barbiturate	-0.14	14,15
69	150146-06-8	Beloxepin	Analgesic	0.82	14,15,17,18
70	55-21-0	Benzamide	-	-0.24	6

	CAS	Name	Possible drug use	Log BB	References
71	71-43-2	Benzene	-	0.32	1,2,5,6,8,10,11,12,14,15,16,19,20,21,22,23,24
72	63659-18-7	Betaxolol	Beta-blocker	0.39	17
73	514-65-8	Biperiden	Anticholinergic	0.85	14,15
74	80-05-7	Bisphenol A	-	-0.12	14,15
75	84379-13-5	Bretazenil	Anxiolytic	-0.09	1,6,10,12,14,15,17
76	25614-03-3	Bromocriptine	Dopamine agonist	-1.10	13,16
77	10457-90-6	Bromperidol	Antipsychotic	1.38	1,10,12,13,16,17,19
78	34915-68-9	Bunitrolol	Beta-blocker	0.38	22
79	34841-39-9	Bupropion (Zyban)	Antidepressant	1.40	17
80	36505-84-7	Buspirone	Anxiolytic	0.48	16
81	94-25-7	Butyl 4-aminobenzoate	Anesthetic	0.42	14,15
82	123-86-4	Butyl acetate	-	0.28	14,15
83	58-08-2	Caffeine	Stimulant	-0.04	1,2,5,6,7,8,9,10,11,12,13,14,15,16,17,18,19,20,21,22,24
84	298-46-4	Carbamazepine	Anticonvulsant	-0.07	1,4,5,6,7,12,13,14,15,16,18,19,20,21,23
85	36507-30-9	Carbamazepine-10,11-Epoxide	Anticonvulsant	-0.34	1,4,6,12,13,14,15,16,18,19,20,21,23
86	75-15-0	Carbon Disulfide	-	0.60	6,10,11,14,15,16,21
87	154-93-8	Carmustine (BCNU)	Anticancer drugs	-0.52	1,6,8,11,12,13,14,15,16,18,20,21,24
88	51781-06-7	Carteolol	Beta-blocker	-0.40	14,15
89	69712-56-7	Cefotetan	Antibiotic	-1.89	16
90	83881-51-0	Cetirizine	Antihistamine	-2.15	17
91	305-03-3	Chlorambucil	Chemotherapy	-1.70	1,8,11,12,18,20,24
92	67-66-3	Chloroform (Trichloromethane)	Inhalational anesthetic	0.25	1,10,11,12,14,15,16
93	50-53-3	Chlorpromazine	Antipsychotic	1.02	1,3,5,6,7,8,9,10,11,12,13,14,15,16,17,18,19,20,21,24
94	51481-61-9	Cimetidine (Y-G1)	Antihistamine/ Peptic ulcer	-1.42	1,3,4,6,7,9,10,11,12,13,16,17,18,19,20,21,23
95	156-59-2	Cis 1,2-dichloroethene	-	-0.13	14,15
96	22316-47-8	Clobazam	Benzodiazepine/ Anxiolytic	0.35	1,10,12,13,14,15,16,17,19
97	4205-90-7	Clonidine (SKB6)	Adrenergic	0.13	1,3,4,5,6,7,9,10,11,12,14,15,16,17,18,19,20,21,23
98	50-36-2	Cocaine	Local anesthetic	0.60	14,15
99	76-57-3	Codeine	Analgesic	0.38	1,6,7,8,9,10,11,12,13,14,15,16,17,18,19,20,21,24
100	486-56-6	Cotinine	Antidepressant	-0.28	6,12,14,15,17
101	52-31-3	Cyclobarbital	Barbiturate	-0.30	17
102	110-82-7	Cyclohexane	-	1.00	10,12,14,15,16
103	75-19-4	Cyclopropane	Inhalational anesthetic	0.04	10,14,15,16
104	59865-13-3	Cyclosporine A	Immunosuppressant	-0.78	22
105	485-35-8	Cytisine	Nicotinic	-1.09	17

	CAS	Name	Possible drug use	Log BB	References
106	486-66-8	Daidzein	Isoflavones	-0.15	14,15
107	133099-04-4	Darifenacin	Urinary incontinence	-0.62	17
108	124-18-5	Decane	-	0.67	14,15
109	57041-67-5	Desflurane	Anesthetic	0.11	16
110	50-47-5	Desipramine	Antidepressant	1.11	1,4,8,9,10,11,12,13,14,15,16,17,18,19,20,21,24
111	22316-55-8	Desmethylclobazam	Benzodiazepine	0.31	1,6,10,12,13,14,15,16,17
112	2095-20-7	Desmonomethylpromazine (Monodesmethylpro.)	Antipsychotic	0.59	1,6,10,12,14,15,16,17
113	439-14-5	Diazepam	Benzodiazepine/ Anxiolytic	0.45	1,2,5,6,7,10,12,13,14,15,16,17,19
114	75-09-2	Dichloromethane	-	-0.23	10,14,15,16
115	69655-05-6	Didanosine	Anti-HIV	-1.03	1,6,8,10,11,14,15,16,17,18,20,21,22,24
116	2095-95-6	Didesipramine (Desmethyldesipramine)	Antidepressant	1.04	1,6,10,13,14,15,16,17
117	60-29-7	Diethyl ether	Anesthetic	0.00	1,6,8,10,11,12,14,15,16,20,21,22,23,24
118	20830-75-5	Digoxin	Cardiac glycoside	-1.23	22
119	58-73-1	Diphenhydramine	Antihistamine	1.26	14,15
120	109-93-3	Divinyl ether (vinyl ether)	Inhalational anesthetic	0.12	10,12,14,15,16
121	57808-66-9	Domperidone	Antiemetic	-0.83	1,4,12,14,15,18
122	120014-06-4	Donepezil (Aricept)	Treatment of Alzheimer's	0.89	17
123	23214-92-8	Doxorubicin	Chemotherapy	-0.83	22
124	469-21-6	Doxylamine	Antihistamine	0.64	14,15
125	13838-16-9	Enflurane	Inhalational anesthetic	0.21	1,6,8,10,11,14,15,16,20,21,22,23,24
126	57-47-6	Eserine (Physostigmine)	Glaucoma	0.08	1,5,6,7,8,11,12,13,14,15,16,18,20,21,24
127	64-17-5	Ethanol	-	-0.15	1,6,8,10,11,12,14,15,16,19,20,21,22,23,24
128	938-73-8	Ethenzamide (o-Ethoxybenzamide and AI-5)	Analgesic	-0.05	14,15
129	94-09-7	Ethyl 4-aminobenzoate	Anesthetic	0.27	14,15
130	141-78-6	Ethyl acetate	-	0.00	14,15
131	637-92-3	Ethyl t-butyl ether	-	0.22	14,15
132	100-41-4	Ethylbenzene	-	0.22	5,10,14,15,16
133	74-85-1	Ethylene (ethene)	Anesthetic	0.31	14,15
134	75-21-8	Ethylene Oxide	-	0.01	14,15
135	33419-42-0	Etoposide	Anticancer drugs	-2.00	16
136	437-38-7	Fentanyl	Opioid analgesic	0.58	14,15
137	83799-24-0	Fexofenadine (Allegra)	Antihistamine	-0.98	17
138	98206-10-1	Flesinoxan	Antidepressant/ Anxiolitic	-0.45	22
139	86386-73-4	Fluconazole	Antifungal	-0.22	17
140	78755-81-4	Flumazenil	Antidote for benzodiazepines	-0.29	1,2,6,10,12,14,15,17

	CAS	Name	Possible drug use	Log BB	References
141	1622-62-4	Flunitrazepam	Benzodiazepine / Hypnotic	0.06	1,6,10,12,13,14,15,16,17,19
142	54910-89-3	Fluoxetine	Antidepressant	0.72	14,15,17
143	69-23-8	Fluphenazine (Triflumethazine)	Neuroleptic/ Antipsychotic	1.51	1,6,7,10,12,13,16,17,19
144	54739-18-3	Fluvoxamine	Obsessive-Compulsive Disorder	0.79	17
145	357-70-0	Galantamine	Alzheimer's disease	0.32	17
146	490-79-9	Gentisic acid	-	0.08	16
147	471-53-4	Glycyrrhetinic acid	Peptic ulcer	-1.40	14,15
148	109889-09-0	Granisetron	Antiemetic	-0.69	1
149	52-86-8	Haloperidol	Antipsychotic	1.34	1,3,5,7,10,12,13,16,17,19
150	151-67-7	Halothane	Anesthetic	0.27	1,6,8,10,11,14,15,16,20,21,22,23,24
151	5579-03-3	HEPP (3-hydroxy-3-phenylpentanamide)	Anticonvulsant	0.04	14,15
152	142-82-5	Heptane	-	0.69	1,6,8,10,11,12,14,15,16,20,21,22,23,24
153	110-54-3	Hexane	-	0.74	1,6,8,10,11,12,14,15,16,20,21,22,23,24
154	56-29-1	Hexobarbital	Barbiturate/Hypnotic	0.04	1,6,10,12,13,14,15,16,17,19
155	68-88-2	Hydroxyzine	Antihistamine	0.34	1,6,8,9,10,11,12,13,14,15,16,17,18,19,20,21,24
156	15687-27-1	Ibuprofen	Analgesic/ NSAID	-0.18	1,2,5,6,7,8,9,10,11,12,13,14,15,16,17,18,19,20,21,24
157	71351-79-6	Icotidine	Antihistamine	-2.00	1,4,6,11,12,16,17,18,20,21,23
158	50-49-7	Imipramine (SKB8)	Antidepressant	1.03	1,3,4,5,6,7,9,10,11,12,13,14,15,16,17,18,19,20,21,23
159	150378-17-9	Indinavir	Aids	-0.74	1,6,10,14,15,16,17,21,22
160	53-86-1	Indomethacin	Analgesic/ NSAID	-1.26	1,2,6,7,8,9,10,11,12,13,14,15,16,18,19,20,21,24
161	110-19-0	Isobutyl acetate	-	0.45	14,15
162	26675-46-7	Isoflurane	Inhalational anesthetic	0.36	1,6,8,10,11,14,15,16,20,21,22,23,24
163	123-92-2	Isopentylacetate	Honey bee pheromone	0.55	14,15
164	108-21-4	Isopropyl acetate	-	0.40	14,15
165	4759-48-2	Isotretinoin (13-cis-Retinoic Acid)	Anti-acne	-0.49	22
166	65277-42-1	Ketoconazole	Antifungal	-0.63	17
167	7439-90-9	Krypton	-	-0.16	10,15,16
168	84057-84-1	Lamotrigine	Antiepileptic	0.29	1,14,15
169	59-92-7	Levodopa	Dopamine-agonist/ Parkinson's	-0.77	13,16
170	77-07-6	Levorphanol	Opioid analgesic	0.00	13,16
171	137-58-6	Lidocaine	Local anesthetic	0.34	14,15
172	53179-11-6	Loperamide	Anti-diarrheal	0.77	17
173	846-49-1	Lorazepam	Anxiolytic/ Hypnotic	0.44	14,15
174	83903-06-4	Lupitidine	Antiulcer	-1.06	1,4,6,11,14,15,16,17,18,20,21,23
175	69-65-8	Mannitol	Osmotherapy	-1.60	14,15

	CAS	Name	Possible drug use	Log BB	References
176	53230-10-7	Mefloquine (AI-8)	Anti-malaria	0.63	14,15
177	5588-33-0	Mesoridazine	Neuroleptic/ Antipsychotic	-0.31	1,6,10,12,13,16,17
178	33817-09-3	Methamphetamine	ADHD	0.93	14,15,16
179	74-82-8	Methane	-	0.04	6,10,11,14,15,16,21,23
180	67-56-1	Methanol	-	0.02	14,15
181	151-83-7	Methohexital	Anesthetic	-0.06	1,6,10,12,14,15,16,17
182	59-05-2	Methotrexate	Anticancer drugs	-1.52	13,16
183	76-38-0	Methoxyflurane	Inhalational anesthetic	0.21	1,10,11,14,15,16
184	79-20-9	Methyl acetate	-	-0.13	14,15
185	1634-04-4	Methyl t-butyl ether	-	0.36	14,15
186	108-87-2	Methylcyclohexane	-	0.96	14,15
187	96-37-7	Methylcyclopentane	-	0.93	1,6,8,10,11,12,14,15,16,20,21,22,23,24
188	37350-58-6	Metoprolol	Beta-blocker	1.15	17
189	24219-97-4	Mianserin	Antidepressant	0.99	1,3,4,5,7,10,12,14,15,16,17,18,19
190	59467-64-0	Midazolam	Benzodiazepine	0.38	1,3,5,6,7,8,9,10,11,12,14,15,16,17,18,19,20,21,24
191	37065-29-5	Miloxacin	Antibacterial	-0.92	14,15
192	85650-52-8	Mirtazapine (Mirtazepine)	Antidepressant	0.53	1,4,10,12,14,15,16,17,18
193	13551-89-8	Misonidazolefluoro (Fluoromisonidazole)	Metabolic marker	-0.01	14,15
194	57-27-2	Morphine	Opioid analgesic	-0.27	1,3,10,12,13,14,15,16,17
195	108-38-3	m-Xylene	-	0.26	10,14,15,16
196	389-08-2	Nalidixic acid	Antibiotic	-0.66	14,15
197	159989-64-7	Nelfinavir (AG-1341)	HIV	-0.93	17
198	7440-01-9	Neon	-	0.20	10,11,15,16
199	129618-40-2	Nevirapine	HIV/ aids	0.00	1,6,8,10,11,13,14,15,16,17,18,20,21,22,24
200	54-11-5	Nicotine	Stimulant	0.36	3,14,15,17
201	7727-37-9	Nitrogen	-	0.03	6,10,11,14,15,16,21,23
202	10024-97-2	Nitrous Oxide	Anesthetic/ Analgesic	0.03	6,10,11,14,15,16,21
203	5638-76-6	N-methyl-2-pyridineethanamine (Betahistine)	Anti-vertigo	-0.33	1,7,10,11,12,14,15,16,17,18,20,21,23
204	111-84-2	Nonane	-	0.52	14,15
205	1225-64-5	Nor-1-Chlorpromazine	Neuroleptic	1.37	1,6,10,12,16,17
206	1088-11-5	Nordazepam (Desmethyldiazepam)	Benzodiazepine	0.52	1,6,10,12,13,14,15,16,17
207	5746-86-1	Nor-nicotine	Stimulant	0.32	17
208	10538-32-6	Northioridazine	Neuroleptic	0.75	1,6,10,12,14,15,16,17
209	67018-85-3	Norverapamil	Antihypertensive	-0.64	16
210	111-65-9	Octane	-	0.69	14,15

	CAS	Name	Possible drug use	Log BB	References
211	132539-06-1	Olanzapine	Antipsychotic	0.78	14,15
212	73590-58-6	Omeprazole	Peptic ulcer	-0.82	6,7,12,17
213	210821-63-9	Org-12962	5-HT2 agonist	1.64	1,4,10,12,17,18
214	65576-45-6	Org-5222 (asenapine)	Neuroleptic/ Antipsychotic	1.03	1,4,10,12,14,15,17,18
215	604-75-1	Oxazepam	Benzodiazepine	0.60	1,2,5,6,7,8,9,10,11,12,13,14,15,16,17,18,19,20,21,24
216	95-47-6	o-Xylene	-	0.39	10,14,15,16
217	611-59-6	Paraxanthine	Stimulant	0.06	1,6,10,12,14,15,16
218	109-66-0	Pentane	-	0.72	1,6,8,10,11,12,14,15,16,20,21,22,23,24
219	359-83-1	Pentazocine	Opioid analgesic	0.54	14,15
220	76-74-4	Pentobarbital	Barbiturate/Hypnotic	0.09	1,5,6,7,8,9,10,11,12,13,14,15,16,18,19,20,21,24
221	628-63-7	Pentyl acetate	-	0.40	14,15
222	54-95-5	Pentylenetetrazole (metrazole)	Anxiogenic	-0.03	14,15
223	66104-22-1	Pergolide	Parkinson's	0.30	16
224	77-10-1	Phencyclidine	Anesthetic	0.56	13,14,15,16
225	50-06-6	Phenobarbital (Luminal)	Barbiturate/ Anticonvulsant	-0.12	17
226	101246-66-6	Phenserine	Alzheimer's	1.00	1,6,8,11,12,16,18,20,21,24
227	50-33-9	Phenylbutazone	Analgesic	-0.52	1,2,5,6,7,10,12,13,14,15,16
228	3376-24-7	Phenyl-N-tert-butylnitrone	-	0.09	12,14,15
229	57-41-0	Phenytoin	Anticonvulsant	-0.06	1,2,5,6,7,10,12,13,14,15,16,19,22
230	13523-86-9	Pindolol	Beta-blocker	-0.14	14,15
231	85532-75-8	PK-11195	-	0.48	14,15
232	92-92-2	p-Phenylbenzoic acid	-	-1.26	14,15
233	6673-35-4	Practolol	Beta-blocker	-0.55	17
234	125-33-7	Primidone	Anticonvulsant	-0.07	13,16
235	59-46-1	Procaine	Local anesthetic	0.05	14,15
236	57-83-0	Progesterone	Luteal support in IVF	1.95	2
237	58-40-2	Promazine	Neuroleptic	1.07	1,3,6,8,9,10,11,12,13,14,15,16,17,18,19,20,21,24
238	146-21-4	Promazine-Sulfoxide	Neuroleptic	-0.48	17
239	60-87-7	Promethazine	Antihistamine	0.82	3
240	107-19-7	propargyl alcohol	-	-0.23	14,15
241	115-07-1	Propene (Propylene)	-	-0.06	14,15
242	525-66-6	Propranolol	Beta-blocker	0.84	1,3,5,6,7,10,12,13,14,15,16,17,19,22
243	109-60-4	Propyl acetate	-	0.12	14,15
244	3595-11-7	Propylhexedrine	Nasal congestion	1.08	17
245	106-42-3	p-Xylene	-	0.35	10,14,15,16

	CAS	Name	Possible drug use	Log BB	References
246	129-00-0	Pyrene	-	0.23	14,15
247	91-84-9	Pyrilamine (Mepyramine)	Antihistamine	0.49	1,4,6,9,10,11,12,13,14,15,16,17,18,19,20,21,23
248	56-54-2	Quinidine	Antiarrhythmic	-0.30	1,5,6,7,10,12,13,14,15,16,17
249	10043-92-2	Radon	Arthritis	-0.12	15
250	66357-35-5	Ranitidine	Antihistamine	-1.23	1,3,4,6,7,9,10,11,12,16,17,18,19,20,21,23
251	87226-41-3	R-Etodolac	Analgesic/ NSAID	-1.42	14,15
252	36791-04-5	Ribavirin	Hepatitis C	-0.67	22
253	106266-06-2	Risperidone	Antipsychotic	-0.02	1,4,5,7,10,12,14,15,16,18
254	123441-03-2	Rivastigmine	Cholinergic	0.88	17
255	99632-94-7	RO19-4603	Benzodiazepine	-0.25	10,17
256	61413-54-5	Rolipram	Anti-inflammatory	0.61	14,15
257	91374-21-9	Ropinirole (SKF101468)	Dopamine agonist	0.11	1,6,10,11,12,14,15,16,17,18,20,21,23
258	18559-94-9	Salbutamol (albuterol)	Bronchospasm	-1.14	7,13,14,15,16
259	69-72-7	Salicylic Acid	Analgesic/ NSAID	-1.12	1,2,5,6,7,8,9,10,11,12,13,14,15,16,17,18,19,20,21,24
260	487-54-7	Salicyluric acid	-	-0.44	1,6,10,12,13,16
261	127779-20-8	Saquinavir	Antiviral/ HIV	-0.97	14,15,17,22
262	174635-69-9	SB 222200	-	0.30	1,8,11,12,14,15,16,20,21,24
263	51-34-3	Scopolamine	Anticholinergic	0.23	17
264	76-73-3	Secobarbital	Barbiturate/ Anticonvulsant	0.20	17
265	79617-96-2	Sertraline	Antidepressant	1.60	17
266	28523-86-6	Sevoflurane	Inhalational anesthetic	0.30	14,15
267	81654-62-8	SKF 89124	Dopamine agonist	-0.33	1,10,11,12,14,15,16,17,18,20,21,23
268	2986-19-8	S-methylisothiourea	-	-0.60	14,15
269	3930-20-9	Sotalol	Beta-blocker	-0.28	17
270	749-02-0	Spiperone	Antipsychotic	0.26	14,15
271	3056-17-5	Stavudine	Antiviral/ HIV	-0.48	14,15,22
272	79637-11-9	Styrene	-	0.45	14,15
273	14759-06-9	Sulforidazine	Neuroleptic	0.18	1,6,10,12,13,14,15,16,17
274	2551-62-4	Sulfur Hexafluoride	-	0.37	6,10,11,14,15,16,21
275	321-64-2	Tacrine	Cholinergic	-0.13	13,16
276	142852-50-4	TAK-147 (Zanapezil)	Cholinergic	1.14	17
277	21489-20-3	Talsupram (LU 5-003)	Antidepressant	0.22	17
278	10540-29-1	Tamoxifen	Breast cancer	0.92	1
279	75-65-0	t-Butanol	-	0.11	14,15
280	98-06-6	t-Butylbenzene	-	0.43	14,15

	CAS	Name	Possible drug use	Log BB	References
281	3178-22-1	t-Butylcyclohexane	-	0.61	14,15
282	124-72-1	Teflurane	Inhalational anesthetic	0.27	1,6,8,10,11,14,15,16,20,21,22,23,24
283	86181-42-2	Temelastine (SKF93944)	Antihistamine	-1.88	1,4,6,11,12,16,17,18,20,21,24
284	91161-71-6	Terbinafine	Antifungal	0.09	14,15,17
285	50679-08-8	Terfenadine	Antihistamine/ Anti-allergic	0.64	17
286	994-05-8	tertiary-Amyl methyl ether	-	0.17	14,15
287	127-18-4	Tetrachloroethylene	-	0.37	14,15
288	83-67-0	Theobromine (3,7-Dimethylxanthine)	Vasodilation	-0.28	1,2,6,10,12,13,14,15,16,17
289	58-55-9	Theophylline	Asthma	-0.31	1,2,5,6,7,8,9,10,11,12,13,14,15,16,17,18,19,20,21,22,24
290	76-75-5	Thiopental (Thiopentone)	Barbiturate/ General anesthetic	-0.17	1,2,10,12,13,14,15,16,17
291	106243-16-7	Thioperamide	Antihistamine	-0.16	1,6,11,12,14,15,16,18,20,21
292	50-52-2	Thioridazine	Neuroleptic	0.26	1,6,7,8,9,10,11,12,14,15,16,17,18,19,20,21,24
293	5630-53-5	Tibolone	Steroid hormone	0.40	1,4,5,10,12,14,15,16,17,18
294	69014-14-8	Tiotidine (SKB10, Y-G10)	Antihistamine	-0.82	1,6,10,11,12,14,15,16,17,18,20,21,23
295	2933-94-0	Toliprolol	Beta-blocker	0.28	14,15
296	108-88-3	Toluene	-	0.34	1,2,5,6,8,10,11,14,15,16,19,20,21,22,23,24
297	156-60-5	trans 1,2-dichloroethene	-	0.04	14,15
298	28911-01-5	Triazolam	Benzodiazepine	0.69	1,5,6,10,12,13,14,15,16,17
299	79-01-6	Trichloroethene	General anesthetic	0.26	1,8,10,11,12,14,15,16,20,21,23,24
300	117-89-5	Trifluoperazine (Trifluoroperazine)	Neuroleptic	1.43	1,6,7,9,11,12,13,14,15,16,17,19,20,21,24
301	146-54-3	Trifluopromazine	Neuroleptic	1.44	8,10,18
302	57-13-6	Urea	Diuretic	-0.14	22
303	99-66-1	Valproic Acid	Anticonvulsant	-0.32	1,6,8,9,10,11,12,14,15,16,17,18,20,21,22,24
304	52-53-9	Verapamil	Antiarrhythmic	-0.61	1,5,6,7,8,9,11,12,13,14,15,16,18,19,20,21,24
305	865-21-4	Vinblastine	Chemotherapy	-0.07	22
306	57-22-7	Vincristine	Chemotherapy	-1.03	22
307	7440-63-3	Xenon	General anesthetic	0.06	10,11,15,16
308	7481-89-2	Zalcitabine	HIV/ aids	-1.18	17,22
309	30516-87-1	Zidovudine	HIV/ aids	-0.72	1,6,8,10,11,14,15,16,17,20,21,22,24
310	104076-38-2	Zolantidine (SKB41)	Antihistamine	0.14	1,4,6,11,12,14,15,16,17,18,20,21,23
311	82626-48-0	Zolpidem	Insomnia	-0.48	17
312	66893-81-0	α-(4-pyridyl-1-oxide)-N-tert-butylnitrone	-	-0.30	12,14,15
313	37115-43-8	α-Hydroxyalprazolam	Benzodiazepine	-1.27	16

References

1. Zhang LY, Zhu H, Oprea TI, Golbraikh A, Tropsha A (2008) QSAR modeling of the Blood-Brain Barrier permeability for diverse organic compounds. Pharmaceut Res 25 (8):1902-1914.

2. Grumetto L, Carpentiero C, Di Vaio P, Frecentese F, Barbato F (2013) Lipophilic and polar interaction forces between acidic drugs and membrane phospholipids encoded in IAM-HPLC indexes: Their role in membrane partition and relationships with BBB permeation data. J Pharmaceut Biomed 75:165-172.

3. Grumetto L, Carpentiero C, Barbato F (2012) Lipophilic and electrostatic forces encoded in IAM-HPLC indexes of basic drugs: Their role in membrane partition and their relationships with BBB passage data. Eur J Pharm Sci 45 (5):685-692.

4. Kelder J, Grootenhuis PDJ, Bayada DM, Delbressine LPC, Ploemen JP (1999) Polar molecular surface as a dominating determinant for oral absorption and brain penetration of drugs. Pharmaceut Res 16 (10):1514-1519.

5. Lu R, Sun J, Wang YJ, Li HY, Liu JF, Fang L, He ZG (2009) Characterization of biopartitioning micellar chromatography system using monolithic column by linear solvation energy relationship and application to predict blood-brain barrier penetration. J Chromatogr A 1216 (27):5190-5198.

6. Shen J, Du YP, Zhao YX, Liu GX, Tang Y (2008) In silico prediction of blood-brain partitioning using a chemometric method called Genetic Algorithm Based Variable Selection. Qsar Comb Sci 27 (6):704-717.

7. Liu JF, Sun J, Wang YJ, Liu XH, Sun YH, Xu H, He ZG (2007) Characterization of microemulsion liquid chromatography systems by solvation parameter model and comparison with other physicochemical and biological processes. J Chromatogr A 1164 (1-2):129-138.

8. Fu XC, Song ZF, Fu CY, Liang WQ (2005) A simple predictive model for blood-brain barrier penetration. Pharmazie 60 (5):354-358.

9. Salminen T, Pulli A, Taskinen J (1997) Relationship between immobilised artificial membrane chromatographic retention and the brain penetration of structurally diverse drugs. J Pharmaceut Biomed 15 (4):469-477.

10. Platts JA, Abraham MH, Zhao YH, Hersey A, Ijaz L, Butina D (2001) Correlation and prediction of a large blood-brain distribution data set - an LFER study. Eur J Med Chem 36 (9):719-730.

11. Norinder U, Haeberlein M (2002) Computational approaches to the prediction of the blood-brain distribution. Adv Drug Deliver Rev 54 (3):291-313.
12. Katritzky AR, Kuanar M, Slavov S, Dobchev DA, Fara DC, Karelson M, Acree WE, Solov'ev VP, Varnek A (2006) Correlation of blood-brain penetration using structural descriptors. Bioorgan Med Chem 14 (14):4888-4917.
13. Karelson M, Dobchev D, Tamm T, Tulp I, Janes J, Tamm K, Lomaka A, Savchenko D, Karelsona G (2008) Correlation of blood-brain penetration and human serum albumin binding with theoretical descriptors. Arkivoc:38-60.
14. Konovalov DA, Coomans D, Deconinck E, Vander Heyden Y (2007) Benchmarking of QSAR models for blood-brain barrier permeation. J Chem Inf Model 47 (4):1648-1656.
15. Abraham MH, Ibrahim A, Zhao Y, Acree WE (2006) A data base for partition of volatile organic compounds and drugs from blood/plasma/serum to brain, and an LFER analysis of the data. J Pharm Sci 95 (10):2091-2100.
16. Garg P, Verma J (2006) In silico prediction of blood brain barrier permeability: An artificial neural network model. J Chem Inf Model 46 (1):289-297.
17. Mente SR, Lombardo F (2005) A recursive-partitioning model for blood-brain barrier permeation. J Comput Aid Mol Des 19 (7):465-481.
18. Ooms F, Weber P, Carrupt PA, Testa B (2002) A simple model to predict blood-brain barrier permeation from 3D molecular fields. Bba-Mol Basis Dis 1587 (2-3):118-125.
19. Escuder-Gilabert L, Molero-Monfort A, Villanueva-Camanas RM, Sagrado S, Medina-Hernandez MJ (2004) Potential of biopartitioning micellar chromatography as an in vitro technique for predicting drug penetration across the blood-brain barrier. Journal of Chromatography B-Analytical Technologies in the Biomedical and Life Sciences 807 (2):193-201.
20. Luco JM (1999) Prediction of the brain-blood distribution of a large set of drugs from structurally derived descriptors using partial least-squares (PLS) modeling. J Chem Inf Comp Sci 39 (2):396-404.
21. Rose K, Hall LH, Kier LB (2002) Modeling blood-brain barrier partitioning using the electrotopological state. J Chem Inf Comp Sci 42 (3):651-666.
22. Usansky HH, Sinko PJ (2003) Computation of log BB values for compounds transported through carrier-mediated mechanisms using in vitro permeability data from brain microvessel endothelial cell (BMEC) monolayers. Pharmaceut Res 20 (3):390-396.

23. Clark DE (1999) Rapid calculation of polar molecular surface area and its application to the prediction of transport phenomena. 2. Prediction of blood-brain barrier penetration. J Pharm Sci 88 (8):815-821.
24. Subramanian G, Kitchen DB (2003) Computational models to predict blood-brain barrier permeation and CNS activity. J Comput Aid Mol Des 17 (10):643-664.

Appendix B. Structural formulas of tested molecules

Name	CAS number	Structural formula
2,2,2-Trifluoroethyl vinyl ether	406-90-6	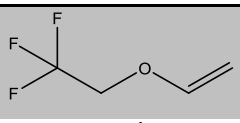
2,6-diisopropylphenol	2078-54-8	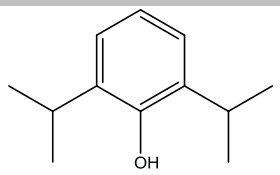
Acetaminophen	103-90-2	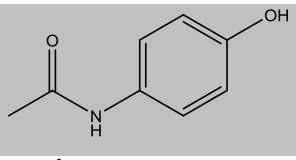
Acetylsalicylic acid	50-78-2	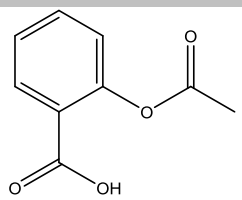
Aminopyrine	58-15-1	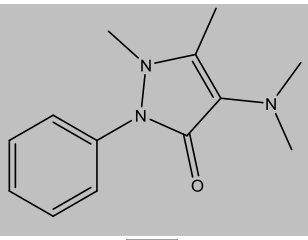
Amitriptyline	50-48-6	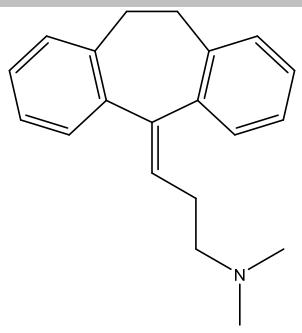
Amobarbital	57-43-2	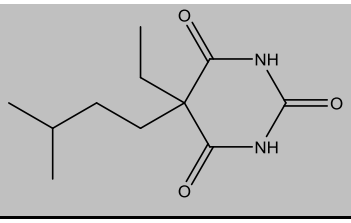

Antipyrine	60-80-0	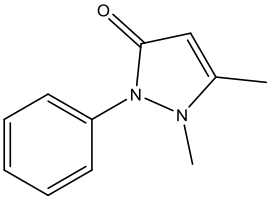
Atenolol	29122-68-7	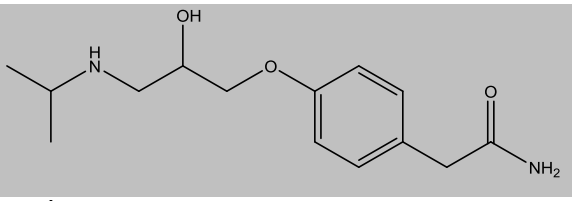
Benzene	71-43-2	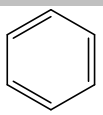
Caffeine	58-08-2	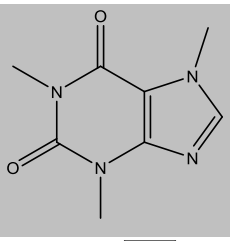
Carbamazepine	298-46-4	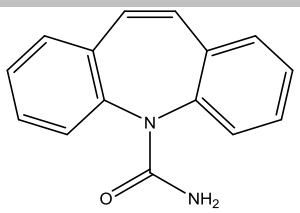
Chlorambucil	305-03-3	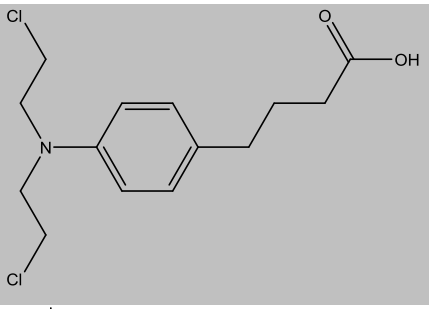
Chlorpromazine	50-53-3	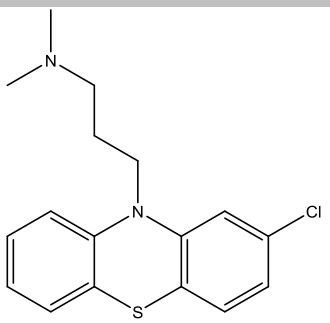
Cimetidine	51481-61-9	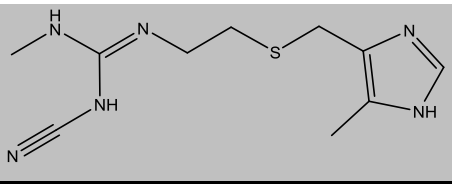

Clonidine	4205-90-7	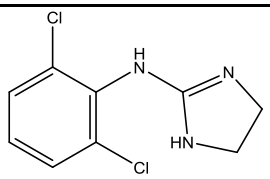
Cotinine	486-56-6	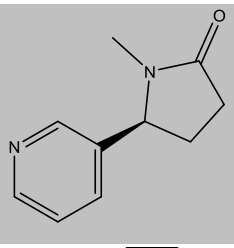
Desipramine	50-47-5	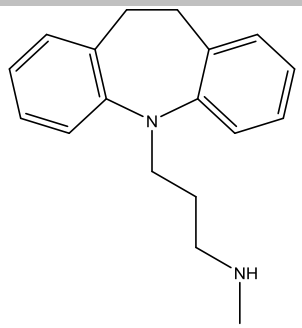
Domperidone	57808-66-9	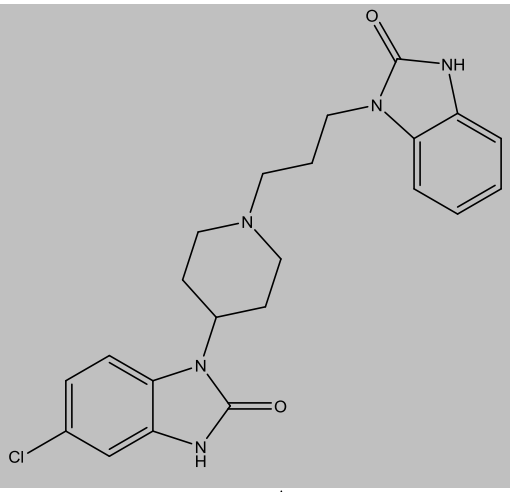
Eserine	57-47-6	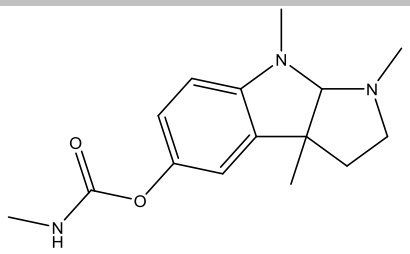
Ethylbenzene	100-41-4	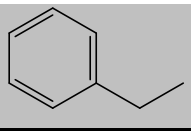

Fluphenazine	69-23-8	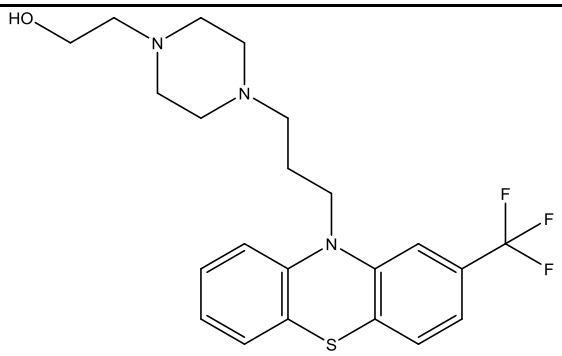
Haloperidol	52-86-8	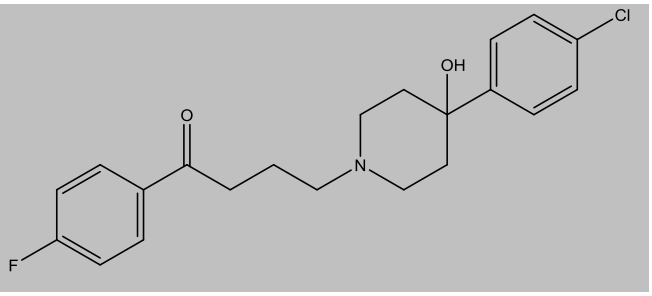
Halothane	151-67-7	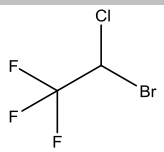
Hexobarbital	56-29-1	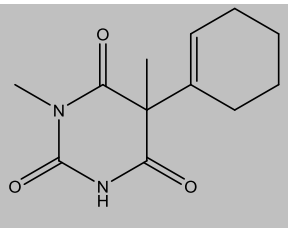
Hydroxyzine	68-88-2	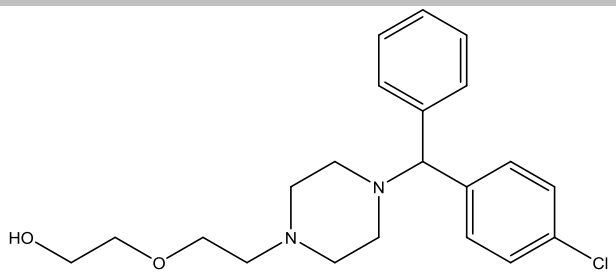
Ibuprofen	15687-27-1	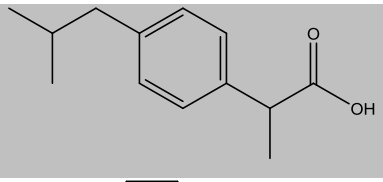
Imipramine	50-49-7	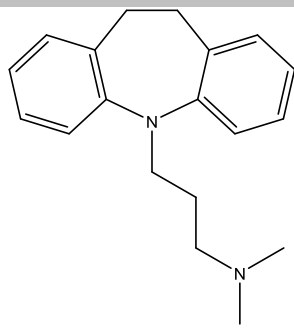

Indomethacin	53-86-1	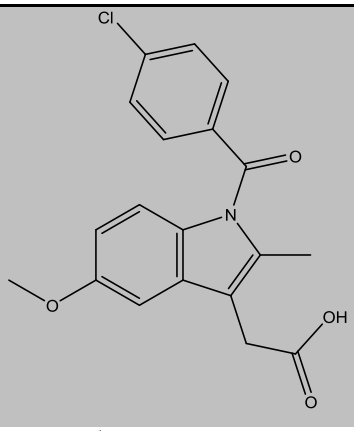
Mianserin	24219-97-4	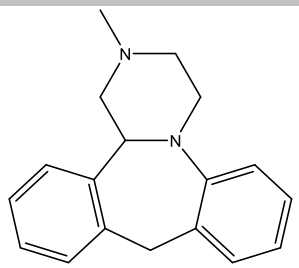
N-methyl-2-pyridineethanamine	5638-76-6	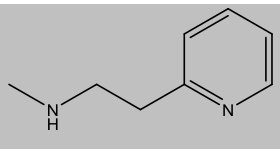
Omeprazole	73590-58-6	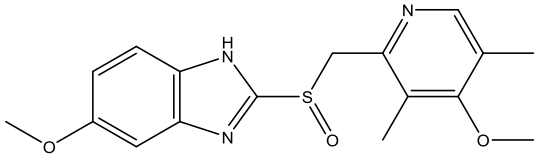
Oxazepam	604-75-1	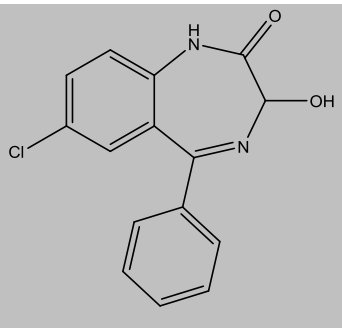
Pentobarbital	76-74-4	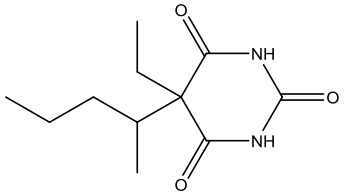
Phenylbutazone	50-33-9	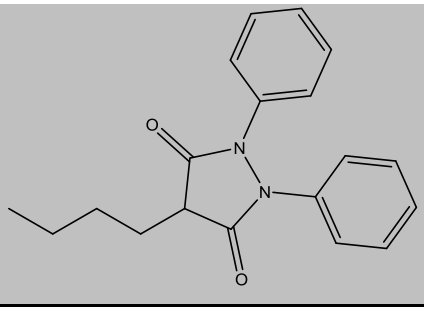

Phenytoin	57-41-0	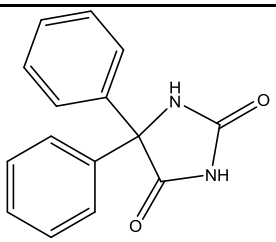
Promazine	58-40-2	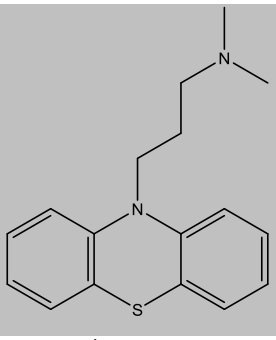
Propranolol	525-66-6	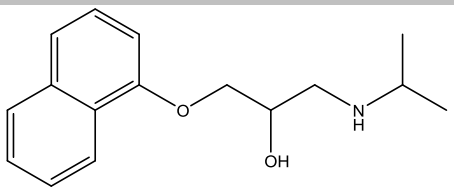
Pyrilamine	91-84-9	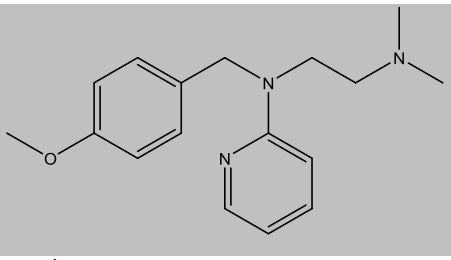
Quinidine	56-54-2	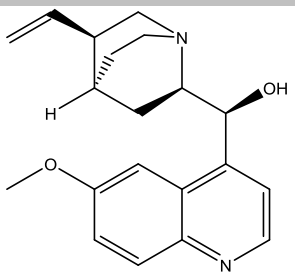
Ranitidine	66357-35-5	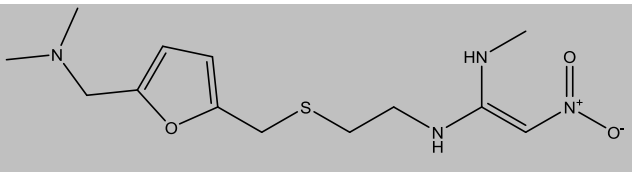
Ropinirole	91374-21-9	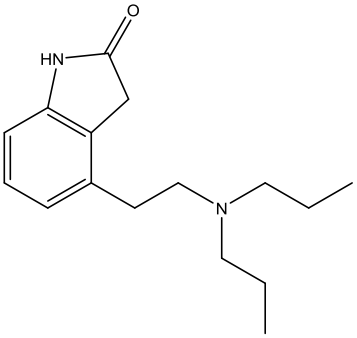

Salicylic acid	69-72-7	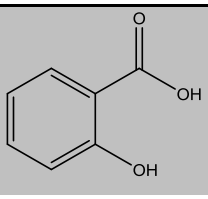
Theobromine	83-67-0	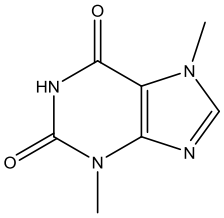
Theophylline	58-55-9	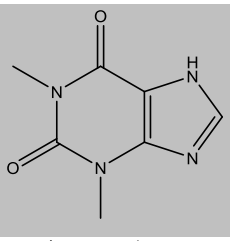
Toluene	108-88-3	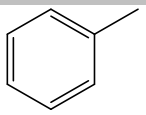
Valproic acid	99-66-1	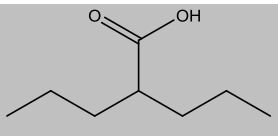
Verapamil	52-53-9	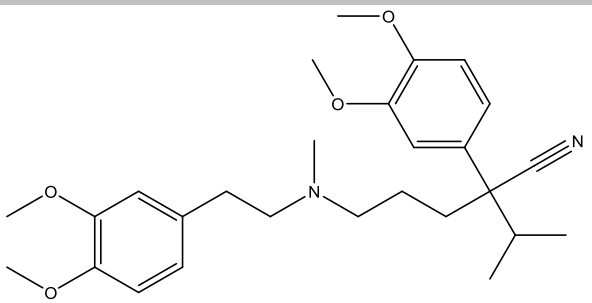
Zidovudine	30516-87-1	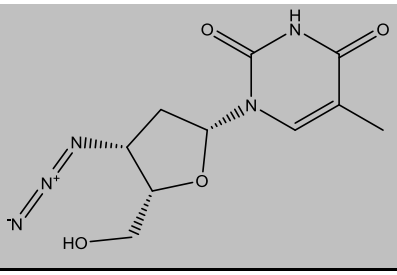

Structural formulas of tested molecules

Appendix C. Wavelengths & computed parameters of evaluated compounds

Table C-1: Experimental values of the logarithm of the brain-blood distribution coefficient (log BB) and calculated structural and physicochemical parameter values.

nr	Compounds	UV (nm)	log BB	α	MW	MR (cm^3)	MV (cm^3)	Pr (cm^3)	Polarizability (x 10^{-24}) (cm^3)	Log P	Log D7.4	Log WSo	WS7.4	PB	MI	MIA	HIA
1	2,2,2-trifluoroethyl vinyl ether	210	0.13	0.0000	126.08	22.50	112.4	223.5	8.92	1.64	1.64	-1.30	6.25	34.210	0	1	79.2
2	2,6-diisopropylphenol	210	0.48	-0.0002	178.27	56.50	188.0	452.3	22.40	3.66	3.66	-3.45	0.06	94.454	0	0	83.2
3	acetaminophen	254	-0.31	-0.0104	151.16	42.40	120.9	326.0	16.81	0.67	0.67	-1.50	5.15	30.134	1	0	90.6
4	acetylsalicylic acid	230	-0.50	-0.9999	180.16	44.52	139.5	370.9	17.65	1.11	-1.93	-1.89	31.70	61.163	0	0	94.9
5	aminopyrine	254	0.00	0.0040	231.29	68.33	196.0	518.8	27.08	0.15	0.15	-0.52	70.20	34.747	0	0	96.0
6	amitriptyline	254	0.98	0.9905	277.40	91.52	257.7	675.1	36.28	4.45	2.68	-5.19	0.11	94.195	0	0	89.5
7	amobarbital	210	0.04	-0.2847	226.27	57.95	211.4	507.3	22.97	1.90	1.90	-2.79	0.37	57.057	0	0	91.5
8	antipyrine	240	-0.10	0.0000	188.23	54.55	162.7	416.1	21.62	0.30	0.29	-0.26	104.00	15.609	0	0	96.4
9	atenolol	270	-1.42	0.9937	266.34	74.25	236.6	613.0	29.43	0.40	-0.63	-1.93	25.30	9.577	0	1	64.3
10	benzene	210	0.37	0.0000	78.11	26.25	89.4	207.2	10.40	1.83	1.83	-1.93	0.93	11.773	0	0	90.9
11	caffeine	210	-0.05	0.0000	194.19	50.38	133.3	364.5	19.97	-0.28	-0.28	-0.63	45.70	15.912	0	0	93.2
12	carbamazepine	210	0.00	0.0000	236.27	69.68	186.5	513.4	27.62	1.84	1.84	-3.53	0.07	72.015	0	0	88.8
13	chlorambucil	254	-1.70	-0.9781	304.21	79.91	243.6	643.7	31.67	2.48	0.87	-3.12	10.20	94.996	1	1	85.2
14	cimetidine	210	-1.42	0.2008	252.34	70.70	198.2	526.0	28.03	0.48	-0.57	-2.11	18.20	46.912	0	0	77.3
15	clonidine	270	0.11	0.7597	230.09	57.28	153.1	409.2	22.70	1.42	1.41	-2.58	0.62	38.729	0	0	95.2
16	cotinine	260	-0.32	0.0013	176.22	49.38	153.6	399.4	19.57	-0.37	-0.37	-0.44	64.10	11.321	0	0	91.1
17	desipramine	254	1.20	0.9987	266.38	84.16	254.2	639.3	33.36	3.10	1.94	-3.57	1.07	92.559	0	0	93.9
18	domperidone	270	-0.78	-0.2403	425.91	114.03	317.4	867.0	45.20	3.73	3.65	-3.34	0.24	95.369	0	0	82.1
19	eserine	240	0.08	0.0499	275.35	77.18	236.0	602.3	30.59	1.99	1.94	-2.17	2.05	70.319	1	1	91.2
20	ethylbenzene	210	0.20	0.0000	106.17	35.80	122.2	283.8	14.19	2.89	2.89	-2.92	0.13	62.578	0	0	86.7
21	fluphenazine	263	1.51	0.7597	437.52	114.30	343.8	885.9	45.31	3.81	3.71	-4.20	0.03	95.557	0	1	91.2
22	hexobarbital	254	0.10	-0.1368	236.27	60.38	192.8	501.8	23.93	1.49	1.49	-2.60	0.60	52.440	0	1	90.7
23	hydroxyzine	210	0.39	0.2847	374.90	105.91	317.1	833.7	41.98	3.18	2.16	-2.96	4.51	92.934	0	0	93.1

Table C-1 (continued)

nr	Compounds	UV (nm)	log BB	α	MW	MR (cm^3)	MV (cm^3)	Pr (cm^3)	Polarizability ($x\ 10^{-24}$) (cm^3)	Log P	Log D7.4	Log WSo	WS7.4	PB	MI	MIA	HIA
24	ibuprofen	270	-0.18	-0.9937	206.28	60.77	200.3	497.6	24.09	3.68	0.94	-4.01	3.51	99.931	0	0	92.4
25	imipramine	240	1.06	0.9844	280.41	88.92	269.2	677.5	35.25	3.97	2.17	-3.98	1.92	93.399	0	0	90.5
26	indomethacin	210	-1.26	-0.9987	357.79	94.59	269.5	707.6	37.49	3.64	1.04	-4.69	3.46	99.088	0	0	91.6
27	mianserin	280	0.99	0.3339	264.36	82.88	223.6	605.9	32.85	4.03	3.15	-3.54	0.59	89.139	0	0	91.0
28	N-methyl-2-pyridineethanamine	254	-0.30	0.9980	136.19	42.12	140.7	345.7	16.69	0.37	-0.22	-0.17	377.00	7.656	0	0	93.0
29	omeprazole	300	-0.82	-0.0467	345.42	94.02	251.8	741.6	37.27	1.99	1.99	-3.75	0.06	94.344	1	0	82.6
30	oxazepam	230	0.61	-0.0001	286.71	76.43	201.8	548.8	30.30	2.18	2.18	-3.68	0.06	92.968	1	1	92.9
31	pentobarbital	210	0.12	-0.2008	226.27	57.89	209.1	507.3	22.95	1.94	1.94	-2.71	0.45	59.667	0	0	91.9
32	phenylbutazone	240	-0.52	0.0013	308.37	88.70	262.7	689.4	35.16	1.93	1.93	-3.56	0.09	92.130	0	0	96.7
33	phenytoin	210	-0.04	-0.1051	252.27	69.58	200.5	531.3	27.58	2.61	2.61	-4.01	0.02	89.658	1	0	95.3
34	propranolol	290	0.64	0.9921	259.34	78.98	237.1	606.1	31.31	1.71	0.58	-3.63	2.74	84.800	1	1	92.2
35	pyrilamine	300	0.49	0.9617	285.38	87.44	262.1	677.3	34.66	1.53	0.45	-2.97	3.96	77.312	0	0	95.7
36	quinidine	254	-0.46	0.9353	324.42	95.78	266.3	728.7	37.97	2.92	1.97	-3.16	2.27	86.151	0	0	95.2
37	ranitidine	230	-1.23	0.8632	314.40	85.64	265.4	687.5	33.95	0.69	-0.22	-4.39	0.50	21.099	0	1	79.8
38	ropinirole	254	0.25	0.9844	260.37	78.36	250.1	630.9	31.06	2.79	0.67	-2.40	12.30	69.841	1	0	88.3
39	salicylic acid	300	-1.10	-1.0000	138.12	35.06	100.3	284.4	13.90	1.86	-1.65	-1.41	52.90	83.046	0	1	90.6
40	theobromine	270	-0.28	-0.0032	180.16	45.05	112.0	319.0	17.86	-0.50	-0.50	-1.47	6.15	29.355	0	1	87.3
41	theophylline	270	-0.29	-0.0592	180.16	43.14	122.9	352.4	17.10	-0.30	-0.30	-0.76	31.40	17.155	0	0	96.7
42	toluene	210	0.37	0.0000	92.14	31.07	105.7	244.9	12.32	2.49	2.49	-2.43	0.34	45.204	0	0	88.5
43	valproic acid	210	-0.22	-0.9968	144.21	40.63	155.5	369.6	16.10	2.59	0.25	-1.97	22.30	86.214	0	0	92.3
44	verapamil	210	-0.70	0.9523	454.60	131.86	429.3	1063.9	52.27	3.77	3.27	-4.95	0.02	92.662	0	0	94.8
45	zidovudine	270	-0.72	0.9937	267.24	68.56	206.9	536.3	27.18	0.25	0.25	-1.43	9.93	30.855	1	1	87.6

α: total molar charge at pH 7.4; MW: molecular weight; MR: molar refractivity; MV: molar volume; Pr: parachor; log P: logarithm of the partition coefficient in an n-octanol/water system of the neutral form of the compound; log D7.4: distribution coefficient of the compound in an n-octanol/water system at pH 7.4; log WSo: intrinsic aqueous solubility; WS7.4: aqueous solubility at pH 7.4; PB: plasma protein binding; MI(A): Ames test mutagenic index; HIA: human intestinal absorption

Table C-2: Experimental values of the logarithm of the brain-blood distribution coefficient (log BB) and calculated structural and physicochemical parameter values.

No.	Compound	UV (nm)	log BB	α	MW	MR (cm^3)	MV (cm^3)	Pr (cm^3)	Polarizability ($x\ 10^{-24}$) (cm^3)	Log P	Log D7.4	Log WSo	WS7.4	PB	MI	MIA	HIA
1	2,2,2-trifluoroethyl vinyl ether	210	0.13	0.0000	126.08	22.50	112.4	223.5	8.92	1.64	1.64	-1.30	6.25	34.210	0	1	79.2
2	2,6-diisopropylphenol	210	0.48	-0.0002	178.27	56.50	188.0	452.3	22.40	3.66	3.66	-3.45	0.06	94.454	0	0	83.2
3	acetaminophen	254	-0.31	-0.0104	151.16	42.40	120.9	326.0	16.81	0.67	0.67	-1.50	5.15	30.134	1	0	90.6
4	acetylsalicylic acid	230	-0.50	-0.9999	180.16	44.52	139.5	370.9	17.65	1.11	-1.93	-1.89	31.70	61.163	0	0	94.9
5	aminopyrine	254	0.00	0.0013	231.29	68.33	196.0	518.8	27.08	0.15	0.15	-0.52	70.20	34.747	0	0	96.0
6	amitriptyline	254	0.98	0.9905	277.40	91.52	257.7	675.1	36.28	4.45	2.68	-5.19	0.11	94.195	0	0	89.5
7	amobarbital	210	0.04	-0.2847	226.27	57.95	211.4	507.3	22.97	1.90	1.90	-2.79	0.37	57.057	0	0	91.5
8	antipyrine	240	-0.10	0.0000	188.23	54.55	162.7	416.1	21.62	0.30	0.29	-0.26	104.00	15.609	0	0	96.4
9	atenolol	270	-1.42	0.9937	266.34	74.25	236.6	613.0	29.43	0.40	-0.63	-1.93	25.30	9.577	0	1	64.3
10	benzene	210	0.37	0.0000	78.11	26.25	89.4	207.2	10.40	1.83	1.83	-1.93	0.93	11.773	0	0	90.9
11	caffeine	210	-0.05	0.0000	194.19	50.38	133.3	364.5	19.97	-0.28	-0.28	-0.63	45.70	15.912	0	0	93.2
12	carbamazepine	210	0.00	1.0000	236.27	69.68	186.5	513.4	27.62	1.84	1.84	-3.53	0.07	72.015	0	0	88.8
13	chlorambucil	254	-1.70	-0.9781	304.21	79.91	243.6	643.7	31.67	2.48	0.87	-3.12	10.20	94.996	1	1	85.2
14	chloropromazine	254	1.06	0.9844	318.86	92.75	262.9	686.9	36.77	5.01	4.17	-5.05	0.02	97.606	0	0	85.9
15	cimetidine	210	-1.42	0.2008	252.34	70.70	198.2	526.0	28.03	0.48	-0.57	-2.11	18.20	46.912	0	0	77.3
16	clonidine	270	0.11	0.7597	230.09	57.28	153.1	409.2	22.70	1.42	1.41	-2.58	0.62	38.729	0	0	95.2
17	cotinine	260	-0.32	0.0013	176.22	49.38	153.6	399.4	19.57	-0.37	-0.37	-0.44	64.10	11.321	0	0	91.1
18	desipramine	254	1.20	0.9987	266.38	84.16	254.2	639.3	33.36	3.10	1.94	-3.57	1.07	92.559	0	0	93.9
19	domperidone	270	-0.78	-0.2403	425.91	114.03	317.4	867.0	45.20	3.73	3.65	-3.34	0.24	95.369	0	0	82.1
20	eserine	240	0.08	-0.9501	275.35	77.18	236.0	602.3	30.59	1.99	1.94	-2.17	2.05	70.319	1	1	91.2
21	ethylbenzene	210	0.20	0.0000	106.17	35.80	122.2	283.8	14.19	2.89	2.89	-2.92	0.13	62.578	0	0	86.7
22	fluphenazine	263	1.51	0.7597	437.52	114.30	343.8	885.9	45.31	3.81	3.71	-4.20	0.03	95.557	0	1	91.2
23	haloperidol	254	1.34	0.9479	375.86	101.01	303.2	797.8	40.04	3.63	2.69	-4.88	0.04	92.115	1	1	90.0
24	halothane	210	0.35	0.0000	197.38	24.31	102.8	223.3	9.63	2.53	2.53	-2.18	1.30	56.404	0	0	77.3
25	hexobarbital	254	0.10	-0.1368	236.27	60.38	192.8	501.8	23.93	1.49	1.49	-2.60	0.60	52.440	0	1	90.7
26	hydroxyzine	210	0.39	0.2847	374.90	105.91	317.1	833.7	41.98	3.18	2.16	-2.96	4.51	92.934	0	0	93.1
27	ibuprofen	270	-0.18	-0.9937	206.28	60.77	200.3	497.6	24.09	3.68	0.94	-4.01	3.51	99.931	0	0	92.4
28	imipramine	240	1.06	0.9844	280.41	88.92	269.2	677.5	35.25	3.97	2.17	-3.98	1.92	93.399	0	0	90.5
29	indomethacin	210	-1.26	-0.9987	357.79	94.59	269.5	707.6	37.49	3.64	1.04	-4.69	3.46	99.088	0	0	91.6
30	mianserin	280	0.99	0.3339	264.36	82.88	223.6	605.9	32.85	4.03	3.15	-3.54	0.59	89.139	0	0	91.0
31	N-methyl-2-pyridineethanamine	254	-0.30	0.9980	136.19	42.12	140.7	345.7	16.69	0.37	-0.22	-0.17	377.00	7.656	0	0	93.0
32	omeprazole	300	-0.82	-0.0467	345.42	94.02	251.8	741.6	37.27	1.99	1.99	-3.75	0.06	94.344	1	0	82.6
33	oxazepam	230	0.61	-0.0001	286.71	76.43	201.8	548.8	30.30	2.18	2.18	-3.68	0.06	92.968	1	1	92.9
34	pentobarbital	210	0.12	-0.2008	226.27	57.89	209.1	507.3	22.95	1.94	1.94	-2.71	0.45	59.667	0	0	91.9

Table C-2 (continued)

No.	Compound	UV (nm)	log BB	α	MW	MR (cm^3)	MV (cm^3)	Pr (cm^3)	Polarizability (x 10^{-24}) (cm^3)	Log P	Log D7.4	Log WSo	WS7.4	PB	MI	MIA	HIA
35	phenylbutazone	240	-0.52	-0.9987	308.37	88.70	262.7	689.4	35.16	1.93	1.93	-3.56	0.09	92.130	0	0	96.7
36	phenytoin	210	-0.04	-0.1051	252.27	69.58	200.5	531.3	27.58	2.61	2.61	-4.01	0.02	89.658	1	0	95.3
37	promazine	254	1.23	0.9844	284.42	87.85	250.9	649.7	34.82	4.18	2.56	-4.41	0.46	90.319	0	0	88.6
38	propranolol	290	0.64	0.9921	259.34	78.98	237.1	606.1	31.31	1.71	0.58	-3.63	2.74	84.800	1	1	92.2
39	pyrilamine	300	0.49	0.9617	285.38	87.44	262.1	677.3	34.66	1.53	0.45	-2.97	3.96	77.312	0	0	95.7
40	quinidine	254	-0.46	0.9353	324.42	95.78	266.3	728.7	37.97	2.92	1.97	-3.16	2.27	86.151	0	0	95.2
41	ranitidine	230	-1.23	0.8632	314.40	85.64	265.4	687.5	33.95	0.69	-0.22	-4.39	0.50	21.099	0	1	79.8
42	ropinirole	254	0.25	0.9844	260.37	78.36	250.1	630.9	31.06	2.79	0.67	-2.40	12.30	69.841	1	0	88.3
43	salicylic acid	300	-1.10	-1.0000	138.12	35.06	100.3	284.4	13.90	1.86	-1.65	-1.41	52.90	83.046	0	1	90.6
44	theobromine	270	-0.28	-0.0032	180.16	45.05	112.0	319.0	17.86	-0.50	-0.50	-1.47	6.15	29.355	0	1	87.3
45	theophylline	270	-0.29	-0.0592	180.16	43.14	122.9	352.4	17.10	-0.30	-0.30	-0.76	31.40	17.155	0	0	96.7
46	toluene	210	0.37	0.0000	92.14	31.07	105.7	244.9	12.32	2.49	2.49	-2.43	0.34	45.204	0	0	88.5
47	valproic acid	210	-0.22	-0.9968	144.21	40.63	155.5	369.6	16.10	2.59	0.25	-1.97	22.30	86.214	0	0	92.3
48	verapamil	210	-0.70	0.9523	454.60	131.86	429.3	1063.9	52.27	3.77	3.27	-4.95	0.02	92.662	0	0	94.8
49	zidovudine	270	-0.72	0.9937	267.24	71.74	215.0	558.7	28.44	0.25	0.25	-1.43	9.93	30.855	1	1	87.6

α: total molar charge at pH 7.4; MW: molecular weight; MR: molar refractivity; MV: molar volume; Pr: parachor; log P: logarithm of the partition coefficient in an n-octanol/water system of the neutral form of the compound; log D7.4: distribution coefficient of the compound in an n-octanol/water system at pH 7.4; logWSo: intrinsic aqueous solubility; WS7.4: aqueous solubility at pH 7.4; PB: plasma protein binding; MI(A): Ames test mutagenic index; HIA: human intestinal absorption

Table C-3: Overview of the values of the calculated structural and physicochemical parameters. In vitro models were created based on the log k values and these parameters.

No.	α	MW	MR (cm^3)	MV (cm^3)	Pr (cm^3)	Polarizability (x 10^{-24}) (cm^3)	Log P	Log D7.4	Log WSo	WS7.4	PB	MI	MIA	HIA	PSA	HBA	HBD	MSA
1	0.0000	126.08	22.50	112.4	223.5	8.92	1.64	1.64	-1.30	6.25	34.210	0	1	79.2	9.23	1	0	158.11
2	-0.0002	178.27	56.50	188.0	452.3	22.40	3.66	3.66	-3.45	0.06	94.454	0	0	83.2	20.23	1	1	331.14
3	-0.0104	151.16	42.40	120.9	326.0	16.81	0.67	0.67	-1.50	5.15	30.134	1	0	90.6	49.33	3	2	222.56
4	-0.9999	180.16	44.52	139.5	370.9	17.65	1.11	-1.93	-1.89	31.70	61.163	0	0	94.9	63.60	4	1	246.17
5	0.0040	231.29	68.33	196.0	518.8	27.08	0.15	0.15	-0.52	70.20	34.747	0	0	96.0	26.79	4	0	367.02
6	0.9905	277.40	91.52	257.7	675.1	36.28	4.45	2.68	-5.19	0.11	94.195	0	0	89.5	3.24	1	0	457.27
7	-0.2847	226.27	57.95	211.4	507.3	22.97	1.90	1.90	-2.79	0.37	57.057	0	0	91.5	75.27	5	2	368.83
8	0.0000	188.23	54.55	162.7	416.1	21.62	0.30	0.29	-0.26	104.00	15.609	0	0	96.4	23.55	3	0	280.13
9	0.9937	266.34	74.25	236.6	613.0	29.43	0.40	-0.63	-1.93	25.30	9.577	0	1	64.3	84.58	5	4	440.41
10	0.0000	78.11	26.25	89.4	207.2	10.40	1.83	1.83	-1.93	0.93	11.773	0	0	90.9	0.00	0	0	135.86
11	0.0000	194.19	50.38	133.3	364.5	19.97	-0.28	-0.28	-0.63	45.70	15.912	0	0	93.2	58.44	6	0	269.15
12	0.0000	236.27	69.68	186.5	513.4	27.62	1.84	1.84	-3.53	0.07	72.015	0	0	88.8	46.33	3	2	312.24
13	-0.9781	304.21	79.91	243.6	643.7	31.67	2.48	0.87	-3.12	10.20	94.996	1	1	85.2	40.54	3	1	443.08
14	0.9844	318.86	92.75	262.9	686.9	36.77	5.01	4.17	-5.05	0.02	97.606	0	0	85.9	6.48	2	0	456.64
15	0.2008	252.34	70.70	198.2	526.0	28.03	0.48	-0.57	-2.11	18.20	46.912	0	0	77.3	88.89	6	3	370.53
16	0.7597	230.09	57.28	153.1	409.2	22.70	1.42	1.41	-2.58	0.62	38.729	0	0	95.2	36.42	3	2	273.18
17	0.0013	176.22	49.38	153.6	399.4	19.57	-0.37	-0.37	-0.44	64.10	11.321	0	0	91.1	33.20	3	0	272.90
18	0.9987	266.38	84.16	254.2	639.3	33.36	3.10	1.94	-3.57	1.07	92.559	0	0	93.9	15.27	2	1	443.34
19	-0.2403	425.91	114.03	317.4	867.0	45.20	3.73	3.65	-3.34	0.24	95.369	0	0	82.1	67.92	7	2	583.57
20	0.0499	275.35	77.18	236.0	602.3	30.59	1.99	1.94	-2.17	2.05	70.319	1	1	91.2	44.81	5	1	441.72
21	0.0000	106.17	35.80	122.2	283.8	14.19	2.89	2.89	-2.92	0.13	62.578	0	0	86.7	0.00	0	0	198.54
22	0.7597	437.52	114.30	343.8	885.9	45.31	3.81	3.71	-4.20	0.03	95.557	0	1	91.2	29.95	4	1	617.34
23	0.9479	375.86	101.01	303.2	797.8	40.04	3.63	2.69	-4.88	0.04	92.115	1	1	90.0	40.54	3	1	544.82
24	0.0000	197.38	24.31	102.8	223.3	9.63	2.53	2.53	-2.18	1.30	56.404	0	0	77.3	0.00	0	0	140.12
25	-0.1368	236.27	60.38	192.8	501.8	23.93	1.49	1.49	-2.60	0.60	52.440	0	1	90.7	66.48	5	1	346.43
26	0.2847	374.90	105.91	317.1	833.7	41.98	3.18	2.16	-2.96	4.51	92.934	0	0	93.1	35.94	4	1	579.98
27	-0.9937	206.28	60.77	200.3	497.6	24.09	3.68	0.94	-4.01	3.51	99.931	0	0	92.4	37.30	2	1	356.78
28	0.9844	280.41	88.92	269.2	677.5	35.25	3.97	2.17	-3.98	1.92	93.399	0	0	90.5	6.48	2	0	478.35
29	-0.9987	357.79	94.59	269.5	707.6	37.49	3.64	1.04	-4.69	3.46	99.088	0	0	91.6	68.53	5	1	476.27

Table C-3 (continued)

No.	α	MW	MR (cm^3)	MV (cm^3)	Pr (cm^3)	Polarizability ($x\ 10^{-24}$) (cm^3)	Log P	Log D7.4	Log WSo	WS7.4	PB	MI	MIA	HIA	PSA	HBA	HBD	MSA
30	0.3339	264.36	82.88	223.6	605.9	32.85	4.03	3.15	-3.54	0.59	89.139	0	0	91.0	6.48	2	0	415.95
31	0.9980	136.19	42.12	140.7	345.7	16.69	0.37	-0.22	-0.17	377.00	7.656	0	0	93.0	24.92	2	1	242.37
32	-0.0467	345.42	94.02	251.8	741.6	37.27	1.99	1.99	-3.75	0.06	94.344	1	0	82.6	77.10	6	1	501.87
33	-0.0001	286.71	76.43	201.8	548.8	30.30	2.18	2.18	-3.68	0.06	92.968	1	1	92.9	61.69	4	2	346.15
34	-0.2008	226.27	57.89	209.1	507.3	22.95	1.94	1.94	-2.71	0.45	59.667	0	0	91.9	75.27	5	2	367.89
35	0.0013	308.37	88.70	262.7	689.4	35.16	1.93	1.93	-3.56	0.09	92.130	0	0	96.7	40.62	4	0	466.42
36	-0.1051	252.27	69.58	200.5	531.3	27.58	2.61	2.61	-4.01	0.02	89.658	1	0	95.3	58.20	4	2	340.95
37	0.9844	284.42	87.85	250.9	649.7	34.82	4.18	2.56	-4.41	0.46	90.319	0	0	88.6	6.48	2	0	440.29
38	0.9921	259.34	78.98	237.1	606.1	31.31	1.71	0.58	-3.63	2.74	84.800	1	1	92.2	41.49	3	2	426.96
39	0.9617	285.38	87.44	262.1	677.3	34.66	1.53	0.45	-2.97	3.96	77.312	0	0	95.7	28.60	4	0	485.16
40	0.9353	324.42	95.78	266.3	728.7	37.97	2.92	1.97	-3.16	2.27	86.151	0	0	95.2	45.59	4	1	483.55
41	0.8632	314.40	85.64	265.4	687.5	33.95	0.69	-0.22	-4.39	0.50	21.099	0	1	79.8	83.58	6	2	484.00
42	0.9844	260.37	78.36	250.1	630.9	31.06	2.79	0.67	-2.40	12.30	69.841	1	0	88.3	32.34	3	1	459.72
43	-1.0000	138.12	35.06	100.3	284.4	13.90	1.86	-1.65	-1.41	52.90	83.046	0	1	90.6	57.53	3	2	183.54
44	-0.0032	180.16	45.05	112.0	319.0	17.86	-0.50	-0.50	-1.47	6.15	29.355	0	1	87.3	67.23	6	1	237.27
45	-0.0592	180.16	43.14	122.9	352.4	17.10	-0.30	-0.30	-0.76	31.40	17.155	0	0	96.7	69.30	6	1	235.19
46	0.0000	92.14	31.07	105.7	244.9	12.32	2.49	2.49	-2.43	0.34	45.204	0	0	88.5	0.00	0	0	168.11
47	-0.9968	144.21	40.63	155.5	369.6	16.10	2.59	0.25	-1.97	22.30	86.214	0	0	92.3	37.30	2	1	281.48
48	0.9523	454.60	131.86	429.3	1063.9	52.27	3.77	3.27	-4.95	0.02	92.662	0	0	94.8	63.95	6	0	781.98

α total molar charge at pH 7.4; MW: molecular weight; MR: molar refractivity; MV: molar volume; Pr: parachor; log P: logarithm of the partition coefficient in an n-octanol/water system of the neutral form of the compound; log D7.4: distribution coefficient of the compound in an n-octanol/water system at pH 7.4; log WSo: intrinsic aqueous solubility; WS7.4: aqueous solubility at pH 7.4; PB: plasma protein binding; MI(A): Ames test mutagenic index; HIA: human intestinal absorption; PSA: polar surface area; HBA: hydrogen bond acceptor; HBD: hydrogen bond donor; MSA: molecular surface area

Table C-4: Overview of the values of the calculated structural and physicochemical parameters. In vitro models were created based on the log k values and these parameters.

No.	α	MW	MR (cm^3)	MV (cm^3)	Pr (cm^3)	Polarizability (x 10^{-24}) (cm^3)	Log P	Log D7.4	Log WSo	WS7.4	PB	MI	MIA	HIA	PSA	HBA	HBD	MSA
1	0.0000	126.08	22.50	112.4	223.5	8.92	1.64	1.64	-1.30	6.25	34.210	0	1	79.2	9.23	1	0	158.11
2	-0.0002	178.27	56.50	188.0	452.3	22.40	3.66	3.66	-3.45	0.06	94.454	0	0	83.2	20.23	1	1	331.14
3	-0.0104	151.16	42.40	120.9	326.0	16.81	0.67	0.67	-1.50	5.15	30.134	1	0	90.6	49.33	3	2	222.56
4	-0.9999	180.16	44.52	139.5	370.9	17.65	1.11	-1.93	-1.89	31.70	61.163	0	0	94.9	63.60	4	1	246.17
5	0.0040	231.29	68.33	196.0	518.8	27.08	0.15	0.15	-0.52	70.20	34.747	0	0	96.0	26.79	4	0	367.02
6	0.9905	277.40	91.52	257.7	675.1	36.28	4.45	2.68	-5.19	0.11	94.195	0	0	89.5	3.24	1	0	457.27
7	-0.2847	226.27	57.95	211.4	507.3	22.97	1.90	1.90	-2.79	0.37	57.057	0	0	91.5	75.27	5	2	368.83
8	0.0000	188.23	54.55	162.7	416.1	21.62	0.30	0.29	-0.26	104.00	15.609	0	0	96.4	23.55	3	0	280.13
9	0.9937	266.34	74.25	236.6	613.0	29.43	0.40	-0.63	-1.93	25.30	9.577	0	1	64.3	84.58	5	4	440.41
10	0.0000	78.11	26.25	89.4	207.2	10.40	1.83	1.83	-1.93	0.93	11.773	0	0	90.9	0.00	0	0	135.86
11	0.0000	194.19	50.38	133.3	364.5	19.97	-0.28	-0.28	-0.63	45.70	15.912	0	0	93.2	58.44	6	0	269.15
12	0.0000	236.27	69.68	186.5	513.4	27.62	1.84	1.84	-3.53	0.07	72.015	0	0	88.8	46.33	3	2	312.24
13	-0.9781	304.21	79.91	243.6	643.7	31.67	2.48	0.87	-3.12	10.20	94.996	1	1	85.2	40.54	3	1	443.08
14	0.9844	318.86	92.75	262.9	686.9	36.77	5.01	4.17	-5.05	0.02	97.606	0	0	85.9	6.48	2	0	456.64
15	0.2008	252.34	70.70	198.2	526.0	28.03	0.48	-0.57	-2.11	18.20	46.912	0	0	77.3	88.89	6	3	370.53
16	0.7597	230.09	57.28	153.1	409.2	22.70	1.42	1.41	-2.58	0.62	38.729	0	0	95.2	36.42	3	2	273.18
17	0.0013	176.22	49.38	153.6	399.4	19.57	-0.37	-0.37	-0.44	64.10	11.321	0	0	91.1	33.20	3	0	272.90
18	0.9987	266.38	84.16	254.2	639.3	33.36	3.10	1.94	-3.57	1.07	92.559	0	0	93.9	15.27	2	1	443.34
19	-0.2403	425.91	114.03	317.4	867.0	45.20	3.73	3.65	-3.34	0.24	95.369	0	0	82.1	67.92	7	2	583.57
20	0.0499	275.35	77.18	236.0	602.3	30.59	1.99	1.94	-2.17	2.05	70.319	1	1	91.2	44.81	5	1	441.72
21	0.0000	106.17	35.80	122.2	283.8	14.19	2.89	2.89	-2.92	0.13	62.578	0	0	86.7	0.00	0	0	198.54
22	0.7597	437.52	114.30	343.8	885.9	45.31	3.81	3.71	-4.20	0.03	95.557	0	1	91.2	29.95	4	1	617.34
23	0.9479	375.86	101.01	303.2	797.8	40.04	3.63	2.69	-4.88	0.04	92.115	1	1	90.0	40.54	3	1	544.82
24	0.0000	197.38	24.31	102.8	223.3	9.63	2.53	2.53	-2.18	1.30	56.404	0	0	77.3	0.00	0	0	140.12
25	-0.1368	236.27	60.38	192.8	501.8	23.93	1.49	1.49	-2.60	0.60	52.440	0	1	90.7	66.48	5	1	346.43
26	0.2847	374.90	105.91	317.1	833.7	41.98	3.18	2.16	-2.96	4.51	92.934	0	0	93.1	35.94	4	1	579.98
27	-0.9937	206.28	60.77	200.3	497.6	24.09	3.68	0.94	-4.01	3.51	99.931	0	0	92.4	37.30	2	1	356.78
28	0.9844	280.41	88.92	269.2	677.5	35.25	3.97	2.17	-3.98	1.92	93.399	0	0	90.5	6.48	2	0	478.35
29	-0.9987	357.79	94.59	269.5	707.6	37.49	3.64	1.04	-4.69	3.46	99.088	0	0	91.6	68.53	5	1	476.27

Table C-4 (continued)

No.	α	MW	MR (cm^3)	MV (cm^3)	Pr (cm^3)	Polarizability (x 10^{-24}) (cm^3)	Log P	Log D7.4	Log WSo	WS7.4	PB	MI	MIA	HIA	PSA	HBA	HBD	MSA
30	0.3339	264.36	82.88	223.6	605.9	32.85	4.03	3.15	-3.54	0.59	89.139	0	0	91.0	6.48	2	0	415.95
31	0.9980	136.19	42.12	140.7	345.7	16.69	0.37	-0.22	-0.17	377.00	7.656	0	0	93.0	24.92	2	1	242.37
32	-0.0467	345.42	94.02	251.8	741.6	37.27	1.99	1.99	-3.75	0.06	94.344	1	0	82.6	77.10	6	1	501.87
33	-0.0001	286.71	76.43	201.8	548.8	30.30	2.18	2.18	-3.68	0.06	92.968	1	1	92.9	61.69	4	2	346.15
34	-0.2008	226.27	57.89	209.1	507.3	22.95	1.94	1.94	-2.71	0.45	59.667	0	0	91.9	75.27	5	2	367.89
35	0.0013	308.37	88.70	262.7	689.4	35.16	1.93	1.93	-3.56	0.09	92.130	0	0	96.7	40.62	4	0	466.42
36	-0.1051	252.27	69.58	200.5	531.3	27.58	2.61	2.61	-4.01	0.02	89.658	1	0	95.3	58.20	4	2	340.95
37	0.9844	284.42	87.85	250.9	649.7	34.82	4.18	2.56	-4.41	0.46	90.319	0	0	88.6	6.48	2	0	440.29
38	0.9921	259.34	78.98	237.1	606.1	31.31	1.71	0.58	-3.63	2.74	84.800	1	1	92.2	41.49	3	2	426.96
39	0.9617	285.38	87.44	262.1	677.3	34.66	1.53	0.45	-2.97	3.96	77.312	0	0	95.7	28.60	4	0	485.16
40	0.9353	324.42	95.78	266.3	728.7	37.97	2.92	1.97	-3.16	2.27	86.151	0	0	95.2	45.59	4	1	483.55
41	0.8632	314.40	85.64	265.4	687.5	33.95	0.69	-0.22	-4.39	0.50	21.099	0	1	79.8	83.58	6	2	484.00
42	0.9844	260.37	78.36	250.1	630.9	31.06	2.79	0.67	-2.40	12.30	69.841	1	0	88.3	32.34	3	1	459.72
43	-1.0000	138.12	35.06	100.3	284.4	13.90	1.86	-1.65	-1.41	52.90	83.046	0	1	90.6	57.53	3	2	183.54
44	-0.0032	180.16	45.05	112.0	319.0	17.86	-0.50	-0.50	-1.47	6.15	29.355	0	1	87.3	67.23	6	1	237.27
45	-0.0592	180.16	43.14	122.9	352.4	17.10	-0.30	-0.30	-0.76	31.40	17.155	0	0	96.7	69.30	6	1	235.19
46	0.0000	92.14	31.07	105.7	244.9	12.32	2.49	2.49	-2.43	0.34	45.204	0	0	88.5	0.00	0	0	168.11
47	-0.9968	144.21	40.63	155.5	369.6	16.10	2.59	0.25	-1.97	22.30	86.214	0	0	92.3	37.30	2	1	281.48
48	0.9523	454.60	131.86	429.3	1063.9	52.27	3.77	3.27	-4.95	0.02	92.662	0	0	94.8	63.95	6	0	781.98
49	0.9937	267.24	61.71	220.9	558.7	23.69	0.25	0.25	-1.43	9.93	30.855	1	1	87.6	108.30	8	2	342.98

α total molar charge at pH 7.4; MW: molecular weight; MR: molar refractivity; MV: molar volume; Pr: parachor; log P: logarithm of the partition coefficient in an n-octanol/water system of the neutral form of the compound; log D7.4: distribution coefficient of the compound in an n-octanol/water system at pH 7.4; log WSo: intrinsic aqueous solubility; WS7.4: aqueous solubility at pH 7.4; PB: plasma protein binding; MI(A): Ames test mutagenic index; HIA: human intestinal absorption; PSA: polar surface area; HBA: hydrogen bond acceptor; HBD: hydrogen bond donor; MSA: molecular surface area

Appendix D. Details of the PLS regression analysis (Figure IV-3)

The Partial Least Squares (PLS) regression analysis, shown in Figure IV-3, was performed with Matlab software. For 23 test compounds, in vivo log BB values were used to construct the y-block (response variable), while calculated molecular descriptors and experimental log k_{IAM} values were used to construct the X-block (descriptor variables) in a log BB prediction model [1]. Both were normalized before PLS analysis.

The k_{IAM} (IAM retention factor) and corresponding log k_{IAM} values on both IAM.PC.DD2 column **1** and Sphingo-IAM column **2** were determined for the 23 test compounds from retention time measurements ($k_{IAM} = (t_r - t_0) / t_0$), as detailed in Table D-1.

Using the IAM.PC.DD2 column **1**, the correlation between in vivo log BB values and predicted in vitro log BB values can be expressed with the following equation. This model explains 96 % of variance in the data.

$$log\ BB = -0.24 + 0.03\ \alpha - 0.53\ MW - 217.78\ MR - 1.31\ MV + 2.48\ Pr + 216.82\ Pol - 0.14\ log\ P - 0.21\ log\ D7.4 + 0.21\ log\ WSo - 0.39\ WS7.4 + 0.17\ PB - 0.15\ MI + 0.04\ MIA + 0.59\ HIA + 0.85\ log\ k_{IAM}$$

Using the Sphingo-IAM column **2**, the correlation between in vivo log BB values and predicted in vitro log BB values can be expressed with the following equation. This model explains 89 % of variance in the data. The data is visually presented in Figure IV-3.

$$log\ BB = -0.25 + 0.37\ \alpha - 0.29\ MW - 36.38\ MR + 0.57\ MV + 0.10\ Pr + 35.88\ Pol - 0.06\ log\ P + 0.20\ log\ D7.4 + 0.36\ log\ WSo - 0.22\ WS7.4 + 0.05\ PB + 0.15\ MI + 0.15\ MIA + 0.28\ HIA + 0.33\ log\ k_{IAM}$$

Table D-1: k_{IAM} values (= (t_r - t_0) / t_0) of 23 test compounds measured on IAM.PC.DD2 column **1** and Sphingo-IAM column **2**.[a]

		20 µL, 50 µg/mL t_0 = 1.20 min	
		IAM.PC.DD2 column **1** 15 cm x 4.6 mm Flow 1 mL/min	Sphingo-IAM column **2** 15 cm x 3 mm Flow 0.5 mL/min
No.	Compound		
1	acetaminophen	0.51	0.72
2	acetylsalicylic acid	0.08	2.49
3	aminopyrine	0.63	0.81
4	amobarbital	1.81	2.78
5	antipyrine	0.51	0.63
6	benzene	1.89	2.87
7	carbamazepine	2.31	3.04
8	cimetidine	1.05	0.83
9	eserine	4.63	1.18
10	ethylbenzene	6.07	11.43
11	hexobarbital	1.27	1.89
12	ibuprofen	0.73	11.95
13	indomethacin	1.66	27.72
14	N-methyl-2-pyridineethanamine	2.85	0.51
15	omeprazole	2.34	3.31
16	oxazepam	5.93	7.77
17	pentobarbital	1.89	2.93
18	phenylbutazone	0.54	10.32
19	phenytoin	3.16	5.07
20	ranitidine	2.75	0.68
21	ropinirole	6.76	1.04
22	salicylic acid	0.06	2.18
23	toluene	3.45	5.66

[a] Conditions: Isocratic elution (25 °C); NH_4OAc_{Aq} buffer (10 mM, pH 7.4) + MeOH (40 % v/v) [2]; Waters 2690 Alliance HPLC chromatograph + Waters 2487 dual λ absorbance detector (210 - 300 nm). Data acquisition/ processing: PeakSimple Chromatography Data System (model 202).

References

1. Escuder-Gilabert L, Molero-Monfort A, Villanueva-Camanas RM, Sagrado S, Medina-Hernandez MJ (2004) Potential of biopartitioning micellar chromatography as an in vitro technique for predicting drug penetration across the blood-brain barrier. Journal of Chromatography B-Analytical Technologies in the Biomedical and Life Sciences 807 (2):193-201.

2. Braddy AC, Janaky T, Prokai L (2002) Immobilized artificial membrane chromatography coupled with atmospheric pressure ionization mass spectrometry. J Chromatogr A 966 (1-2):81-87.

Details of the PLS regression analysis (Figure IV-3)

Appendix E. Curriculum Vitae

CURRICULUM VITAE
MIKE DE VRIEZE

22/11/1985
Heurnestraat 306
9700 Oudenaarde
0498/ 10 14 02
mikedevrieze@gmail.com

EDUCATION

2009 – present	**PhD in Chemistry** Ghent University Titel: "The use of biopartitioning chromatography as an in-vitro technique to predict drug absorption" Promotor: prof. dr. Frederic Lynen
2010 – 2012	**Teacher training** Het Perspectief Ghent, magna cum laude
2004 – 2009	**Master in Chemistry** Ghent University, cum laude Master thesis: "Fractionation of lipid classes in biological liquids" Promotor: prof. dr. Pat Sandra
2003 – 2004	**1st Candidature Civil Engineer** Ghent University

PUBLICATIONS

- Verzele D, Lynen F, De Vrieze M, Wright AG, Hanna-Brown M, Sandra P (2012) Development of the first sphingomyelin biomimetic stationary phase for immobilized artificial membrane (IAM) chromatography. Chem Commun 48 (8):1162-1164

- De Vrieze M, Lynen F, Chen K, Szucs R, Sandra P (2013) Predicting drug penetration across the blood-brain barrier: comparison of micellar liquid chromatography and immobilized artificial membrane liquid chromatography. Anal Bioanal Chem 405 (18):6029-6041
- De Vrieze M, Verzele D, Szucs R, Sandra P, Lynen F (2014) Evaluation of sphingomyelin, cholester, and phosphatidylcholine-based immobilized artificial membrane liquid chromatography to predict drug penetration across the blood-brain barrier. Anal Bioanal Chem 406 (25):6179-6188
- Malengier B, Goessens T, Mafo FF, De Vrieze M, Van Langenhove L, Wanji S, Lynen F (2014) Model-based determination of the influence of textile fabric on bioassay analysis and the effectiveness of a textile slow-release system of DEET in mosquito control. Pest Manag Sci 71 (8): 1165-1174
- Van de Velde T, De Vrieze M, Surmont P, Bodé S, Drechsler P (2015) A geochemical study on the bitumen from Dosariyah (Saudi-Arabia): tracking Neolithic-period bitumen in the Persian Gulf. J Archaeol Sci 57: 248-256
- De Vrieze M, Janssens P, Szucs R, Van der Eycken J, Lynen F (2015) In vitro prediction of human intestinal absorption and blood-brain barrier partitioning: development of a lipid analog for micellar liquid chromatography. Anal Bioanal Chem 407 (24):7453-7466

PRESENTATIONS

- De Vrieze M. Predicting drug penetration across the blood–brain barrier: comparison of micellar liquid chromatography and immobilized artificial membrane liquid chromatography. HTC-13, Bruges, Belgium, January 27-31, 2014
- De Vrieze M, Lynen F. Assessment of a novel phosphocholine based micellar LC approach and of immobilized artificial membrane phases for improved prediction of in vivo drug behavior. HPLC 2015, Geneva, Switzerland, June 21-25, 2015

POSTER PRESENTATIONS

- De Vrieze M, Lynen F, Sandra P. Predicting drug penetration across the blood-brain barrier: comparison of micellar liquid chromatography and immobilized artificial membrane liquid chromatography. HTC-12, Bruges, Belgium, February 1-3, 2012

- De Vrieze M, Lynen F, Chen K, Szucs R, Sandra P. Predicting drug penetration across the blood-brain barrier: comparison of micellar liquid chromatography and immobilized artificial membrane liquid chromatography. HPLC 2013, Amsterdam, The Netherlands, June 16-20, 2013
- Nguyen MT, De Vrieze M, Van de Walle D, Van Hoed V, Lynen F, Dewettinck K. Analysis of glycolipids in vegetable lecithin with HPLC-ELSD. HTC-13, Bruges, Belgium, January 27-31, 2014
- De Vrieze M, Lynen F, Verzele D, Szucs R, Sandra P. Predicting drug penetration across the blood-brain barrier: comparison of different stationary phases for immobilized artificial membrane liquid chromatography. HTC-13, Bruges, Belgium, January 27-31, 2014
- De Vrieze M, Janssens P, Szucs R, Van der Eycken J, Lynen F. Synthesis of a phosphocholine based lipid for improved micellar LC based in vitro predictions of human intestinal absorption and blood-brain barrier partitioning. HPLC 2015, Geneva, Switzerland, June 21-25, 2015 **"Best Poster at HPLC2015 – Geneva"**

Dankwoord

Ter afsluiting van deze thesis zou ik graag iedereen willen bedanken die rechtstreeks of onrechtstreeks heeft bijgedragen aan het verwezenlijken van dit doctoraat.

In de eerste plaats wil ik mijn promotor professor Frédéric Lynen hartelijk bedanken voor alle jaren van begeleiding sinds het begin van mijn masterthesis in 2008. Tijdens mijn doctoraat kon ik altijd bij u terecht voor het bespreken van resultaten, het nalezen van manuscripten, praktische tips bij het oplossen van instrumentele problemen en het bespreken van het te volgen parcours. Dankzij uw perspectief en expertise heb ik meermaals nieuwe ideeën opgedaan.

Ook mijn co-promotor professor Pat Sandra zou ik hierbij van harte willen bedanken om me toe te laten mijn doctoraat aan te vatten als assistent na mijn masterthesis. Dankzij u heb ik voor dit uitdagende onderwerp kunnen kiezen. Uw ideeën en input tijdens de eerste jaren van mijn doctoraat hebben de basis gelegd voor een groot deel van het traject dat ik gevolgd heb.

I would like to thank Laure Hitzel and Roman Szucs. Thanks to your input, some general guidelines were created at the start of this project and some necessary calculations could be performed.

I would also like to thank the members of the reading committee for the critical evaluation of my thesis and the valuable suggestions.

Mijn collega’s van de Separation Science Group zou ik ook willen bedanken voor de aangename (werk)sfeer en natuurlijk ook voor de hulp bij het oplossen van problemen. Doorheen mijn 7 jaren in het labo zijn er heel wat mensen de revue gepasseerd, ik hoop dat ik dus niemand over het hoofd zie. In elk geval: bedankt aan Kevin, Pieter, Tim, Olivier, Sander, Seppe, Piotr, Jente, Maarten, Thomas, Bram, Marc, Vivienne, Maria, Mirka, Willem, Michael, Barbara, Mai, Bess, Kai, Li, Engda, Stefan, Melissa, Anna, Hanka, Lucia, Eva, Martha, Matthias, Beatriz, Dieter, Giacomo, Ravindra, Ameur, Yasemin en Tahisa!

Ook het overige personeel van de vakgroep Organische en Macromoleculaire Chemie en de leden van de centrale werkplaats zou ik graag bedanken voor de leuke conversaties en hulp bij allerhande zaken. Freddy en Tom, die intussen enkele jaren vertrokken zijn, zou ik hierbij zeker ook willen vermelden.

Verder wil ik nog een speciaal woord van dank richten aan Pieter. Niet enkel ken ik jou al van in de wieg en kan ik je logischerwijze als mijn oudste vriend bestempelen. Samen hebben we de kleuterschool en lagere school doorlopen en per toeval eindigde onze opleiding ook samen. Vooral de laatste twee jaar van mijn doctoraat heb ik frequent gesteund op jouw hulp; zonder die hulp zouden mijn syntheses helemaal niet zo vlot gelopen zijn.

Mijn familie en vrienden wil ik ook bedanken. Het samenzijn en de mogelijkheid om te kunnen praten over allerhande zaken zorgde ervoor dat ik kon blijven ontspannen en dit hielp me dan ook om mijn werk-gerelateerde moeilijkheden te relativeren.

Tenslotte wil ik mijn vrouw Kim bedanken. Zes jaar doctoraat is een redelijk lange periode, in ons geval lang genoeg voor een hele hoop belangrijke gebeurtenissen, zoals samenwonen, trouwen, en vier huizen kopen (t.t.z. één effectief huis en vervolgens nog drie kinderen). Bedankt om er altijd te zijn voor mij en steeds te luisteren naar mijn dagelijkse avonturen. Ook tijdens de drukke momenten (en dat waren er wel redelijk wat: extra opleidingen, verbouwingen, kindjes, …) en momenten dat ik mijn twijfels had om dit doctoraat af te ronden, heb je me steeds zo goed als mogelijk geholpen en mij gemotiveerd om verder te gaan. Ik hoop dat we samen nog zeer veel mogen meemaken en altijd kunnen blijven rekenen op elkaars steun.

Aan iedereen, BEDANKT,
Mike